Institut für Anorganische Chemie

Visible-Light-Driven Aerobic Oxidation Reactions Catalyzed by Riboflavin Tetraacetate

Dissertation

Zur Erlangung des Doktorgrades der Naturwissenschaften

Dr. rer. nat.

an der Fakultät Chemie und Pharmazie der Universität Regensburg

vorgelegt von:

Bernd Mühldorf

aus Burglengenfeld

Regensburg 2016

Der experimentelle Teil der vorliegenden Arbeit wurde in der Zeit zwischen November 2012 und Dezember 2015 unter Anleitung von Prof. Dr. Robert Wolf am Institut für Anorganische Chemie der Universität Regensburg angefertigt. Meinem Betreuer danke ich herzlich für die Überlassung dieses spannenden Projektes sowie für die hervorragende Betreuung und Unterstützung.

Die Arbeit wurde angeleitet von: Prof. Dr. Robert Wolf

Promotionsgesuch eingereicht am: 18.04.2016

Tag der mündlichen Prüfung: 29.04.2016

Promotionsausschuss:	Vorsitz	Prof. Dr. Richard Buchner
	Erstgutachter	Prof. Dr. Robert Wolf
	Zweitgutachter	Prof. Dr. Burkhard König
	Dritter Prüfer	Prof. Dr. Arno Pfitzner

Prologue

This thesis reports on photocatalytic oxidation reactions catalyzed by the vitamin B_2 derivative riboflavin tetraacetate (RFT). The dissertation seeks to expand the field of RFT-mediated oxidation reactions, mainly focusing on the challenging visible-light-driven oxygenation of C−H bonds with air as terminal oxidant. Chapter 1 reviews recent developments in the field of photocatalytic C−H bond oxygenation. In chapter 2, we show that the photooxygenation of electron-deficient benzylic substrates is feasible by modifying the reduction potential of RFT with Lewis acids. Expanding the scope of benzylic substrates accessible with flavin photocatalysis, chapter 3 delineates how the addition of a non-heme iron complex as co-catalyst improves the performance of RFT. In chapter 4, the RFT/non-heme iron system was used for the epoxidation of cycloalkenes. In addition to flavin-mediated C−H bond oxygenations, an aim was to apply RFT as oxidation catalyst for challenging transformations. Therefore, in chapter 5 we present two routes for the direct esterification of aldehydes based on flavin photocatalysis. Chapter 6 describes an enzyme-inspired artificial photosystem for the challenging oxidative chlorination of arenes using chloride anions as Cl source. Chapter 7 summarizes the results of this thesis.

Art & Science

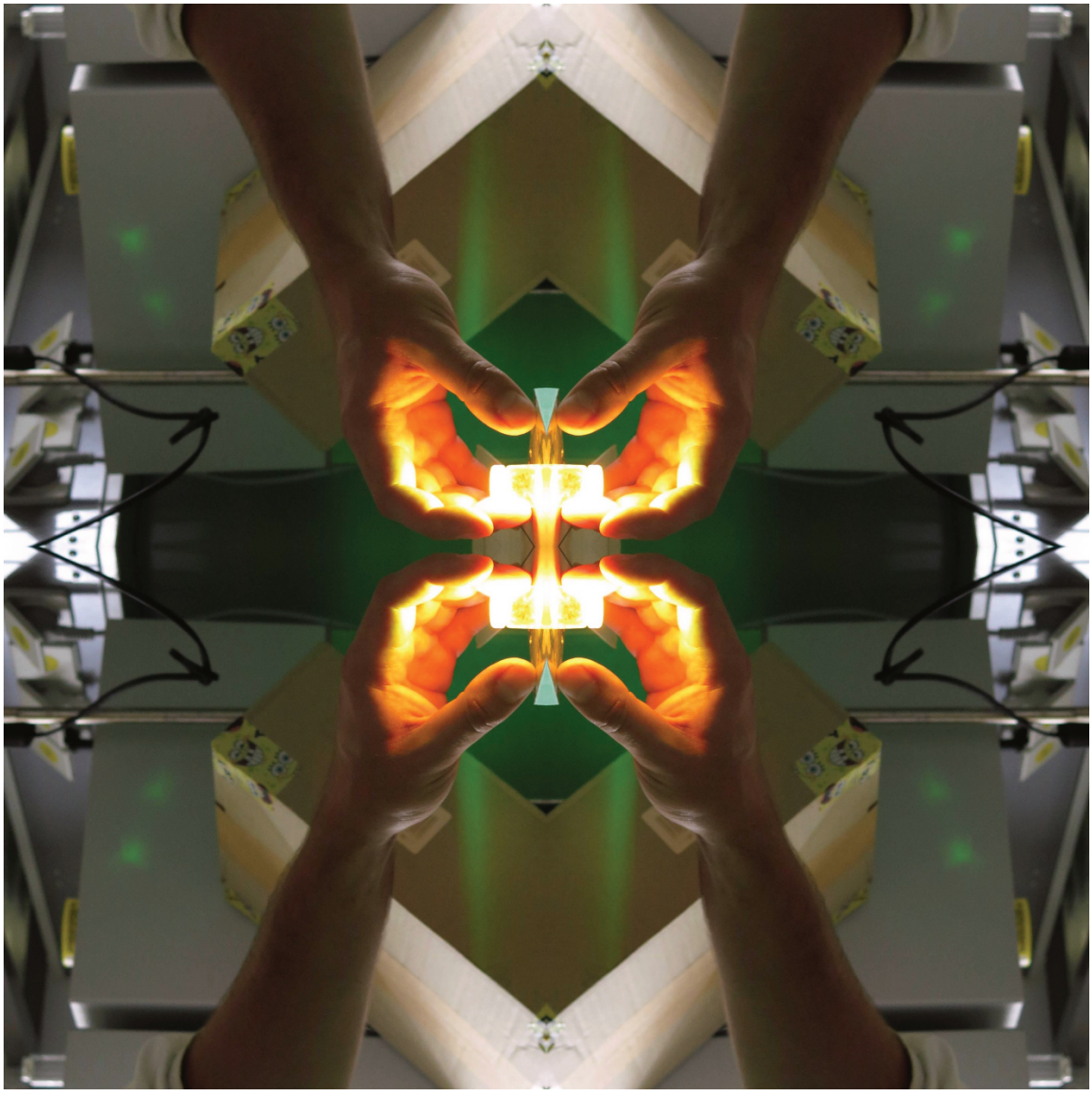

Robert Weindl, 2015

Table of Contents

Art & Science

Johanna Schuster, Spectaculum, 2015

1 Homogeneous Visible-Light-Driven C−H Bond Oxygenation

The selective C−H bond oxygenation of organic molecules is a challenging task from both a laboratory and industrial point of view. C−H bonds are thermodynamically strong and chemically inert thus their direct activation is a difficult task.[1,2] Dioxygen is the best oxidant from an atom-economic point of view, easily accessible and does not produce hazardous by-products, but direct transformations with dioxygen are kinetically hindered due to its triplet ground state.[3] Therefore, dioxygen has to be activated first to highly reactive intermediates such as hydroxyl radicals, hydroperoxides, or peroxides, which intrinsically diminishes the chemo-, stereo- and regioselectivity.

Nature utilizes enzymes to mediate the selective oxygen transfer of one or both oxygen atoms from O_2 to the organic molecule. A plethora of transition metal-based enzymes is capable of activating dioxygen and performing the selective oxygenation of C−H bonds (alkane hydroxylation) or C=C bonds (epoxidation and *cis*-dihydroxylation of alkenes). For instance, heme enzymes (cytochrome P450) perform the selective hydroxylation of alkanes and epoxidation of alkenes with dioxygen under mild conditions (Scheme 1a),[4,5] whereas non-heme enzymes (e.g. Rieske dioxygenase) bearing a 2-His-1-carboxylate facial triad motif catalyze the *cis*-dihydroxylation of alkenes (Scheme 1b).[6–10] Enzymes are substrate specific and the isolation and handling of the enzymes is often challenging and not suitable for large-scale reactions. Thus, the development of bioinspired catalysts which mimic the active center of the enzyme, has raised immense interest over the last years.[11] Most of these bioinspired heme and non-heme metal complexes are not able to activate dioxygen directly, but need strong organic oxidants to generate reactive intermediates that resemble those generated in the enzyme with dioxygen.[12] Therefore, catalysts which utilize dioxygen under mild conditions using visible light irradiation are highly desirable. Visible light is an inexhaustible source of energy. Over the past several years, synthetic photochemistry has attracted increasing attention, since light triggers reactions that are uniquely feasible *via* photochemistry. The combination of visible light irradiation and biomimetic metal catalysis with O_2 as oxidant is a green and sustainable alternative to traditional methods. This field has attracted much interest recently and is extensively reviewed in the first chapter.

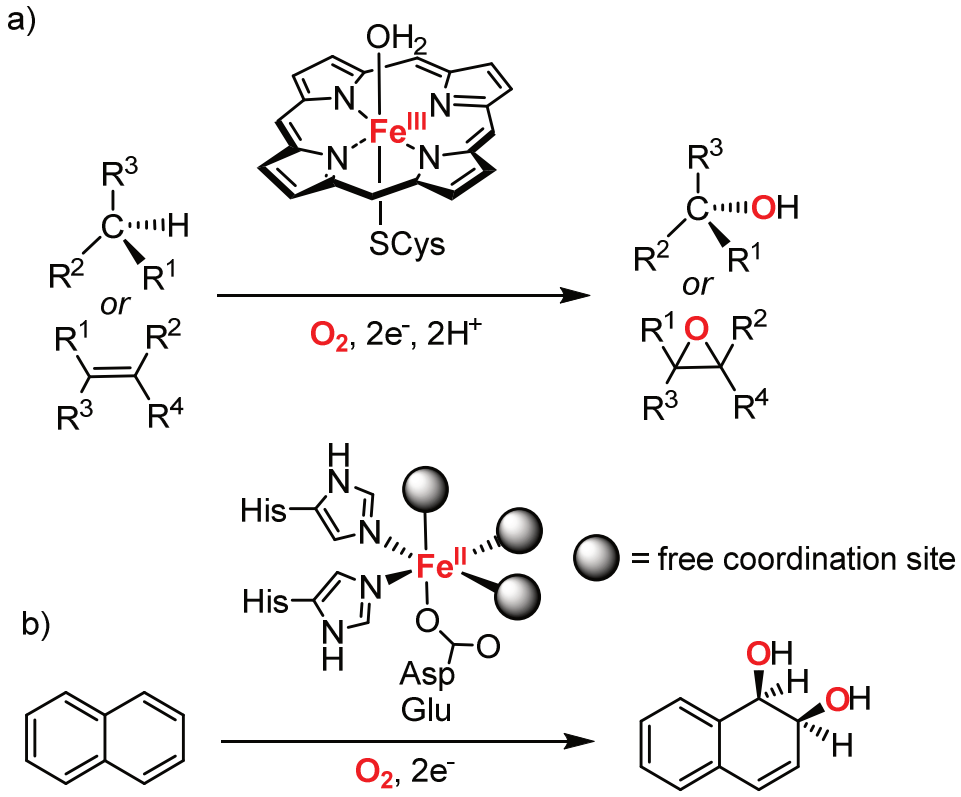

Scheme 1. a) Schematic representation of the active site of the heme-protein cytochrome P450, which effectively performs the hydroxylation of alkanes and epoxidation of alkenes;[4,5] b) Schematic representation of the active site of the non-heme protein Rieske-dioxygenase with 2-His-1-carboxylate facial triad motif for the selective *cis*-hydroxylation of alkenes;[6-10] Cys = cysteine, His = histidine, Asp = aspartic acid, Glu = glutamic acid.

Simultaneously to biomimetic transition metal catalysis, $[Ru(bpy)_3]^{2+}$[13–15] and organic dyes (methylene blue, eosin Y, etc.) have been extensively studied. These visible light absorbing chromophores have mainly been applied to catalyze the synthesis of complex organic molecules *via* photoredox catalysis, while only a few reports have studied their potential as oxygenation catalysts. The recent development of acridinium-based organophotocatalysts has tremendously enriched the field of visible-light-driven oxygenation reactions. These results are therefore reviewed here as well.

Much progress has been made for heterogeneous photooxygenation of various substrates with visible light.[16–23] This review intends to shed light on recent progress in the complementary *homogeneous* visible-light-driven photooxygenation of C−H bonds. Oxygenation reactions based on energy transfer such as singlet oxygen sensitization are not discussed in this review, since they have been reviewed elsewhere.[24,25]

1.1 Metal Porphyrin and Porphyrinoid Catalysts

1.1.1 Iron

Mononuclear Porphyrin Catalysts

The reactivity of iron porphyrins as photocatalysts is of great interest for the selective oxygenation of organic compounds owing to their ability to utilize O_2 for oxygenation reactions. Classically, Fe(III) porphyrins need stoichiometric quantities of co-reductants to be catalytically active. In 1987, Suslick and co-workers reported the first photocatalytic hydroxylation of hydrocarbons with dioxygen using an [(tpp)Fe(III)Cl] complex (**1**, tpp = 5,10,15,20-tetraphenylporphyrin dianion, Scheme 2) without the need of a co-reductant.[26] Cyclohexene is oxygenated to the allylic products cyclohexen-3-ol (23%) and cyclohexen-3-one (77%) with 150 turnovers. Hennig *et al*. reported that the photocatalytic oxygenation of α-pinene with **1** yielded a mixture of oxygenated products with high turnover up to TON 1500.[27] A serious obstacle of iron porphyrin complexes is their high sensitivity toward free radical attacks and oxidative degradation. The stability of these catalysts is significantly increased by introducing aryl groups bearing electron withdrawing substituents in the *meso*-position of the porphyrin framework. Therefore, Maldotti and co-workers applied a *meso*-tetraarylporphyrin complex with an axial ligand OH^-, [(tdcpp)Fe(III)OH] (**2**, tdcpp = 5,10,15,20-tetra(2,6-dichlorphenyl)porphyrin dianion, Scheme 2) as catalyst for the selective oxygenation of cyclohexane to cyclohexanone (61%) and cyclohexanol (39%) by O_2 under visible light irradiation (λ = 350−450 nm).[28] Additionally, introducing electron-withdrawing groups such as Cl or Br in the *β*-position of the pyrrole moiety gave complexes of the type [(tdcp$R^1{}_8$)Fe(III)OH] (tdcp$R^1{}_8$ = 5,10,15,20-tetra(2,6-dichlorphenyl)octa-*β*-halogenidoporphyrin dianion, **3** (R^1 = Cl), **4** (R^1 = Br), Scheme 2) with further improved durability, but with only slight effect on the product distribution.[28]

In all cases, visible light excitation of the complexes [(porph)Fe(III)X] (porph = tpp, tdcpp or tdcp$R^1{}_8$, X = Cl or OH) leads to the homolysis of the Fe−X bond, which yields [(porph)Fe(II)] and $Cl^\bullet$ or $OH^\bullet$ radicals (Scheme 2, step *i*). The subsequent abstraction of a hydrogen atom from RH by $X^\bullet$ yields alkane radicals $R^\bullet$, which form the observed oxygenated products *via* a peroxy radical chain autoxidation. The regeneration of the iron catalyst [(porph)Fe(III)X] is proposed to occur *via* the autoxidation of [(porph)Fe(II)], yielding the *μ*-oxo bridged complex $[(porph)Fe(III)]_2O$ (step *ii*). In the case of **1**, HCl is believed to regenerate the complex (step *iii*), whereas in the case of **2**, the photodisproportionation of $[Fe(III)(porph)]_2O$[29] and subsequent hydrogen abstraction by a high-valent oxo-iron(IV) species regenerates the catalyst (step *iv*).[30] The role of

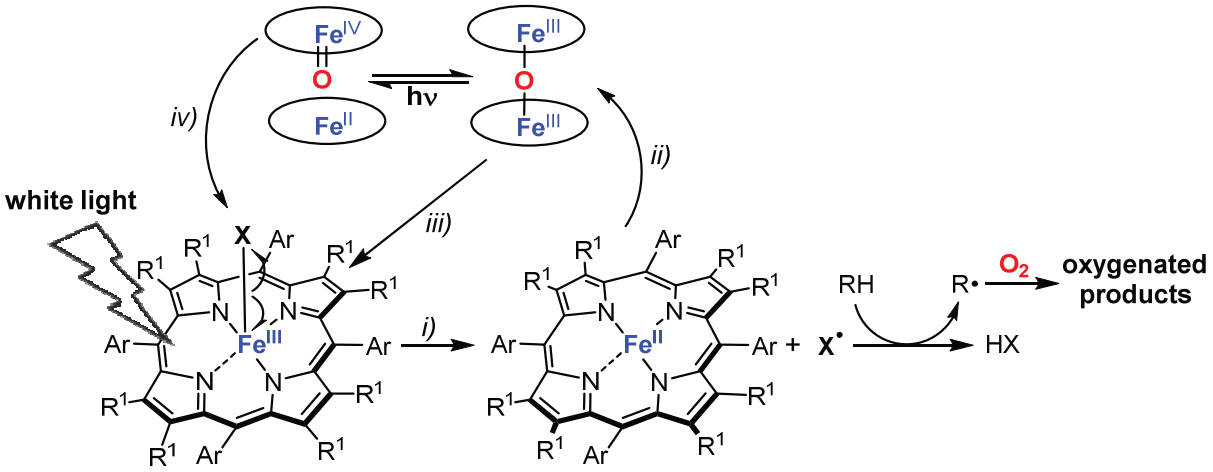

1 Ar = phenyl; X = Cl
2 Ar = 2,6-dichlorphenyl; X = OH
3 Ar = 2,6-dichlorphenyl; X = OH; R^1 = Cl
4 Ar = 2,6-dichlorphenyl; X = OH; R^1 = Br

Scheme 2. Photooinitiated homolysis of the Fe–X bond in [(porph)Fe(III)X] complexes (step *i*) leads to the generation of $X^{\bullet}$ radicals, which subsequently abstract hydrogen atoms from RH and yield oxygenated products *via* peroxy radical chain autoxidation. The reduced catalyst forms a μ-oxo bridged complex (step *ii*). Depending on the porphyrin moiety, the μ-oxo bridged complex directly regenerates the catalyst in the presence of acids (step *iii*) or *via* photodisproportionation (step *iv*).

[(porph)Fe(III)X] catalysts seems to be limited to induce radical chain reactions. This reactivity substantially differs from the role of iron porphyrins in naturally occurring monooxygenase enzymes such as cytochrome P450, where the strong oxidizing agent is a highly reactive iron(IV)-oxo porphyrin π radical cation, [(porph$^{\bullet+}$)Fe(IV)(O)], also known as compound I (cpd I).[31] Groves *et al.* showed that [(tpp$^{\bullet+}$)Fe(IV)(O)] (**5**) is generated from the synthetic model complex **1** by oxygen-atom transfer from an active oxygen species such as iodosylbenzene.[32] However, this high-valent oxo-species does not seem to be accessible selectively by excitation of [(porph)Fe(III)X] with visible light under aerobic conditions as described above. Nevertheless, a closer examination of the product distribution for various substrate/catalyst ratios in the photocatalytic oxygenation of α-pinene revealed the preferred formation of α-pinene oxide in the presence of **1**.[33] Hennig and co-workers concluded that [(tpp$^{\bullet+}$)Fe(IV)(O)] or [(tpp)Fe(IV)(O)] (**6**) may be involved in addition to the radical chain pathway. These species may be formed by the well-known peroxide shunt mechanism between **1** and hydroperoxyl radicals or hydroperoxides that result from α-pinene radicals after hydrogen abstraction. In agreement with this observation, alkenes with strained carbon double bonds preferentially gave epoxides, whereas allylic oxygenation was mainly observed for unstrained alkenes. Thus, the proposed reaction mechanisms more likely involves [(tpp)Fe(IV)(O)], comparable to compound II (cpd II) in cytochrome P450 enzymes as the catalytically active species.[27,34]

The epoxidation of strained alkenes by **6** is analogous to epoxidation reactions using [(tpp$^{\bullet+}$)Fe(IV)(O)], but its reactivity is significantly lower than that of [(tpp$^{\bullet+}$)Fe(IV)(O)], presumably due to the lower electrophilicity of [(tpp)Fe(IV)(O)].

These biologically inspired approaches showed that photooxygenation of hydrocarbons with [(porph)Fe(III)X] is possible, but suffers from low selectivities due to autoxidative processes initiated by the homolysis of the Fe−X bond. Additionally, the selective formation of high-valent iron-oxo species such as cpd I was not feasible in a photocatalytic procedure. Very recently, Zhang *et al.* selectively generated [(tpp$^{\bullet+}$)Fe(IV)(O)] (**7b**) from [(tpp)Fe(III)(BrO_3)] (**7**) by photoinitiated heterolysis of the Fe−O bond *via* a putative [(tpp)Fe(V)(O)]$^+$ complex (**7a**, Scheme 3, step *i*).[35] The subsequent intramolecular electron transfer from the porphyrin moiety to iron(V) yields the valence tautomer [(tpp$^{\bullet+}$)Fe(IV)(O)] (**7b**, step *ii*), as confirmed by UV-vis spectroscopy. In the case of [(tpfpp)Fe(III)(BrO_3)] (**8**, tpfpp = 5,10,15,20-tetrakis(pentafluoro)phenylporphyrin dianion), which exhibits a highly electron deficient porphyrin moiety, no formation of [(tdfpp$^{\bullet+}$)Fe(IV)(O)] is observed. Instead, the [(tdfpp)Fe(IV)(O)] complex (**8b**) is formed *via* the comproportionation of the proposed [(tdfpp)Fe(V)(O)]$^+$ complex (**8a**) and **8** (step *iii*).The electron transfer from the tdfpp ligand to iron(V) seems to be unfavored due to the higher redox potential of tdfpp compared to tpp. Kinetic studies showed that the oxygenation reaction of [(tpp$^{\bullet+}$)Fe(IV)(O)] with alkenes is about two to three orders of magnitude higher in comparison with those of [(tdfpp)Fe(IV)(O)]. This is in agreement with the observation that cpd I is a more efficient oxidant than cpd II and impressively shows the importance of the selective formation of high-valent iron-oxo species, although the reaction is not catalytic yet and the oxygen source is derived from the BrO_3^- anion.

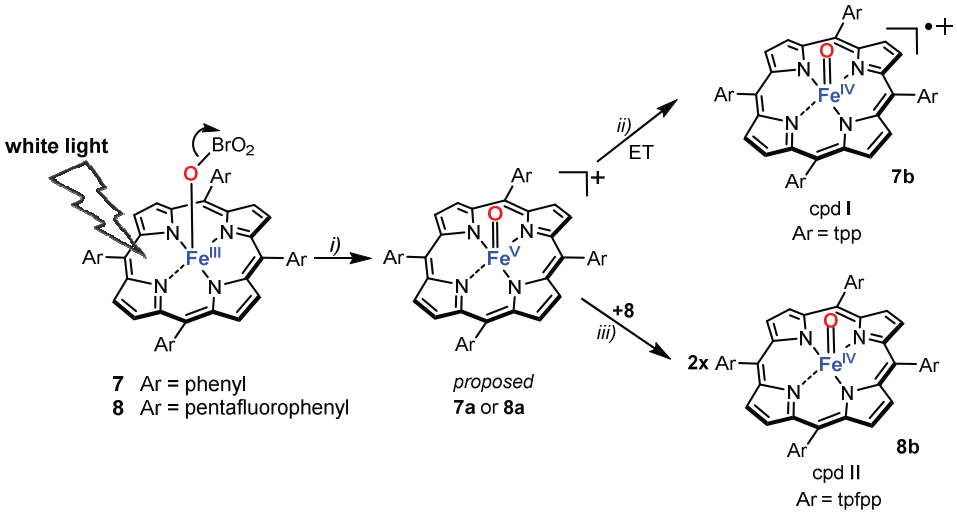

Scheme 3. Photoinitiated generation of high-valent porphyrin iron-oxo derivatives.

As shown by Zhang *et al.*, biomimetic [(porph$^{\bullet+}$)Fe(IV)(O)] complexes (cpd I mimics) are more reactive than [(porph)Fe(IV)(O)] (cpd II mimics).[35] Nevertheless they do not

exhibit the high reactivity necessary for hydrocarbon oxidation reactions, which is assumed to be performed by cpd I in cytochrome P450. For example, oxygenation of cyclohexane does not occur when the model porphyrin complex [(tmp$^{\bullet+}$)Fe(IV)(O)] (tmp = 5,10,15,20-tetramesitylporphyrin dianion) or [(tmp)Fe(IV)(O)] are applied. However, the oxygenation of cyclohexane readily occurs when [(tmp)Fe(III)Cl] is used in the presence of a sacrificial oxidant such as *m*-chloroperoxybenzoic acid (*m*CPBA). Therefore, the authors suggest that an [(tmp)Fe(V)(O)]$^{+}$ species is the real oxidant, which is accessible with the strong oxidant *m*CPBA. A genuine iron(V)-oxo porphyrin species remains to be comprehensively characterized, but laser flash photolysis experiments indicate its existence.[36] Photolysis of the metastable species [(tmp)Fe(IV)(ClO_4)$_2$] by 355 nm laser light gave a highly reactive species that reacts with alkenes five orders of magnitude faster than the cpd I analogue [(tmp$^{\bullet+}$)Fe(IV)(O)(ClO_4^-)]. The authors tentatively assigned this species to a true iron(V)-oxo species. Additionally, photolysis of metastable porphyrin-iron(IV) diperchlorates by Newcomb *et al.* produced a highly reactive transient porphyrin-iron(V)-oxo complex, which oxidizes alkenes, styrenes and benzylic C−H bonds in two-electron oxo-transfer reactions. The reaction rate is also several orders of magnitude faster than oxidations by iron(IV)-oxo porphyrin radical cations.[37]

Mononuclear Corrole Catalysts

Although biolocially inspired complexes are suitable for mimicking the iron porphyrin moiety of cytochrome P450 synthetic applications often suffer from oxidative degradation of the porphyrin framework in the absence of the protecting surrounding of the enzyme.[38] Thus, the modification of the porphyrin ring was intensively investigated in order to stabilize high-valent oxo-species and to prevent oxidation of the porphyrin core. One approach is the use of corrole, a fully unsaturated tetrapyrrolic macrocycle found in nature. Corroles differ from porphyrins by the absence of one *meso*-carbon atom in the macrocyclic backbone.[39] Corroles act as trianionic ligands, while porphyrins are typically dianionic. As a consequence, corroles support metals in higher oxidation states than porphyrins.

The aerobic oxidation of triphenylphosphine by a Cr(III) corrole complex was reported, where the active species is a Cr(V)-oxo intermediate.[40] Inspired by this work, Newcomb and co-workers reported that the laser flash photolysis (λ = 350 nm) of 5,10,15-tris(pentafluorophenyl)corrole iron(IV) chlorate (**9**) gave a highly reactive iron−oxo transient identified as an iron(V)-oxo species (**10**, Scheme 4). The transient was shown to be an oxo transfer agent in a preparative reaction with *cis*-cyclooctene. The new transient

is more than six orders of magnitude more reactive with typical organic reductants than expected for an iron(IV)-oxo corrole radical cation and 100 times more reactive than an

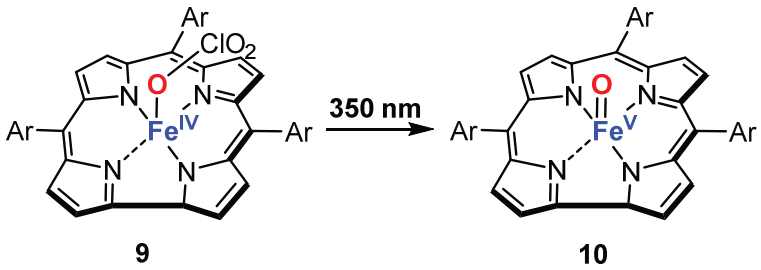

9 **10**

Scheme 4. Photochemical generation of a highly reactive iron(V)-oxo transient **10**.

analogous, positively charged iron(IV)-oxo porphyrin radical cation.[41]

Dinuclear Porphyrin Catalysts

Bis-iron(III)-μ-oxo porphyrin complexes have received much attention since they were observed as intermediates in the photooxygenation of hydrocarbons by monomeric porphyrin complexes.[30] Nocera *et al.* developed the first cofacial bisporphyrin system bearing a dibenzofuran spacer (Scheme 5) to perform the photooxygenation of dimethylsulfide under irradiation with white light with high selectivities (90%) for the sulfoxidation.[42] Further modification of the porphyrin framework, i.e. the introduction of electron-withdrawing C_6F_5 groups in the *meso*-position of the porphyrin unit, led to a higher oxidation power of the metalloporphyrin. Thus, the visible-light-driven epoxidation of olefins[43] and the photooxygenation of hydrocarbons[44] was feasible using air as terminal oxidant (Scheme 5). The general catalytic cycle for the photooxygenation of hydrocarbons with bis-iron(III)-μ-oxo porphyrin **11** involves the photoinitiated cleavage of the thermally inert Fe−O bond[29,45] to generate an [(porph)Fe(II) linked (porph)Fe(IV)(O)] pair (**11a**). This reactive intermediate is capable to transfer an oxygen atom to the substrate with concomitant formation of reduced [(porph)Fe(II) linked (porph)Fe(II)] subunits (**11b**), which are easily regenerated by dioxygen to **11**.

The catalyst motif is not strictly limited to bis-iron(III)-μ-oxo porphyrin complexes since Karlin *et al.* demonstrated the first photochemical oxidations with a bis-iron(III)-μ-oxo complex, which exhibits one porphyrin and one non-heme moiety.[46] The porhyrin framework is covalently linked similar to Nocera's system. This complex was capable to perform the oxygenation of triphenylphosphine, tetrahydrofuran or toluene. Nevertheless, the efficiency is dramatically lower compared to the related bis-iron(III)-μ-oxo porphyrin complexes.

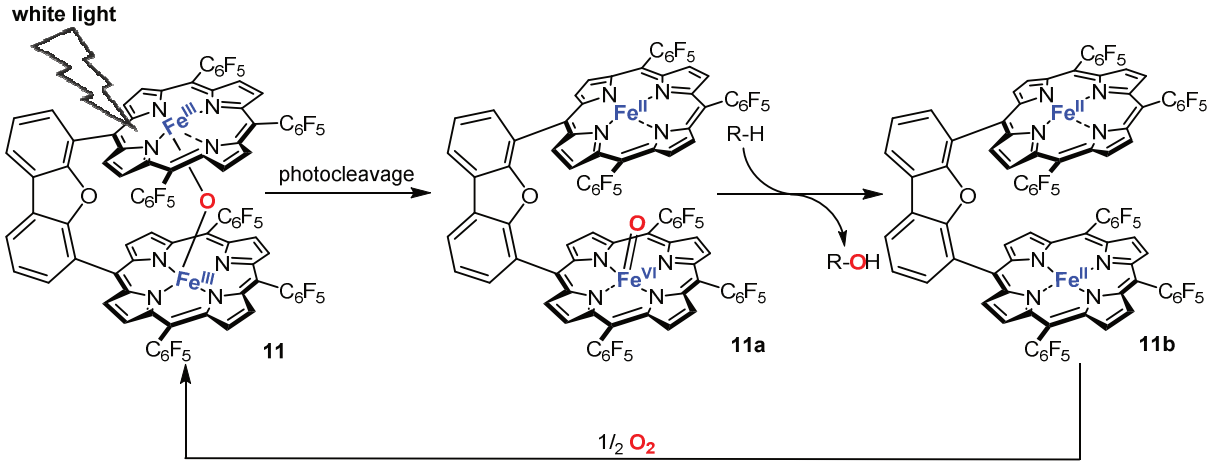

Scheme 5. Photocatalytic oxygenation of hydrocarbons by the bis-iron(III)-μ-oxo pacman porphyrin using atmospheric oxygen and visible light.

Dinuclear Corrole Catalysts

Newcomb described the visible-light-driven epoxidation of *cis*-cyclooctene to *cis*-cyclooctene oxide (yield >95%, ~200 turnovers) on a preparative scale (5 mmol) in the presence of a bis-iron(IV)-μ-oxo corrole dimer (**12**, Scheme 6). In analogy to the bis-iron(III)-μ-oxo pacman porphyrin by Nocera, the catalysis proceeds by photoinitiated homolysis of the Fe–O bond to give a putative iron(V)-oxo corrole species (**13**) and an iron(III) corrole (**14**). The formation of **13** was suggested by its similar high reactivity in comparison to [(tpp)Fe(V)(O)](ClO$_4$).[47]

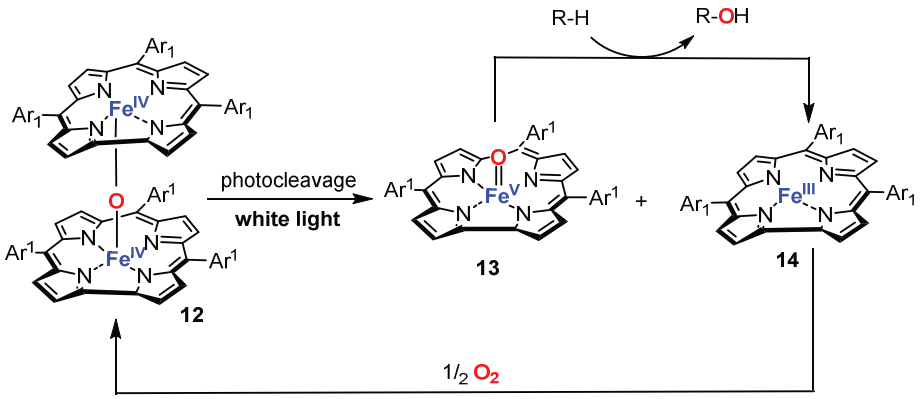

Scheme 6. Photogeneration of an iron(V)-oxo corrole species for oxygenation reactions; Ar$_1$ = C$_6$F$_5$.

1.1.2 Manganese

Porphyrin Catalysts

Manganese porphyrins have attracted special attention because their high-valent oxo species are related to manganese oxo species in the oxygen-evolving center (OEC) of photosystem II. High-valent metal-oxo complexes have been prepared peroxy acids, hydrogen peroxide, iodosylarenes, and dioxygen in the presence of reductants. Until 2015, there was only one report of photocatalytic olefin oxidation with O_2 using manganese porphyrins. Hennig and co-workers reported the catalytic oxygenation of alkenes using (tetraarylporphyrinato)manganese(III) complexes with molecular oxygen and visible light, resulting in the formation of mixtures of epoxide and allylic oxygenation products.[48] The reaction suffers from low selectivity due to autoxidative processes initiated by the manganese porphyrin, which yield the allylic oxidation products by a radical chain mechanism. On the contrary, epoxide formation is due to at least one high-valent manganese-oxo species present in the reaction mixture. The low epoxide yield suggests that the predominant mechanism is a radical chain.

In 2015, Goldberg *et al.* reported the photocatalytic oxidation of 10-methyl-9,10-dihydroacridine ($AcrH_2$) to 10-methyl-(9,10*H*)-acridone (Acr=O) by O_2 with manganese(III) porphyrins, i.e. [(tmp)Mn(III)OH] (**15**, tmp = 5,10,15,20-tetramesitylporphyrin dianion) and [(tpfpp)Mn(III)(CH_3COO)] (**16**, tpfpp = 5,10,15,20-tetrakis(pentafluoro)phenylporphyrin dianion) under visible light irradiation ($\lambda > 480$ nm) in oxygen-saturated benzonitrile at room temperature.[49] Catalyst **15** is approximately three times more effective for the oxygenation of AcrH than **16**. The proposed mechanism (Scheme **7**) involves the excitation of the [(porph)Mn(III)] complex to [(porph)Mn(III)]* (step *i*), which reacts with O_2 to produce a putative[(porph)Mn(IV)($O_2^{\bullet-}$)] complex

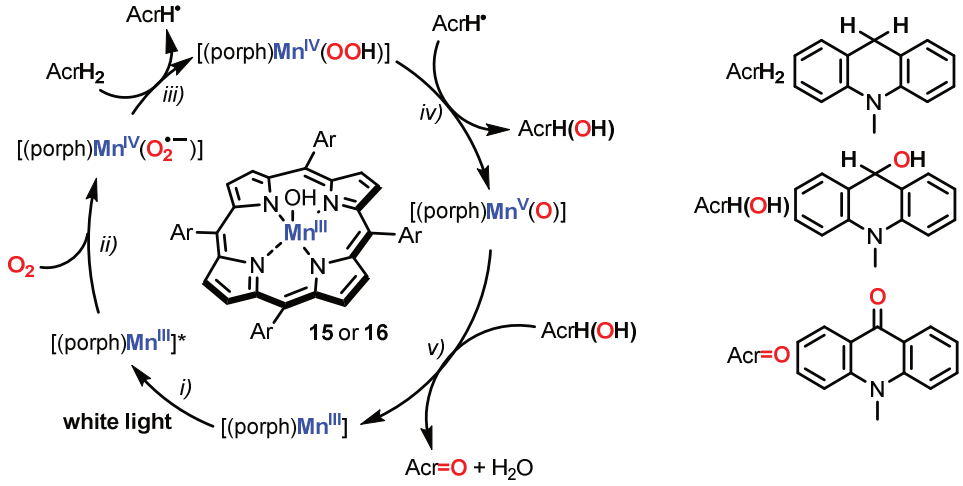

Scheme 7. Proposed mechanism for the visible-light-driven photooxygenation of AcrH to Acr=O by manganese(III) porphyrin complexes **15** (Ar = 2,4,6-trimethlyphenyl) or **16** (Ar = C_6F_5).

(step *ii*). Hydrogen-atom transfer from $AcrH_2$ generates a hydroperoxo complex [(porph)Mn(IV)(OOH)] and $AcrH^{\bullet}$ (step *iii*). The subsequent reductive O−O bond cleavage by $AcrH^{\bullet}$ produces [(porph)Mn(V)(O)] and AcrH(OH) (step *iv*), followed by the subsequent oxidation of AcrH(OH) by [(porph)Mn(V)(O)] to yield the desired product Acr=O with concomitant regeneration of [(porph)Mn(III)] (step *v*).

Corrolazine Catalysts

Goldberg and co-worker investigated the properties of the corrolazine ligand, which is a *meso*-N-substituted analogue of corrole. As a trianionic ligand, corrolazine more strongly supports higher metal oxidation states than porphyrins. The authors reported that the excitation of the Mn(III) complex [(tbp_8Cz)Mn(III)] (**17**, tbp_8Cz = octakis(*p-tert*-butylphenyl)-corrolazine trianion) with visible light in the presence of O_2 yields the Mn(V)-oxo complex [(tbp_8Cz)Mn(V)(O)] (**18**) as confirmed by UV-vis and ^{1}H-NMR spectroscopy (Scheme 8).[50] This complex is a rare example of a first-row transition metal complex capable of activating dioxygen directly from its initial oxidation state +3.

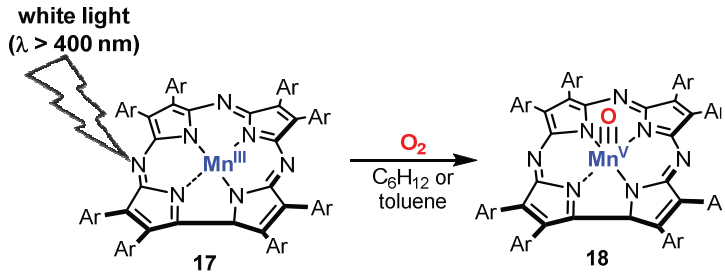

Scheme 8. Photogeneration of a high-valent Mn-oxo species in the presence of dioxygen; Ar = *p-tert*-butylphenyl.

Control experiments confirmed that the photogeneration of **18** occurs *via* a free radical mechanism. Thus the formation of **18** is suppressed when radical inhibitors are added. Additionally, the generation of **18** is also feasible in the dark when radical initiators are present. Mechanistic studied revealed that this radical process is initiated by excitation of **17** (Scheme 9, step *i*) followed by reaction with O_2, which may produce a Mn(IV)-superoxide complex [Mn(IV)$O_2^{\bullet-}$] (step *ii*). This species abstracts a hydrogen atom from the solvent R-H (cyclohexane or toluene) to give $R^{\bullet}$ and Mn(IV)−OOH (step *iii*), which is subsequently cleaved to **18** and $OH^{\bullet}$ radicals (step *iv*). The alkyl radicals $R^{\bullet}$ derived from the solvent are trapped by O_2 to yield alkylperoxy/alkylhydroperoxide species ($ROO^{\bullet}$/ROOH, step *v*) and further propagate or terminate (step *vi*) the radical chain.

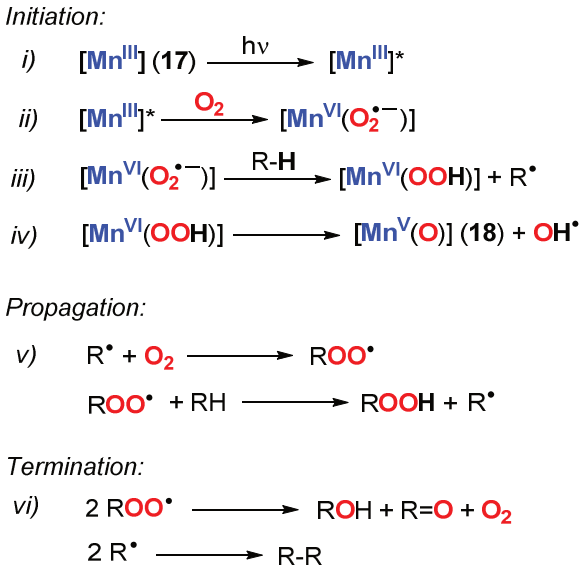

Scheme 9. Free radical chain mechanism for the formation of **18**.

Irradiation of a mixture of an excess of triphenylphosphine (PPh_3, 1300 equiv.) and **17** for 60 min in a dioxygen-saturated cyclohexane solution resulted in the rapid production of triphenylphosphine oxide ($OPPh_3$, TON = 535). The photogenerated oxygenation catalyst **18** transfers the oxygen atom to PPh_3 and regenerates **17**. The source of the oxygen atom in $OPPh_3$ was confirmed to be air, and a singlet oxygen pathway was ruled out.[50]

Building on these investigations, Goldberg *et al.* investigated the generation of **18** in the inert solvent benzonitrile (PhCN).[51] As expected, step *iii* in Scheme 9 does not proceed in PhCN alone, since no radical initiation is possible. The formation of **18** is not observed in this case. However, **18** is formed in the presence of hexamethylbenzene (HMB). Similar to cyclohexane (*vide supra*, **f**), HMB acts as initiator for the radical chain forming the hexamethylbenzene radical which transforms into the benzyl alcohol and the corresponding ketone, whereas **18** accumulates in the reaction mixture because no further reaction occurs. Unfortunately, **18** is unable to oxidize strong C−H bonds with a bond dissociation free energy BDFE >69 kcal mol^{-1}. Thus, the oxygenation of 10-methyl-9,10-dihydroacridine ($AcrH_2$, BDFE = 76 kcal mol^{-1}) to 10-methyl-(9,10*H*)-acridone (Acr=O) may be performed catalytically (Scheme 10a), whereas the selective hydroxylation of toluene (BDFE = 87 kcal mol^{-1}) was therefore limited to strictly stoichiometric reactions (Scheme 10b). Further studies revealed that the addition of a strong acid gave access to a catalytic procedure. Addition of Brookhart´s acid ($[H(OEt_2)_2][B(C_6F_5)_4]$) to **17** in benzene successfully enabled the photocatalytic oxygenation of toluene derivatives.[52] For example, HMB is oxygenated to the corresponding benzyl alcohol PMB-OH (TON = 18) and ketone PMB-CHO (TON = 9). Strict control of the proton content is crucial. While the monoprotonated Mn(III) complex $[(tbp_8Cz(H))Mn(III)]^+$ (**19**) is a catalytically active, the deprotonated $[(tbp_8Cz(H_2))Mn(III)]^{2+}$ complex (**20**) is inactive.

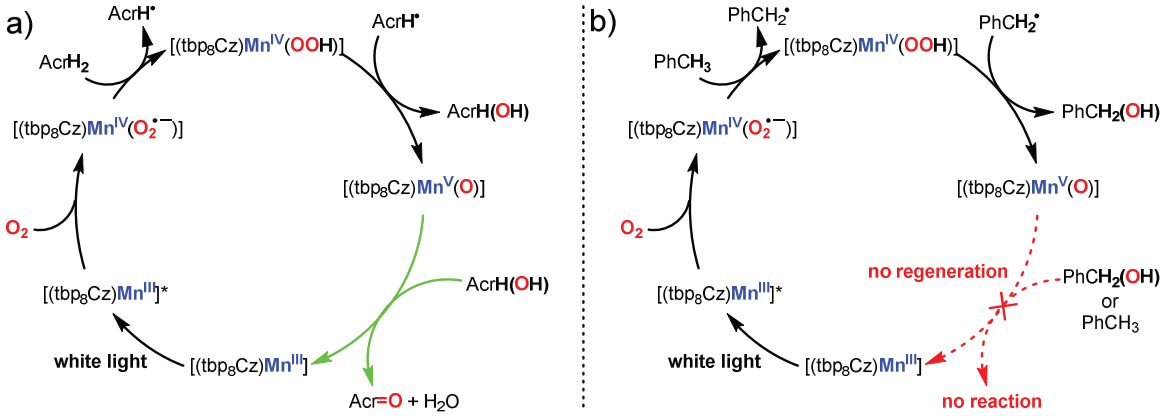

Scheme 10. a) Photocatalytic oxygenation of $AcrH_2$ to Acr=O by **17** in PhCN; b) photochemical generation of **18** from **17** in PhCN in the presence of toluene under concomitant formation of stoichiometric amounts of benzyl alcohol.

The proposed reaction mechanism is depicted in Scheme 11. Excitation of **19** in the presence of O_2 generates a putative $[(tbp_8Cz(H))Mn(IV)(O_2^{\bullet-})]^+$ complex, which abstracts a hydrogen atom from the substrate hexamethylbenzene (HMB), yielding the benzyl radical HMB$^\bullet$ and $[(tbp_8Cz(H))Mn(IV)(OOH)]^+$. The latter species is supposed to perform the hydroxylation of HMB$^\bullet$ *via* homolysis of the O–O bond and subsequent rebound of the concomitantly formed OH$^\bullet$ radical. The recombination of the OH$^\bullet$ radical with HMB$^\bullet$ yields the hydroxylated product pentamethylbenzyl alcohol (PMB-OH). Additionally, the oxidized $[(tbp_8Cz(H))Mn(V)(O)]^+$ complex is formed, which is able to oxygenate HMB to PMB-OH and regenerate **19**. In summary, the addition of a proton source gives access to the catalytic oxygenation of HMB, whereas in the absence of protons, the reaction is strictly limited to stoichiometric formation of PMB-OH.

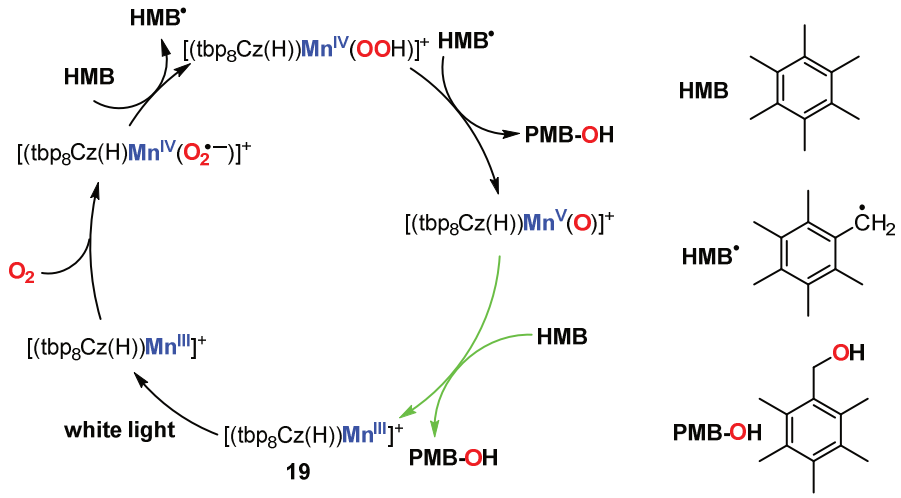

Scheme 11. Proposed reaction mechanism for the photocatalytic oxygenation of HMB by **19**.

1.1.3 Ruthenium

Mononuclear Porphyrin Catalysts

Inoue *et al*. reported the visible-light-driven oxygenation of alkenes in the presence of carbonyl-coordinated 5,10,15,20-tetramesitylporphyrinatoruthenium(II), [(tmp)Ru(II)(CO)] (**21**), as a photosensitizer and oxygenation catalyst at the same time. Hexachloroplatinate(IV) was applied as an electron acceptor in alkaline aqueous acetonitrile under degassed conditions (Scheme 12).[53]

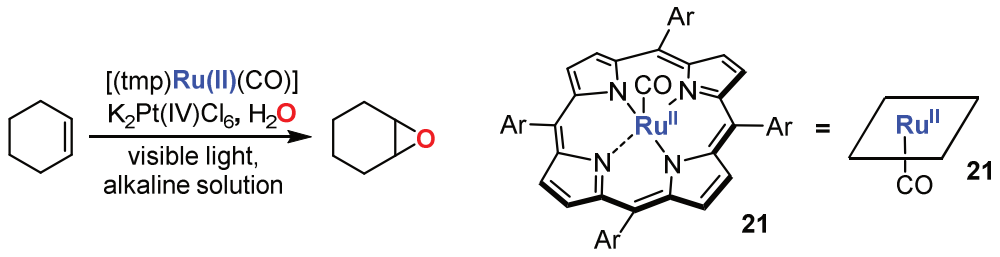

Scheme 12. Photooxygenation of cyclohexene to cyclohexene oxide in the presence of ruthenium catalyst **21** and electron acceptor $K_2Pt(IV)Cl_6$ with water as oxygen source under anaerobic conditions.

This reaction significantly differs from the oxygenation reactions reported in the chapters before. The source of the oxygen atom is water and not dioxygen as confirmed by $H_2{}^{18}O$-labelling experiments. Additionally, the authors ruled out the involvement of higher oxidation states of Ru, such as Ru(IV), Ru(V) or Ru(VI), since no reaction occurred in a control experiment with [(tmp)Ru(VI)$(O)_2$]. This is in contrast to metal porphyrin catalyzed oxygenation reactions, where a high selectivity is only obtained with metal ions in high oxidation states. Nevertheless, the oxygenation of cyclohexene, *cis*-stilbene, styrene and norbornene was achieved in high selectivity. The proposed reaction mechanism is based on an electron transfer from the excited triplet state of **21** to K_2PtCl_6, which yields the radical cation [(tmp$^{\bullet+}$)Ru(II)(CO)] (Scheme 13). Under neutral conditions, no further reaction occurs, whereas the key intermediate [(tmp)Ru(III)(OH)(CO)] is formed in the presence of OH^- anions. Successive deprotonation generates the oxygenation catalyst [(tmp)Ru(III)(O)(CO)]$^-$ which transfers the oxygen atom to the substrate. The reduced species [(tmp)Ru(I)(CO)]$^-$ or its tautomer [(tmp$^{\bullet-}$)Ru(II)(CO)] is reoxidized to **21** by another equivalent of K_2PtCl_6.

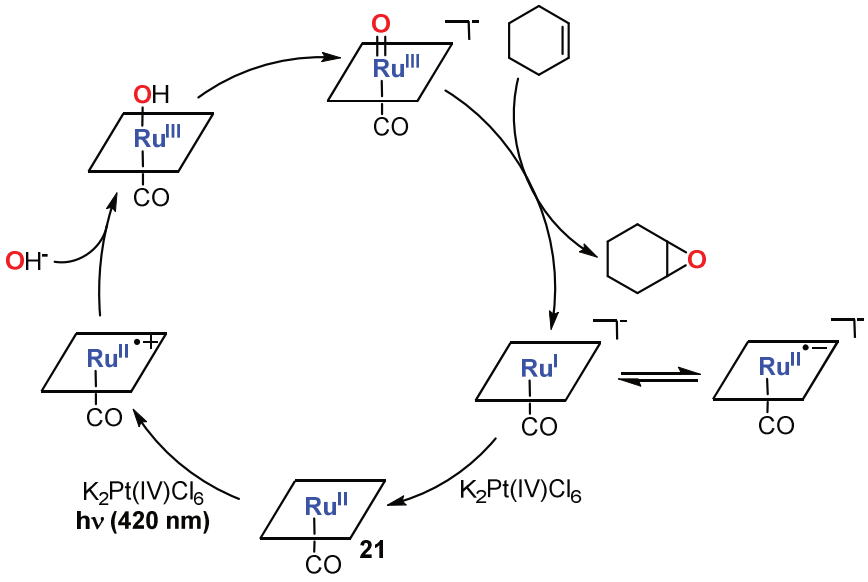

Scheme 13. Proposed mechanism for the photooxygenation of cyclohexene by **21**.

Dinuclear Porphyrin Catalysts

Newcomb *et al.* demonstrated that bis-ruthenium(IV)-μ-oxo porphyrins are efficient precursors for high-valent ruthenium(V)-oxo transients and catalyze the visible-light-promoted oxygenation of alkenes and activated hydrocarbons using atmospheric oxygen (Scheme 14). The most efficient catalyst was a [(4-CF_3-tpp)(Ru(IV)OH]$_2$O precursor (**22**, 4-CF_3-tpp = 5,10,15,20-tetra(4-(trifluoromethyl)phenyl)porphyrin dianion). The oxygenation of *cis*-cyclooctene (4 mmol) was carried out with 0.5 µmol of catalyst **22** in 5 mL of oxygen-saturated solution. After 24 h of photolysis with visible light (λ_{max} = 420 nm), *cis*-cyclooctene oxide was obtained as the only identifiable oxidation product (>95% by GC) with ca. 250 turnovers. Cyclohexene, in contrast, is susceptible to allylic oxidation, thus primarily 2-cyclohexen-1-one and 2-cyclohexen-1-ol along with minor formation of epoxide are obtained. The competing formation of allylic products was also observed for bis-iron(III)-μ-oxo porphyrin complexes by Nocera.[43] Activated hydrocarbons including triphenylmethane, diphenylmethane, ethylbenzene, and xanthenes were oxidized to the corresponding alcohols and/or ketones with total TONs ranging from 560 to 2900. The observed photocatalytic oxidation is ascribed to a photodisproportionation mechanism of **22** to afford [(4-CF_3-tpp)(Ru(III)OH] (**23**) and ruthenium(V)-oxo species [(4-CF_3-tpp)(Ru(V)OH] (**24**), whereas the latter species oxygenates the substrate and is reduced to **23** (Scheme 14).[54] In the presence of dioxygen, **22** is regenerated from two equivalents of **23**.

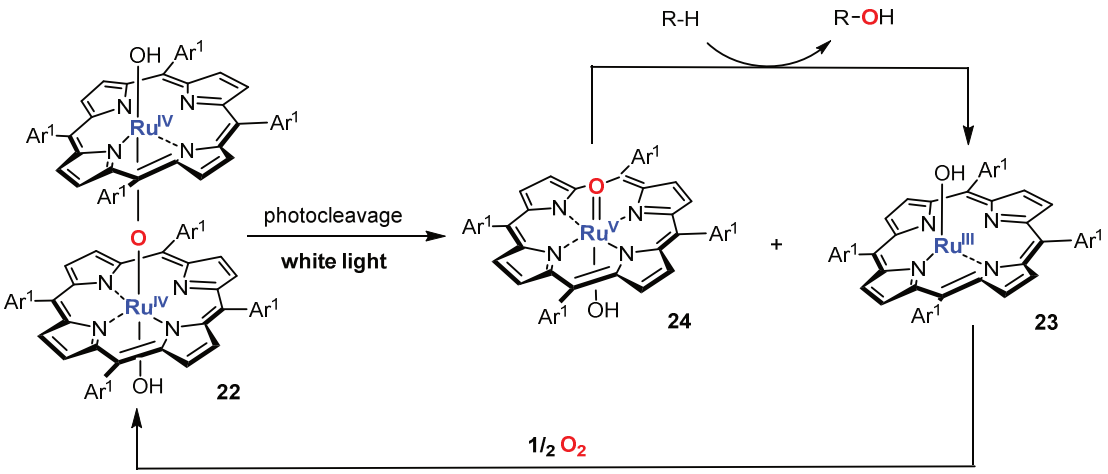

Scheme 14. Photocatalytic Aerobic Oxidation by the bis-ruthenium(IV)-μ-oxo porphyrin complex **22**; (Ar^1 = 4-(trifluoromethyl)phenyl).

1.1.4 Antimony

The group of Hida extensively investigated the photochemical properties of high-valent metalloporphyrins such as Sb(V), P(V), Ge(IV) and Sn(IV) tetraphenylporphyrins in the presence of various kinds of electron donors. The photooxygenation of cyclohexene to 2-cyclohexen-1-one was achieved with antimony(V)tetraphenylporphyrin, [(tpp)Sb(V)$(OH)_2$]Br (**25**, [(tpp)Sb(V)]) in the presence of the additives methylviologen (MV^{2+}, 1,1'-Dimethyl-4,4'-bipyridinium dichloride) and triphenylphosphine (PPh_3) in aqueous solution (Scheme 15). [55][56] The reaction is performed under anaerobic conditions; the source of the oxygen atom is water. Photoexcitation of **25** with visible light (λ_{max} = 420 nm) leads to the formation of the triplet excited state of **25** (Scheme 16,step *i*), which is effectively quenched by the sacrificial electron donor PPh_3 (step *ii*). This electron transfer generates [($tpp^{\bullet-}$)Sb(V)] and $PPh_3^{\bullet+}$. In the presence of one equivalent of the electron acceptor MV^{2+} and cyclohexene, $PPh_3^{\bullet+}$ is supposed to form

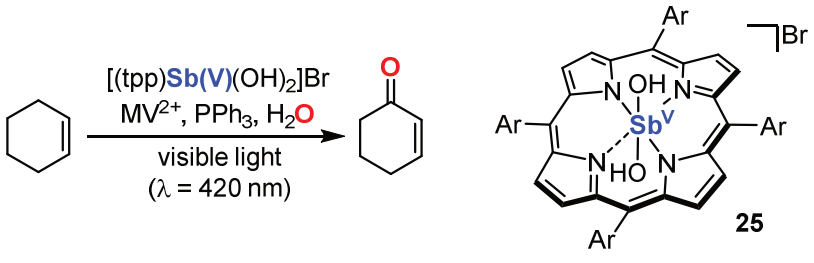

Scheme 15. Photooxygenation of cyclohexene to 2-cyclohexen-1-one in the presence of PPh_3, MV^{2+} and the photocatalyst **25**, Ar = phenyl.

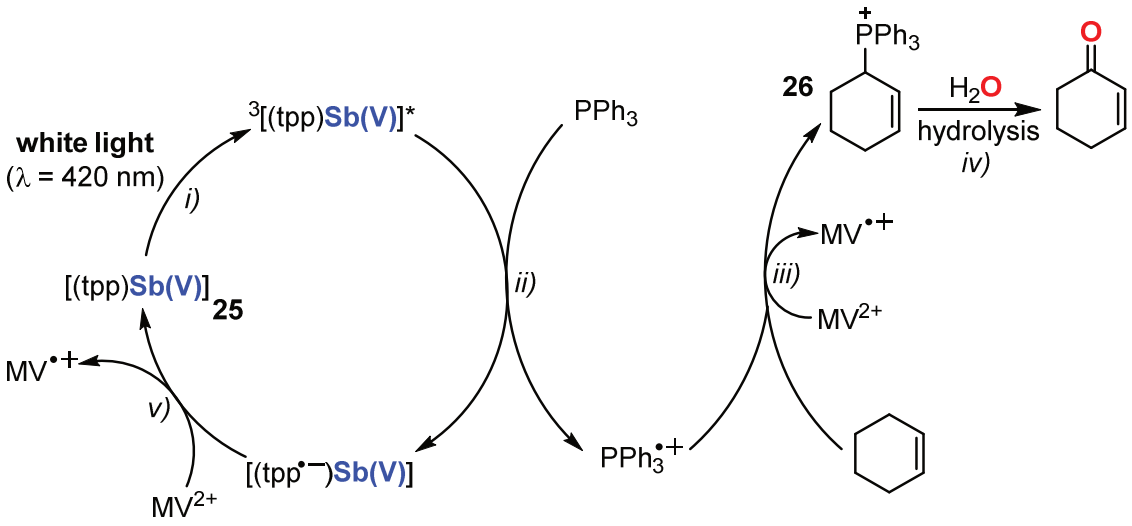

Scheme 16. Proposed mechanism for the photooxygenation of cyclohexene to 2-cyclohexen-1-one catalyzed by **25** in the presence of PPh_3 and MV^{2+}.

the adduct (2-cyclohexen-1-yl)triphenylphosphonium ion (**26**, step *iii*), which is subsequently hydrolyzed to 2-cyclohexen-1-one (step *iv*). The photocatalyst **25** is regenerated by oxidative quenching of [(tpp$^{\bullet-}$)Sb(V)] by MV^{2+} (step *v*).

Very interestingly, the substitution of PPH_3 by KOH in MeCN/water (95/5) under otherwise identical conditions yielded epoxides instead of cyclohexanone, nevertheless the efficiency of this oxygenation reaction was only modest. [57,58] The sacrificial electron acceptor $K_2Pt(IV)Cl_6$ was observed to be a more efficient regeneration agent for the photosensitizer **25** than MV^{2+}. Therefore, Inoue used [(tpp)Sb(V)$(OH)_2$]PF_6 (**27**) in the presence of $K_2Pt(IV)Cl_6$ for the oxygenation of cyclohexene and obtained a mixture of products, consisting of 2-cyclohexen-1-ol (34%), 1,2-dichlorocyclohexane (36%), 2-chlorocyclohexanol (20%), cyclohexene oxide (2%), and small amounts of 3,3'-bicyclohexenyl, 3-acetaminocyclohexene, and cyclohexanone.[59] The formation of chlorinated products (1,2-dichlorocyclohexane, 15%) was suppressed by addition of $AgNO_3$ due to precipitation of Cl^- which originate from $K_2Pt(IV)Cl_6$ .Additionally, formation of cyclohexene oxide (6%) and cyclohexanone (34%) was enhanced. The product distribution drastically changes when [(tpp)Sb(V)$(OCH_3)_2$]Br (**28**) was applied as a sensitizer.[60] Under anaerobic conditions mainly 2-cyclohexen-1-ol (TON = 20) and 3,3'-bicyclohexenyl in aqueous MeCN solution are obtained. Excitation of **28** leads to the formation of the excited triplet state (Scheme 17, step *i*), which is effectively quenched by $K_2Pt(IV)Cl_6$, generating the radical cation of **28** (step *ii*). In the presence of a reductant such as cyclohexene, **28** is regenerated under concomitant formation of the cyclohexene cation radical (step *iii*). The formation of 2-cyclohexen-1-ol can be plausibly explained by

the nucleophilic attack of water on the cyclohexene cation radical and the following oxidation (step *iv*), whereas 3,3'-bicyclohexenyl is formed *via* dimerization of cyclohexene cation radicals (step *v*).

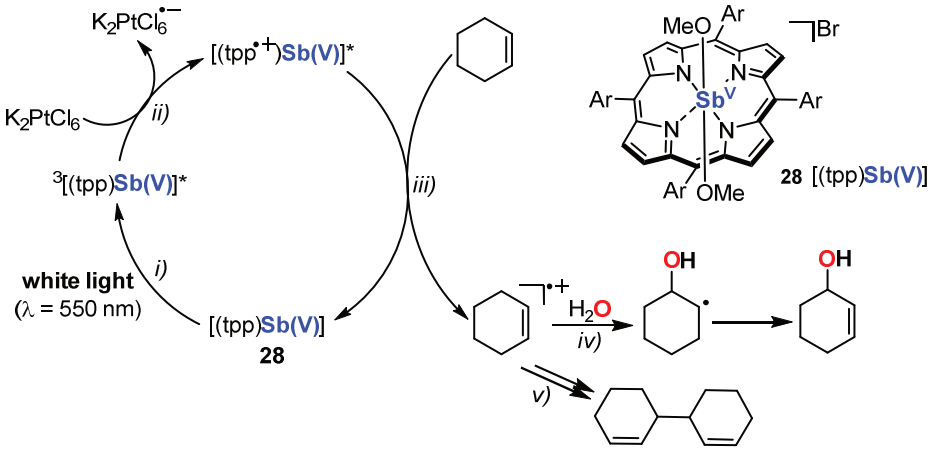

Scheme 17. Photooxygenation of cyclohexene to 2-cyclohexen-1-ol and 3,3'-bicyclohexenyl in the presence of the catalyst **28** and the sacrificial electron acceptor $K_2Pt(IV)Cl_6$.

1.1.5 Summary

In summary, the development of artificial iron porphyrin complexes inspired by cytochrome P450 for the aerobic oxidation of hydrocarbons led to various insights into the reactivity of iron-oxo species over the last 30 years. In the beginning, Fe(III) porphyrin halides seemed to serve as simple radical chain initiators for autoxidative processes, but further modification of the porphyrin moiety gave access to catalysts which stabilize distinct high-valent iron-oxo species. Unfortunately, these complexes only gave access to [(porph)Fe(IV)(O)] or (porph$^{\bullet+}$)Fe(IV)(O) which exhibit low reactivity for hydrocarbon oxygenation, although the latter species is assumed to be the predominant oxidant in cytochrome P450. Additionally, in the absence of the protective enzyme environment, these catalysts are prone to oxidative degradation which limits the use of iron porphyrins as practical photocatalysts. Nocera *et al*. significantly improved the catalytic efficiency by employing a bis-iron(III)-μ-oxo porphyrin complex with an organic spacer which serves to preorganize two iron centers in a cofacial arrangement. Laser flash photolysis experiments indicate that an iron(V)-oxo species is in principle accessible by visible light irradiation of artificially designed iron(III) porphyrin or iron(IV) corrole complexes, but these systems are not fully understood yet and their practical application in preparative synthesis is still limited. Furthermore, Mn(III) porphyrin and Mn(III) corrolazine complexes are capable of catalyzing the visible-light-driven oxygenation of weak C−H bonds. The formation of a distinct Mn(V)-oxo species was selectively achieved *via* a solvent initiated radical process or in the presence of other hydrogen atom donors such as

toluene derivatives in inherent solvents. Unfortunately the obtained Mn(V)-oxo species exhibits a surprising stability towards hydrocarbons with strong C−H bonds, therefore the oxygenation of benzylic substrates such as hexamethylbenzene is strictly limited to stoichiometric reactions unless the exact quantity of a strong hydrogen donor is added.

Both the iron and manganese porphyrin/porphyrinoid systems mainly rely on the reductive activation of dioxygen inspired by cytochrome P450 or other heme/non-heme enzymes, whereas Ru and Sb porphyrin complexes mainly oxidize water in a process inspired by Photosystem II. For example, ruthenium porphyrin complexes, such as [(tmp)Ru(II)(CO)], are suitable catalysts for the oxygenation of alkenes. In contrast to other metal porphyrin catalysts, no high-valent ruthenium-oxo species is involved for a selective oxygenation reaction and water acts as oxygen source. Additionally, bis-ruthenium(IV)-μ-oxo porphyrin complexes are suitable for the oxygenation of alkenes and activated hydrocarbons and are quite related in reactivity to Nocera's bis-iron(III)-μ-oxo porphyrin pacman system. Next to Fe, Mn, and Ru, high-valent metalloporphyrins such as Sb(V), P(V), Ge(IV) and Sn(IV) tetraphenylporphyrins are able to oxygenate various substrates. Hida showed that [(tpp)Sb(V)$(OMe)_2$]Br performs the selective photooxygenation of cyclohexene to 2-cyclohexen-1-ol in the presence of a sacrificial electron acceptor K_2Pt(IV)Cl_6 with water as oxygen source. Nevertheless, these antimonyporphyrin complexes have to be prepared from a Sb(III) precursor with strong oxidants (such as bromine) first, and often need an excess of sacrificial electron acceptors. Thus, the main progress of the last years was achieved in the reductive activation of dioxygen by iron and manganese complexes.

1.2 Tris(2,2'-bipyridine)ruthenium(II) ([Ru(bpy)$_3$]$^{2+}$) and Derivatives

Burstall and co-workers reported salts of [Ru(bpy)$_3$]$^{2+}$ (bpy = 2,2'-bipyridine) for the first time in 1936.[61] This complex absorbs visible light at 452 nm, is chemically robust and an excited triplet state ^{3}[Ru(bpy)$_3$]$^{2+}$* (lifetime 890 ns in CH_3CN), which is sufficiently long-lived to compete with deactivation processes and perform electron transfer reactions to engage organic transformations.[14,15,62] The photoexcited complex acts a single electron oxidant in the presence of reductive quenchers (NEt_3, DIPEA, EDTA, ascorbate, etc.), yielding the strong reductant [Ru(bpy)$_3$]$^+$ (–1.33 V *vs* SCE in CH_3CN), whereas the strong oxidant [Ru(bpy)$_3$]$^{3+}$ (+1.29 V *vs* SCE in CH_3CN) is formed in the presence of oxidative quenchers (Ar-N_2^+, Ar-NO_2 viologens, etc.). Depending on the choice of the sacrificial substrate, the [Ru(bpy)$_3$]$^{2+}$ catalyst is capable to trigger single electron photoreduction or photooxidation processes, respectively.[13]

After its discovery, [Ru(bpy)$_3$]$^{2+}$ was only rarely used as a photocatalyst for organic synthesis. Starting from 1987 until the first decade of the 21th century, [Ru(bpy)$_3$]$^{2+}$ mainly catalyzed photoreduction reactions.[13] Since 2008, reports by Yoon[63], MacMillan[64] and Stephenson[65] remarkably accelerated the development of this transition metal compound as a potent photocatalyst to achieve unique bond formations not feasible with established protocols. The photoredox chemistry of [Ru(bpy)$_3$]$^{2+}$ was reviewed very recently.[66] Here, we would like to highlight the few examples where [Ru(bpy)$_3$]$^{2+}$ or a derivative is used as photooxygenation catalysts.

In 2003, Zen and co-workers reported the first photocatalytic system for the selective oxygenation of sulfides to sulfoxides by dioxygen on a novel heterogeneous multicomponent nafion membrane containing a lead ruthenate pyrochlore catalyst (Pyc) and a [Ru(bpy)$_3$]$^{2+}$ photosensitizer.[67] In 2011, the group of Jiao *et al.* disclosed a novel, efficient photooxidation of α-aryl halogen derivatives to the corresponding α-aryl carbonyl compounds at room temperature (Scheme 18).[68]

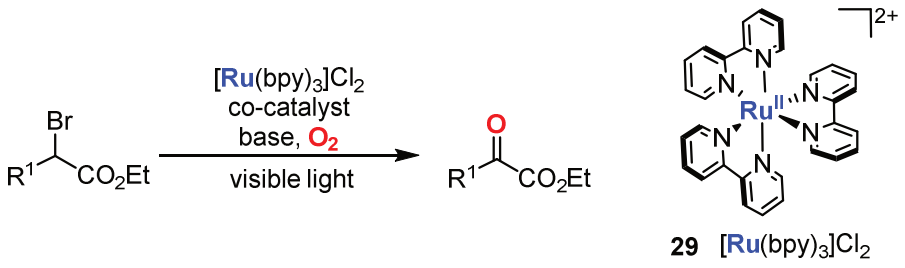

Scheme 18. Photocatalytic oxygenation of α-aryl halogen derivatives with [Ru(bpy)$_3$]$^{2+}$.

The reaction is efficiently catalyzed by [Ru(bpy)$_3$]Cl_2 (**29**) and co-catalyst 4-methoxypyridine (**30**) in the presence of a base under aerobic conditions. The oxygenation

of various α-haloarylacetic esters to their corresponding α-aryl carbonyl compounds proceeds in good to excellent yields while both chloride and bromide are tolerated as leaving groups. Also 1,2-diphenylethane-1,2-dione (benzil) derivatives are accessible in good to excellent yields, whereas 9-flourenone and benzophenone derivatives are only obtained in moderate yields. Extensive studies and control experiments led to the proposed mechanism depicted in Scheme 19. As initial step, the co-catalyst **30** forms a pyridinium salt with the α-aryl halogen compound (step *i*). In the presence of air and a base an unknown radical intermediate is generated (step *ii*), which is supposed to act as a reductive quencher for photoexcited **29*** generating the $[Ru(bpy)_3]^+$ (step *iii*). This reduced Ru(I) species triggers the single electron transfer from $[Ru(bpy)_3]^+$ to another equivalent of pyridinium salt, yielding the dihydropyridyl radical (step *iv*), which generates the benzyl radical *via* C–N bond homolysis (step *v*). The benzyl radical is trapped by dioxygen (step *vi*), and the desired product is obtained *via* an alkoxyl radical intermediate under concomitant formation of superoxide radical anions $O_2^{\bullet-}$ (step *vii*).

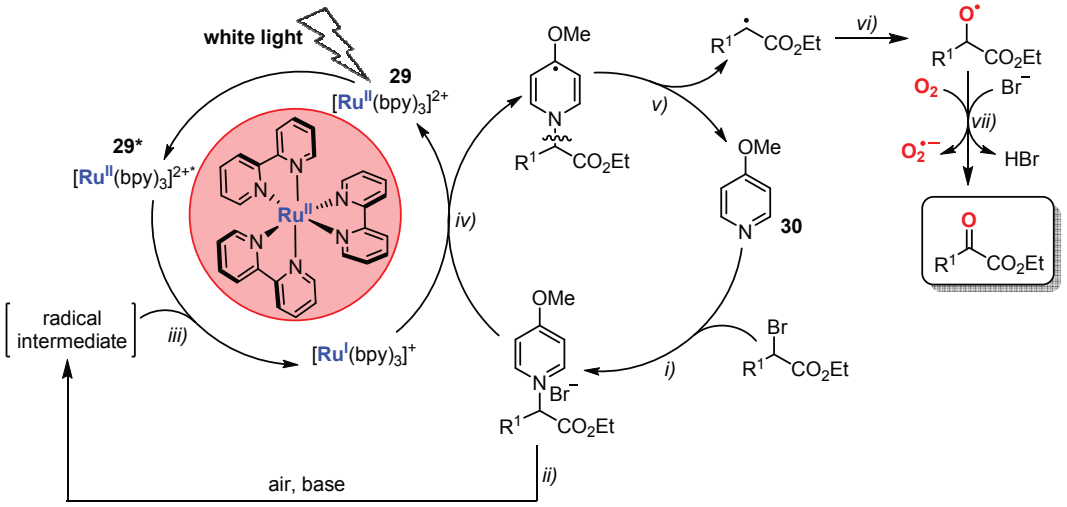

Scheme 19. Proposed mechanism for the photooxygenation of α-aryl halogen derivatives with $[Ru(bpy)_3]^{2+}$.

Xiao *et al.* reported the visible-light-driven hydroxylation of arylboronic acids to aryl alcohols. This reaction is effectively mediated by $[Ru(bpy)_3]^{2+}$ in the presence of the reductive quencher DIPEA (*N*,*N*-Diisopropylethylamine) in air (Scheme 20).[69]

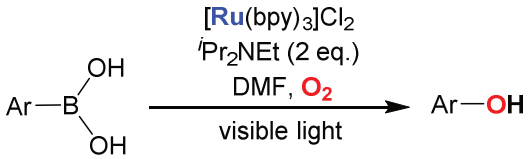

Scheme 20. Visible-light-driven hydroxylation of arylboronic acids by **29**.

A wide range of arylboronic acids bearing electron-neutral, electron-donating, and electron withdrawing substituents were smoothly oxidized to the corresponding aryl alcohols in good to excellent yields. Electron-rich phenols, which are difficult to obtain by traditional methods, are easily accessible with this photocatalytic method. Computational and experimental investigations gave insight into the reaction mechanism as shown in Scheme 21. The reductive quenching of $[Ru(bpy)_3]^{2+*}$ by the tertiary alkylamine yields $[Ru(bpy)_3]^{+}$ (step *i*). In the presence of air the chromophore **29** is regenerated and $O_2^{\bullet-}$ is formed (step *ii*), a Lewis base which readily reacts with the Lewis acidic boron atom to generate the intermediate **31** (step *iii*). The radical anion **31** abstracts a hydrogen atom from the alkyl ammonium radial cation $NEt_3^{\bullet+}$ to form intermediate **32** (step *iv*). The formation of the hydroxylated product occurs by rearrangement of **32** into **33** (step *v*) with subsequent hydrolysis.

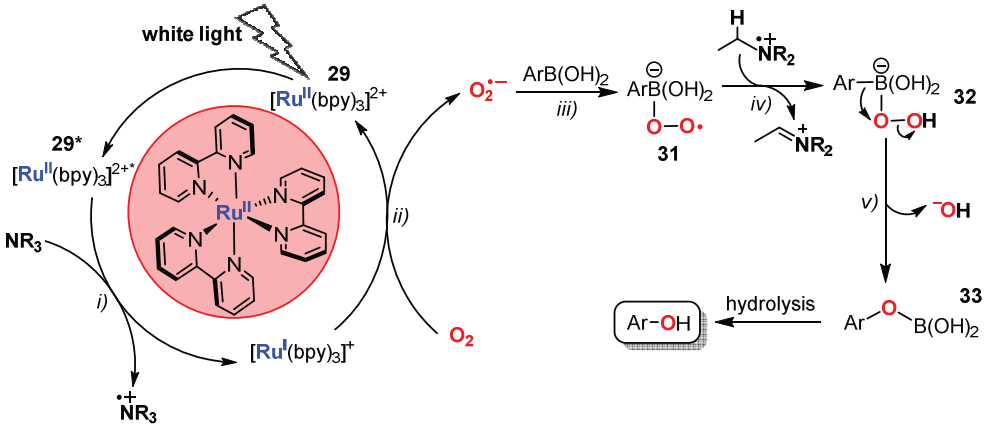

Scheme 21. Proposed mechanism for the photooxygenation of arylboronic acids by **29**.

Structurally novel endoperoxides are synthesized by the photocatalytic cyclization of bis(styrene) substrates with molecular oxygen reported by Yoon *et al.*.[70] The most effective catalyst for this transformation is $[Ru(bpz)_3]^{2+}$ (**34**, bpz = 2,2'-bipyrazin), which exhibits a higher reduction potential (+1.4 V *vs* SCE) compared to $[Ru(bpy)_3]^{2+}$ (+0.8 V *vs* SCE) in its excited state due to the more electron-deficient ligand. Thus, the electron transfer from bis(styrene) derivatives **35** (+1.1 V *vs* SCE) to $[Ru(bpz)_3]^{2+*}$ becomes feasible, generating the reduced $[Ru(bpz)_3]^{+}$ species and the radical cation **36** as displayed in Scheme 22 (step *i*). **36** readily reacts with triplet oxygen in a [2+2+2] cycloaddition, which yields a six-membered radical cation **37** (step *ii*). This intermediate **37** is supposed to be reduced to the desired endoperoxide **38** by $[Ru(bpz)_3]^{+}$ regenerating **34**. It is noteworthy, that these endoperoxides are not accessible in a singlet oxygen pathway, since no product formation is observed with the well-known $^1O_2$ photosensitizer tetraphenylporphyrin (tpp). Interestingly, 9,10-dicyanoantracene (DCA), which is the common photocatalyst for aerobic [2+2+2] cycloadditions, is not successful. This is attributed to the fact that DCA sensitizes the formation of superoxide radical anions $O_2^{\bullet-}$.

The scope of Yoon's methodology is quite extensive, mainly due to the absence of $O_2^{\bullet-}$ formation by $[Ru(bpz)_3]^{2+}$. The endoperoxides are believed to be promising inhibitors of cancer cell growth as shown by their biological activity profiles.

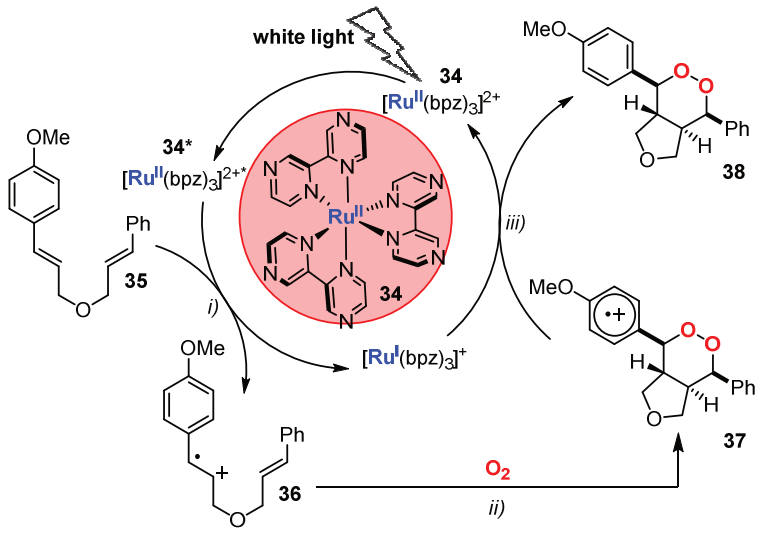

Scheme 22. Proposed mechanism for the aerobic [2+2+2] cycloadditions of bis(styrene) derivative **35** to **38** catalyzed by the chromophore **34**.

In summary, next to their application as photoreduction catalysts and catalysts for the formation of unique bonds, $[Ru(bpy)_3]^{2+}$ and $[Ru(bpz)_3]^{2+}$ are also potent oxygenation catalysts. Jiao *et al.* reported the photooxidation of α-aryl halogen derivatives to the corresponding α-aryl carbonyl compound, whereas Xiao *et al.* disclosed a powerful protocol for the visible-light-driven hydroxylation of arylboronic acids to aryl alcohols. Additionally, structurally novel endoperoxides, which are not feasible with singlet oxygen, are now accessible by the photocatalytic cyclization of bis(styrene) substrates with molecular oxygen in the presence of the strong oxidant $[Ru(bpz)_3]^{2+}$ as shown by Yoon *et al.*.[70]

1.3 Organic dyes

1.3.1 Eosin Y (EY)

Eosin Y (EY), a long known dye molecule, is used in many applications, i.e. a pH indicator, for cell staining[71] and halide determination by Fajans[72], and very recently as photocatalyst in organic synthesis.[73–76] The photochemical properties are very well investigated[77,78] and the dye found application as a cheap and non-toxic alternative to expensive transition metal catalysts.[73] Eosin Y effectively absorbs green light (λ_{max} = 539 nm, ε ~ 60000 M^{-1} cm^{-1}) and after excitation, a rapid intersystem crossing to the lowest triplet state ^{3}EY* (lifetime of 24 µs) occurs, which is the key intermediate in electron transfer processes mediated by EY. Next to its ability to trigger electron transfer processes, EY is known to promote energy transfer.[79] The synthetic application of EY in photoredox chemistry has recently been reviewed[80], mainly focusing on reduction and oxidation reactions, as well as arylation, trifluormethylation, and cooperative processes. Complementary to this review, we highlight the recent applications of EY as a photocatalyst for oxygenation reactions.

Xiao *et al.* reported the visible-light-driven hydroxylation of arylboronic acids to aryl alcohols, which is effectively mediated by the transition metal photocatalyst $[Ru(bpy)_3]^{2+}$ under aerobic conditions (*vide supra*).[69] In a single example, $[Ru(bpy)_3]^{2+}$ was successfully substituted by Eosin Y (**39**, Scheme 23).[69] Irradiation of a mixture containing 4-methoxyphenylboronic acid, Eosin Y (2 mol%) and two equivalents of the sacrificial electron donor *N*,*N*-Diisopropylethylamine (DIPEA) gave 4-methoxyphenol in 90% yield after 96 hours under aerobic conditions. The excitation of Eosin Y in the presence of DIPEA leads to an electron transfer from DIPEA to the dye molecule, yielding $DIPEA^{\bullet+}$ and $EY^{\bullet-}$. The regeneration of the catalyst is easily achieved by dioxygen generating the superoxide radical anion $O_2^{\bullet-}$, which readily reacts with 4-methoxyphenylboronic acid. The desired product is obtained after a series of rearrangements and hydrolysis similar to those reported by Xiao (see Scheme 21).[69]

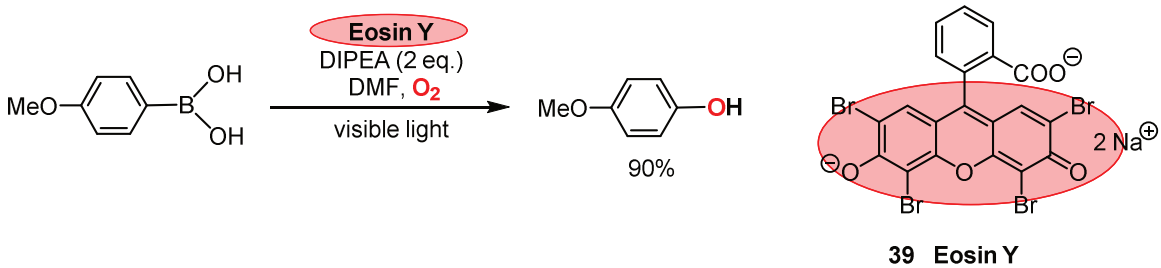

39 **Eosin Y**

Scheme 23. Hydroxylation of 4-methoxyphenylboronic acid *via* visible light catalysis using **39**.

Sun and co-workers reported the visible-light-driven aerobic transformation of arylmethyl bromides to the corresponding benzyl alcohols and aldehydes by EY in DMSO (Scheme 24).[81] The reaction temperature is crucial, since the benzyl alcohol is the main product at room temperature, whereas the formation of the benzaldehyde is favored at elevated temperatures. Control experiments confirmed the decisive role of dioxygen, but unfortunately no further mechanistic studies were performed.

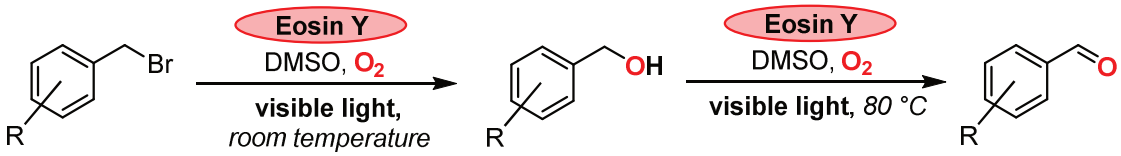

Scheme 24. Aerobic photooxygenation of arylmethyl bromides to benzyl alcohols and benzaldehydes catalyzed by **39**.

Yadav and co-workers reported the desulfurization of thioamides to amides, which is effectively catalyzed by EY in air (Scheme 25).[82] Irradiation of EY (green LEDs, step *i*) leads to a single electron transfer from the thioamide to EY*, yielding $EY^{\bullet-}$ and thioamid radical cation (step *ii*). The chromophore is easily regenerated by atmospheric dioxygen, yielding the superoxide radical anion $O_2^{\bullet-}$ (step *iii*), which is suggested to react with the thioamid radical cation (step *iv*). This intermediate converts to the desired amide with concomitant formation of elemental sulfur (step *v*). Control experiments additionally confirmed that a singlet oxygen pathway is not relevant, since the reaction is not improved under a neat dioxygen atmosphere and no influence on the yield is observed in the presence of an effective singlet oxygen quencher. The desulfurization of various secondary and tertiary thioamides was achieved and a wide range of functional groups was tolerated.

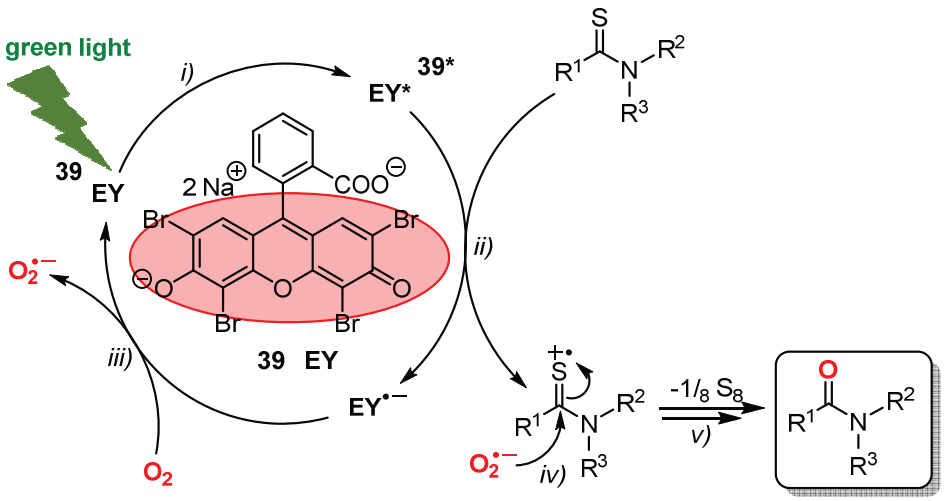

Scheme 25. Proposed mechanism for the desulfurization of thioamides to amides by **39**.

1.3.2 Methylene Blue (MB^+)

Methylene Blue (MB^+) is a member of the thiazine dye family which exhibits a maximum absorption at ~670 nm. This dye is extensively used as test reagent for the visible-light-driven degradation of organic molecules catalyzed by heterogeneous TiO_2 catalysts.[83,84] Nevertheless, the photoredox catalysis of MB^+ under homogeneous conditions is little explored.[85] Seeking to develop a transition-metal-free catalyst system, Sciano and co-workers substituted $[Ru(bpy)_3]^{2+}$ (**29**) by MB^+ (**40**) in the oxidative hydroxylation of arylboronic acids reported by Xiao *et al.* (Scheme 26).[86] A key observation of this work was that $^3MB^{+}$* was more efficient than **29*** under otherwise identical conditions, although the substrate scope is by far not as extensive as in Xiao's study. The improved efficiency is due to an effective quenching of the excited triplet state $^3MB^{+}$* by the sacrificial electron donor (DIPEA), generating the reduced form of methylene blue $MB^{\bullet}$ and $DIPEA^{\bullet+}$ in a single electron transfer process. In the presence of dioxygen, $MB^{\bullet}$ acts as an electron donor and regenerates the chromophore with concomitant formation of $O_2^{\bullet-}$, which subsequently generated the desired phenol (see Scheme 21). This procedure impressively shows that a cheap organic dye is a promising alternative to an expensive and potentially toxic transition metal catalyst.

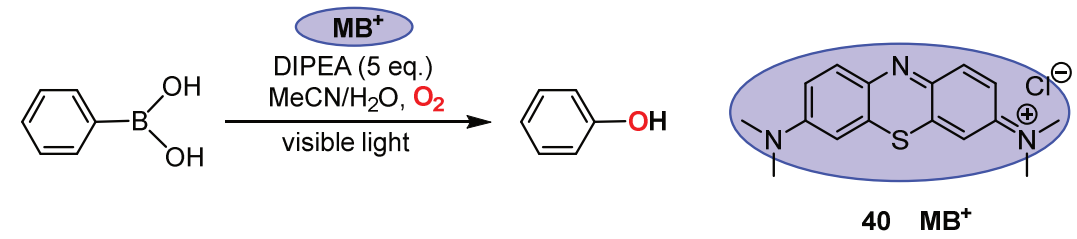

Scheme 26. Photooxidative hydroxylation of arylboronic acids with **40**.

1.3.3 2,3-Dichloro-5,6-dicyano-*p*-benzoquinone (DDQ)

2,3-Dichloro-5,6-dicyano-*p*-benzoquinone (DDQ, **41**) is a well-known and powerful organic oxidizing reagent for a number of organic transformations. Recently, DDQ has recently drawn attention as a potent photocatalyst.[87] DDQ absorbs light in the visible region (λ_{max} = 470 nm in CH_2Cl_2). Photoexcited DDQ spontaneously relaxes into the long-lived n−π* triplet excited state ^{3}DDQ* by intersystem crossing.[88] The reduction potential of ^{3}DDQ* (E_{red} = 3.18 V *vs* SCE)[88] is significantly higher than of the ground state ^{1}DDQ (E_{red} = 0.51 V *vs* SCE)[89], thus the oxidation of challenging substrates such as benzene with a high oxidation peak potential (E_0^p = 2.48 *vs*. SCE) becomes feasible. Fukuzumi *et al.* demonstrated that the photooxidation of benzene readily occurs with stoichiometric quantities of DDQ in water to yield phenol under anaerobic conditions (Scheme 27).[90]

The oxidation of benzene with water as the oxygen source yields the reduced chromophore 2,3-dichloro-5,6-dicyanohydroquinone (**42**, $DDQH_2$).

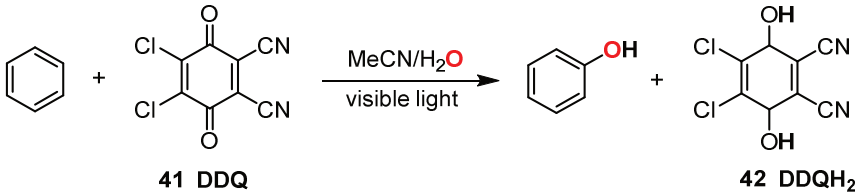

Scheme 27. Stoichiometric oxygenation of benzene to phenol by **41**.

Tert-butyl nitrite (TBN)[91] as an appropriate sacrificial oxidant for the regeneration of DDQ from $DDQH_2$ under aerobic conditions enabled a photocatalytic protocol. The reaction mechanism is depicted in Scheme 28.

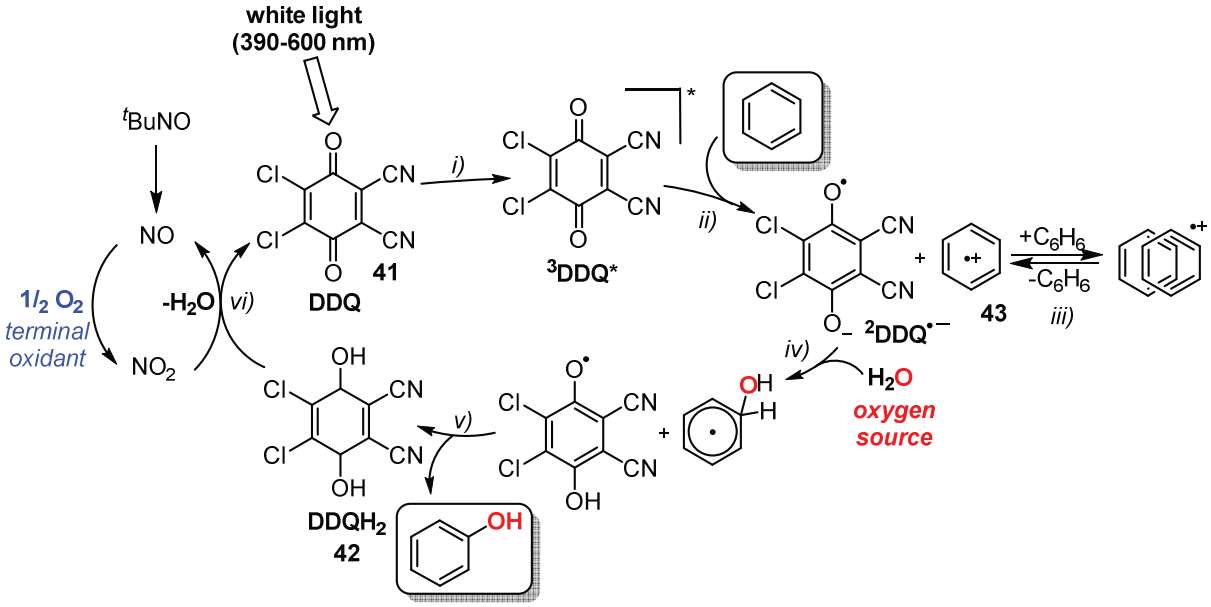

Scheme 28. Proposed mechanism for the photooxygenation of benzene to phenol with water as oxygen source and dioxygen as terminal oxidant catalyzed by **41**.

The excitation of **41** with visible light generates ^{3}DDQ* (step *i*). The electron transfer between ^{3}DDQ* and benzene proceeds very effectively (step *ii*), because the free energy change is largely negative (ΔG_{ET} = -0.7 eV). This electron transfer yields the reduced radical anion $^2DDQ^{\bullet-}$ and the benzene radical cation (**43**) which is equilibrium with a π-dimer radical cation formed between **43** and another equivalent of benzene (step *iii*). **43** (or the dimer) is supposed to react with water to yield the OH-adduct radical (step i*v*), which subsequently yields phenol and $DDQH_2$ after hydrogen abstraction (step *v*). The regeneration of DDQ is effectively carried out by dioxygen as terminal oxygen *via* NO_2 generated from TBN (step *vi*). It is noteworthy, that no overoxidation of phenol is observed, although this oxidation is much easier than the oxidation of benzene. The back electron transfer from $^2DDQ^{\bullet-}$ to the initially formed phenol radical cation is much faster

as compared to the back electron transfer from $^2DDQ^{\bullet-}$ to the benzene radical cation. Thus the back electron transfer event is too fast to compete with an effective dissociation of $^2DDQ^{\bullet-}$ and the phenol radical cation and no further transformation occurs.[90]

1.3.4 3-Cyano-1-methylquinolinium ion ($QuCN^+$)

The 3-cyano-1-methylquinolinium ion (**44**, $QuCN^+$) also acts as an efficient organic photocatalyst for the aerobic selective hydroxylation of benzene.[92] In contrast to DDQ where the triplet state is strongly oxidizing, the reactive species is the singlet excited state $^1QuCN^{+}$* (E_{red} *vs*. SCE = 2.72 V). Additionally, dioxygen directly regenerates $QuCN^+$ under concomitant formation of hydrogen peroxide and no sacrificial oxidant (such as TBN) is needed as mediator (Scheme 29).

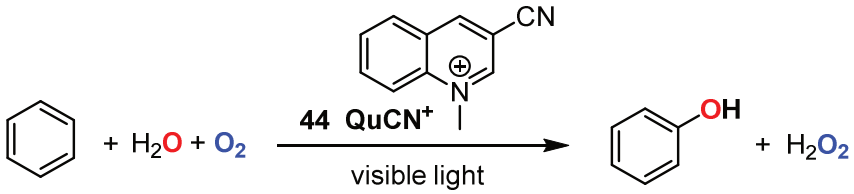

Scheme 29. Photocatalytic oxygenation of benzene to phenol by **44**.

In the initial step, the electron transfer between $^1QuCN^{+}$* and benzene yields $^2QuCN^{\bullet}$ (step *i*) and the benzene radical cation and/or π-dimer radical cation (step *ii*, Scheme 30). In the presence of water the OH-adduct radical is generated similar to the DDQ/benzene system (step *iii*, see Scheme 28). $^2QuCN^{\bullet}$ reduces O_2 to $HO_2^{\bullet}$ (step *iv*), which is supposed to abstract a hydrogen atom from the OH-radical cation to yield phenol with concomitant generation of H_2O_2 (step *v*).

Use of 3-phenyl-1-propanol instead of benzene gave chromans under otherwise identical conditions.[93] In a subsequent study, the substitution of water by various alcohols yielded alkoxybenzenes, which are valuable precursors to pharmaceutics and perfumes.[94]

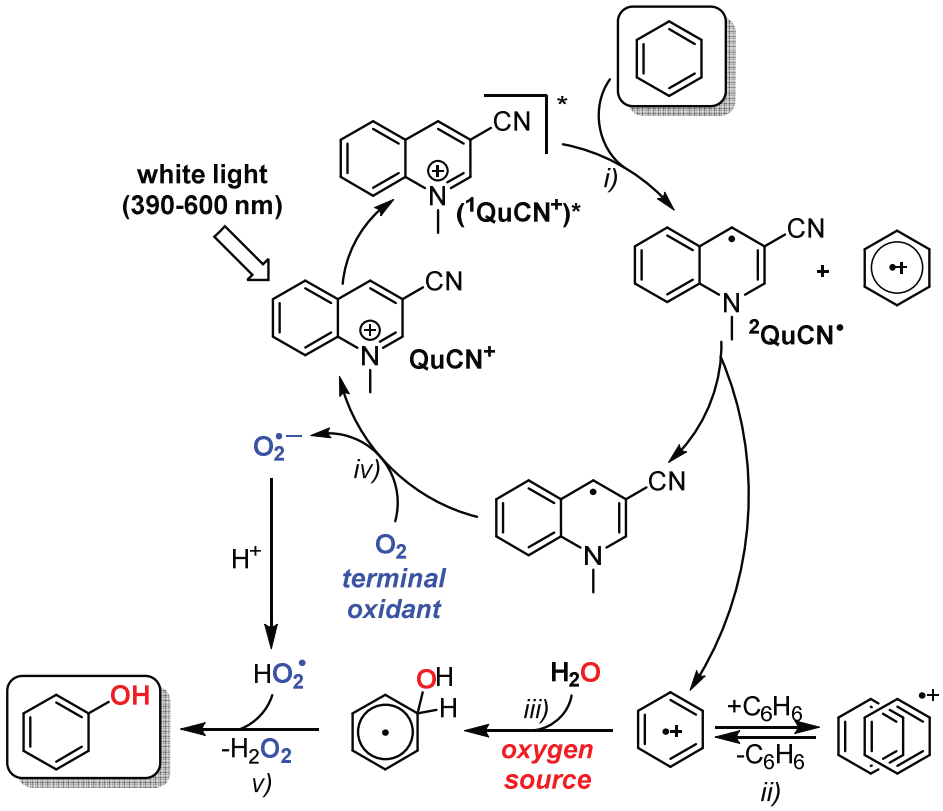

Scheme 30. Proposed mechanism for the photocatalytic oxygenation of benzene by **44**.

1.3.5 Acridinium ions (Acr⁺-R, R = H, Ph or Mes)

Fukuzumi and co-workers synthesized the electron donor-acceptor linked molecule 9-mesityl-10-methylacridinium ion (**45**, Acr⁺-Mes, Scheme 31)[95], which was extensively used in several organic transformations such as arene bromination[96], cycloaddition reactions[97] and for the selective formation of products with anti-Markovnikov selectivity.[98–100] This catalyst absorbs blue light ($\lambda > 450$ nm) and exhibits excellent oxidizing capabilities in its excited state ($E_{red} = 2.06$ V *vs* SCE in MeCN). The X-ray crystal structure revealed that the mesityl group is orientated nearly perpendicular to the acridinium moiety, which supports the formation of a long-lived charge-shift state Acr•-Mes•⁺ after excitation (lifetime = 2 h at 203 K).[95] The combination of fast charge separation but slow charge recombination connected with its high reduction potential makes Acr⁺-Mes an efficient electron-transfer photocatalyst for the selective oxygenation of challenging substrates as shown in this chapter.[101,102] Some derivatives of Acr⁺-Mes such as the 10-methylacridinium ion (**46**, Acr⁺-H) and 10-methyl-9-phenylacridinium (**47**, Acr⁺-Ph) have also been used for various oxygenation reactions, whereas their reaction pattern and substrate scope significantly differs from Acr⁺-Mes. These differences will also be illustrated in this chapter.

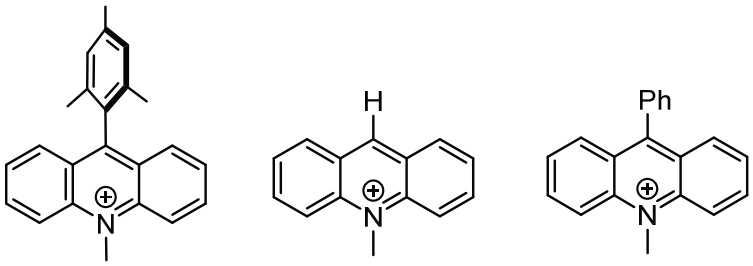

45 Acr^+-Mes **46** Acr^+-H **47** Acr^+-Ph

Scheme 31. Acridinium derived catalysts.

Photocatalytic oxygenation of toluene derivatives

The photocatalytic oxygenation of toluene derivatives as model substrates in the presence of acridinium ions as photocatalysts has been extensively studied by Fukuzumi *et al.*.Visible light irradiation of the absorption band (λ_{max} = 358 and 417 nm) of Acr^+-H in oxygen-saturated acetonitrile containing *p*-xylene with white light results in formation of *p*-tolualdehyde in a moderate yield (37%) after 24 h.[103] The product yield is improved to 66%, when acetonitrile is replaced by the less polar solvent chloroform under otherwise identical experimental conditions. The photooxygenated product yield is further improved to 100% when Acr^+-H is replaced by Acr^+-Ph in chloroform (Scheme 32).[104]

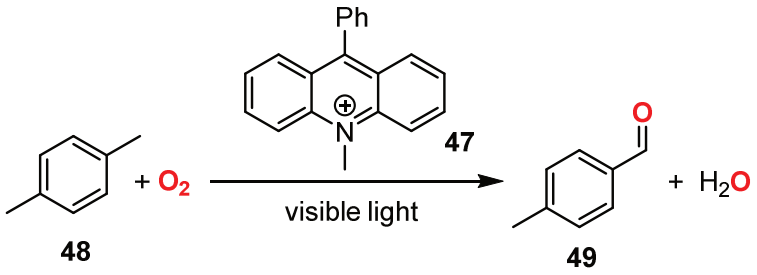

Scheme 32. Photooxygenation of *p*-xylene by the acridinium derivative Acr^+-Ph (**47**).

The reaction mechanism for the Acr^+-Ph photosensitized oxygenation of *p*-xylene is depicted in Scheme 33. Fluorescence emission quenching experiments confirmed that an efficient photoinduced electron transfer from *p*-xylene (**48**) to the excited singlet state $^1Acr^+$-Ph* (step *i*) generates ^{2}Acr-Ph$^\bullet$ and the *p*-xylene radical cation (**48a**, step *ii*), which is in equilibrium with the dimer radical cation (step *iii*). The subsequent deprotonation of **48a** forms the *p*-methylbenzyl radical (**48b**, step *iv*), which is readily trapped by dioxygen to give the corresponding peroxyl radical (**48c**, step *v*). After protonation (step *vi*), the hydroperoxide **48d** selectively transforms to *p*-tolualdehyde **49** (step *vii*).

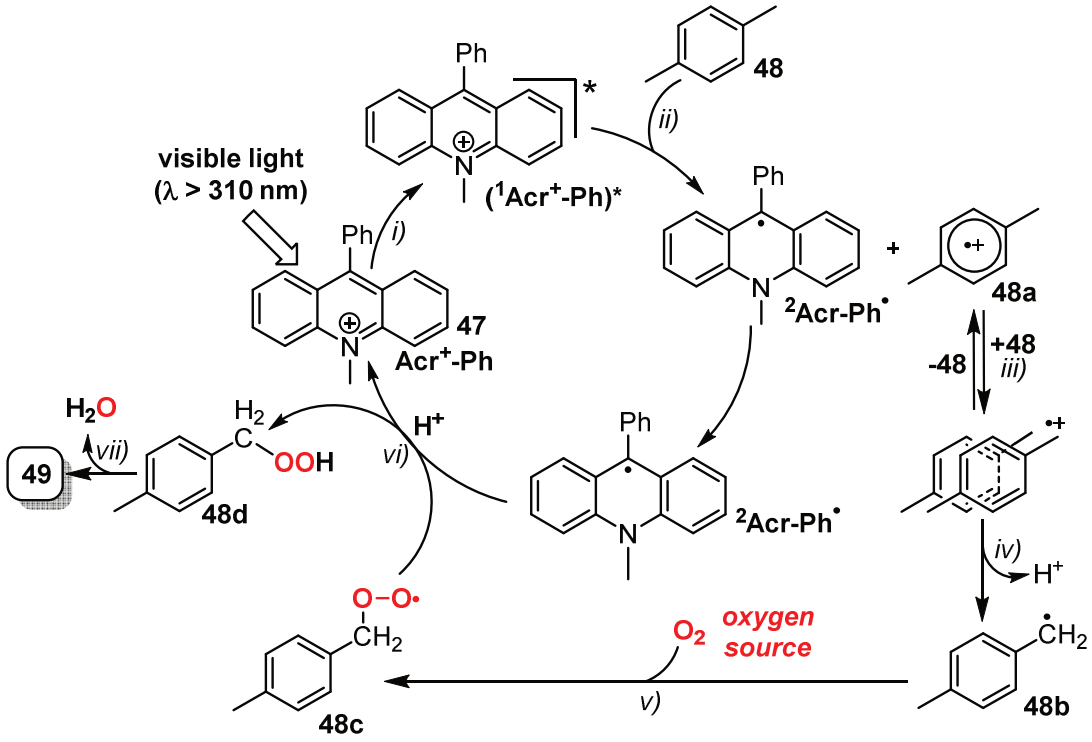

Scheme 33. Proposed mechanism for the photocatalytic oxygenation of p-xylene by **47**.

A better yield is obtained by employing Acr$^+$-Ph instead of Acr$^+$-H. This is presumably ascribed to the energetically more unfavored back electron transfer from ^{2}Acr-Ph$^\bullet$ to **48a** compared to ^{2}Acr-H$^\bullet$. Additionally, Acr$^+$-Ph exhibits a higher durability than Acr$^+$-H. The steric effect of the phenyl group prohibits the radical coupling between AcrR$^\bullet$ and the *p*-methylbenzyl radical, which is a possible decomposition pathway of the catalyst.[104]

For these reasons, Acr$^+$-Ph is mostly preferred compared to Acr$^+$-H as a photocatalyst for various transformations, such as the oxygenation of 4,4'-dimethylbiphenyl[105], α-methylstyrene[106] and pivalic acid (^{t}BuCOOH)[107]. The reaction mechanism for these reactions is comparable to that in Scheme 33.

Ohkuba *et al.* substituted Acr$^+$-Ph (or Acr$^+$-H) by Acr$^+$-Mes in the photocatalytic oxygenation of *p*-xylene (Scheme 34).[108] Visible light irradiation of Acr$^+$-Mes in oxygen-saturated acetonitrile containing *p*-xylene with a xenon lamp attached with a color glass filter (λ = 380–500 nm) for 80 min resulted in formation of *p*-tolualdehyde (34%), *p*-methylbenzyl alcohol (10%) and H_2O_2 (30%). A perfect 100% yield of *p*-tolualdehyde and H_2O_2 was achieved with the slightly modified catalyst 9-mesityl-2,7,10-trimethlyacridinium ion (**50**, Me$_2$Acr$^+$-Mes) bearing two methyl groups at the 2 and 7 position of the acridinium moiety.

Interestingly, the by-product in this oxygenation is hydrogen peroxide and not water as in the case of Acr$^+$-Ph (or Acr$^+$-H). There have been extensive studies on the photocatalytic formation of H_2O_2 or photocatalytic oxygenation of aromatic substrates, but no combined

process has been known so far. The photocatalytic reaction is initiated by an intramolecular electron transfer from the mesitylene group to the Acr^+ moiety of R_2Acr^+-Mes (R = H or Me) which affords the electron transfer state $R_2Acr^{\bullet}$-$Mes^{\bullet+}$as shown in Scheme 34. This is in sharp contrast to Acr^+-Ph, where the electron transfer occurs from the substrate to the singlet state $^1Acr^+$-Ph*. The electron transfer from *p*-xylene to the $Mes^{\bullet+}$ moiety yields $R_2Acr^{\bullet}$-Mes and the *p*-xylene radical cation **48a**, which transforms to the corresponding benzyl alcohol **51** and **49**. The benzyl alcohol **51** is oxidized to **49** in a photocatalytic process as depicted in **Scheme 34**. Dioxygen rapidly reacts with $R_2Acr^{\bullet}$-Mes to regenerate the catalyst, yielding $O_2^{\bullet-}$, which subsequently generates H_2O_2.

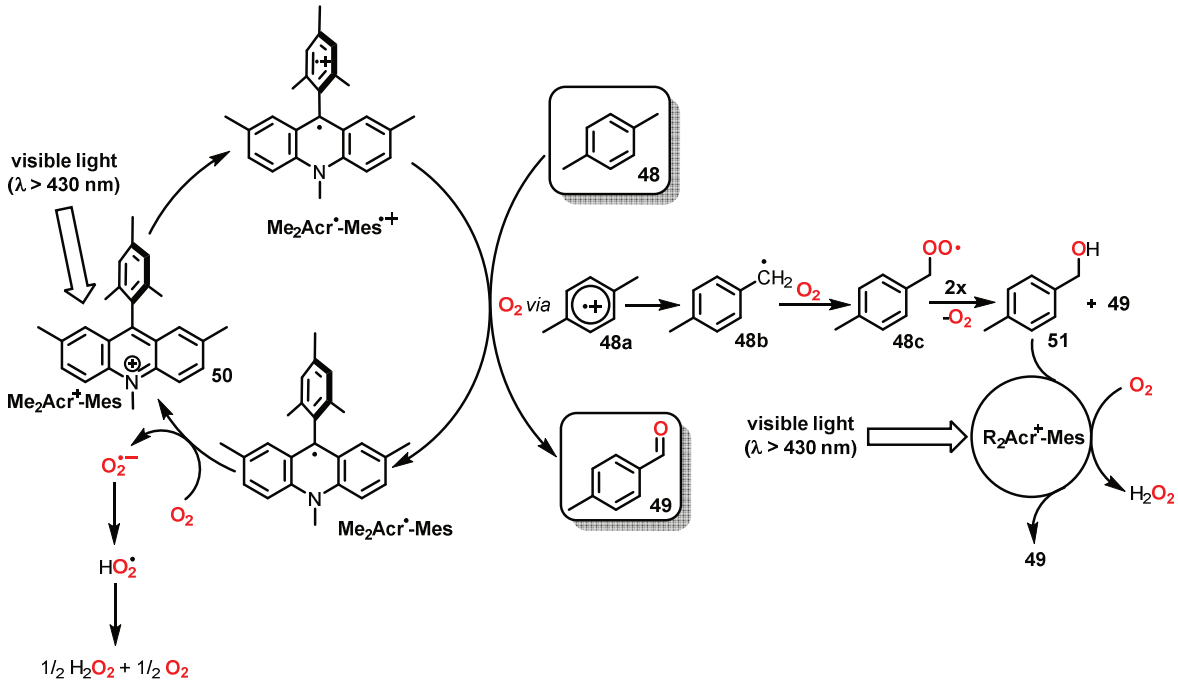

Scheme 34. Proposed mechanism of the photooxygenation of *p*-xylene by Acr^+-Mes.

Addition of aqueous sulfuric acid also improves the overall yield, mainly due to an enhanced protonation of the *p*-xylene radical cation and the disproportionation of $O_2^{\bullet-}$.[108] The remarkably improvement of the reactivity by applying Me_2Acr^+-Mes instead of Acr^+-Mes is attributed to its increased reducing ability by introducing two the electron-donating methyl groups. Indeed, $Me_2Acr^{\bullet}$-$Mes^{\bullet+}$ reduces O_2 two orders of magnitude more efficient than $Acr^{\bullet}$-$Mes^{\bullet+}$, which might be the reason for the improved photocatalytic activity.

The catalytic efficiency of Acr^+-Mes in the photooxygenation of *p*-xylene is also dramatically improved in the presence of $[Cu(II)(TPA)](ClO_4)_2$ (TPA = tris(2-pyridylmethyl)amine), which efficiently reacts with $O_2^{\bullet-}$ yielding the dicopper(II)peroxo complex $[\{Cu(II)(TPA)\}_2O_2]$ preventing the degradation of the photocatalyst.[109,110] The composite photocatalyst composed of Acr^+-Mes@AlMCM-41 (AlMCM-41 = nanosized

mesoporous silica–alumina) and $[Cu(II)(TPA)](ClO_4)_2$ exhibited the highest catalytic activity and durability in the photocatalytic oxygenation of *p*-xylene with O_2.

Acr^+-Mes also catalyzes the oxygenation of durene, mesitylene[108], other benzylic substrates[111], methyl-substituted naphthalenes,[112] and triphenylphosphine,[113] but fails with even more challenging substrates such as toluene or cyclohexane. The reduction potential of R_2Acr^+-Mes (R = H or Me) of the excited charge-shifted state $R_2Acr^{\bullet}$-$Mes^{\bullet+}$ (2.06 V *vs* SCE in MeCN) is sufficient for activated toluene derivatives, but too low for toluene (E_{ox} = 2.20 V). The scope of Acr^+-Mes was significantly expanded by adding hydrochloric acid to the Acr^+-Mes/substrate mixture, which made the oxygenation of toluene, toluene derivatives bearing electron-withdrawing groups[114] and even cyclohexane[114,115] feasible (Scheme 35). After excitation of **45** (step *i*), the crucial step of this reaction is an efficient electron transfer from Cl^- to the $Mes^{\bullet+}$ moiety yielding $Cl^{\bullet}$ (step *ii*), which abstracts a hydrogen atom from cyclohexane (step *iii*). The carbon centered radical is trapped by O_2, generating the peroxy radical (step *iv*), which disproportionate to an equimolar mixture of cyclohexanone and cyclohexanol (step *v*). Hydrogen peroxide is the sole by-product generated by the reduction of O_2 to $O_2^{\bullet-}$ by the $Acr^{\bullet}$ moiety which regenerates the catalyst **45** (step *vi*). The oxygenation of toluene (and its derivatives) selectively forms the desired aromatic aldehydes.

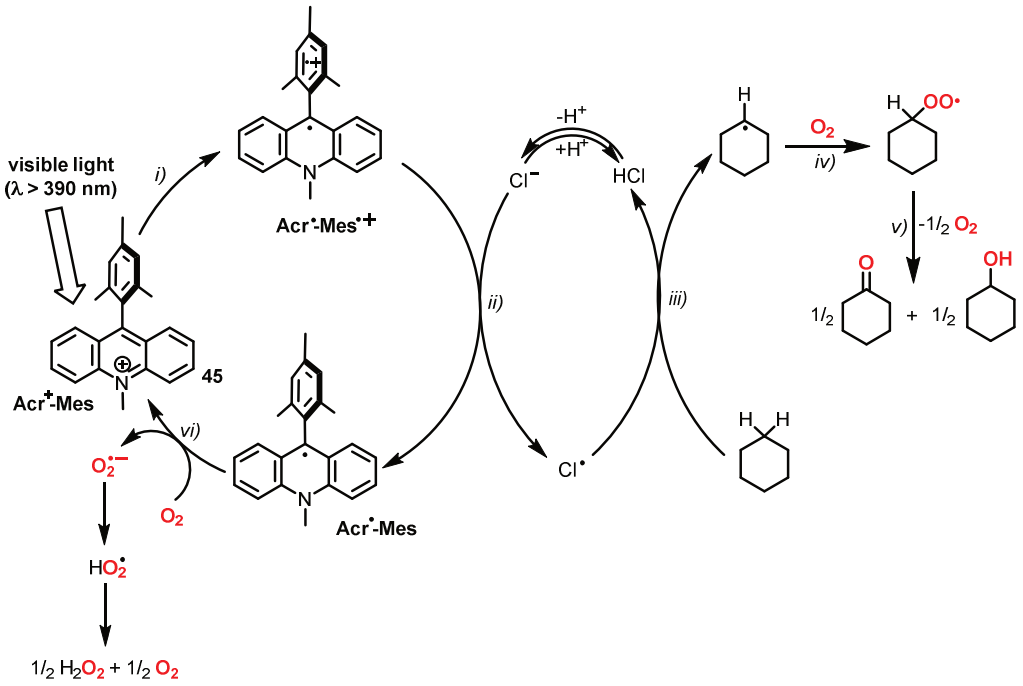

Scheme 35. Photocatalytic oxygenation of cyclohexane by Acr^+-Mes.

Photocatalytic cycloaddition reactions

The long-lived charge-shifted excited state, $Acr^{\bullet}$-$Mes^{\bullet+}$, provides an efficient way to produce radical cations and radical anions simultaneously. The oxidizing ability of the $Mes^{\bullet+}$ group is capable of generating radical cations, $D^{\bullet+}$, in the presence of suitable electron donors, whereas the reducing ability of $Acr^{\bullet}$ moiety gives access to radical anions, $A^{\bullet-}$, in the presence of electron acceptors. The direct coupling between $D^{\bullet+}$ and $A^{\bullet-}$ might yield a new molecule D-A.

The [2 + 2] cycloaddition of dioxygen (O_2 = A in this case) with tetraphenylethylene (TPE = D) to the corresponding 1,2-dioxyethan (D-A) impressively illustrates this strategy (Scheme 36).[116] After excitation of **45** (step *i*), the electron transfer occurs TPE (E_{ox} = 1.56 V *vs* SCE) to the $Mes^{\bullet+}$ group (E_{red} = 1.88 V *vs* SCE) is thermodynamically feasible, generating $TPE^{\bullet+}$ ($D^{\bullet+}$) and $Acr^{\bullet}$-Mes (step *ii*). Simultaneously, the electron transfer from the $Acr^{\bullet}$ moiety to O_2 regenerates the catalyst with concomitant formation of $O_2^{\bullet-}$ ($A^{\bullet-}$, step *iii*). Recombination of these radicals generates the 1,2-dioxyethane (step *iv*), which is further transformed to benzophenone as final oxygenation product *via* photocatalytic O─O cleavage (step *v*).

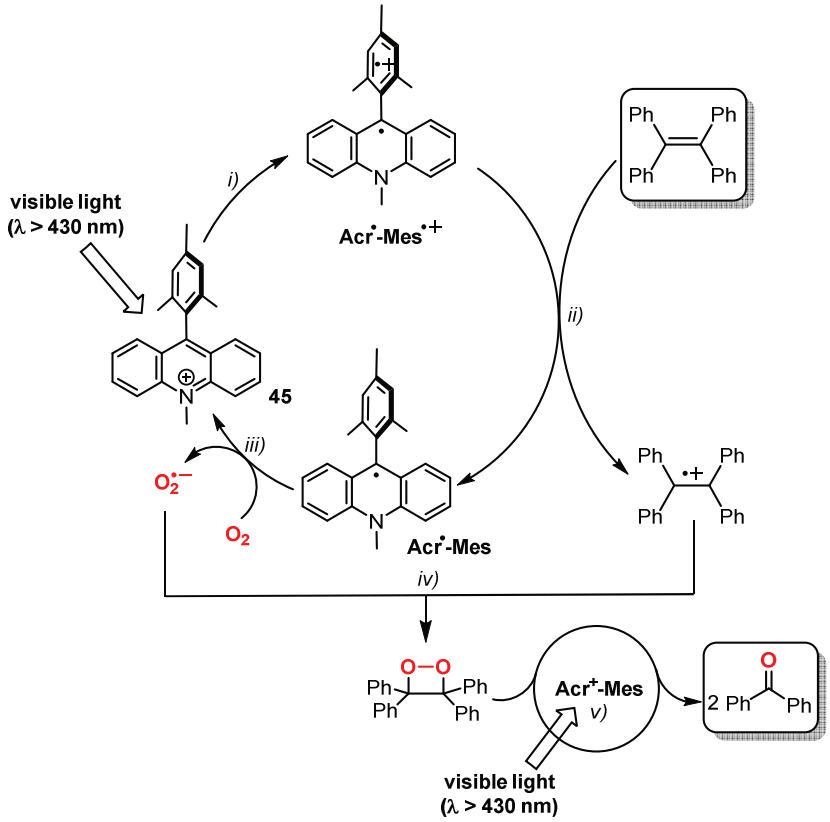

Scheme 36. Photocatalytic [2 + 2] cycloaddition of TPE and O_2 catalyzed by Acr^{+}-Mes.

It is noteworthy that the common preparation strategy for 1,2-dioxyethanes with singlet dioxygen does not give any product with the electron-poor alkene TPE. This observation

emphasizes the unique reactivity pattern of Acr^+-Mes, which is in principle capable to sensitize $^1O_2$ or perform electron transfer reactions depending on the substrate present.[112] When TPE is substituted by anthracene, the [4 + 2] cycloaddition of $O_2^{\bullet-}$ to the anthracene radical cation yields the corresponding epidioxyanthracene, which is further oxidized to antraquinone under prolonged irradiation.[117] When 9,10-dimethylanthracene was used, the desired dimethylepidioxyanthracene was isolated in 99% yield and no overoxidation was observed.[117]

Photooxidation of nitrate for alkyne oxygenation

The group of König *et al.* utilized Acr^+-Mes as an efficient photocatalyst for the challenging oxidation of nitrate to nitrate radicals $NO_3^{\bullet}$. The latter is generated *in situ* in the reaction mixture under aerobic conditions and subsequently reacts with diphenylacetylene (**52**) to yield benzophenone (**53**) and benzil (**54**, Scheme 37)[118]. Fluorescence emission spectroscopy revealed that the oxidation of NO_3^- occurs *via* quenching of a singlet excited state of Acr^+-Mes. Quenching of the long-lived triplet state by NO_3^- was not detected by laser flash photolysis.[95] This reaction pattern differs from the oxygenation reactions described by Fukuzumi (*vide supra*), where the key intermediate is the long-lived charge-shift state. The oxidation of diphenylacetylene by $NO_3^{\bullet}$ yields the vinyl radical adduct (**55**), which performs a γ-fragmentation after $NO_2^{\bullet}$ elimination (Scheme 37a). The resulting carbene intermediate (**56**) rearranges to intermediate **57**. An oxidative decarboxylation yields benzophenone in the presence of dioxygen. Benzil is obtained in a competing pathway from the vinyl radical adduct *via* a 5-*endo* cyclization (**58**) with concomitant loss of $NO^{\bullet}$ (Scheme 37b).

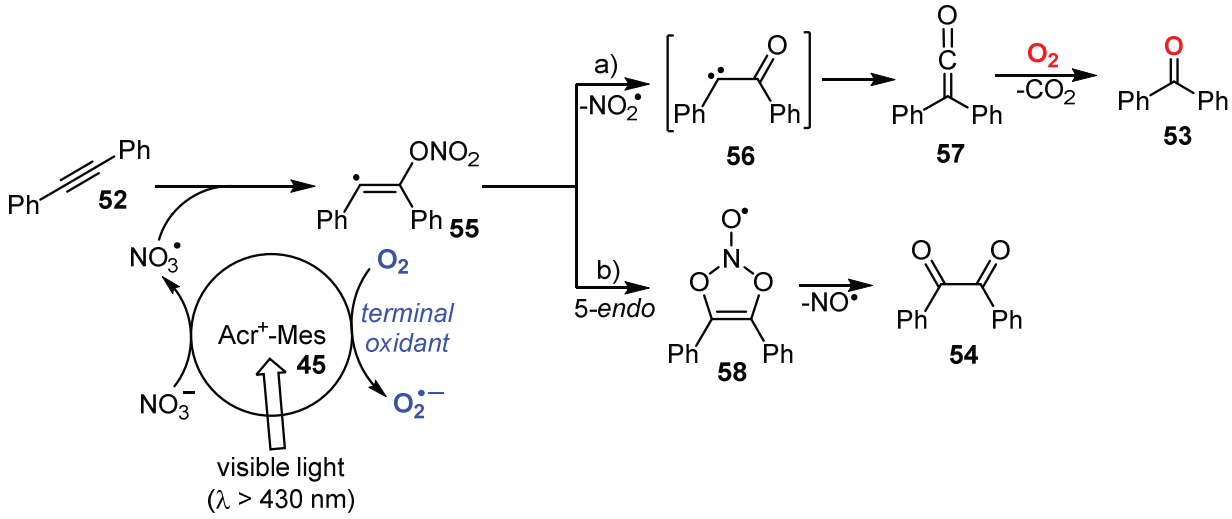

Scheme 37. Proposed mechanism for the photocatalytic oxygenation of aromatic alkynes in the presence of Acr+-Mes triggered by nitrate radicals.

1.3.6 Antraquinone-2,3-dicarboxylic acid (AQN)

Itoh *et al.* reported the direct photooxygenation of methylbenzenes to the corresponding carboxylic acids in the presence of catalytic amounts of $MgBr_2 \cdot Et_2O$[119]. The photo-initiated generation of bromo radicals leads to the formation of benzyl radicals *via* hydrogen abstraction, which are subsequently trapped by dioxygen yielding the desired carboxylic acid. In further studies, the direct esterification of methylbenzenes to the corresponding methyl esters was achieved with catalytic amounts of CBr_4 in MeOH.[120] Similar to $MgBr_2 \cdot Et_2O$, the hydrogen abstraction by bromo radicals yields aldehydes, which form dimethyl acetals in the presence of methanol. The subsequent oxygenation of the dimethyl acetals leads to methyl esters. Similar results are obtained if the toxic reagent CBr_4 is substituted by the visible light photocatalyst antraquinone-2,3-dicarboxylic acid (**59**, AQN) under otherwise identical conditions (Scheme 38).[121]

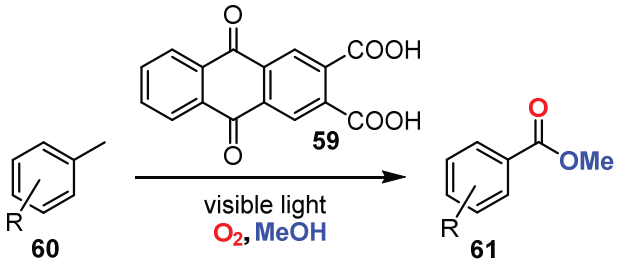

Scheme 38. Visible-light-driven transformation of methylbenzene derivatives to the corresponding esters catalyzed by AQN in the presence of dioxygen and methanol.

A plausible reaction mechanism is depicted in Scheme 39. The excitation of AQN leads to hydrogen abstraction from the methylbenzene derivative **60** yielding the benzyl radical **60a** and AQNH•. The authors did not exclude a direct electron transfer from the **60** to AQN*. Benzyl radical **60a** is trapped by dioxygen, yielding the peroxyl radical **60b**, which regenerates the catalyst *via* hydrogen abstraction from AQNH• with concomitant formation of **60c**. The aldehyde **60d** is generated from **60c** and, in the presence of MeOH, the dimethyl acetal **60e** is formed, which is photocatalytically oxidized to the desired methyl esters **61** *via* a peroxyradical pathway initiated by AQN*.

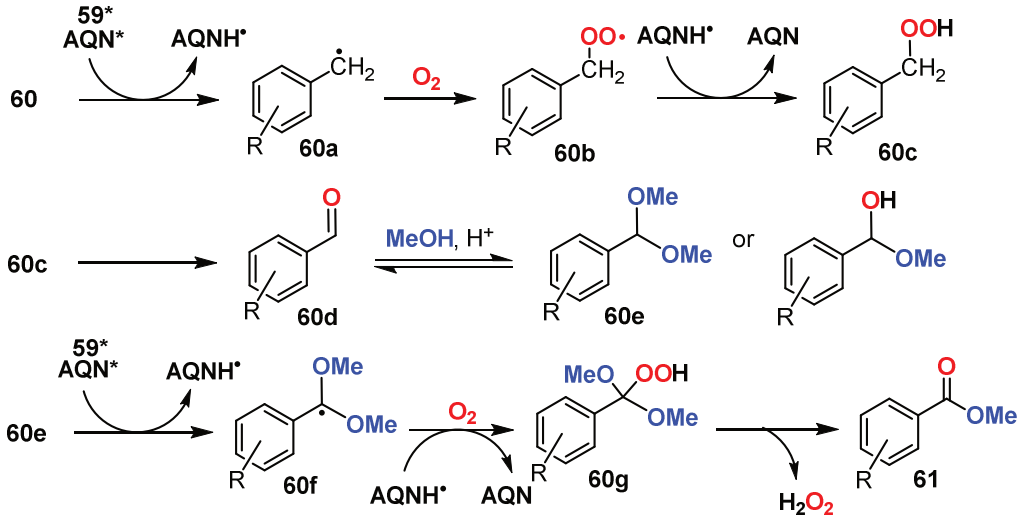

Scheme 39. Proposed reaction mechanism for the photooxygenation of methylbenzenes to the corresponding esters.

1.3.7 Riboflavin tetraacetate (RFT)

The important role of flavins as photoreceptors and redox cofactors in nature has inspired the use of synthetic flavin analogues as bioinspired photocatalysts.[122,123] The most prominent example, riboflavin tetraacetate (RFT)[124], catalyzes the aerobic photooxidation of benzyl alcohols,[125–128] benzyl amines,[129] sulfoxides[130] and [2 + 2] cycloadditions[131]. Very recently, we reported that a photocatalytic system consisting of RFT/benzyl alcohol/acetic acid efficiently mimics the enzyme activity of FAD-dependent halogenases (FAD = flavin adenine dinucleotide) for the challenging oxidative chlorination of arenes with chloride and air as terminal oxidant. These results will be extensively summarized in chapter 6 of this thesis. A particularly intriguing application of RFT is the oxygenation of methylbenzenes, styrenes and phenylacetic acids reported by König and co-workers.[132] The oxygenation of *p*-methoxytoluene, *p*-*tert*-butyl-toluene and *p*-xylene to the corresponding aldehydes was achieved in the presence of RFT (20 mol%) and irradiation with blue light in a MeCN/water mixture (1/1) in moderate yields of 58%, 40% and 43%, respectively. The oxygenation of fluorene and α-tetrahydronaphthalene only gave 16% and 34% yield of fluorenone and α-tetralone. Mechanistic studies revealed an electron transfer from the test substrate 4-methoxytoluene (**62**) to the triplet excited state ^{3}RFT* to yield ^{2}RFT$^{\bullet-}$ and the benzyl radical cation **62a** (step *i*), which is subsequently deprotonated to the benzyl radical **62b** (step *ii*, Scheme 40). **62b** is able to form covalent adducts with ^{2}RFT$^{\bullet-}$ (step *iii*). The N5 adduct **63** is oxidized to the neutral radical **63a** as confirmed by absorption spectroscopy (step *iv*). **63a** subsequently fragments after electron transfer into the benzyl alcohol **64** under concomitant formation of hydrogen peroxide and

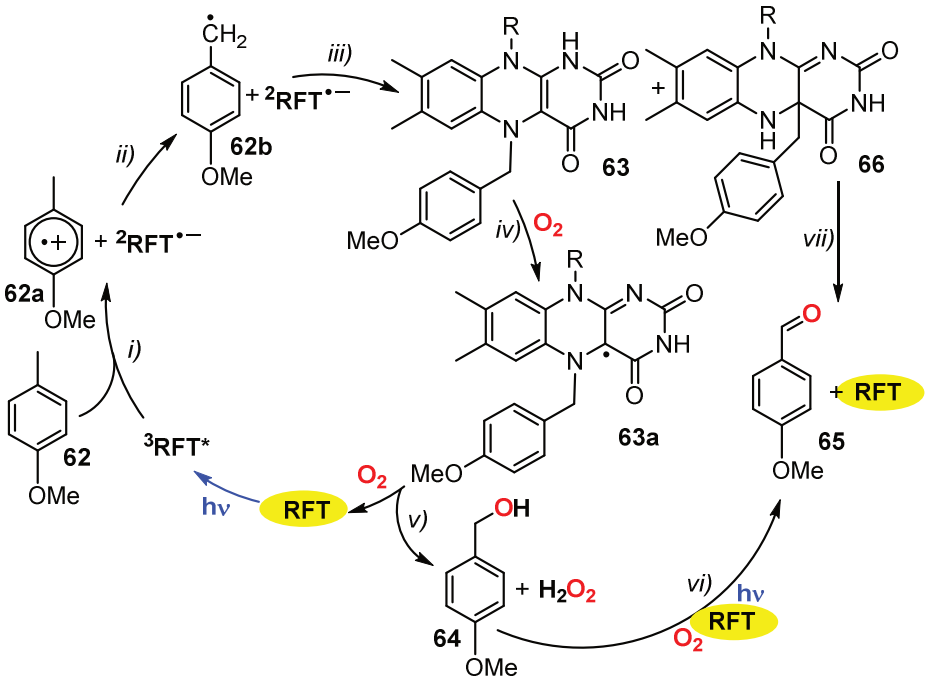

Scheme 40. Proposed mechanism for the oxygenation of methylbenzenes by RFT.

regeneration of the chromophore (step *v*). **64** is further oxidized to the corresponding aldehyde **65** in a flavin-mediated oxidation process (step *vi*). The covalent C4a adduct **66** directly yields the desired benzaldehyde **65** and RFT (step *vii*). Additionally, the oxygenation of stilbene derivatives gave aldehydes *via* photo-oxidative cleavage of the double bond, whereas tolane was oxidized to benzil. In all cases, the yields were moderate or poor, whereas the photooxidative decarboxylation of phenylacetic acids to aldehydes was achieved in excellent yields. For all compounds, the key step is an electron transfer from the substrate to ^{3}RFT*. Furthermore, the experimental data do not indicate an oxidation *via* singlet oxygen. Unfortunately, moderate product yields were achieved for most substrates. This is mainly due to a competing polymerization reaction after the electron transfer event. Additionally, the substrate scope is narrow due to the low reduction potential of ^{3}RFT*. Fukuzumi *et al.* found that the redox potential of RFT can be modified by metal ion coordination.[133] Complexes of RFT with Mg^{2+}, Zn^{2+}, Yb^{3+} and Sc^{3+} ions have a significantly more positive reduction potential E_{red} (^{1}RFT*/^{2}RFT$^{\bullet-}$) in the excited singlet state. In particular, the Sc^{3+} system appears promising as it features high fluorescence quenching rate constants of (^{1}RFT–2Sc^{3+})* in the presence of alkyl- and methoxy-substituted benzenes.[134] This indicates an efficient single electron transfer from the substrate to (^{1}RFT–2Sc^{3+})*, which is a prerequisite for photocatalytic activity. Chapter 2 of this thesis will describe that the enhanced reduction potential of RFT coordinating to scandium triflate enables the challenging photocatalytic C–H oxidation of electron-deficient alkylbenzenes and benzyl alcohols. The scope of benzylic C–H bond oxidation reactions was further expanded with a mixture of RFT and the biomimetic non-heme iron

complex $[Fe(TPA)(MeCN)_2](ClO_4)_2$ (TPA = tris(2-pyridylmethyl)amine). An RFT catalyzed photocycle and the independent action of the iron complex as a catalyst for H_2O_2 disproportionation and alkyl benzene oxygenation ensure high yields and selectivities and will be extensively discussed in chapter 3 of this thesis.

1.3.8 Summary

Organic dyes such as Eosin Y and methylene blue are attractive alternatives to transition metal complexes in photoredox catalysis. They are typically less expensive and less toxic, easy to handle and even outperform organometallic and inorganic catalysts in some cases as exemplified for the visible-light-driven hydroxylation of arylboronic acids to aryl alcohols by Eosin Y or MB^+ (chapters 1.3.1 and 1.3.2). Additionally, the desulfurization of thioamides to amides and the transformation of arylmethyl bromides to the corresponding benzyl alcohols and aldehydes is easily achieved with Eosin Y.

Organic photocatalysts such as DDQ and QuCN exhibit enormous high reduction potentials in their excited states, thus the challenging oxygenation of benzene to phenol becomes feasible (chapters 1.3.3 and 1.3.4). The key step is the one-electron transfer from benzene to ^{3}DDQ* or ^{1}QuCN*. This oxidation yields the benzene radical cation which is trapped by water and subsequently transformed into the desired product. In the case of DDQ, the catalytic procedure needs a sacrificial oxidant to regenerate the catalyst, whereas in the case of QuCN atmospheric oxygen is sufficient.

Acridinium ions such as Acr^+-Mes, Acr^+-Ph, and Acr^+-H have attracted much attention as catalysts of several types of organic transformations such as arene bromination, cycloaddition reactions, and for the selective formation of anti-Markovinov alkene addition products (chapter 1.3.5). They have been successfully applied for the oxygenation of *p*-xylene, durene, mesitylene or other benzylic substrates, methyl-substituted naphthalenes and triphenylphosphine, but failed for more challenging substrates such as toluene or cyclohexane. The reduction potential of excited Acr^+-Mes is too low to trigger an electron transfer from these substrates to the chromophore. Fukuzumi elegantly circumvented this obstacle by applying the mediator HCl for this challenging oxygenation reaction. An efficient electron transfer from Cl^- to the $Mes^{\bullet+}$ moiety of excited Acr^+-Mes yields $Cl^\bullet$ which abstracts a hydrogen atom from cyclohexane or toluene. The following addition of dioxygen yields the desired products. This chromophore also exhibits a long-lived charge-shift state $Acr^\bullet$-$Mes^{\bullet+}$ after excitation, which provides an efficient way to produce radical cations and radical anions simultaneously. This ability gave access to 1,2-dioxyethane in a [2 + 2] cycloaddition of dioxygen to tetraphenylethylene (TPE), which is not possible with singlet oxygen; the preferred reagent for this kind of transformations.

Antraquinone-2,3-dicarboxylic acid as catalyst gave access to the direct transformation of esters from methylbenzene derivatives (chapter 1.3.6). In this oxygenation reaction, no electron transfer between the substrate and the excited chromophore is assumed, instead the improved ability of AQN* (compared to AQN) to abstract a hydrogen atom from the substrate is the key step.

Riboflavin tetraacetate (RFT) performs the oxygenation of methlybenzenes, styrenes, and phenylacetic acids, but these reactions often suffer from low yields (chapter 1.3.7). The key step is the electron transfer from the substrate to a photoexcited RFT molecule, which triggers the oxygenation reaction under concomitant formation of hydrogen peroxide. Unfortunately, the reduction potential of RFT is limited, thus the substrate scope is narrow. Nevertheless, RFT is a green and easy accessible alternative for traditional protocols, which often involve toxic chemicals in stoichiometric quantities. The addition of the Lewis-acid $Sc(OTf)_3$ to RFT yields a complex exhibits a significantly higher reduction potential and effectively catalyzes the oxygenation of electron-poor benzylic substrates (see chapter 2 of this thesis). The scope was even extended by applying a catalyst mixture consisting of RFT and a non-heme iron complex $[Fe(TPA)(MeCN)_2](ClO_4)_2$. The photocatalytic performance of RFT is enhanced by the iron complex, which acts a catalyst for H_2O_2 disproportionation and alkylbenzene oxygenation at the same time (see chapter 3 of this thesis).

1.4 Photocatalysis Coupled with Transition Metal Catalysis

1.4.1 Heme and Non-Heme Metal Complexes

As shown in chapter 2, manganese and iron porphyrins are capable of performing the *reductive activation of dioxygen* for the oxygenation of organic substrates, following equation 1:

$$R{-}H + \mathbf{O_2} + 2e^- + 2H^+ \rightarrow R{-}\mathbf{O}H + H_2O \quad (1)$$

Since water is the most abundant reactant that can be used as oxygen source, the *oxidative activation of H_2O* in analogy to equation 2 is a promising alternative:

$$R{-}H + \mathbf{H_2O} - 2e^- - 2H^+ \rightarrow R{-}\mathbf{O}H \quad (2)$$

The two-electron oxidation of water for catalytic oxygenation reactions classically requires strong oxidants such as cerium(IV) ammonium nitrate. Nam *et. al.* developed the first photocatalytic oxidative activation of water in oxygenation reactions of various substrates *in the absence of dioxygen and strong oxidants*.[135] They reported highly efficient photocatalytic olefin epoxidation, alkane hydroxylation and sulfoxidation reactions by using manganese(III) porphyrins, [(porph)Mn(III)(OH)] (**67**), as a catalyst, $[Ru(II)(bpy)_3]^{2+}$ (**29**) as a photocatalyst, $[Co(III)(NH_3)_5Cl]^{2+}$ (**68**) as a low-cost and weak one-electron oxidant, and water as an oxygen source.

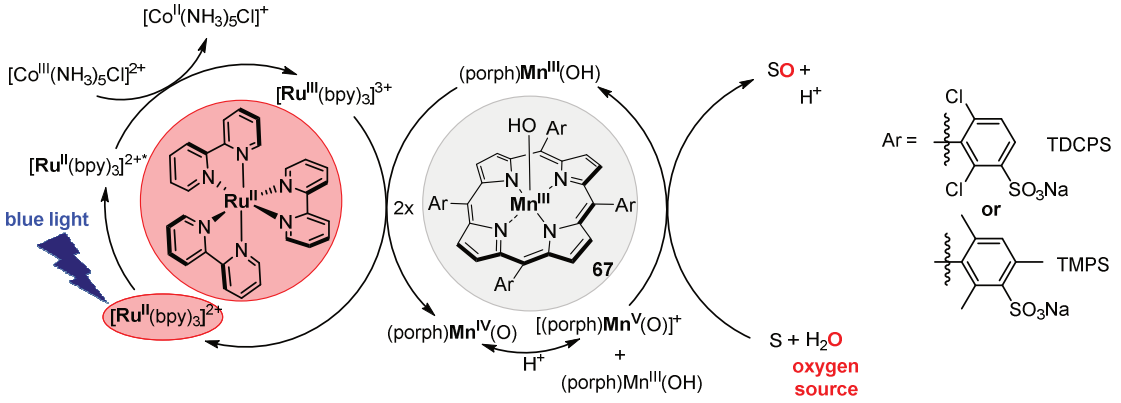

Scheme 41. Visible-light-driven oxygenation of a substrate, S, catalyzed by an *in situ* generated oxygenation catalyst, $[(porph)Mn(V)(O)]^+$.

The proposed mechanism is depicted in Scheme 41. The excitation of the photocatalyst $[Ru(II)(bpy)_3]^{2+}$ in the presence of the sacrificial electron acceptor $[Co(III)(NH_3)_5Cl]^{2+}$ leads to the efficient formation of $[Ru(III)(bpy)_3]^{3+}$, which oxidizes **67** to [(porph)Mn(IV)(OH)]. The subsequent disproportionation of two equivalents of [(porph)Mn(IV)(OH)] generates one equivalent of **67** and one equivalent of the oxidant $[(porph)Mn(V)(O)]^+$, which performs the oxygenation of the substrate. The oxygen atom derives from the water molecule, as confirmed by $H_2{}^{18}O$-labelling experiments.

Based on this work, Sun *et al.* coupled the $[Ru(II)(bpy)_3]^{2+}/[Co(III)(NH_3)_5Cl]^{2+}$ photosystem with a non-heme manganese(II) complex, $[Mn(II)(BQCN)](OTf)_2$ (**69**, BQCN = *N,N'*-dimethyl-*N,N'*-bis(8-quinolyl)cyclohexanediamine, Scheme 42).[136] The *in situ* photogenerated [Mn(IV)(BQCN)(O)] complex is able to oxidize benzyl alcohol to benzaldehyde *via* a hydrogen atom transfer mechanism (HAT) and sulfides to sulfoxides *via* an oxygen atom transfer mechanism (OAT). Fukuzumi[137] and Costas[138] showed that biomimetic non-heme iron(II) complexes bearing pentadentate pyridyl ligands such as $[Fe(II)(N4Py)(MeCN)](OTf)_2$ (**70**, N4Py = *N,N*-bis(2-pyridylmethyl)-*N*-bis(2-pyridyl)methylamine, Scheme 42) and $[Fe(II)(Me_2TACN)(MeCN)](OTf)_2$ (**71**, Me_2TACN = *N*-methyl-*N'*,*N''*-bis(2-pyridylmethyl)-1,4,7-triazacyclononane, Scheme 42) are also suitable oxygenation catalysts as well when coupled with the $[Ru(II)(bpy)_3]^{2+}/[Co(III)(NH_3)_5Cl]^{2+}$ photosystem. The photogenerated oxoiron(IV) species are capable to perform the oxygenation of thioanisole to thioanisole oxide. Very recently, Mahy *et al*. combined the $[Ru(II)(bpy)_3]^{2+}/[Co(III)(NH_3)_5Cl]^{2+}$ photosystem with a Mn(III)-corrole complex (**72**, Scheme 42) to generate a high-valent Mn(V)-oxo species. The addition of the protein bovine serum albumin (BSA) enables enantioselective oxidation of organic substrates.[139]

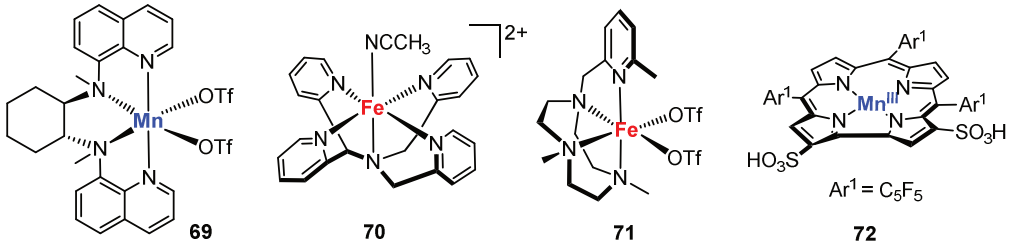

69 **70** **71** **72**

Scheme 42. Iron and manganese complexes under study.

Banse *et al.* developed a supramolecular assembly consisting of a Ru(II)-photocatalyst linked with a non-heme iron catalyst (**73**), which is an oxygenation catalyst for triphenylphosphine (Scheme 43).[140] Excitation of the chromophore with visible light in the presence of a sacrificial electron acceptor $[Co(III)(NH_3)_5Cl]^{2+}$ (EA) triggers a cascade of one electron transfer reactions, leading to the formation of a high valent iron(IV)–oxo species [Fe(IV)(O)] from an iron(II)-aqua complex. This oxygen atom transfer catalyst subsequently oxidizes PPh_3 to $OPPh_3$, using the initially bound water molecule as the oxygen source. A TON of 3.2 was determined in a buffered solution after 10 minutes of irradiation (λ= 450 nm), which corresponds to a 20% efficiency with respect to the amount of $[Co(III)(NH_3)_5Cl]^{2+}$ used.

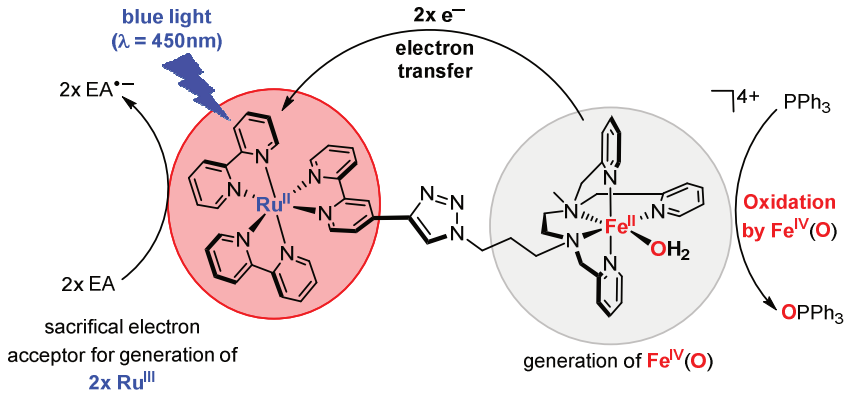

Scheme 43. Structure of the supramolecular assembly **73** catalyzing the photooxygenation of PPh_3.

1.4.2 Copper Complexes

Next to the non-heme/heme metal complexes, several Cu(I) complexes inspired by metalloenzymes such as dopamine *β*-monooxygenase are known to activate dioxygen. The Cu(I) species produce a Cu(II)(O_2) complex, which performs the oxygenation reaction and yields an inactive Cu(II)-complex. The key challenge is the regeneration of the active Cu(I) species, which is classically achieved by addition of a sacrificial reductant. Unfortunately, the competitive reduction of the active Cu(II)(O_2) species in the presence of the sacrificial reductant diminished the efficiency dramatically (Scheme 44a), thus few bioinspired copper(I) complexes are catalytically active.

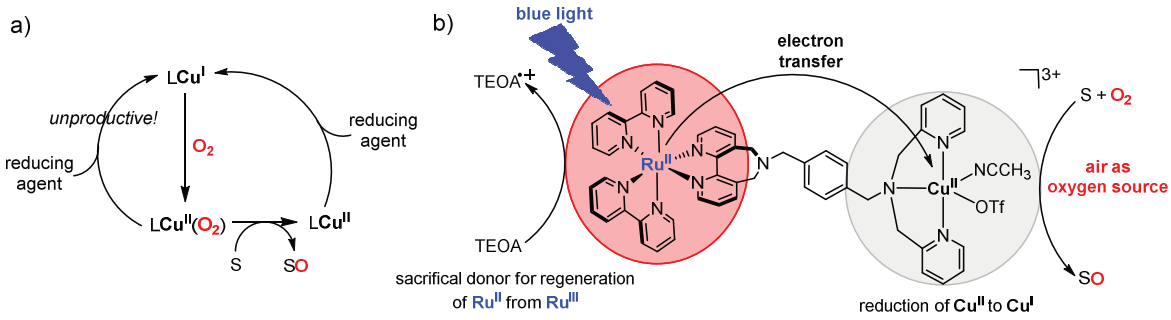

Scheme 44. a) Productive *vs.* unproductive regeneration LCu(I) in copper catalyzed oxygenation reactions; b) Ruthenium(II)-Copper(II) dyad for the visible-light-driven oxygenation of substrates; TEOA = triethanolamine.

Ménage *et al.* developed a Ruthenium(II)-copper(II) dyad (**74**, Ru^{II}_{phot}-Cu^{II}_{cat}), consisting of a Ru(II)-photocatalyst covalently linked to a copper(II) oxygenation precatalyst, which performs the photooxygenation of various substrates mediated by dioxygen (Scheme 44b).[141] Excitation of the Ru(II) subunit leads to an efficient electron transfer to the Cu(II) precatalyst, yielding the active Cu(I) moiety, which is the prerequisite for dioxygen activation. The regeneration of the photosensitizer unit is effectively achieved by addition

of the sacrificial electron donor triethanolamine (TEOA). A covalent connection between the Ru-based photosensitizer and the Cu(II) catalyst for O_2 activation allows a controlled delivery of reducing equivalents that overcomes the undesired Cu(II)(O_2) reduction by the reducing reagent. This dyad proved to be efficient for the catalytic oxygenation of sulfides, phosphines, and alkenes. In a typical reaction, the substrate (ca. 50 mM), the catalyst Ru^{II}_{phot}-Cu^{II}_{cat} (ca. 0.5 mM), and TEOA (ca. 100 mM) were dissolved in oxygen-saturated acetonitrile and irradiated with a blue LED (λ_{max} = 468 nm) for 8 h. The oxygenation of sulfides to sulfoxides was achieved nearly quantitatively and selectively in high turnovers (TON ~ 90-100), except 4-nitrothioanisol bearing an electron-withdrawing group (TON = 8). PPh_3 gave $OPPh_3$ quantitatively after 1.5 h (TON = 100), whereas indene gave the corresponding *cis*-diol in moderate yields of 36%. Cycloalkenes are converted to the corresponding 1-cycloalk-2-enones in moderate yields after 16 h.

1.4.3 Ruthenium Complexes

Effective electron transfer from a photoexcited chromophore to a redox active catalyst across a bridging ligand is the key step in an effective oxygenation reaction in the artificial Ru^{II}_{phot}-Cu^{II}_{cat} dyad designed by Ménage and co-workers (*vide supra*). In recent years, dinuclear Ru complexes analogous to this dyad have attracted considerable attention of several research groups. One Ru center (Ru_{phot}) acts a light-harvesting antenna, inspired by the light-harvesting unit P680 in the photosystem II (PS II), whereas the other Ru center (Ru_{cat}−OH_2) is the active catalyst. Ru_{phot} and Ru_{cat}−OH_2 are connected by a bridging ligand, which guarantees an effective electron transfer. The role of the linker between Ru_{phot} and Ru_{cat}−OH_2 is crucial, thus only a few assemblies have been published so far, i.e. for the oxidation of water[142–144] (similar to the oxygen evolving complex (OEC) in PS II) and the oxidation of alcohols.[145–148] Additionally, a few dyads (Scheme 45) catalyze the visible-light-driven oxygenation of sulfides to sulfoxides, which is of potential interest in the pharmaceutical and petroleum industries.[149–152] The initial step in the catalytic mechanism is the oxidation of excited Ru_{phot}(II)* by an electron acceptor generating Ru_{phot}(III), which is subsequently reduced by the Ru_{cat}(II)−OH_2 moiety yielding Ru_{cat}(III)−OH. This one electron transfer cascade is repeated, yielding the active oxidant Ru_{cat}(IV)(O), which oxygenates the substrate. A suitable dyad system is supposed to fulfil various requirements, such as a) effective harvesting of visible light by Ru_{phot}, b) effective electron transfer from the oxygenation catalyst Ru_{cat}−OH_2 to Ru_{phot}(III), and c) effective oxygenation of the substrate with water as the oxygen source. One of the most efficient dyads for sulfoxidations is the recent example reported by Fu and co-workers (Scheme 45). The oxygenation of thioanisole (10 mM) to thioanisole oxide was achieved within

745 turnovers and 99% selectivity in the presence of the electron-acceptor $[Co(III)(NH_3)_5Cl]^{2+}$ (20 mM).

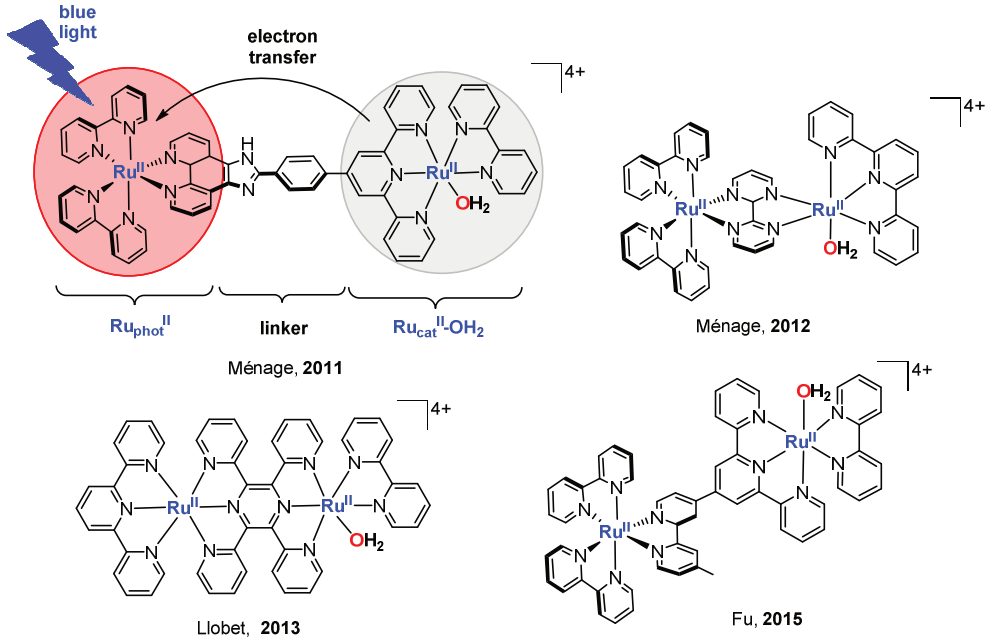

Scheme 45. Ru^{II}_{phot}-Ru^{II}_{cat} dyads for the photooxygenation of sulfides.

1.4.4 Biocatalytic Oxygenation

Biocatalytic oxygenation chemistry is a rapidly evolving field in which monooxygenases are the tools of choice for catalyzing many industrially important synthetic transformations.[153] However, their use in preparative applications is hampered by the intrinsic requirement for reducing equivalents such as the expensive nicotine-amide cofactors NAD(P)H and $NAD(P)^+$, which are commonly regenerated by glucose dehydrogenase in the presence of *β*-D-glucose as sacrificial donor (Scheme 46a). The group of Hollmann *et al.* developed a visible-light-driven non-enzymatic system that uses cheap, non-toxic, and easily accessible organic reagents as replacement for the NAD(P)H/glucose dehydrogenase system (Scheme 46b).[154] The redox co-factor FAD (flavin adenine dinucleotide) substitutes NAD(P)H as reducing agent, which is able to regenerate the Bayer-Villiger monooxygenase (BVMO) under visible light irradiation. In the presence of EDTA (ethylenediaminetetraacetate) as a sacrificial donor, which acts a substitute for *β*-D-glucose, an efficient combination of photocatalysis and enzyme catalysis has been developed. This simplified system was successfully applied for the enantioselective monooxygenase-catalyzed Bayer-Villiger reaction of ketones.[154]

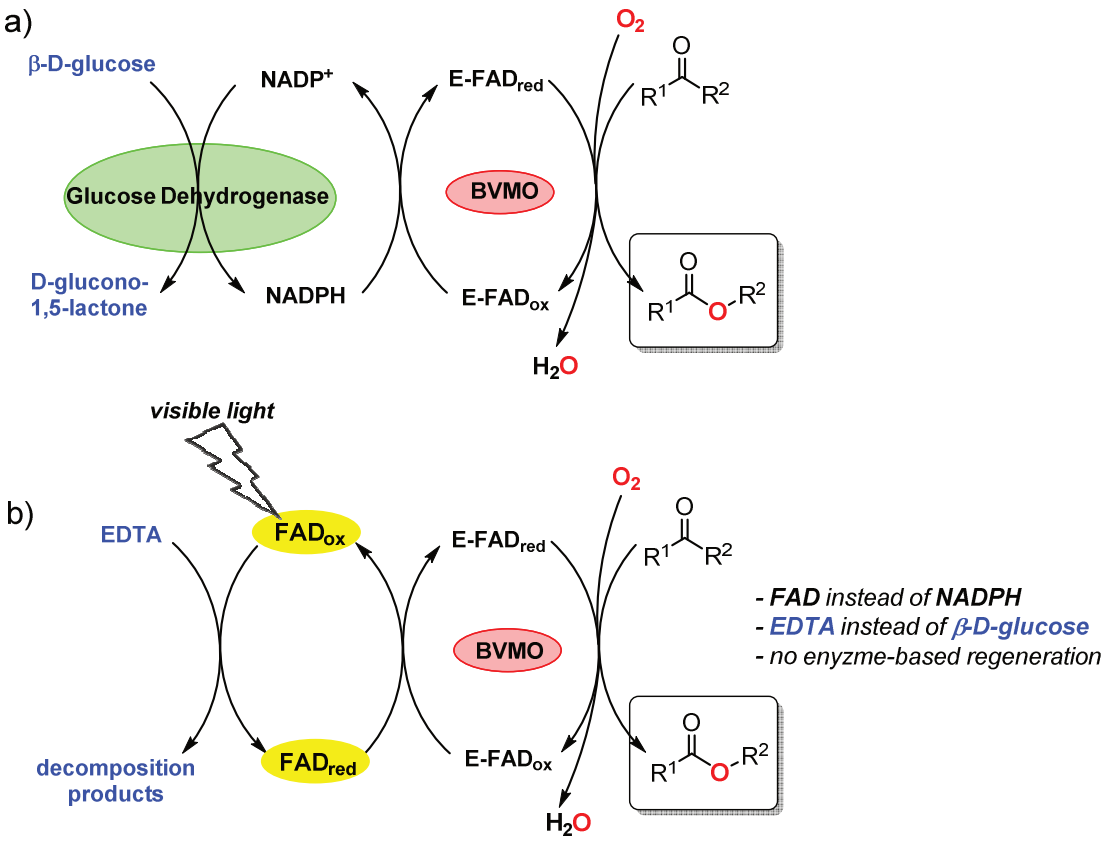

Scheme 46. a) Traditional enzyme-coupled regeneration of the reducing agent NADPH by glucose dehydrogenase in the presence of *β*-D-glucose and glucose dehydrogenase; b) visible-light-driven regeneration of the monooxygenase BVMO by FAD in the presence of EDTA.

In a following study, the monooxygenase was substituted by chloroperoxidase (*CPO*), which does not need a reducing agent, since this class of enzymes reacts *via* the hydrogen peroxide shunt mechanism. Unfortunately, *CPO* is rather stable towards high H_2O_2 concentrations, presumably due to oxidative degradation of the heme prosthetic group. Portionwise addition of H_2O_2 improved the overall yield, Hollmann *et al.* showed that the photochemical *in situ* generation of H_2O_2 by RFT/EDTA (RFT = riboflavin tetraacetate, see chapter 1.3.7) with air as terminal oxidant significantly promotes the *CPO*-driven oxidation of sulfides, benzyl alcohols and indole in aqueous phosphate buffer solutions (Scheme 47).[155] The identical system also works in a biphasic system to circumvent solubility problems which often occur for many organic reactants in aqueous media.[156] The excitation of RFT with blue light oxidizes EDTA and yields the reduced flavin species $RFTH_2$, which is easily regenerated by dioxygen under concomitant formation of H_2O_2. This slow production of H_2O_2 significantly improves the yield in the oxygenation of thioanisole to the corresponding sulfoxide from 30% (stoichiometric addition of H_2O_2, TON = 4900) to 100% (TON = 22400).

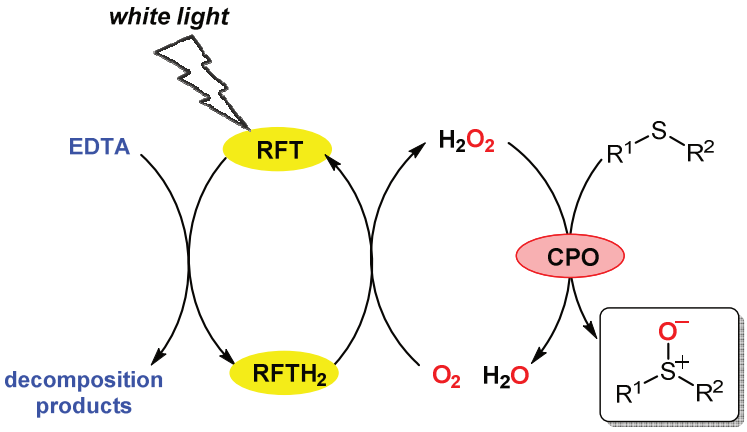

Scheme 47. Light-driven *in situ* H_2O_2 generation to promote CPO-catalyzed sulfoxidation reactions.

When *CPO* is substituted by *AaeAPO* (Agrocybe aegerita aromatic peroxygenase) the challenging enantiospecific hydroxylation of alkanes and epoxidation of alkenes becomes feasible.[157] Visible light irradiation (light bulb) of a mixture, containing photocatalyst FMN (flavin adenosine mononucleotide, 50 µM, 5 mol%), EDTA (1 mM), *AaeAPO* (40 nM, 0.004 mol%), and ethylbenzene (1 mM) gave *(R)*-1-phenylethanol (TON = 11470, *ee* >97%). The direct addition of H_2O_2 to *AaeAPO*/ethylbenzene in the dark is significantly less efficient (TON = 6000, *ee* = 97%). In addition, cyclohexane was hydroxylated to cyclohexanol in excellent efficiency (TON = 17900), whereas *n*-octane only reacted sluggishly (TON = 1040). The artificial photosystem EDTA/FMN/*AaeAPO* was also applied for the epoxidation of styrene and its derivatives. Styrene was converted to styrene oxide very efficiently (TON = 10390, *ee* > 4.6%), whereas a distinct dependency of the substitution pattern of the C=C double bond was observed. For example, *cis*-β-methyl styrene was converted efficiently (TON = 4740, *ee* > 99%) while its *trans* isomer only gave poor yields (TON < 500, *ee* = 4%). Additionally, cyclohexene was converted into the corresponding epoxide (TON = 3970) and allylic alcohol (TON = 1980) at a ratio of approximately 2 to 1.

1.4.5 Summary

The combination of $[Ru(bpy)_3]^{2+}$ photocatalysis with metal porphyrins and non-heme metal catalysts and a cheap, non-toxic electron acceptor such as $[Co(III)(NH_3)_5Cl]^{2+}$ enables the photocatalytic formation of high-valent metal oxo-species that oxygenate various substrates, such as sulfide to sulfoxide, sodium *p*-styrene sulfonate to the corresponding epoxide, and sodium 4-ethylbenzene sulfonate to the corresponding alcohol. The source of oxygen is water and not dioxygen in contrast to the vast majority of photocatalytic procedures described in chapter 1.1.

Dyads consisting of a photosensitizer covalently linked to an oxygenation catalyst also proved to be efficient catalysts. Most examples consist of a ruthenium-based photosensitizer Ru_{phot}, which is a derivate of $[Ru(bpy)_3]^{2+}$ and acts as a light harvester. A second Ru_{cat}−OH_2 complex, with a water molecule coordinated to ruthenium, performs the oxygenation reaction. The addition of an *electron acceptor* to $Ru_{phot}(II)$* triggers the light-induced electron transfer cascade *from the oxygenation catalyst* $Ru_{cat}(II)$−OH_2 to yield the active species $Ru_{cat}(IV)(O)$ for the sulfoxidation. Here, water covalently bound to the oxygenation complex is the oxygen source.

Ménage and co-workers impressively demonstrated that a dyad consisting of a $Ru_{phot}(II)$ moiety covalently linked to a Cu(II) catalyst oxygenates sulfides, phosphines, and alkenes with dioxygen as oxygen source. In contrast to the diruthenium-based assemblies which require a sacrificial electron acceptor, the addition of an *electron donor* to the $Ru_{phot}(II)$* moiety subsequently initiates the *electron transfer to the copper(II) center* to generate copper(I) as active species. This species activates dioxygen and performs the oxygen atom transfer to the substrate. The active copper(I) species is easily regenerated from copper(II) without the need of a sacrificial reductant, which was the main drawback of copper(I) oxygenation chemistry.

The combination of photocatalysis with enzyme catalysis enables the development of effective biocatalytic oxygenation reactions. A purely organic photocatalyst system based on photoactive riboflavin tetraacetate (RFT) and EDTA as a cheap sacrificial reductant was developed by Hollmann and co-workers. This system generates the oxidant H_2O_2 *in situ* in low concentrations. The performance of enzyme-catalyzed reactions such as the *CPO*- and *AaeAPO*-catalyzed sulfoxidation and enantiospecific hydroxylation of alkanes was significantly improved with respect to related reactions where H_2O_2 was added as terminal oxidant.

1.5 References

[1] A. Gunay, K. H. Theopold, *Chem. Rev.* **2010**, *110*, 1060–1081.

[2] A. S. Goldman, K. I. Goldberg, in *Act. Funct. CH Bonds*, American Chemical Society, **2004**, pp. 1–43.

[3] E. Roduner, W. Kaim, B. Sarkar, V. B. Urlacher, J. Pleiss, R. Gläser, W.-D. Einicke, G. A. Sprenger, U. Beifuß, E. Klemm, C. Liebner, H. Hiernoymus, S.-F. Hsu, B. Plietker, S. Laschat, *ChemCatChem* **2013**, *5*, 82–112.

[4] B. Meunier, S. P. de Visser, S. Shaik, *Chem. Rev.* **2004**, *104*, 3947–3980.

[5] I. Schlichting, J. Berendzen, K. Chu, A. M. Stock, S. A. Maves, D. E. Benson, R. M. Sweet, D. Ringe, G. A. Petsko, S. G. Sligar, *Science* **2000**, *287*, 1615–1622.

[6] E. Y. Tshuva, S. J. Lippard, *Chem. Rev.* **2004**, *104*, 987–1012.

[7] M. Costas, M. P. Mehn, M. P. Jensen, L. Que, *Chem. Rev.* **2004**, *104*, 939–986.

[8] M. M. Abu-Omar, A. Loaiza, N. Hontzeas, *Chem. Rev.* **2005**, *105*, 2227–2252.

[9] E. I. Solomon, T. C. Brunold, M. I. Davis, J. N. Kemsley, S.-K. Lee, N. Lehnert, F. Neese, A. J. Skulan, Y.-S. Yang, J. Zhou, *Chem. Rev.* **2000**, *100*, 235–350.

[10] P. C. A. Bruijnincx, I. L. C. Buurmans, S. Gosiewska, M. A. H. Moelands, M. Lutz, A. L. Spek, G. van Koten, R. J. M. Klein Gebbink, *Chem. – Eur. J.* **2008**, *14*, 1228–1237.

[11] M. Costas, K. Chen, L. Que Jr., *Coord. Chem. Rev.* **2000**, *200–202*, 517–544.

[12] E. P. Talsi, K. P. Bryliakov, *Coord. Chem. Rev.* **2012**, *256*, 1418–1434.

[13] F. Teplý, *Collect. Czechoslov. Chem. Commun.* **2011**, *76*, 859–917.

[14] D. M. Schultz, T. P. Yoon, *Science* **2014**, *343*, 1239176.

[15] C. K. Prier, D. A. Rankic, D. W. C. MacMillan, *Chem. Rev.* **2013**, 5322–5363

[16] S. Tang, W. Wu, Z. Fu, S. Zou, Y. Liu, H. Zhao, S. R. Kirk, D. Yin, *ChemCatChem* **2015**, *7*, 2637–2645.

[17] R. Yuan, S. Fan, H. Zhou, Z. Ding, S. Lin, Z. Li, Z. Zhang, C. Xu, L. Wu, X. Wang, X. Fu, *Angew. Chem. Int. Ed.* **2013**, *52*, 1035–1039.

[18] J. Long, S. Wang, Z. Ding, S. Wang, Y. Zhou, L. Huang, X. Wang, *Chem. Commun.* **2012**, *48*, 11656–11658.

[19] Y. Zhang, N. Zhang, Z.-R. Tang, Y.-J. Xu, *Chem. Sci.* **2012**, *3*, 2812–2822.

[20] Y. Shiraishi, N. Saito, T. Hirai, *J. Am. Chem. Soc.* **2005**, *127*, 12820–12822.

[21] Y. Shiraishi, Y. Teshima, T. Hirai, *Chem. Commun.* **2005**, 4569–4571.

[22] H. Sun, F. Blatter, H. Frei, *J. Am. Chem. Soc.* **1996**, *118*, 6873–6879.

[23] Z. Zheng, B. Huang, X. Qin, X. Zhang, Y. Dai, M.-H. Whangbo, *J. Mater. Chem.* **2011**, *21*, 9079–9087.

[24] M. C. DeRosa, R. J. Crutchley, *Coord. Chem. Rev.* **2002**, *233–234*, 351–371.

[25] D. Ashen-Garry, M. Selke, *Photochem. Photobiol.* **2014**, *90*, 257–274.

[26] D. N. Hendrickson, M. G. Kinnaird, K. S. Suslick, *J. Am. Chem. Soc.* **1987**, *109*, 1243–1244.

[27] L. Weber, R. Hommel, J. Behling, G. Haufe, H. Hennig, *J. Am. Chem. Soc.* **1994**, *116*, 2400–2408.

[28] A. Maldotti, C. Bartocci, G. Varani, A. Molinari, P. Battioni, D. Mansuy, *Inorg. Chem.* **1996**, *35*, 1126–1131.

[29] R. M. Richman, M. W. Peterson, *J. Am. Chem. Soc.* **1982**, *104*, 5795–5796.

[30] D.-H. Chin, G. N. La Mar, A. L. Balch, *J. Am. Chem. Soc.* **1980**, *102*, 4344–4350.

[31] I. G. Denisov, T. M. Makris, S. G. Sligar, I. Schlichting, *Chem. Rev.* **2005**, *105*, 2253–2278.

[32] J. T. Groves, Y. Watanabe, *J. Am. Chem. Soc.* **1988**, *110*, 8443–8452.

[33] L. Weber, R. Hommel, J. Behling, G. Haufe, H. Hennig, *J. Am. Chem. Soc.* **1994**, *116*, 2400.

[34] L. Weber, G. Haufe, D. Rehorek, H. Hennig, *J. Chem. Soc. Chem. Commun.* **1991**, 502–503.

[35] T.-H. Chen, N. Asiri, K. W. Kwong, J. Malone, R. Zhang, *Chem. Commun.* **2015**, *51*, 9949–9952.

[36] R. Zhang, R. E. P. Chandrasena, E. Martinez, J. H. Horner, M. Newcomb, *Org. Lett.* **2005**, *7*, 1193–1195.

[37] Z. Pan, Q. Wang, X. Sheng, J. H. Horner, M. Newcomb, *J. Am. Chem. Soc.* **2009**, *131*, 2621–2628.

[38] M. Christmann, *Angew. Chem. Int. Ed.* **2008**, *47*, 2740–2742.

[39] I. Aviv, Z. Gross, *Chem. Commun.* **2007**, 1987–1999.

[40] A. Mahammed, H. B. Gray, A. E. Meier-Callahan, Z. Gross, *J. Am. Chem. Soc.* **2003**, *125*, 1162–1163.

[41] D. N. Harischandra, R. Zhang, M. Newcomb, *J. Am. Chem. Soc.* **2005**, *127*, 13776–13777.

[42] B. J. Pistorio, C. J. Chang, D. G. Nocera, *J. Am. Chem. Soc.* **2002**, *124*, 7884–7885.

[43] J. Rosenthal, B. J. Pistorio, L. L. Chng, D. G. Nocera, *J. Org. Chem.* **2005**, *70*, 1885–1888.

[44] J. Rosenthal, T. D. Luckett, J. M. Hodgkiss, D. G. Nocera, *J. Am. Chem. Soc.* **2006**, *128*, 6546–6547.

[45] M. W. Peterson, D. S. Rivers, R. M. Richman, *J. Am. Chem. Soc.* **1985**, *107*, 2907–2915.

[46] I. M. Wasser, H. C. Fry, P. G. Hoertz, G. J. Meyer, K. D. Karlin, *Inorg. Chem.* **2004**, *43*, 8272–8281.

[47] D. N. Harischandra, G. Lowery, R. Zhang, M. Newcomb, *Org. Lett.* **2009**, *11*, 2089–2092.

[48] L. Weber, J. Behling, G. Haufe, H. Hennig, *J. Für Prakt. ChemieChemiker-Ztg.* **1992**, *334*, 265–268.

[49] J. Jung, K. Ohkubo, D. P. Goldberg, S. Fukuzumi, *J. Phys. Chem. A* **2014**, *118*, 6223–6229.

[50] K. A. Prokop, D. P. Goldberg, *J. Am. Chem. Soc.* **2012**, *134*, 8014–8017.

[51] J. Jung, K. Ohkubo, K. A. Prokop-Prigge, H. M. Neu, D. P. Goldberg, S. Fukuzumi, *Inorg. Chem.* **2013**, *52*, 13594–13604.

[52] H. M. Neu, J. Jung, R. A. Baglia, M. A. Siegler, K. Ohkubo, S. Fukuzumi, D. P. Goldberg, *J. Am. Chem. Soc.* **2015**, *137*, 4614–4617.

[53] S. Funyu, T. Isobe, S. Takagi, D. A. Tryk, H. Inoue, *J. Am. Chem. Soc.* **2003**, *125*, 5734–5740.

[54] E. Vanover, Y. Huang, L. Xu, M. Newcomb, R. Zhang, *Org. Lett.* **2010**, *12*, 2246–2249.

[55] S. Takagi, T. Okamoto, T. Shiragami, H. Inoue, *J. Org. Chem.* **1994**, *59*, 7373–7378.

[56] H. Inoue, S. Funyu, Y. Shimada, S. Takagi, *Pure Appl. Chem.* **2005**, *77*, DOI 10.1351/pac200577061019.

[57] H. Inoue, M. Sumitani, A. Sekita, M. Hida, *J. Chem. Soc. Chem. Commun.* **1987**, 1681–1682.

[58] H. Inoue, T. Okamoto, Y. Kameo, M. Sumitani, A. Fujiwara, D. Ishibashi, M. Hida, *J. Chem. Soc. [Perkin 1]* **1994**, 105–111.

[59] S. Takagi, M. Suzuki, T. Shiragami, H. Inoue, *J. Am. Chem. Soc.* **1997**, *119*, 8712–8713.

[60] T. Shiragami, K. Kubomura, D. Ishibashi, H. Inoue, *J. Am. Chem. Soc.* **1996**, *118*, 6311–6312.

[61] F. H. Burstall, *J. Chem. Soc. Resumed* **1936**, 173–175.

[62] F. Teplý, *Collect. Czechoslov. Chem. Commun.* **2011**, *76*, 859–917.

[63] M. A. Ischay, M. E. Anzovino, J. Du, T. P. Yoon, *J. Am. Chem. Soc.* **2008**, *130*, 12886–12887.

[64] D. A. Nicewicz, D. W. C. MacMillan, *Science* **2008**, *322*, 77–80.

[65] J. M. R. Narayanam, J. W. Tucker, C. R. J. Stephenson, *J. Am. Chem. Soc.* **2009**, *131*, 8756–8757.

[66] C. K. Prier, D. A. Rankic, D. W. C. MacMillan, *Chem. Rev.* **2013**, *113*, 5322–5363.

[67] J.-M. Zen, S.-L. Liou, A. S. Kumar, M.-S. Hsia, *Angew. Chem. Int. Ed.* **2003**, *42*, 577–579.

[68] Y. Su, L. Zhang, N. Jiao, *Org. Lett.* **2011**, *13*, 2168–2171.

[69] Y.-Q. Zou, J.-R. Chen, X.-P. Liu, L.-Q. Lu, R. L. Davis, K. A. Jørgensen, W.-J. Xiao, *Angew. Chem. Int. Ed.* **2012**, *51*, 784–788.

[70] J. D. Parrish, M. A. Ischay, Z. Lu, S. Guo, N. R. Peters, T. P. Yoon, *Org. Lett.* **2012**, *14*, 1640–1643.

[71] M. E. Selsted, H. W. Becker III, *Anal. Biochem.* **1986**, *155*, 270–274.

[72] K. Fafans, O. Hassel, *Z. Für Elektrochem. Angew. Phys. Chem.* **1923**, *29*, 495–500.

[73] M. Neumann, S. Füldner, B. König, K. Zeitler, *Angew. Chem. Int. Ed.* **2011**, *50*, 951–954.

[74] K. Fidaly, C. Ceballos, A. Falguières, M. S.-I. Veitia, A. Guy, C. Ferroud, *Green Chem.* **2012**, *14*, 1293–1297.

[75] M. Majek, A. Jacobi von Wangelin, *Angew. Chem. Int. Ed.* **2015**, *54*, 2270–2274.

[76] Z. Yang, H. Li, L. Zhang, M.-T. Zhang, J.-P. Cheng, S. Luo, *Chem. – Eur. J.* **2015**, *21*, 14723–14727.

[77] T. Lazarides, T. McCormick, P. Du, G. Luo, B. Lindley, R. Eisenberg, *J. Am. Chem. Soc.* **2009**, *131*, 9192–9194.

[78] A. Penzkofer, A. Beidoun, *Chem. Phys.* **1993**, *177*, 203–216.

[79] J. Zhang, L. Wang, Q. Liu, Z. Yang, Y. Huang, *Chem. Commun.* **2013**, *49*, 11662–11664.

[80] D. P. Hari, B. König, *Chem. Commun.* **2014**, *50*, 6688–6699.

[81] J. Li, H. Wang, L. Liu, J. Sun, *RSC Adv.* **2014**, *4*, 49974–49978.

[82] A. K. Yadav, V. P. Srivastava, L. D. S. Yadav, *New J. Chem.* **2013**, *37*, 4119–4124.

[83] R. Asahi, T. Morikawa, T. Ohwaki, K. Aoki, Y. Taga, *Science* **2001**, *293*, 269–271.

[84] X. Chen, L. Liu, P. Y. Yu, S. S. Mao, *Science* **2011**, *331*, 746–750.

[85] S. P. Pitre, C. D. McTiernan, H. Ismaili, J. C. Scaiano, *ACS Catal.* **2014**, *4*, 2530–2535.

[86] S. P. Pitre, C. D. McTiernan, H. Ismaili, J. C. Scaiano, *J. Am. Chem. Soc.* **2013**, *135*, 13286–13289.

[87] S. B. Bharate, *Synlett* **2006**, 0496–0497.

[88] S. M. Hubig, T. M. Bockman, J. K. Kochi, *J. Am. Chem. Soc.* **1997**, *119*, 2926–2935.

[89] S. Fukuzumi, K. Ohkubo, Y. Tokuda, T. Suenobu, *J. Am. Chem. Soc.* **2000**, *122*, 4286–4294.

[90] K. Ohkubo, A. Fujimoto, S. Fukuzumi, *J. Am. Chem. Soc.* **2013**, *135*, 5368–5371.

[91] Z. Shen, J. Dai, J. Xiong, X. He, W. Mo, B. Hu, N. Sun, X. Hu, *Adv. Synth. Catal.* **2011**, *353*, 3031–3038.

[92] K. Ohkubo, T. Kobayashi, S. Fukuzumi, *Angew. Chem. Int. Ed.* **2011**, *50*, 8652–8655.

[93] S. Fukuzumi, K. Ohkubo, *Org. Biomol. Chem.* **2014**, *12*, 6059–6071.

[94] K. Ohkubo, T. Kobayashi, S. Fukuzumi, *Opt. Express* **2012**, *20*, A360.

[95] S. Fukuzumi, H. Kotani, K. Ohkubo, S. Ogo, N. V. Tkachenko, H. Lemmetyinen, *J. Am. Chem. Soc.* **2004**, *126*, 1600–1601.

[96] K. Ohkubo, K. Mizushima, R. Iwata, S. Fukuzumi, *Chem. Sci.* **2011**, *2*, 715–722.

[97] J.-M. M. Grandjean, D. A. Nicewicz, *Angew. Chem. Int. Ed.* **2013**, *52*, 3967–3971.

[98] D. S. Hamilton, D. A. Nicewicz, *J. Am. Chem. Soc.* **2012**, *134*, 18577–18580.

[99] T. M. Nguyen, D. A. Nicewicz, *J. Am. Chem. Soc.* **2013**, *135*, 9588–9591.

[100] A. J. Perkowski, D. A. Nicewicz, *J. Am. Chem. Soc.* **2013**, *135*, 10334–10337.

[101] S. Fukuzumi, K. Ohkubo, *Org. Biomol. Chem.* **2014**, *12*, 6059–6071.

[102] S. Fukuzumi, K. Ohkubo, *Chem. Sci.* **2013**, *4*, 561–574.

[103] K. Ohkubo, S. Fukuzumi, *Org. Lett.* **2000**, *2*, 3647–3650.

[104] K. Ohkubo, K. Suga, K. Morikawa, S. Fukuzumi, *J. Am. Chem. Soc.* **2003**, *125*, 12850–12859.

[105] K. Suga, K. Ohkubo, S. Fukuzumi, *J. Phys. Chem. A* **2005**, *109*, 10168–10175.

[106] K. Suga, K. Ohkubo, S. Fukuzumi, *J. Phys. Chem. A* **2003**, *107*, 4339–4346.

[107] K. Suga, K. Ohkubo, S. Fukuzumi, *J. Phys. Chem. A* **2006**, *110*, 3860–3867.

[108] K. Ohkubo, K. Mizushima, R. Iwata, K. Souma, N. Suzuki, S. Fukuzumi, *Chem. Commun.* **2010**, *46*, 601–603.

[109] S. Fukuzumi, K. Doi, A. Itoh, T. Suenobu, K. Ohkubo, Y. Yamada, K. D. Karlin, *Proc. Natl. Acad. Sci.* **2012**, *109*, 15572–15577.

[110] Y. Yamada, K. Maeda, K. Ohkubo, K. D. Karlin, S. Fukuzumi, *Phys. Chem. Chem. Phys.* **2012**, *14*, 9654–9659.

[111] H. Yi, C. Bian, X. Hu, L. Niu, A. Lei, *Chem. Commun.* **2015**, *51*, 14046–14049.

[112] A. G. Griesbeck, M. Cho, *Org. Lett.* **2007**, *9*, 611–613.

[113] K. Ohkubo, T. Nanjo, S. Fukuzumi, *Bull Chem Soc Jpn* **2006**, *79*, 1489.

[114] K. Ohkubo, K. Mizushima, S. Fukuzumi, *Res. Chem. Intermed.* **2012**, *39*, 205–220.

[115] K. Ohkubo, A. Fujimoto, S. Fukuzumi, *Chem. Commun.* **2011**, *47*, 8515–8517.

[116] K. Ohkubo, T. Nanjo, S. Fukuzumi, *Org. Lett.* **2005**, *7*, 4265–4268.

[117] H. Kotani, K. Ohkubo, S. Fukuzumi, *J. Am. Chem. Soc.* **2004**, *126*, 15999–16006.

[118] T. Hering, T. Slanina, A. Hancock, U. Wille, B. König, *Chem. Commun.* **2015**, *51*, 6568–6571.

[119] S. Hirashima, A. Itoh, *Photochem. Photobiol. Sci.* **2007**, *6*, 521–524.

[120] S. Hirashima, T. Nobuta, N. Tada, T. Miura, A. Itoh, *Org. Lett.* **2010**, *12*, 3645–3647.

[121] N. Tada, Y. Ikebata, T. Nobuta, S. Hirashima, T. Miura, A. Itoh, *Photochem. Photobiol. Sci.* **2012**, *11*, 616–619.

[122] S. Ghisla, V. Massey, *Eur. J. Biochem.* **1989**, *181*, 1–17.

[123] E. Silva, A. M. Edwards, Eds. , *Flavins: Photochemistry and Photobiology*, Royal Society Of Chemistry, Cambridge, **2006**.

[124] G. de Gonzalo, M. W. Fraaije, *ChemCatChem* **2013**, *5*, 403–415.

[125] H. Schmaderer, P. Hilgers, R. Lechner, B. König, *Adv. Synth. Catal.* **2009**, *351*, 163–174.

[126] J. Svoboda, H. Schmaderer, B. König, *Chem. – Eur. J.* **2008**, *14*, 1854–1865.

[127] R. Cibulka, R. Vasold, B. König, *Chem. – Eur. J.* **2004**, *10*, 6223–6231.

[128] B. König, Ed. , *Chemical Photocatalysis*, De Gruyter, **n.d.**

[129] R. Lechner, B. König, *Synthesis* **2010**, *2010*, 1712–1718.

[130] J. Dad'ová, E. Svobodová, M. Sikorski, B. König, R. Cibulka, *ChemCatChem* **2012**, *4*, 620–623.

[131] V. Mojr, E. Svobodová, K. Straková, T. Neveselý, J. Chudoba, H. Dvořáková, R. Cibulka, *Chem Commun* **2015**, *51*, 12036–12039.

[132] R. Lechner, S. Kümmel, B. König, *Photochem. Photobiol. Sci.* **2010**, *9*, 1367.

[133] S. Fukuzumi, S. Kuroda, T. Tanaka, *J. Am. Chem. Soc.* **1985**, *107*, 3020.

[134] S. Fukuzumi, K. Yasui, T. Suenobu, K. Ohkubo, M. Fujitsuka, O. Ito, *J. Phys. Chem. A* **2001**, *105*, 10501–10510.

[135] S. Fukuzumi, T. Kishi, H. Kotani, Y.-M. Lee, W. Nam, *Nat. Chem.* **2011**, *3*, 38–41.

[136] X. Wu, X. Yang, Y.-M. Lee, W. Nam, L. Sun, *Chem. Commun.* **2015**, *51*, 4013–4016.

[137] H. Kotani, T. Suenobu, Y.-M. Lee, W. Nam, S. Fukuzumi, *J. Am. Chem. Soc.* **2011**, *133*, 3249–3251.

[138] A. Company, G. Sabenya, M. González-Béjar, L. Gómez, M. Clémancey, G. Blondin, A. J. Jasniewski, M. Puri, W. R. Browne, J.-M. Latour, et al., *J. Am. Chem. Soc.* **2014**, *136*, 4624–4633.

[139] C. Herrero, A. Quaranta, R. Ricoux, A. Trehoux, A. Mahammed, Z. Gross, F. Banse, J.-P. Mahy, *Dalton Trans.* **2015**, *45*, 706–710.

[140] C. Herrero, A. Quaranta, M. Sircoglou, K. Sénéchal-David, A. Baron, I. M. Marín, C. Buron, J.-P. Baltaze, W. Leibl, A. Aukauloo, et al., *Chem. Sci.* **2015**, *6*, 2323–2327.

[141] W. Iali, P.-H. Lanoe, S. Torelli, D. Jouvenot, F. Loiseau, C. Lebrun, O. Hamelin, S. Ménage, *Angew. Chem. Int. Ed.* **2015**, *54*, 8415–8419.

[142] N. Kaveevivitchai, R. Chitta, R. Zong, M. El Ojaimi, R. P. Thummel, *J. Am. Chem. Soc.* **2012**, *134*, 10721–10724.

[143] D. L. Ashford, D. J. Stewart, C. R. Glasson, R. A. Binstead, D. P. Harrison, M. R. Norris, J. J. Concepcion, Z. Fang, J. L. Templeton, T. J. Meyer, *Inorg. Chem.* **2012**, *51*, 6428–6430.

[144] F. Li, Y. Jiang, B. Zhang, F. Huang, Y. Gao, L. Sun, *Angew. Chem. Int. Ed.* **2012**, *51*, 2417–2420.

[145] W. Chen, F. N. Rein, B. L. Scott, R. C. Rocha, *Chem. – Eur. J.* **2011**, *17*, 5595–5604.

[146] W. Chen, F. N. Rein, R. C. Rocha, *Angew. Chem. Int. Ed.* **2009**, *48*, 9672–9675.

[147] D. Chao, W.-F. Fu, *Dalton Trans.* **2013**, *43*, 306–310.

[148] D. Chao, W.-F. Fu, *Chem. Commun.* **2013**, *49*, 3872–3874.

[149] O. Hamelin, P. Guillo, F. Loiseau, M.-F. Boissonnet, S. Ménage, *Inorg. Chem.* **2011**, *50*, 7952–7954.

[150] P. Guillo, O. Hamelin, P. Batat, G. Jonusauskas, N. D. McClenaghan, S. Ménage, *Inorg. Chem.* **2012**, *51*, 2222–2230.

[151] P. Farràs, S. Maji, J. Benet-Buchholz, A. Llobet, *Chem. – Eur. J.* **2013**, *19*, 7162–7172.

[152] T.-T. Li, F.-M. Li, W.-L. Zhao, Y.-H. Tian, Y. Chen, R. Cai, W.-F. Fu, *Inorg. Chem.* **2015**, *54*, 183–191.

[153] A. Taglieber, F. Schulz, F. Hollmann, M. Rusek, M. T. Reetz, *ChemBioChem* **2008**, *9*, 565–572.

[154] F. Hollmann, A. Taglieber, F. Schulz, M. T. Reetz, *Angew. Chem. Int. Ed.* **2007**, *46*, 2903–2906.

[155] D. I. Perez, M. M. Grau, I. W. C. E. Arends, F. Hollmann, *Chem. Commun.* **2009**, 6848.

[156] E. Churakova, I. W. C. E. Arends, F. Hollmann, *ChemCatChem* **2013**, *5*, 565–568.

[157] E. Churakova, M. Kluge, R. Ullrich, I. Arends, M. Hofrichter, F. Hollmann, *Angew. Chem. Int. Ed.* **2011**, *50*, 10716–10719.

2 Photocatalytic Benzylic C−H Bond Oxidation with a Flavin Scandium Complex[a]

Bernd Mühldorf and Robert Wolf

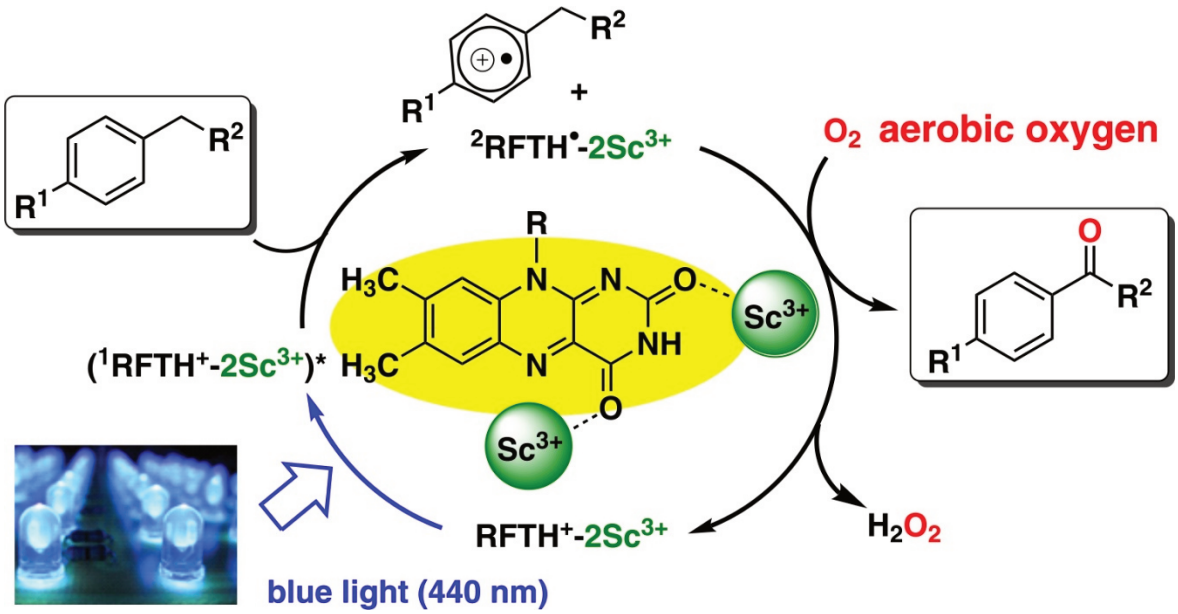

[a] Bernd Mühldorf and Robert Wolf, *Chem. Commun.*, **2015**, *51*, 8425-8428; DOI: 10.1039/C5CC00178A; First published online 05 Feb 2015

2.1 Introduction

The important role of flavins as photoreceptors and redox cofactors in nature has inspired the use of synthetic flavin analogues as bioinspired photocatalysts.[1] The most prominent example, riboflavin tetraacetate (RFT), catalyses the aerobic photooxidation of benzyl alcohols,[2] benzyl amines,[3] and sulfoxides (Scheme 1).[4-5] A particularly intriguing application of RFT is the photocatalytic C−H bond oxidation of alkyl benzenes to the corresponding aldehydes.[6-7] Spectroscopic studies revealed an initial electron transfer from the aromatic substrate to the singlet excited state ^{1}RFT* as the basis of this process.[8] However, the limited reduction potential $E_0(^1RFT^*/^2RFT^-) = 1.67$ V vs. SCE exclusively allows the oxidation of very few selected substrates which feature strongly electron-donating arene substituents. Most other substrates are unsuccessful, because their oxidation potential is too positive.

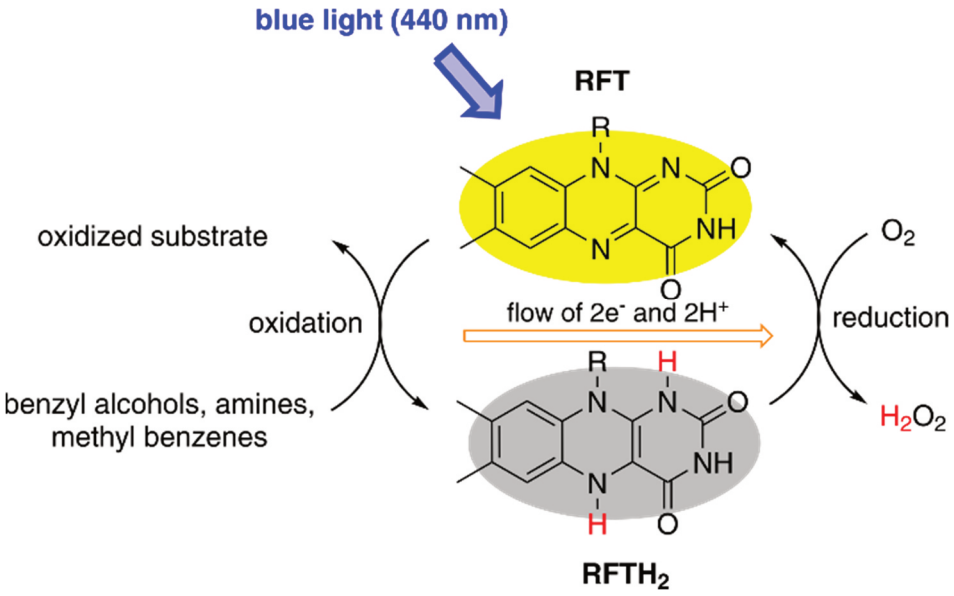

Scheme 1: Photocatalytic cycle for the aerobic oxidation of various organic substrates with riboflavin tetraacetate (RFT) and blue light[5]

Fukuzumi et al. found that the redox potential of RFT can be modified by metal ion coordination.[9] As shown in Figure 1, complexes of RFT with Mg^{2+}, Zn^{2+}, Yb^{3+} and Sc^{3+} ions have a significantly more positive reduction potential $E_0(^1RFT^*/^2RFT^-)$ in the excited singlet state. In particular, the Sc^{3+} system appears promising as it features high fluorescence quenching rate constants of $(^1RFT\text{-}2Sc^{3+})^*$ in the presence of alkyl- and methoxy-substituted benzenes.[8] This indicates an efficient single electron transfer from the substrate to $(^1RFT\text{-}2Sc^{3+})^*$, which is a prerequisite for photocatalytic activity.

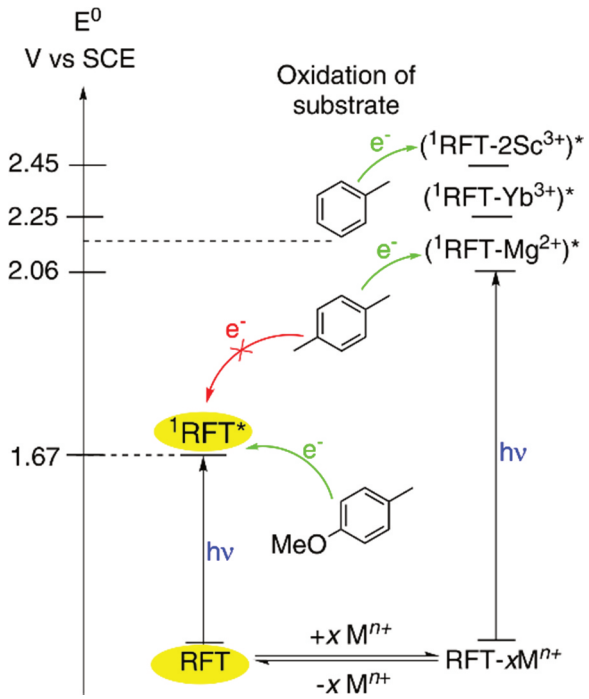

Figure 1: Enhanced reduction potentials $E^0(^1RFT^*/^2RFT^{-})$ of RFT-metal ion complexes (RFT-xM^{y+}).[8-9]

2.2 Results and Discussion

The reaction of ethylbenzene (**1**) to acetophenone (**2**) was chosen as a benchmark (Scheme 2), because **1** shows a high oxidation peak potential ($E_p^0(\mathbf{1}^{+\bullet}/\mathbf{1})$ = 2.14 vs SCE) and therefore cannot be oxidized by ^{1}RFT* alone.[8]]

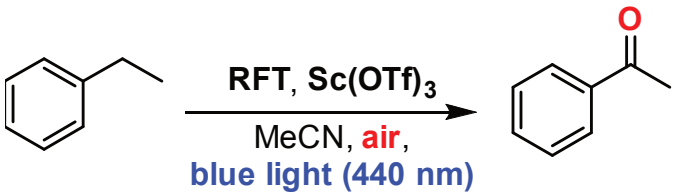

Scheme 2: Photocatalytic oxidation of ethylbenzene (**1**) to acetophenone (**2**)

A screening of various Lewis acids (Table S1, ESI†) and solvents (Table S2†) indicated $Sc(OTf)_3$ in acetonitrile to be the best choice. Irradiation of **1** (0.02 mmol) in CH_3CN for 2.5 h with blue light (440 nm) in the presence of RFT (10 mol%) and $Sc(OTf)_3$ (20 mol%) afforded acetophenone **2** in 58% yield. Substrate **1** was completely consumed, and the formation of H_2O_2 was confirmed by UV-vis spectroscopy (Figure S1†). Note that **2** is formed in <10% yield in the absence of Sc^{3+}-ions, while $Mg(OTf)_2$ and $Zn(OTf)_2$ gave only very low yields of **2**. The reaction is significantly accelerated by higher Sc^{3+} concentrations (Figure S2†). In order to reduce the amount of $Sc(OTf)_3$ required, the effect of acids and other additives was investigated (Table S3†). Importantly,

1 is converted nearly four times as fast in the presence of HCl (30 mol%) with the same $Sc(OTf)_3$ concentration (Figure S3†). Using this optimized system, we subsequently assessed the substrate scope (Table 1).

Toluene is converted to benzaldehyde in 71% yield, while *p*-*tert*-butylbenzaldehyde and *p*-chlorbenzaldehyde are obtained in 68% and 84% yield, respectively (entry 1). Benzylethers do not give the corresponding esters, but benzaldehydes (entry 3). Diarylmethylene derivatives (entry 4) and benzyl alcohols (entries 5 and 6) are oxidised with good to excellent yields as well. Triphenylmethane and diphenylacetic acid both yield

Table 1: Photocatalytic oxidation: Scope and limitations

Entry	Substrate	Product	No Sc^{3+} Yield [%][b]	R	Conv. [%][b]	Yield [%][b]
1	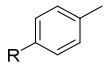	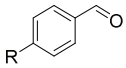	0	H	96	71
			5	^{t}Bu	100	68
			8	Me[d]	100	62
			0	Cl[d]	100	84
			0	CN	56	29
			0	CO_2Me	44	15
2	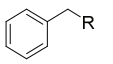	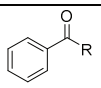	3	Me	100	60
			0	CO_2Me	92	49
3[c]	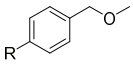	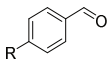	0	H	93	90
			5	OMe	100	63
4	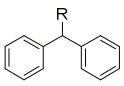	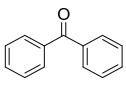	4	H	100	93
			6	Ph	89	52
			23	COOH	n.d.	80
5	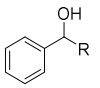		17	H	100	95
			0	Me	100	81
6[c]	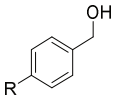	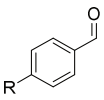	7	F	100	88
			12	Cl	100	73
			14	Br	100	84
			0	CF_3	63	53
			0	NO_2[d]	66	44

[a] All reactions were performed with substrate (0.02 mmol), RFT (10 mol%), HCl (37%, 0.8 µL) and $Sc(OTf)_3$ (4.6 mM) in 1 mL MeCN and irradiated with blue light (440 nm, 3 W) for 2.5 h when not indicated otherwise (see [d]). [b] Conversion and yield determined by GC-FID integration. [c] no HCl added; n.d. = not determined. [d] Irradiation time: 0.5 h (R = Me), 1 h (R = Cl) and 7 h (R = NO_2).

benzophenone *via* oxidative C–C cleavage.[10] Note that the oxidations of *p*-trifluorobenzyl alcohol and *p*-nitrobenzyl alcohol proceed selectively, but the reaction speed is slow, resulting in an incomplete conversion.

Control experiments confirmed that the reaction does not proceed in the dark, in the absence of RFT or under anaerobic conditions (Table S4†, entries 1–5). When the reaction was carried out in an atmosphere of pure dioxygen, slower bleaching of RFT was observed (Fig. S4†), but the yield of **2** did not improve (Table S4†, entry 6). Moreover, a very similar yield (44%) was obtained in deuterated acetonitrile, therefore, a singlet oxygen pathway seems unlikely (Table S4†, entries 7 and 8).[11-12]

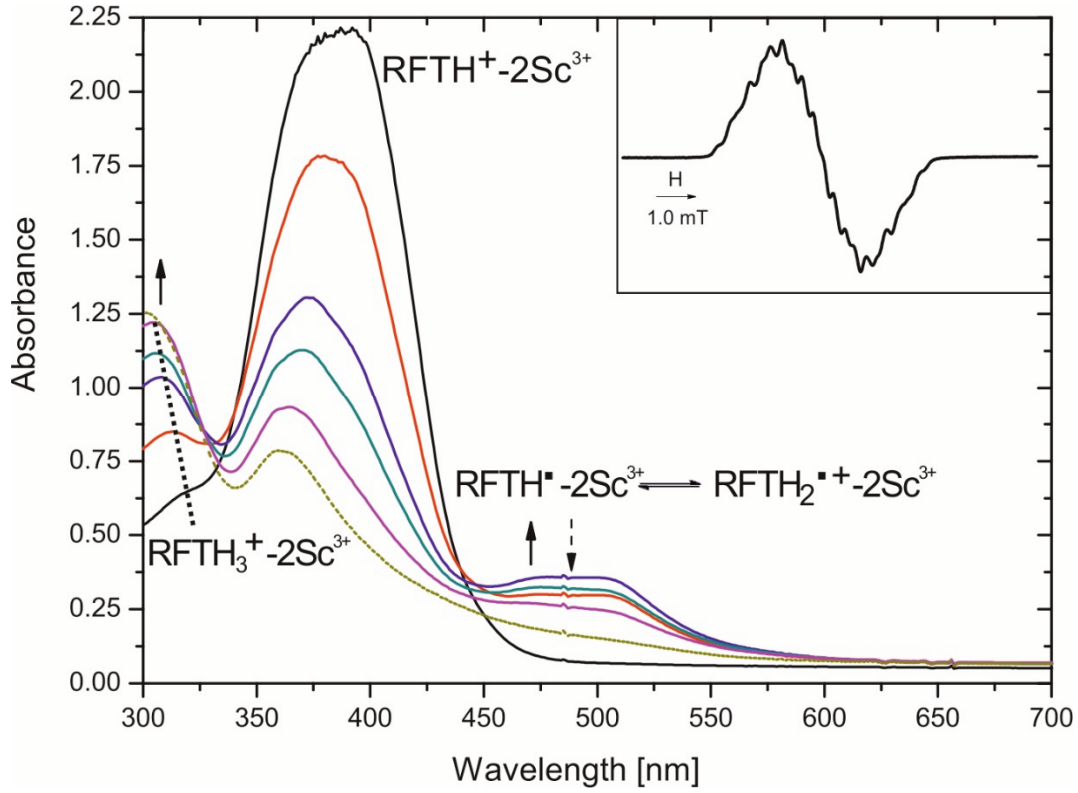

Figure 2: UV-vis absorption spectra of ethylbenzene (5.8 mM) and RFT (0.14 mM) in the presence of $Sc(OTf)_3$ (0.68 mM) and HCl (2.7 mM) during irradiation with blue light in deaereated MeCN at 298 K under nitrogen (straight: 0 s, 60 s, 120 s, 180 s, 360s; dashed: 2h). Inset: ESR-spectrum of $^{2}RFTH_2^{\bullet+}$-$2Sc^{3+}$ generated in the photocatalytic reaction RFT (3.0 mM) with ethylbenzene (20 mM), $Sc(OTf)_3$ (10 mM) and 10 mM $HClO_4$ in deaerated MeCN at 298 K. Parameters obtained by computer simulation: g = 2.0033, $a(N^5)$ = 6.7 G, $a(N^{10})$ = 4.6 G, $a(H^5)$ = 10.6 G, $a(3H^8)$ = 2.9 G, $a(N^{10}\text{-}CH_2)$ = 4.3 G; see the ESI for the labelling scheme.

The reaction mechanism was probed by UV-vis spectroscopy. Before starting to irradiate a mixture of **1**, RFT, $Sc(OTf)_3$ and HCl in acetonitrile with blue light (440 nm), an absorption band can be identified at λ_{max} = 390 nm both under aerobic conditions (Figure S5†) and under argon (Figure 2). This band may be assigned to $RFTH^+$-$2Sc^{3+}$ by comparison with the characteristic spectrum of uncoordinated $RFTH^+$.[13] The IR spectrum of the mixture shows that the C=O stretching bands are shifted to lower frequency compared to those of $RFTH^+$ in the absence of metal ions (Table S5†). This indicates that the scandium(III) ions coordinate to the carbonyl groups in $RFTH^+$-$2Sc^{3+}$.[8]

No structural information is presently available on the scandium(III) complexes in solution, though it seems likely that these correspond to neutral or cationic complexes or clusters with the general composition $[Sc_xX_y(RFTH_n)_z]^{m+}$ (X = OTf or Cl). We choose to designate the species involved in the catalytic mechanism as $RFTH_n^{m+}$-$2Sc^{3+}$ for simplicity.

A possible catalytic cycle is displayed in Scheme 3. In line with previous fluorescence quenching experiments by Fukuzumi *et al.*, we propose that the electron transfer occurs between the substrate and the photoexcited flavin metal complex ($^1RFTH^+$-$2Sc^{3+}$)* in its singlet state (step *i*).[8] This electron transfer produces the ethylbenzene radical cation **4** and the protonated flavin radical complex $^2RFTH^{\bullet}$-$2Sc^{3+}$. It seems likely that the $^2RFTH^{\bullet}$-$2Sc^{3+}$ complex is then protonated to yield $^2RFTH_2^{\bullet+}$-$2Sc^{3+}$, while the strongly acidic ethylbenzene radical cation **4** is deprotonated to the benzyl radical **5** (step *ii*).[14] The pK_a of the closely-related $RFTH_2^{+\bullet}$ radical is approximately 2, while the pK_a of a toluene radical cation in MeCN is estimated to −12 to −13.[17] $^2RFTH_2^{\bullet+}$-$2Sc^{3+}$ should give rise to a broad absorptions at λ_{max} = 400–550 nm similar to those of the uncoordinated dihydroflavin radical cation $^2RFTH_2^{\bullet+}$.[15] Such a broad band is indeed observed in the UV-vis spectrum of the reaction mixture under argon (Figure 2). In addition, the ESR spectrum of the reaction mixture of **1**, RFT, $Sc(OTf)_3$ for $^2RFTH_2^{\bullet+}$-$2Sc^{3+}$.[8] The hyperfine coupling constants obtained by computer simulation are similar to those reported for free $^2RFTH_2^{\bullet+}$.[16] The ESR spectrum of a mixture of **1**, RFT, $Sc(OTf)_3$ and HCl (instead of $HClO_4$, Figure S6†) is more complicated and thus defied a satisfactory simulation so far. This is presumably due to the formation of an equilibrium between $RFTH_2^{\bullet+}$-$2Sc^{3+}$ and $RFTH^{\bullet}$-$2Sc^{3+}$ with the weaker acid HCl.

There are at least two conceivable pathways that connect the benzyl radical **5** with the final product **2** (Scheme 3). One possibility is that $^2RFTH2^{\bullet+}$-$2Sc^{3+}$ recombines with **5** to form a covalent RFT-benzyl radical adduct (not shown in Scheme 3), which rapidly collapses under irradiation in air to product **2** and $RFTH^+$-$2Sc^{3+}$ (**3**).[19] However, this pathway seems less likely based on the UV-vis spectra of the reaction mixture, where characteristic broad absorptions are expected for such an adduct at λ_{max} = 600–630 nm. An alternative pathway is the conversion of **5** into the benzylperoxyl radical **6**, which subsequently transforms into **2** *via* the benzyl hydroperoxide.[18] As observed for $^2RFTH_2^{\bullet+}$, $^2RFTH_2^{\bullet+}$-$2Sc^{3+}$ may disproportionate into oxidized $RFTH^+$-$2Sc^{3+}$ and the reduced dihydroflavin $RFTH_3^+$-$2Sc^{3+}$ (step *iii*).[15] The formation of the latter species is supported by the observation of an absorption band at 295 nm that increases over time (see Figure 2).[15] $RFTH_3^+$-$2Sc^{3+}$ can react with dioxygen, regenerating **3** while producing H_2O_2 (Figure S8†).[16] In addition, $RFTH^+$-$2Sc^{3+}$ (**3**) may also be regenerated by the direct reaction of $^2RFTH_2^{\bullet+}$-$2Sc^{3+}$ with O_2 (step *iv,* Figure S7†). This process may conceivably be facili-

tated by Lewis acid coordination.[20] We presume that the mechanism of the catalytic oxidation of benzyl alcohols (Table S1, entries 5 and 6) is analogous to the one previously suggested by Fukuzumi *et al.* for the oxidation *p*-chlorobenzyl alcohol.[8] The proposed catalytic cycle involves an initial electron transfer from the substrate to (^{1}RFT-2Sc^{3+})*, followed by proton transfer forming the hydroxybenzyl radical (*p*-R-C$_6$H$_4$CHOH$^\bullet$) and protonated RFT radical anion (^{2}RFTH$^\bullet$-2Sc^{3+})*. Subsequent H atom transfer between these species yields the aldehyde and RFTH$_2$-2Sc^{3+}.

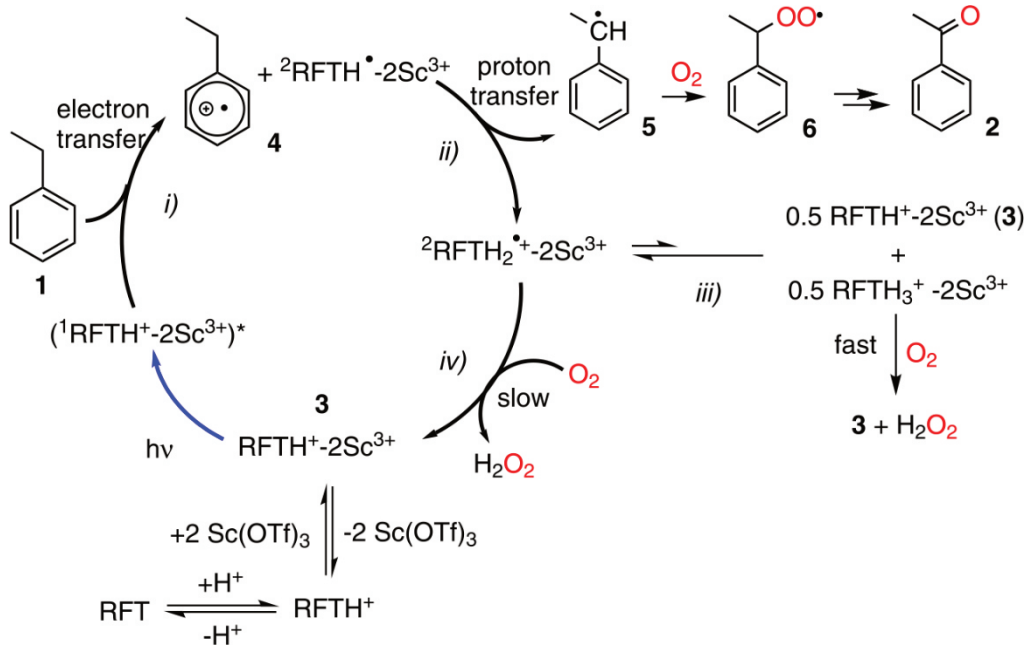

Scheme 3: Proposed mechanism for the photocatalytic aerobic oxidation of ethylbenzene (**1**) to acetophenone (**2**) with RFT in the presence of Sc^{3+}-ions and HCl.

2.3 Conclusion

In summary, RFT/scandium triflate is an efficient photocatalytic system for the aerobic oxidation of alkylbenzenes and electron deficient benzyl alcohols. The results show that the well-known effect of Lewis acid coordination on the redox potential of flavins[6] can be exploited to improve their photocatalytic properties. An extension of this principle, and an exploration of the effects of other metal ions including redox-active ones, is shown in the next chapter.

2.4 References

[1] a) S. Ghisla and V. Massey, *Eur. J. Biochem.*, **1989**, *181*, 1–17; b) E. Silva and A. M. Edwards, Eds., *Flavins: Photochemistry and Photobiology*, Royal Society of Chemistry, Cambridge, **2006**, vol. 6.

[2] a) H. Schmaderer, P. Hilgers, R. Lechner and B. König, *Adv. Synth. Catal*., **2009**, *351*, 163–174; b) J. Svoboda, H. Schmaderer and B. König, *Chem. – Eur. J*., **2008**, *14*, 1854–1865; c) R. Cibulka, R. Vasold and B. König, *Chem. – Eur. J.*, **2004**, *10*, 6223–6231; d) B. König, S. Kümmel, R. Cibulka in B. König, ed., Chemical Photocatalysis, de Gruyter, Berlin, **2013**, p. 44-61.

[3] R. Lechner and B. König, *Synthesis*, **2010**, 1712–1718

[4] J. Dad´ová, E. Svobodová, M. Sikorski, B. König and R. Cibulka, *ChemCatChem*, **2012**, *4*, 620–623.

[5] U. Megerle, M. Wenninger, R.-J. Kutta, R. Lechner, B. König, B. Dick and E. Riedle, *Phys. Chem. Chem. Phys.*, **2011**, *13*, 8869.

[6] a) J. Rosenthal, T. D. Luckett, J. M. Hodgkiss and D. G. Nocera, *J. Am. Chem. Soc*., **2006,** *128*, 6546–6547; b) K. Ohkubo and S. Fukuzumi, *Org. Lett*., **2000**, *2*, 3647–3650; c) K. Ohkubo, K. Suga, K. Morikawa and S. Fukuzumi, *J. Am. Chem. Soc*., **2003**, *125*, 12850–12859.

[7] R. Lechner, S. Kümmel and B. König, *Photochem. Photobiol. Sci*., **2010**, *9*, 1367.

[8] S. Fukuzumi, K. Yasui, T. Suenobu, K. Ohkubo, M. Fujitsuka and O. Ito, *J. Phys. Chem. A*, **2001**, *105*, 10501–10510.

[9] S. Fukuzumi, S. Kuroda and T. Tanaka, *J. Am. Chem. Soc*., **1985**, *107*, 3020.

[10] R. Akaba, M. Kamata, H. Itoh, A. Nakao, S. Goto, K. Saito, A. Negishi, H. Sakuragi and K. Tokumaru, *Tetrahedron Lett*., **1992**, *33*, 7011–7014.

[11] a) E. Sikorska, M. Sikorski, R. P. Steer, F. Wilkinson and D. R. Worrall*, J. Chem. Soc. Faraday Trans.*, **1998**, *94*, 2347–2353; b) E. Sikorska, I. Khmelinskii, A. Komasa, J. Koput, L. F. V. Ferreira, J. R. Herance, J. L. Bourdelande, S. L. Williams, D. R. Worrall, M. Insińska-Rak and M. Sikorski, *Chem. Phys.*, **2005**, *314*, 239–247.

[12] Related reactions proceed *via* a singlet oxygen pathway: a) J. Dad'ová, E. Svobodová, M. Sikorski, B. König and R. Cibulka, *ChemCatChem*, **2012**, *4*, 620–623; b) S. Fukuzumi, K. Tanii and T. Tanaka, *J. Chem. Soc. Perkin Trans. 2*, **1989**, 2103–2108.

[13] P. Hemmerich, C. Veeger and H. C. S. Wood, *Angew. Chem. Int. Ed. Engl*., **1965**, *4*, 671–687.

[14] P. F. Heelis, *Chem. Soc. Rev*., **1982**, *11*, 15–39.

[15] S. Fukuzumi and S. Kuroda, *Res. Chem. Intermed*., **1999**, *25*, 789.

[16] S. Fukuzumi and T. Kojima, *J. Biol. Inorg. Chem*., **2008**, *13*, 321–333.

[17] a) M. M. Green and S. L. Mielke, *J. Org. Chem*., **1984**, *49*, 1276–1278; b) A. M. de P. Nicholas and D. R. Arnold, *Can. J. Chem*., **1982**, *60*, 2165–2179.

[18] S. Fukuzumi, S. Kuroda, T. Goto, K. Ishikawa and T. Tanaka, *J. Chem. Soc. Perkin Trans. 2*, **1989**, 1047.

[19] a) W. H. Walker, P. Hemmerich and V. Massey, *Eur. J. Biochem*., **1970**, *13*, 258–266; b) W. H. Walker, P. Hemmerich and V. Massey, *Helv. Chim. Acta*, **1967**, *50*, 2269–2279; c) R. Lechner, S. Kümmel and B. König, *Photochem. Photobiol. Sci.,* **2010**, *9*, 1367 and references therein.

[20] K. Ohkubo, S. C. Menon, A. Orita, J. Otera and S. Fukuzumi, *J. Org. Chem*., **2003**, *68*, 4720–4726.

2.5 Supporting Information

2.5.1 General considerations

Materials

Most starting materials were purchased from commercial suppliers and freshly distilled or used as received. RFT was synthesized by esterification of commercial available riboflavin.[1]

Representative procedure: Oxidation of Ethylbenzene

Ethylbenzene (0.02 mmol) was added to RFT (10 mol%), $Sc(OTf)_3$ (20 mol% unless indicated otherwise) and hydrochloric acid (37%, 0.8 μL) in 1 mL acetonitrile. The reaction vial was placed in a cooling block to maintain a constant temperature and the vials were irradiated with blue LEDs (440 nm, 6 W LED unless indicated otherwise) while stirring with a magnetic stirring bar. After 2.5 h of irradiation, *n*-pentadecane or cyclooctanone (internal standard), saturated Na_2CO_3 and brine were added. The organic phase was extracted with ethylacetate and subjected to GC-FID analysis. The retention time was verified with authentic samples.

The formation of H_2O_2 was monitored by a standard method.[2] A diluted acetonitrile solution was treated with an excess amount of NaI. The concentration of I_3^- formed was determined by UV-Vis spectroscopy (λ_{max} = 362 nm, ε = 13000 $M^{-1}cm^{-1}$).

ESR spectroscopy

RFT (3 mM), ethylbenzene (10 mM), $Sc(OTf)_3$ (10 mM) and HCl (10 mM) were dissolved in degassed MeCN (1 mL). An aliquot was placed in a closed glas tube, irradiated and introduced into the ESR apparatus (Magnettech miniscope MS400). Simulations of the ESR spectra were performed with the Easyspin software 4.5.5 implemented in MATLAB R2012a.[3] Labelling scheme for the simulated hfc couplings:

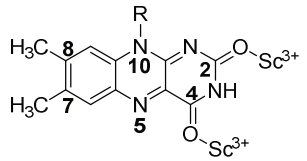

R = $CH_2CH(OAc)CH(OAc)CH(OAc)CH_2(OAc)$

References

[1] S. Alagaratnam, N. J. Meeuwenoord, J. A. Navarro, M. Hervás, M. A. De la Rosa, M. Hoffmann, O. Einsle, M. Ubbink and G. W. Canters, *FEBS J.*, **2011**, *278*, 1506–1521.

[2] R. D. Mair and A. J. Graupner, *Anal Chem.*, **36**, 194.

[3] S. Stoll and A. Schweiger, *J. Magn. Reson.*, **2006**, *178*, 42–55.

2.5.2 Photocatalytic oxidation of ethylbenzene – influence of the Lewis acid. (Table S1)

Table S1. Photocatalytic oxidation of ethylbenzene – influence of the Lewis acid.

Entry	Lewis acid	Conv. [%][b]	Yield [%][b]
1	$Sc(OTf)_3$	81	38
2	$Mg(OTf)_2$	19	1
3	$La(OTf)_3$	25	2
4	$Zn(OTf)_2$	30	3
5	$AlCl_3$	31	6

[a] All reactions were performed with ethylbenzene (0.02 mmol), RFT (10 mol%), and Lewis acid (4.6 mM) in 1 mL MeCN and irradiated for 2.5 h with blue light (440 nm). [b] Conversion of 1 and yield of 2 determined by GC-FID.

2.5.3 Photocatalytic oxidation of ethylbenzene – influence of the solvent. (Table S2)

Table S2. Photocatalytic oxidation of ethylbenzene – influence of the solvent.

Entry[a]	MeCN/Solvent	Conv. [%][b]	Yield [%][b]
1	MeCN	89	45
2	MeCN/H_2O	96	15
3	MeCN/EtOH	25	3
4	MeCN/EtOAc	61	24
5	MeCN/Acetone	70	27
6	MeCN/$CHCl_3$	86	41
7	MeCN/isoprop.	23	1
8	MeCN/DMSO	18	0
9	MeCN/DMF	20	0

[a] All Reactions were performed with ethylbenzene (0.02 mmol), RFT (10 mol%) and $Sc(OTf)_3$ (4.6 mM) in 1 mL MeCN/solvent=1:1 (v/v %) The samples were exposed to atmospheric oxygen and placed in a cooling block during irradiation (2.5 h) with blue light (440 nm). [b] Conversion and yield determined by GC-FID integration.

2.5.4 Hydrogen peroxide formation in the photocatalytic oxidation of ethylbenzene (Figure S1)

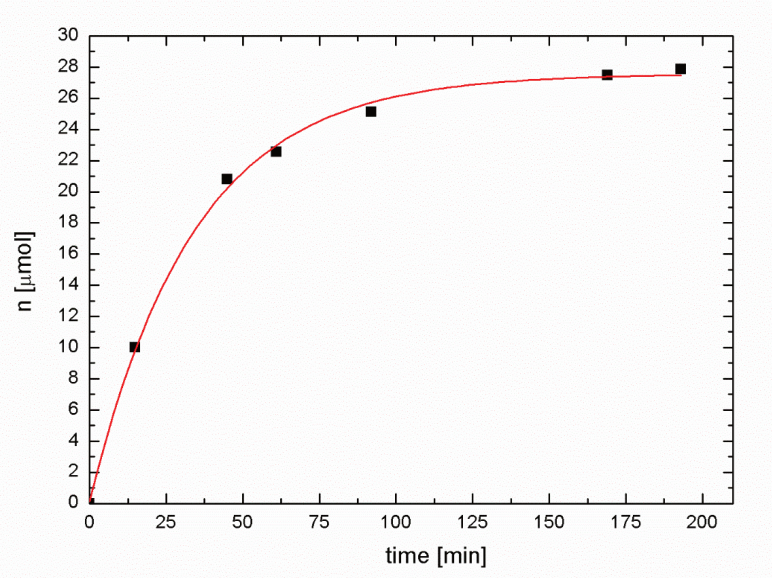

Figure S1. Hydrogen peroxide formation (▪) in the photocatalytic oxidation of ethylbenzene (0.02 mmol) in the presence of RFT (10 mol%) and $Sc(OTf)_3$ (38 mol%) in MeCN at room temperature.

2.5.5 Photocatalytic oxidation of ethylbenzene – Influence of the concentration of $Sc(OTf)_3$ (Figure S2)

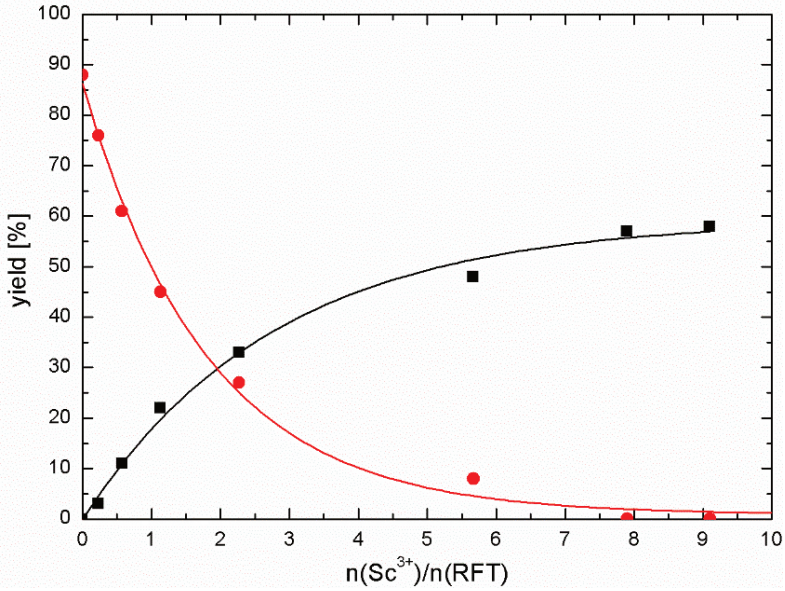

Figure S2. Photocatalyic aerobic oxidation of ethylbenzene (0.02 mmol) in presence of RFT (10 mol%) and various concentrations of $Sc(OTf)_3$ in 1 mL MeCN under irradiation (2.5 h) with blue light at 440 nm.

2.5.6 Photocatalytic oxidation of ethylbenzene – Influence of various additives (Table S3)

Table S3. Photocatalytic oxidation of ethylbenzene – Influence of various additives.

Entry[a]	Additive	Conv. [%][b]	Yield [%][b]
1	none	89	45
2	thiourea (30 mol%)	70	31
3	NaAc(aq) (30 mol%)	27	1
4	NaOH(aq) (30 mol%)	25	2
5	HCl (37%, 0.8 µL, 32 mol%)	100	59
6	HAc (30 mol%)	82	39
7	benzoic acid (30 mol%)	87	41
8	H_2O	40	10

[a] All reactions were performed with ethylbenzene (0.02 mmol), additive, RFT (10 mol%) and $Sc(OTf)_3$ (4.6 mM) in 1 mL MeCN. For all entries except 3, 4 and 8 the solvent was neat MeCN. The solvent mixture was MeCN/water = 7/1 (v/v%) for entries 3 and 8, and MeCN/water = 22/1 for entry 4. The samples were exposed to atmospheric oxygen and placed in a cooling block irradiation (2.5 h) with blue light (440 nm). [b] Conversion and yield were determined by GC-FID integration.

2.5.7 Photocatalytic oxidation of ethylbenzene – Influence of HCl (Figure S3)

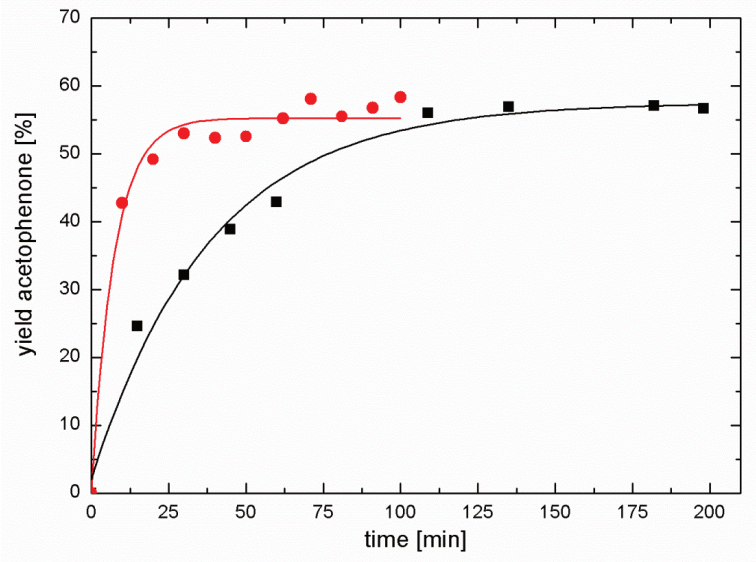

Figure S3. Photocatalytic oxidation of ethylbenzene (0.02 mmol) with RFT (10 mol%) and $Sc(OTf)_3$ (38 mol%) in the absence of HCl (▪) and in presence of 30 mol% HCl (●) during irradiation with blue light (440 nm, 3 W, 1 h).

2.5.8 Photocatalytic oxidation of ethylbenzene – control experiments. (Table S4)

Table S4. Photocatalytic oxidation of ethylbenzene – control experiments.

Entry	Conditions[a]	Conv. [%][b]	Yield [%][b]
1	standard cond.	100	52
2	no Sc^{3+}	33	8
3	no RFT	21	0
4	no irradiation	19	0
5	no (atmospheric) O_2	35	traces
6[c]	O_2 (100%)	100	50
7	CD_3CN	100	44
8[c]	CD_3CN, O_2 (100%)	100	44

[a] All reactions were performed with ethylbenzene (0.02 mmol), RFT (10 mol%), HCl (37%, 0.8 µL) and $Sc(OTf)_3$ (4.6 mM) in 1 mL MeCN. The samples were exposed to atmospheric oxygen and placed in a cooling block during irradiation (1 h) with blue light (440 nm). [b] Conversion and yield determined by GC-FID integration. [c] O_2: oxygen saturated solution.

2.5.9 UV-vis spectra – influence of dioxygen. (Figure S4)

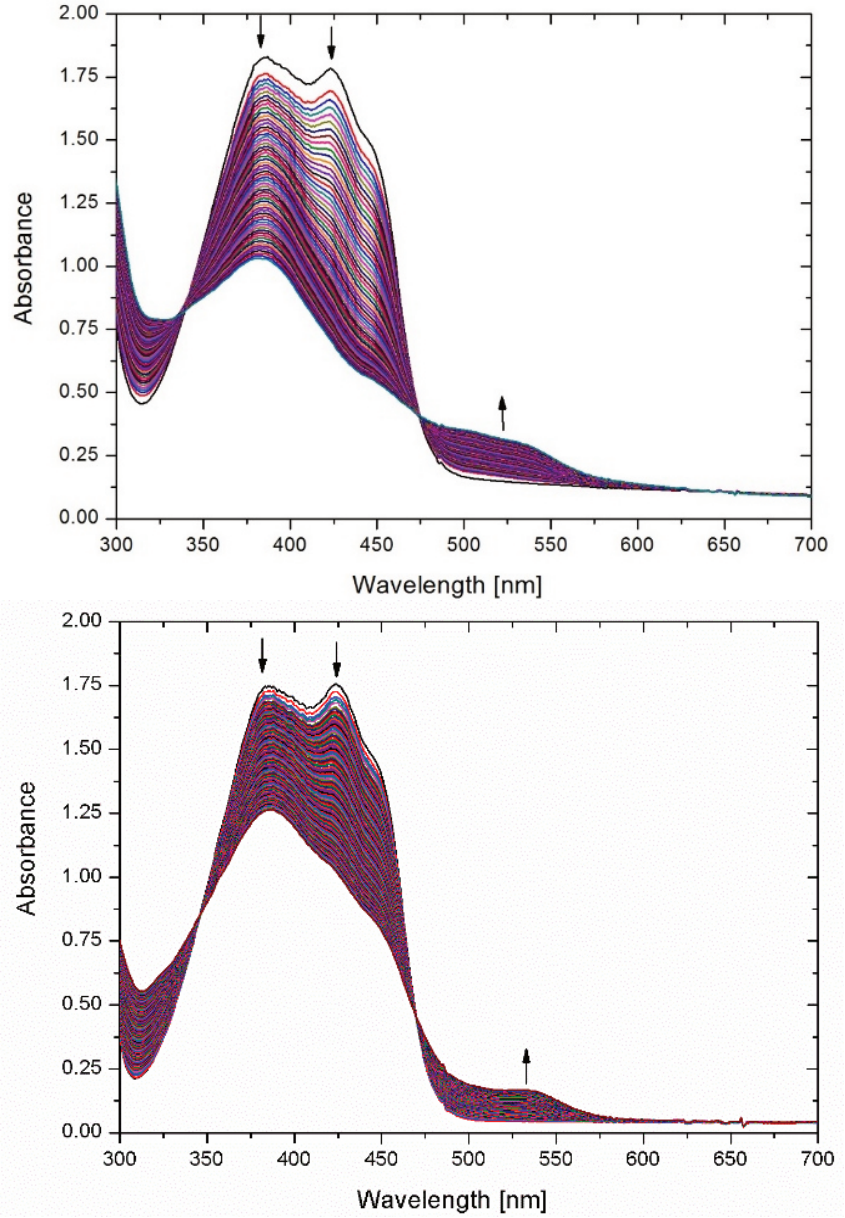

Figure S4. Electronic absorption spectra of ethylbenzene (58 mM) and RFT (0.14 mM) in the presence of $Sc(OTf)_3$ (0.68mM) while irradiating with blue light under atmospheric oxygen (left) and in a dioxygen purged solution (right) in MeCN at 298 K. The spectra were measured over 2 h (120 s between each spectrum displayed).

2.5.10 UV-vis spectra – influence of HCl (Figure S5)

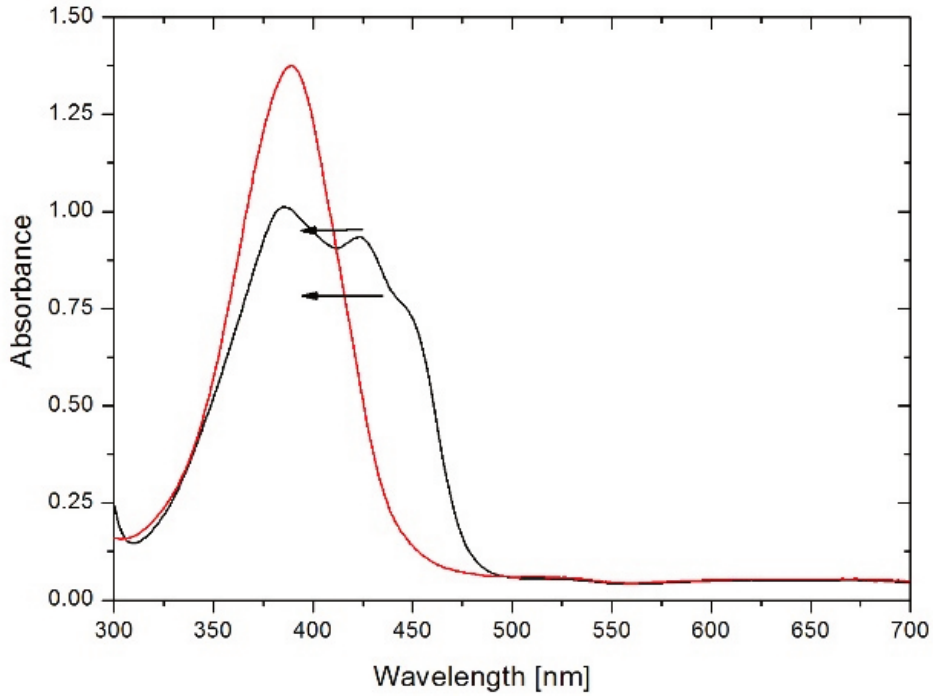

Figure S5. Electronic absorption spectra of ethylbenzene (5.8 mM) and RFT (0.07 mM) in the presence of $Sc(OTf)_3$ (0.34 mM) during irradiation with blue light under aerobic conditions in absence of HCl (black) and in presence of HCl (2.7 mM, red) in MeCN at room temperature.

Integral of the absorption spectrum (red) calculated numerically by OriginPro 8:

$$\int_{306}^{500} \text{red curve dx} = 111.67$$

Integral of the absorption spectrum (black) calculated numerically by OriginPro 8:

$$\int_{306}^{500} \text{black curve dx} = 111.72$$

2.5.11 IR data (Table S5)

Table S5. The ν(C=O) frequencies of the C^2- and C^4-carbonyl groups of RFT in the absence of Sc^{3+}, in the presence of Sc^{3+} and in the presence of Sc^{3+} and HCl in MeCN.

additive	ν(C^2=O)	ν(C^4=O)
none[a]	1689	1718
Sc^{3+} [b]	1606	1677
Sc^{3+} / HCl [c]	1606	1660–1680 (br)

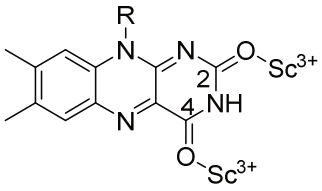

[a] In the absence of metal ions. [b] c(Sc^{3+}) = 30 mM. [c] c(Sc^{3+}) = 30 mM, c(HCl) = 10 mM, in this case the ν(C^4=O) frequency overlaps with the N-H out-of-plane frequency

2.5.12 ESR-spectrum generated in the photocatalytic reaction of RFT with ethylbenzene and $Sc(OTf)_3$. (Figure S6)

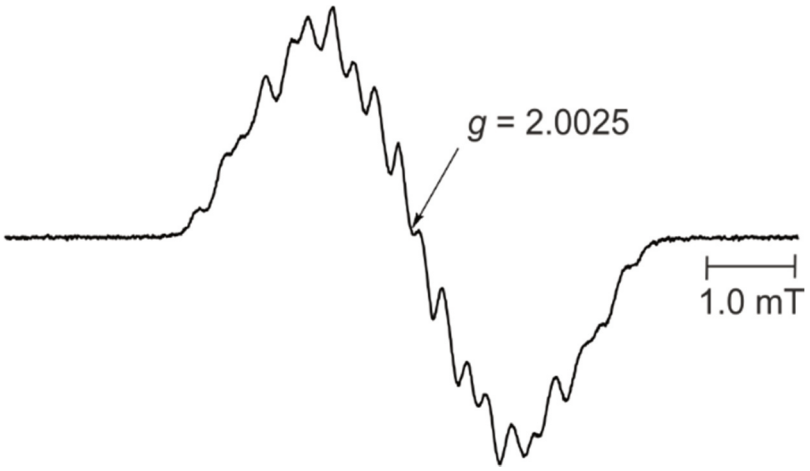

Figure S6. ESR-spectrum generated in the photocatalytic reaction RFT (3.0 mM) with ethylbenzene (10 mM) and $Sc(OTf)_3$ (10 mM) in presence of 10 mM HCl in deaerated MeCN at 298 K.

2.5.13 Monitoring of electronic absorption spectra of ethylbenzene, RFT and $Sc(OTf)_3$ during irradiation with blue light in deaterated MeCN (Figure S7)

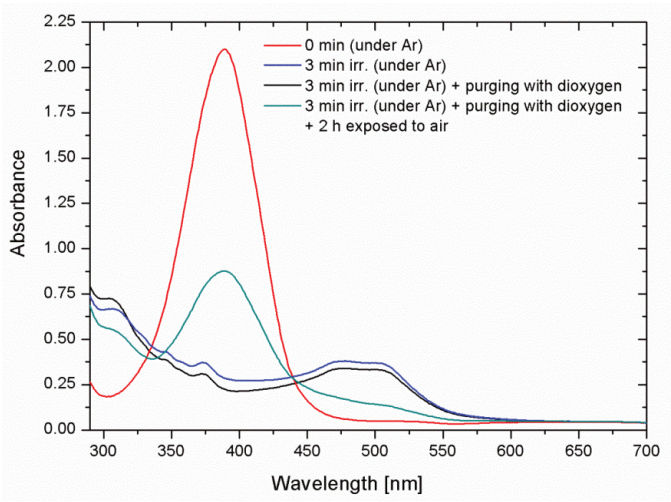

Figure S7. Electronic absorption spectra of ethylbenzene (58 mM) and RFT (0.14 mM) in the presence of $Sc(OTf)_3$ (0.68 mM) before irradiation (red), after 3 min of irradiation with blue light in deaterated MeCN (blue), after 3 min of irradiation with blue light in deaterated MeCN and purging the solution with dioxygen (black), after 3 min of irradiation with blue light in deaterated MeCN and purging the solution with dioxygen and 2 h exposing to atmospheric oxygen (green).

2.5.14 Monitoring of electronic absorption spectra of ethylbenzene, RFT and $Sc(OTf)_3$ under aerobic conditions during irradiation (Figure S8)

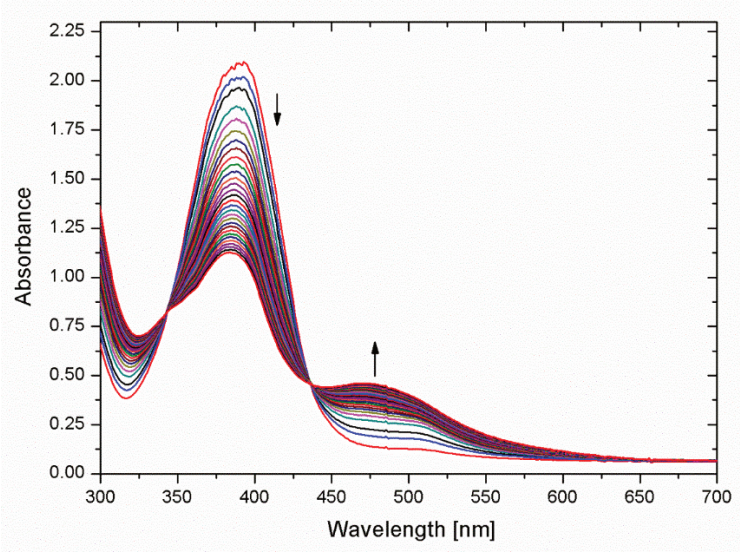

Figure S8. Electronic absorption spectra of ethylbenzene (58 mM) and RFT (0.14 mM) in the presence of $Sc(OTf)_3$ (0.68mM) while irradiating with blue light under atmospheric oxygen in MeCN at 298 K. The spectra were measured over 1 h (120 s between each spectrum displayed).

3 C−H Photooxygenation of Alkylbenzenes Catalyzed by Riboflavin Tetraacetate and a Non-Heme Iron Catalyst[a]

Bernd Mühldorf and Robert Wolf

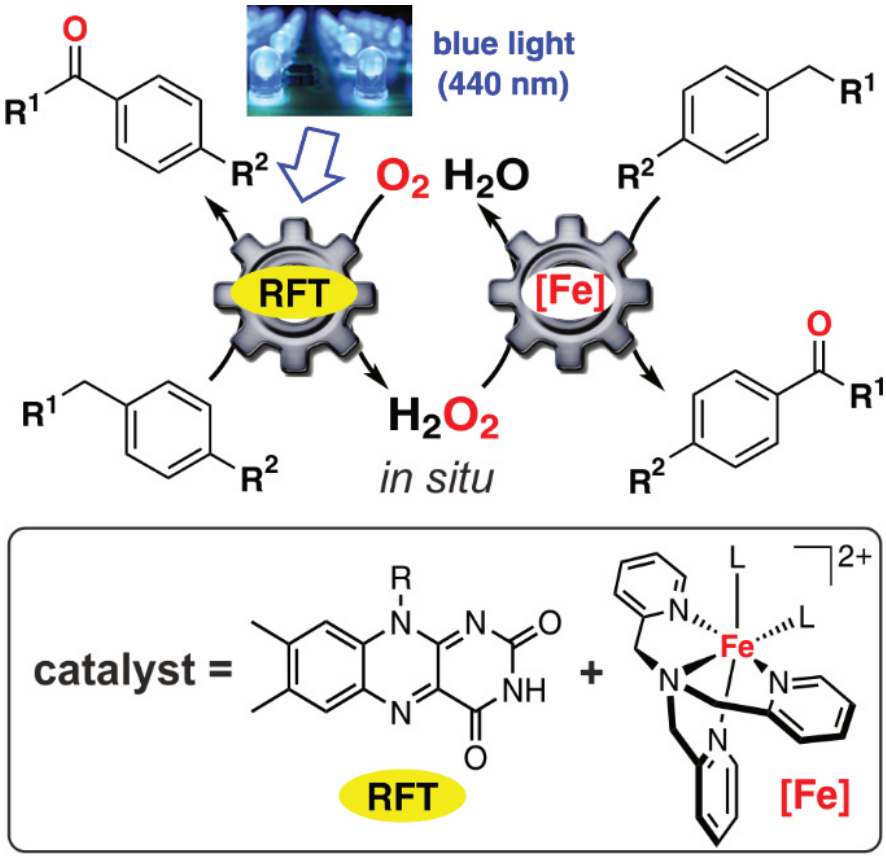

[a] Reprinted (adapted) with permission from John Wiley and Sons (License Number: 3745351248062), Bernd Mühldorf and Robert Wolf, Angew. Chem. Int. Ed. **2016**, *55*, 427 –430; Angew. Chem. **2016**, *128*, 437 –441; first published online 10 Nov 2015

3.1 Introduction

The photocatalytic oxygenation of alkylbenzenes using dioxygen and visible light is an atom economical and benign alternative to classical methods.[1] Only a few photocatalysts perform this type of transformation.[2–5] Organic dyes such as 1,4-dicyanonapthalene, the 10-phenyl-9-methylacridinium ion and the 3-cyano-1-methylquinolinium ion as well as iron porphyrins and manganese porphyrinoids catalyze the photooxygenation of toluene derivatives and related substrates.[3,4] Some heterogeneous catalysts have also been reported.[5]

The vitamin B_2 derivative riboflavin tetraacetate (RFT) is a promising and versatile catalyst for the visible-light driven photooxidation of benzyl alcohols,[6] benzyl amines,[7] and sulfides.[8] Moreover, a derivative of RFT was very recently applied for [2+2]-cycloadditions.[9] However, the C–H oxygenation of alkylbenzenes is difficult using RFT alone.[10] The additive $Sc(OTf)_3$ enables the oxygenation of alkylbenzenes with electron-withdrawing substituents, but this $Sc(OTf)_3$/RFT system still performs poorly for various other benzylic substrates.[11,12] We now report that a dual catalyst consisting of RFT and the tris(2-pyridylmethyl)amine complex $[Fe(TPA)(MeCN)_2](ClO_4)_2$ (**4**)[13] efficiently catalyzes the challenging photooxygenation of alkylbenzenes. The catalytic activity of **4** for H_2O_2 disproportionation and alkylbenzene oxygenation appears to be key for the high efficiency of this catalyst combination.

The formation of hydrogen peroxide as a by-product is a major drawback of the previously established RFT-catalyzed photocycle (Scheme 1, step i).[14] H_2O_2 degrades RFT under irradiation. As a result, ketone and benzyl alcohol are obtained as a product mixture in poor yields due to rapid photocatalyst bleaching (SI, chapters 2 and 3).[10,15] We wondered whether this problem could be solved by adding a metal complex that catalyzes H_2O_2 disproportionation or utilizes photochemically generated H_2O_2 as an oxidant. It is worth mentioning in this context that a photobiocatalytic tandem catalyst developed by Hollmann *et al.* enables impressive stereospecific visible-light driven sulfoxidations, alkene epoxidations and C–H hydroxylations.[16] This system uses a catalyst combination of flavin mononucleotide and a peroxidase enzyme and EDTA as a sacrificial electron donor. Feringa *et al.* reported that bioinspired iron complexes with tetra- and pentadentate nitrogen ligands catalyze the oxidation of ethylbenzene and 4-ethylanisole, using H_2O_2 as an oxidant (Scheme 1, step ii), albeit with low yields and selectivities.[17] Moreover, the ability of such iron complexes to catalyze H_2O_2 disproportionation (Scheme 1, step iii) is well-known.[18] Lower H_2O_2 concentrations could enable a higher

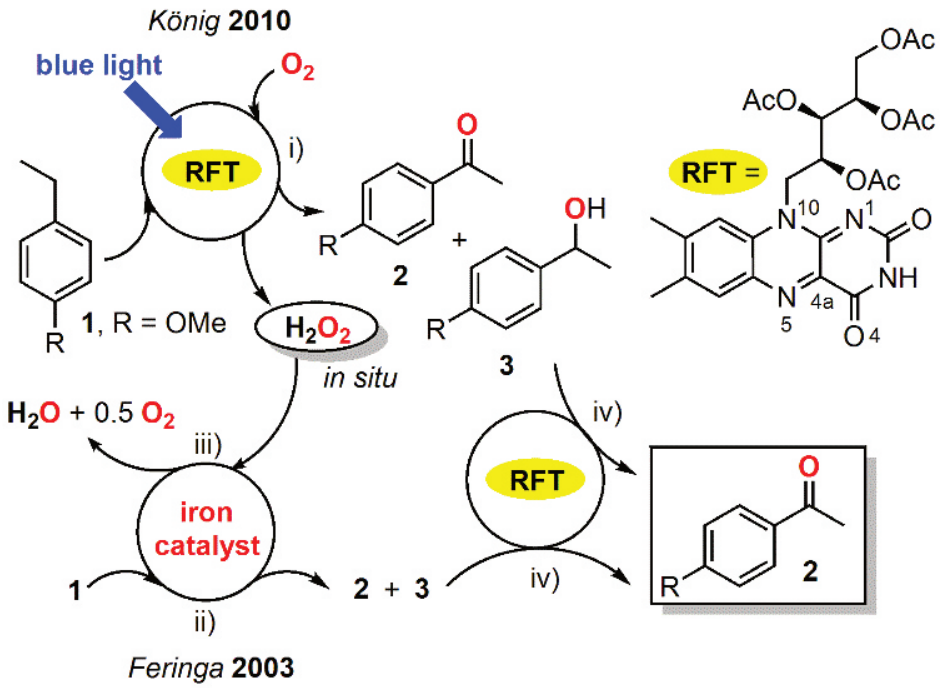

Scheme 1. Proposed dual catalysis for the oxidation of benzylic substrates exemplified for the oxidation of 4-ethylanisole (**1**) to 4-acetylanisole (**2**) and 4-methoxy-α-methylbenzyl alcohol (**3**).

photostability of RFT, allowing the flavin-mediated oxidation of the benzyl alcohol to the ketone (Scheme 1, step iv) to proceed.[14,15]

3.2 Results and Discussions

We initially tested the effect of adding selected biomimetic iron complexes on the benchmark oxidation reaction of 4-ethylanisole (**1**) to 4-acetylanisole (**2**) and 4-methoxy-α-methylbenzyl alcohol (**3**; Figure 1; SI, chapters 2 and 4). In line with previous results by König *et al.*, the photooxygenation of **1** with RFT gave unsatisfactory yields for **2** (30%) and **3** (12%) in the absence of a co-catalyst.[10] In contrast, ketone **2** was obtained exclusively in a high yield (80%) when a mixture of RFT (10 mol%) and **4** (8 mol%) was employed as catalyst. In the initial stages of the reaction, ketone **2** and benzyl alcohol **3** are formed simultaneously (Figure 1), but **3** is subsequently converted to **2** by an RFT-catalyzed process (Scheme 1, step iv).[14] The related non-heme iron complexes **5**[19] and **6**[20] gave a similar time profile as **4**, but the reactions took longer to go to completion (Figure 1). Other non-heme iron complexes and binary iron salts such as $Fe(ClO_4)_x$ (x = 2 or 3) turned out to be less efficient (SI, chapters 2 and 4).

RFT/**4** was the most expedient catalyst combination, hence we subsequently investigated its substrate scope (Table 1). Esters are obtained from benzylethers selectively in very

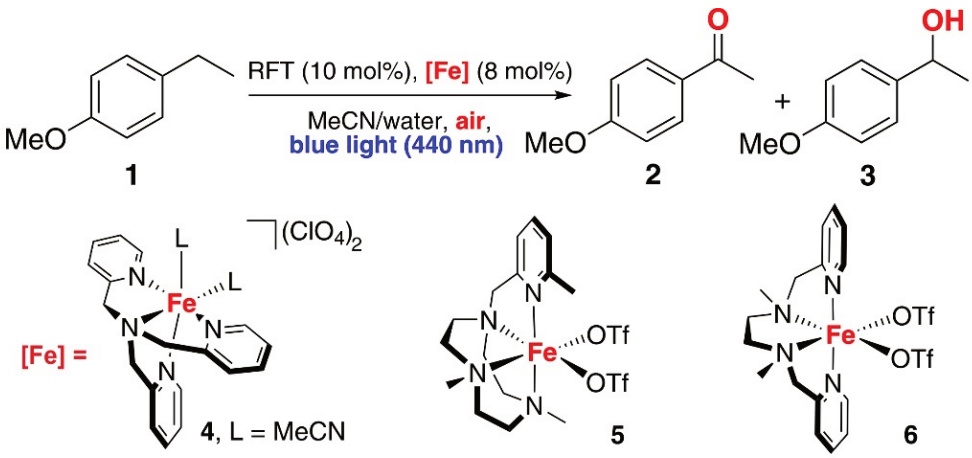

entry	co-catalyst	yield of **2** [%][a]	yield of **3** [%][a]
1	-	30	12
2	MnO_2	60	8
3	$Fe(ClO_4)_2$	62	0
4	$Fe(ClO_4)_3$	67	0
5	**4**	80	0
6	**5**	66	5
7	**6**	58	5

[a] All reactions were performed with substrate (0.02 mmol), RFT (10 mol%), iron catalyst (8 mol%) in 1.5 mL MeCN/H_2O (1/1, v/v%) and irradiated with blue light (440 nm, 3 W) for 60 min. Conversion and yield were determined by GC-FID integration.

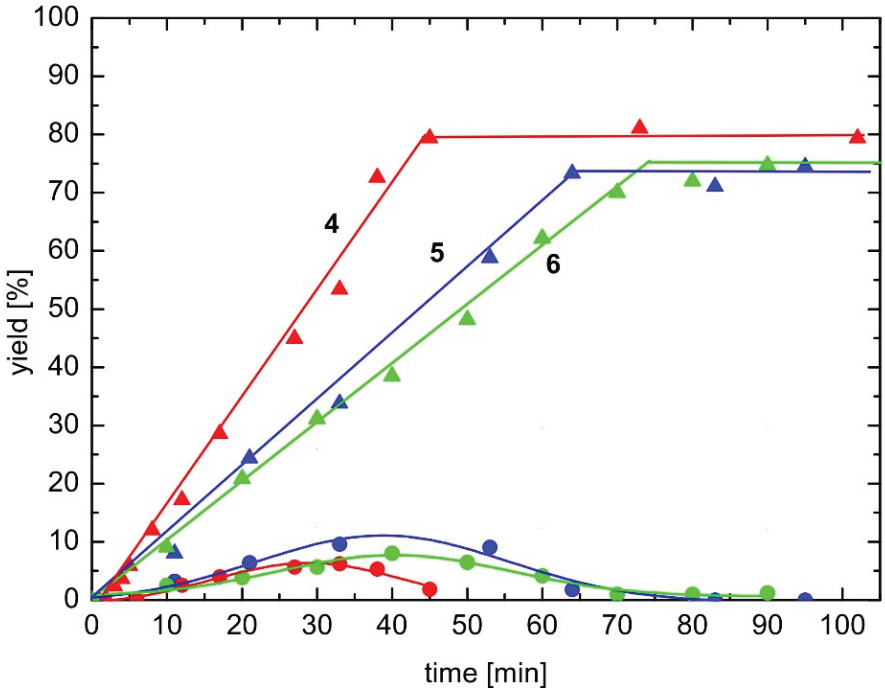

Figure 1. Reaction time profiles for the oxygenation of **1** (0.02 mmol) to **2** (▲) and **3** (●) catalyzed by RFT (10 mol%) in the presence of an iron complex (8 mol%) in MeCN/H_2O (1/1, v/v%): **4** (red), **5** (blue) and **6** (green); lines are visual guides only.

good yields (entry 1). Xanthene affords xanthen-9-one in an excellent yield of 96% (entry 2). Similarly, the oxidation of thioxanthene is fast and proceeds quantitatively. Remarkably, overoxidation was not observed although the oxidation of sulfides to sulfoxides is known to proceed via an RFT-catalyzed singlet oxygen pathway in the absence of a co-catalyst.[8] Isochromane, indane and tetrahydronaphthalene are converted to the corresponding ketones with good yields (entries 3 and 4). The photocatalytic oxygenation of tolane gives benzil in a moderate yield of 48% (entry 5), whereas *trans*-stilbene affords benzaldehyde in 76% yield (entry 6). *Para*-substituted ethylbenzenes afford the

Table 1. Substrate scope of the photocatalytic C–H oxygenation of alkylbenzenes and related substrates.[a,b]

Entry	Substrate	Product	R,n,X	Irr. time [h]	Yield [%][b]
1[c]	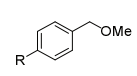	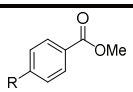	H OMe	24 3.0	79 84
2[c]	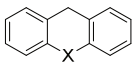	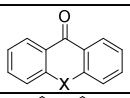	O S	1.5 0.1	96 99
3		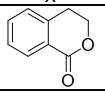	-	2.5	66
4[e]			1 2	2.0 2.0	70 70
5		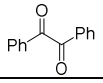	-	2.5	48
6	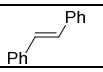		-	1.5	76
7	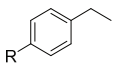	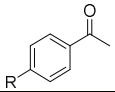	OMe Br[d] H[d]	2.5 2.5 1.0	80 72 74
8		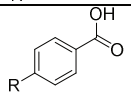	OMe Cl[d] Br[d]	8 5 5	80 60 62
9	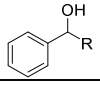	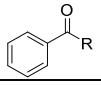	H Me	2.5 2.5	81 68
10	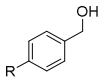		F Cl Br NO_2 CO_2Me CF_3	2.5 1.0 2.5 16 4.5 8	74 74 72 71 83 60

[a] Unless noted otherwise, the reactions were performed with substrate (0.02 mmol), RFT (10 mol%), $[Fe(TPA)(MeCN)_2](ClO_4)_2$ (**4**, 2 mol%) in 1.5 mL $MeCN/H_2O$ (1/1 v/v) and irradiated with blue light (440 nm, 3 W); [b] results of analogous experiments using MnO_2 and $Fe(ClO_4)_3$ as co-catalysts are given in the supporting information (chapter 2); [c] conversion and yield determined by GC-FID integration; [d] solvent MeCN, **4** (8 mol%); [e] solvent MeCN, additive $HClO_4$ (30 mol%); [f] **4** (8 mol%).

corresponding acetophenones in good yields when $HClO_4$ (30 mol%) is added (entry 7). Toluene derivatives are rapidly converted to aldehydes and subsequently to the corresponding carboxylic acids (entry 8) *via* an iron-catalyzed aerobic oxidation process (SI, chapter 4). Benzyl alcohols with strongly electron-withdrawing *para*-substituents (R = NO_2, CO_2Me, CF_3) are also converted very efficiently to the corresponding aldehydes (entries 9 and 10). For synthetic applications, an efficient separation of the catalysts from the product is highly desirable. As shown by UV-vis spectroscopy, both catalyst components are easily removed by adsorption on basic alumina, while <1% of product are lost in this operation (SI, chapter 4). The benchmark oxygenation of **1** does not proceed in the dark, in the absence of RFT or under an N_2 atmosphere (SI, chapter 2). The presence of water is crucial for a high reaction rate (SI, chapter 4). Product yield and substrate conversion are unaffected when the reaction iscarried out in an atmosphere of pure dioxygen, and the yield of **2** was 60% in CD_3CN/D_2O (1:1 v/v%; SI, chapters 2 and 4). Thus, a singlet oxygen pathway appears unlikely.[21] While RFT/**4** efficiently catalyzes the photooxygenation of alkylbenzenes, RFT alone only shows a modest catalytic activity (SI, chapter 2). Insight into the striking effect of the co-catalyst was gained from spectroscopic investigations and reaction monitoring studies. Fluorescence emission quenching experiments revealed an enhanced quenching of the excited singlet state, ^{1}RFT*, in the presence of various metal complexes and metal salts (SI, chapter 2). However, there seems to be no correlation between the magnitude of the Stern-Volmer constants and the catalyst competence, which indicates that the observed emission quenching is probably unproductive. An ESI-MS investigation of RFT/**4** (SI, chapter 4) revealed the signals of $[Fe(TPA)(MeCN)]^{2+}$ (*m/z* = 193.5) and $RFTH^+$ (*m/z* = 545.2). Additional signals are apparent at *m/z* = 445.1, 889.5 and 989.5, which may indicate the formation of an adduct between RFT and **4** (SI, chapter 4). Nonetheless, the UV-vis and IR spectra of the catalyst mixture correspond to a superposition of the individual spectra of **4** and RFT, which shows that the partial complex formation observed by ESI-MS, if at all present at the lower catalytic concentrations, does not affect the ground state of the photocatalyst.

While a direct interaction between RFT and the co-catalyst thus does not seem to be responsible for the improved catalytic properties, metal-catalyzed H_2O_2 disproportionation is important. The rapid photobleaching of RFT observed in the absence of a co-catalyst is effectively diminished when complex **4** is added (SI, chapter 4). Compared to using RTF alone, the yields of **2** (30%) and **3** (12%) improve with manganese dioxide as a co-catalyst instead of **4** (SI, chapters 2 and 4) to 60% and 8%, respectively. MnO_2 has no oxygenation activity, therefore, this increase must be attributed to its activity as an H_2O_2

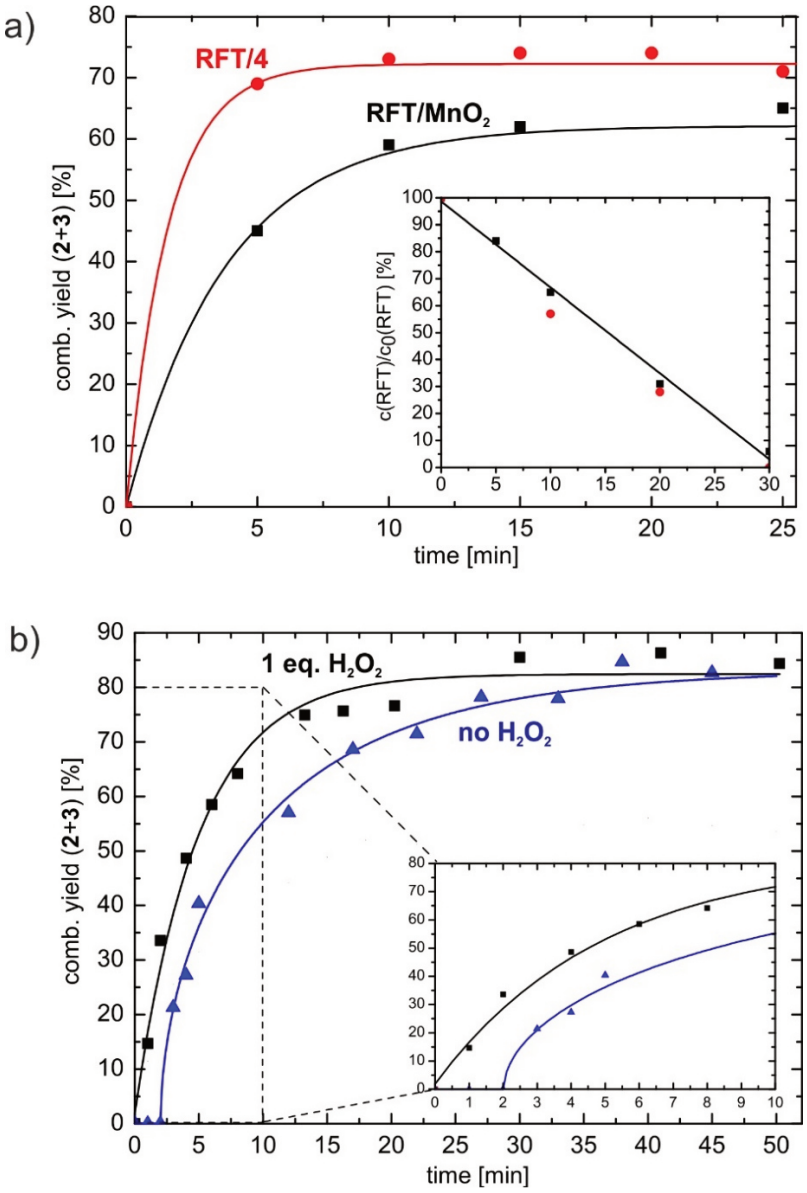

Figure 2. a) Reaction time profile of the photooxygenation of **1** (0.02 mmol) to **2** and **3** catalyzed by RFT/MnO_2 (■, black) and RFT/**4** (●, red) with RFT (8 mol%), MnO_2 (20 mg) or **4** (0.5 mol%); the combined yield is defined as the sum of the molar yields of **2** and **3** divided by the molar amount of converted starting material **1**; the relative concentration of RFT was determined by the change of the absorbance A at λ_{max} = 443 nm (inset); b) reaction time profile of the photooxygenation of **1** (0.02 mmol) to **2** and **3** catalyzed by RFT/**4** in the absence of additional H_2O_2 (▲, blue) and with 1 equiv. H_2O_2 added (■, black) before starting to irradiate at 440 nm; catalyst loadings: RFT (8 mol%), **4** (8 mol%); the inset shows a magnification of the reaction time profile; lines are visual guides only.

disproportionation catalyst. The efficiencies of the RFT/**4** and RFT/MnO_2 combinations can be compared directly when the concentration of the co-catalysts are adjusted such that the same bleaching rate of RFT is maintained (Figure 2a). Even using 0.5 mol% **4**, the combined yield of **2** and **3** is still substantially higher for RFT/**4** compared to RFT/MnO_2. Note that RFT/MnO_2 also performs significantly worse than RFT/**4** for the oxygenation of related alkylbenzenes (SI, chapter 2). Considering that MnO_2 and **4** are

efficient H_2O_2 disproportionation catalysts under these conditions, it seems likely that the higher yields of **2** obtained with RFT/**4** may be attributed to the additional oxygenation activity of the iron complex (Scheme 1, step ii). An additional monitoring study further supports the relevance of the oxygenation activity of the iron complex. Using the RFT/**4**, the formation of **2** and **3** is initially slow (<2% yield after 2 min, Figure 2b). Subsequently, the reaction rate starts to increase rapidly. By contrast, a high initial rate is found when H_2O_2 (1 equiv.) is added immediately before starting to irradiate. In this case, a substantial yield of **2** (35%) is already detected after the first two minutes. This change in the reaction kinetics is likely attributed to the ability of the iron catalyst to perform the oxygenation of **1** independently from RFT as soon as H_2O_2 is present in the reaction solution. A plausible mechanism is based on the well-investigated reaction between **4** and H_2O_2.[22] Spectroscopic and kinetic studies have shown that the addition of H_2O_2 to **4** in acetonitrile gives rise to a low-spin iron(III) hydroperoxo complex, $[Fe^{III}(TPA)(OOH)]^{2+}$, which has been proposed to convert to the putative iron(V) oxidant $[Fe^{V}(TPA)(O)OH]^{2+}$.[22,23]

3.3 Conclusion

In conclusion, the combination of the photocatalyst riboflavin tetraacetate (RFT) with the bioinspired complex $[Fe(TPA)(MeCN)_2](ClO_4)_2$ (**4**) affords a readily accessible, cheap, and efficient catalyst for the visible-light driven aerobic C–H bond oxidation of alkylbenzenes. The reactivity of the iron complex with photocatalytically generated H_2O_2 is key to ensure high conversions and selectivities. Our experiments indicate that **4** acts as an H_2O_2 disproportionation catalyst and an oxygenation catalyst at the same time. Other recently reported dual photoxygenation catalysts rely on the direct photocatalytic generation of reactive transition metal-oxo species.[24] Different to the complementary enzyme-based photobiocatalytic tandem catalyst reported by Hollmann *et al.*, the present system uses a transition metal co-catalyst; a sacrificial electron donor is not required.[16] The application of a wider range of co-catalysts and an extension to other useful substrate classes are currently under investigation.

3.4 References

[1] M. Hudlicky, *Oxidations in Organic Chemistry*, ACS Monograph No. 186, American Chemical Society, Washington DC, 1990.

[2] reviews on photocatalytic oxygenations: a) S. Fukuzumi, *Dalton Trans.* **2015**, *44*, 6696; b) S. Fukuzumi, K. Ohkubo, *Chem. Sci.* **2013**, *4*, 561.

[3] selected examples using organic photosensensitizers: a) J. Jung, K. Ohkubo, D. P. Goldberg, S. Fukuzumi, *J. Phys. Chem. A* **2014**, *118*, 6223; b) G. Pandey, S. Pal, R. Laha, *Angew. Chem. Int. Ed.* **2013**, *52*, 5146; *Angew. Chem.* **2013**, *125*, 5250; c) S. Fukuzumi, K. Doi, A. Itoh, T. Suenobu, K. Ohkubo, Y. Yamada, K. D. Karlin, *PNAS* **2012**, *109*, 15572; d) S. Fukuzumi, J. Yuasa, N. Satoh, T. Suenobu, *J. Am. Chem. Soc.* **2004**, *126*, 7585–7594, e) K. Ohkubo, S. Fukuzumi, *Org. Lett.* **2000**, *2*, 3647.

[4] selected examples using photosensitizers based on porphyrin or porphyrinoid complexes: a) H. M. Neu, J. Jung, R. A. Baglia, M. A. Siegler, K. Ohkubo, S. Fukuzumi, D. P. Goldberg, *J. Am. Chem. Soc.* **2015**, *137*, 4614; b) J. Rosenthal, T. D. Luckett, J. M. Hodgkiss, D. G. Nocera, *J. Am. Chem. Soc.* **2006**, *128*, 6546; c) L. Weber, R. Hommel, J. Behling, G. Haufe, H. Hennig, *J. Am. Chem. Soc.* **1994**, *116*, 2400.

[5] a) H. Yuzawa, H. Yoshida, *Top. Catal.* **2014**, *57*, 984; b) M. Carraro, M. Gardan, G. Scorrano, E. Drioli, E. Fontananova, M. Bonchio, *Chem. Commun.* **2006**, 4533.

[6] a) R. Cibulka, R. Vasold, B. König, *Chem. Eur. J.* **2004**, *10*, 6223; b) B. König, S. Kümmel, R. Cibulka in *Chemical Photocatalysis*, De Gruyter, Berlin (B. König, ed.), **2013**, pp. 45–66.

[7] R. Lechner, B. König, *Synthesis* **2010**, *2010*, 1712.

[8] J. Dad'ová, E. Svobodová, M. Sikorski, B. König, R. Cibulka, *ChemCatChem* **2012**, *4*, 620.

[9] V. Mojr, E. Svobodová, K. Straková, T. Neveselý, J. Chudoba, H. Dvořáková, R. Cibulka, *Chem Commun.* **2015**, *51*, 12036.

[10] R. Lechner, S. Kümmel, B. König, *Photochem. Photobiol. Sci.* **2010**, *9*, 1367.

[11] a) S. Fukuzumi, K. Yasui, T. Suenobu, K. Ohkubo, M. Fujitsuka, O. Ito, *J. Phys. Chem. A* **2001,** *105*, 10501; b) S. Fukuzumi, S. Kuroda, T. Tanaka, *J. Am. Chem. Soc.* **1985**, *107*, 3020.

[12] B. Mühldorf, R. Wolf, *Chem. Commun.* **2015**, *51*, 8425.

[13] P. D. Oldenburg, A. A. Shteinman, L. Que, Jr. *J. Am. Chem. Soc.* **2005**, *127*, 15672.

[14] a) U. Megerle, M. Wenninger, R.-J. Kutta, R. Lechner, B. König, B. Dick, E. Riedle, *Phys. Chem. Chem. Phys.* **2011**, *13*, 8869; b) C. Feldmeier, H. Bartling, K. Magerl, R. M. Gschwind, *Angew. Chem. Int. Ed.* **2015**, *54*, 1347; *Angew. Chem*. **2015**, *127*, 1363.

[15] See the supporting information for further experimental details.

[16] a) E. Churakova, M. Kluge, R. Ullrich, I. Arends, M. Hofrichter, F. Hollmann, *Angew. Chem. Int. Ed.* **2011**, *50*, 10716; *Angew. Chem.* **2011**, *123*, 10904; b) D. I. Perez, M. M. Grau, I. W. C. E. Arends, F. Hollmann, *Chem. Commun.* **2009**, 6848.

[17] M. Klopstra, R. Hage, R. M. Kellogg, B. L. Feringa, *Tetrahedron Lett.* **2003**, *44*, 4581.

[18] a) J. Paschke, M. Kirsch, H.-G. Korth, H. de Groot, R. Sustmann, *J. Am. Chem. Soc.* **2001**, *123*, 11099; b) A. Ghosh, D. A. Mitchell, A. Chanda, A. D. Ryabov, D. L. Popescu, E. C. Upham, G. J. Collins, T. J. Collins, *J. Am. Chem. Soc.* **2008**, *130*, 15116.

[19] I. Prat, A. Company, T. Corona, T. Parella, X. Ribas, M. Costas, *Inorg. Chem.* **2013**, *52*, 9229.

[20] G. J. P. Britovsek, J. England, A. J. P. White, *Inorg. Chem.* **2005**, *44*, 8125.

[21] E. Sikorska, I. Khmelinskii, A. Komasa, J. Koput, L. F. V. Ferreira, J. R. Herance, J. L. Bourdelande, S. L. Williams, D. R. Worrall, M. Insińska-Rak, et al., *Chem. Phys.* **2005**, *314*, 239.

[22] review: W. N. Oloo, L. Que, Jr. *Acc. Chem. Res.* **2015**, *48*, 2612.

[23] a) K. Chen, L. Que, Jr. *J. Am. Chem. Soc.* **2001**, *123*, 6327; b) K. Chen, M. Costas, J. Kim, A. K. Tipton, L. Que, Jr. *J. Am. Chem. Soc.* **2002**, *124*, 3026; c) A. Mairata i Payeras, R. Y. N. Ho, M. Fujita, L. Que, Jr. *Chem. Eur. J.* **2004**, *10*, 4944.

[24] a) X. Wu, X. Yang, Y.-M. Lee, W. Nam, L. Sun, *Chem. Commun.* **2015**, *51*, 4013, b) A. Company, G. Sabenya, M. González-Béjar, L. Gómez, M. Clémancey, G. Blondin, A. J. Jasniewski, M. Puri, W. R. Browne, J.-M. Latour, et al., *J. Am. Chem. Soc.* **2014**, *136*, 4624; c) W. Iali, P.-H. Lanoe, S. Torelli, D. Jouvenot, F. Loiseau, C. Lebrun, O. Hamelin, S. Menage, *Angew. Chem. Int. Ed.* **2015**, *54*, 8415; *Angew. Chem*. **2015**, *127*, 8535.

3.5 Supporting Information

3.5.1 Experimental section

Materials

RFT and the non-heme iron complexes **4**–**8** were prepared according known literature procedures.[S1-S5] All other chemicals were obtained commercially (Sigma Aldrich, VWR) and used as received.

Representative procedure for the oxygenation of 4-ethylanisole

4-Ethylanisole (**1**, 0.02 mmol) was added to RFT (10 mol%) and $[Fe(TPA)(MeCN)_2](ClO_4)_2$ (**4**, 2 mol% or noted otherwise) in 1.5 mL (acetonitrile/water 1/1 v/v). The reaction vial was placed in a cooling block to maintain ambient temperature, and the vials were irradiated with blue LEDs (440 nm, 3 W LED) while stirring with a magnetic stirring bar. After 2.5 h of irradiation, *n*-pentadecane (internal standard),

saturated Na_2CO_3 and brine were added. The organic phase was extracted with ethylacetate and subjected to GC-FID analysis. The retention time was verified with authentic samples.

The formation of benzoic acid derivatives was determined by GC analysis of the corresponding methyl esters. The esterification was performed as follows: The solvent was evaporated from the reaction mixture in vacuo. Then, methanol (1 mL) and toluene (1 mL) were added. Trimethylsilyldiazomethane ($TMSCH_2N_2$, 20 eq.) was carefully added and stirred for 30 min at room temperature. The mixture was quenched with acetic acid (37%, 15 µL) and *n*-pentadecane as internal standard was added. The addition of Na_2CO_3 (saturated solution), brine were subsequently added. The organic phase was extracted with ethylacetate and subjected to GC-FID analysis.

Monitoring the formation of hydrogen peroxide

The formation of H_2O_2 was monitored by a standard method. A diluted acetonitrile solution was treated with an excess of NaI(s). The concentration of I_3^- formed was determined by UV-vis spectroscopy (λ_{max} = 362 nm, ε = 13000 $M^{-1}cm^{-1}$).

Removal of the catalysts

The reaction mixture in neat MeCN was filtered over basic alumina and washed with several portions of ethylacetate. The internal standard (*n*-pentadecane), saturated Na_2CO_3 and brine were added to the clear solution and the organic phase was subjected to GC-FID analysis. The addition of 2,2'-bipyridine (bpy) to an aliquot of the filtrate and an aliquot containing an excess of ascorbic acid (reduction of Fe^{3+}-ions) did not give the intensely colored $[Fe(bpy)_3]^{2+}$-complex (UV-vis spectroscopy), which shows that iron complexes or salts were absent in the organic phase.

MeCN/water mixtures were quenched with saturated Na_2CO_3 and brine and subsequently extracted with ethylacetate. The coloured organic phase was filtered over basic alumina. Then, *n*-pentadecane (internal standard) was added to the clear filtered solution. This mixture was then subjected to GC-FID analysis.

Fluorescence emission quenching

A fluoresence cuvette containing RFT (c_{RFT} = $7.8 \cdot 10^{-6}$ $mol \cdot L^{-1}$) was placed in a fluoresence spectrometer (Casy Eclipse Varian). The solution was irradiated at 440 nm and the maximum emission intensity, I_0^{max}(λ = 506 nm), was determined. The addition of various volumina of a stock solution, containing RFT (c_{RFT} = $7.8 \cdot 10^{-6}$ $mol \cdot L^{-1}$) and the quencher, Q, yielded the concentration dependent emission intensity, I^{max}(λ = 506 nm). A Stern-Volmer plot of I_0^{max}/I_o vs. c(Q) provided the quenching constant, K_{SV}.

3.5.2 Tables with additional catalytic results, results of control experiments, and fluorescence quenching constants.

Table S1. Screening of co-catalysts for the photooxygenation of 4-ethylanisole (**1**).

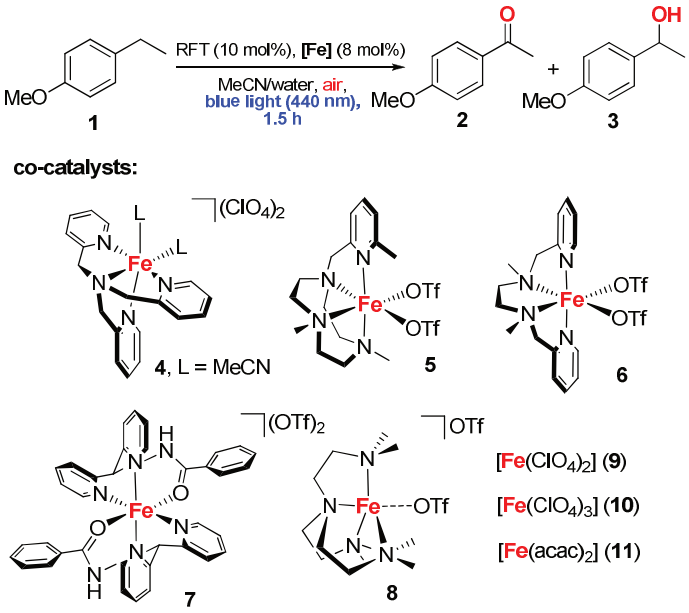

entry	co-catalyst	yield of 2 [%][b]	yield of 3 [%][b]
1	**-**	30	12
2	**4**	80	0
3	**5**	66	5
4	**6**	58	5
5	**7**	70	0
6	**8**	27	15
7	**9**	62	0
8	**10**	67	0
9	**11**	51	12
10	**MnO_2**	60	8

[a] All reactions were performed with substrate (0.02 mmol), RFT (10 mol%), iron catalyst (8 mol%) in 1.5 mL MeCN/H_2O (1/1 v/v) and irradiated with blue light (440 nm, 3 W) for 60 min. [b] Conversion and yield determined by GC-FID integration.

Table S2. Photocatalytic oxygenation of alkylbenzenes with RFT/MnO_2.[a]

Entry	Substrate	Product	No MnO_2 Yield [%][b]	R,n,X	Irr. time[b][h]	Yield [%][b]
1[c]	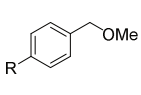	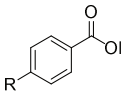	26	OMe	3.0	17
2[c]	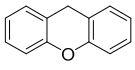	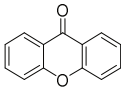	35	-	1.5	68
3			7	1	2.0	18
			8	2	2.0	29
4			38	-	2.5	65
5	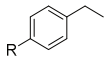	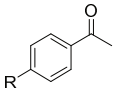	54	Br[d]	2.5	30
			42	H[d]	1.0	10
6	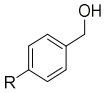		40	F	2.5	71
			50	Cl	1.0	60
			49	Br	2.5	72

[a] Unless otherwise noted, all reactions were performed with substrate (0.02 mmol), RFT (10 mol%), MnO_2 (3 mg, 60 mol%) in 1.5 mL MeCN/H_2O (1/1 v/v) and irradiated with blue light (440 nm, 3 W); [b] conversion and yield were determined by GC-FID integration; [c] solvent MeCN, MnO_2 (3 mg); [d] solvent MeCN, addition of $HClO_4$ (30 mol%).

Table S3. Photocatalytic oxygenation in the presence of $Fe(ClO_4)_3 \cdot H_2O$ (**10**).[a]

Entry	Substrate	Product	No [Fe] Yield [%][b]	R,n,X	Irr. time[b][h]	Yield [%][b]
1[c]	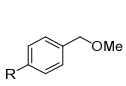	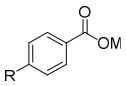	26	OMe	3.0	8[f]
2[c]	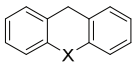	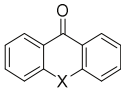	35	O	1.5	84
3[e]			7	1	2.0	46
			8	2	2.0	57
4		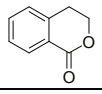	38	-	2.5	71
5	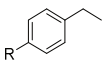	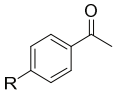	54	Br[d]	2.5	69
			42	H[d]	1.0	43[g]
6	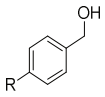		40	F	2.5	53
			50	Cl	1.0	68
			49	Br	2.5	63

[a] Unless otherwise noted, the reactions were performed with substrate (0.02 mmol), RFT (10 mol%), $Fe(ClO_4)_3 \cdot H_2O$ (**10**, 2 mol%) in 1.5 mL MeCN/H_2O (1/1 v/v) and irradiated with blue light (440 nm, 3 W); [b] conversion and yield were determined by GC-FID integration; [c] solvent MeCN; $Fe(ClO_4)_3 \cdot H_2O$ (8 mol%); [d] solvent MeCN, addition of $HClO_4$ (30 mol%); [e] $Fe(ClO_4)_3 \cdot H_2O$ (8 mol%); [f] 6% 4-methoxybenzaldehyde detected; [g] 5% 1-phenyl alcohol detected.

Table S4. Photocatalytic oxygenation of toluene derivatives with RFT in the presence of $HClO_4$.[a]

Entry	Substrate	Product	R,n,X	Conv. [%][b]	Yield [%][b]
1	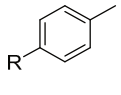	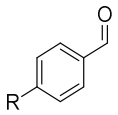	^{t}Bu	100	76
			Cl	83	51
			Br	85	53
			Me	100	35[b]
			OMe	50	20
			H	81	42
			CN	50	27
			CO_2Me	26	7

[a] All reactions were performed with substrate (0.02 mmol), RFT (10 mol%) and $HClO_4$ (30 mol%) in 1.5 mL MeCN and irradiated (2.5 h) with blue light (440 nm, 3 W); conversion and yield were determined by GC-FID integration; [b] 11% terephthalaldehyde additionally detected.

Table S5. Photocatalytic oxygenation of 4-ethylanisole (**1**) – control experiments.[a]

Entry	conditions	Yield of 2 [%][b]	Yield of 3 [%][b]
1	-	**80**	**0**
2	no **4**	30	12
3	dark	0	0
4	no RFT	0	0
5	no air	0	7
6	oxygen saturated solution	80	1
7	CD_3CN/D_2O as solvent	60	0

[a] All reactions were performed with substrate **1** (0.02 mmol), RFT (10 mol%), **4** (8 mol%), MeCN/water (1.5 mL, 1/1 v/v), irradiation with blue LED (440 nm, 3 W) for 1.5 h; [b] conversion and yield were determined by GC-FID.

Table S6. Fluoresence emission quenching – Stern-Volmer constants.[a]

Iron catalyst	K_{SV} [L·mol^{-1}]
4	1248±18
5	236±8
6	288±19
7	1314±43
8	151±23
11	4297±129

[a] A fluorescence cuvette containing RFT (c_{RFT} = 7.8·10^{-6} mol·L^{-1}) was placed in a fluorescence spectrometer and various amounts of a stock solution, containing RFT (c_{RFT} = 7.8·10^{-6} mol·L^{-1}) and the iron catalyst (0–80 eq. referring to RFT) were added. The solution was excited at 440 nm and the emission intensity, I^{max}, was determined at 506 nm.

Table S7. Oxygenation of 4-ethylanisole (**1**) with H_2O_2 and an iron catalyst.[a]

Catalyst	TON(**2**)/TON(**3**)[a]	TON(**2**)/TON(**3**)[b]
4	1.2/1.1	1.7/2.0
5	2.6/3.6	8.0/7.6
6	3.2/1.6	3.4/2.1
7	0.7/0.4	1.5/0.8
8	0.0/0.0	not tested
10	2.9/0.9	3.2/1.4
MnO_2	0.0/0.0	0.0/0.0

[a] Oxygenation of **1** (0.4 mmol) in the presence of a metal catalyst (0.5 mol%) dissolved in 1 mL MeCN and the direct addition of H_2O_2 (30%, 2 mmol) dissolved in 1 mL MeCN; [b] oxygenation of **1** (0.4 mmol) in the presence of a metal catalyst (0.5 mol%) dissolved in 1 mL MeCN, syringe pump addition of H_2O_2 (30%, 2 mmol) dissolved in 1 mL MeCN at a rate of 0.3 mL/h.

Table S8. Photocatalytic C–H oxygenation of alkylbenzenes and related substrates using RFT in the absence of a co-catalyst.[a]

Entry	Substrate	Product	R,n,X	Irr. Time [h]	Yield [%][b]
1[c]	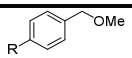	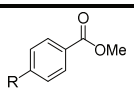	H	24	12
			OMe	3.0	26
2[c]	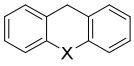	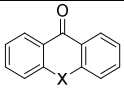	O	1.5	35
			S	0.1	18
3	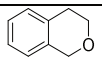	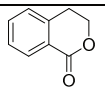	-	2.5	38
4			1	2.0	7
			2	2.0	8
5			-	2.5	20
6		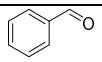	-	1.5	38
7	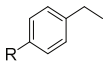	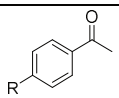	OMe	2.5	34
			Br[d]	2.5	54
			H[d]	1.0	42
8	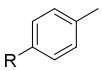	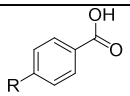	OMe	8	0
			Cl[d]	5	0
			Br[d]	5	0
9	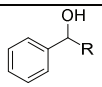	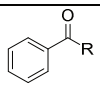	H	2.5	52
			Me	2.5	30
10	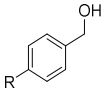		F	2.5	40
			Cl	1.0	50
			Br	2.5	49
			NO_2	16	19
			CO_2Me	4.5	39
			CF_3	8	24

[a] All reactions were performed with substrate (0.02 mmol) and RFT (10 mol%) in 1.5 mL MeCN/H_2O (1/1 v/v) and irradiated with blue light (440 nm, 3 W). Deviations from these conditions are marked in brackets. [b] Conversion and yield determined by GC-FID integration; [c] solvent MeCN [d] solvent MeCN, additive $HClO_4$ (30 mol%).

3.5.3 UV-vis spectroscopic reaction monitoring

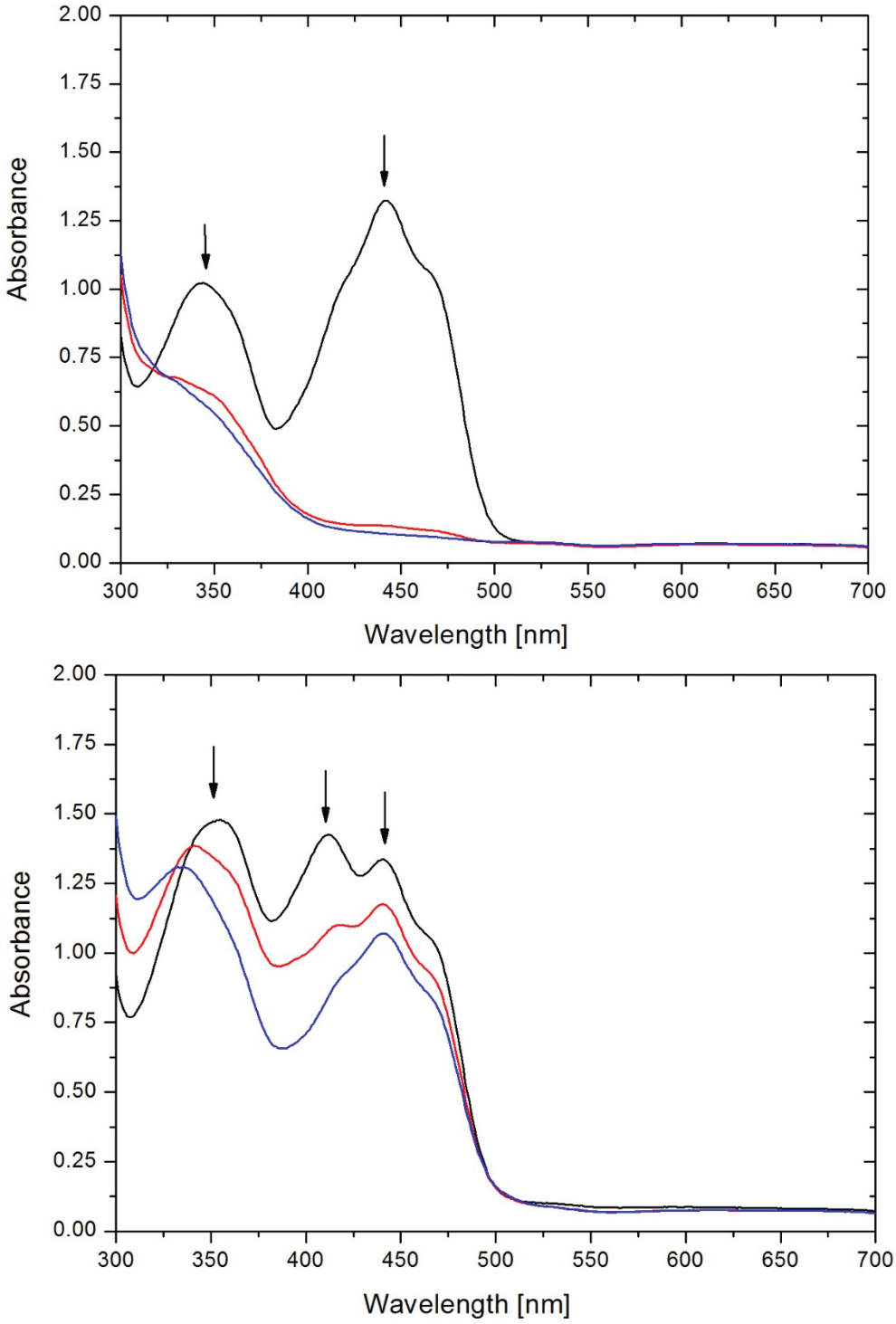

Figure S1. UV-vis spectra of the addition of various amounts of 30% H_2O_2 (0 µL, 2µL and 15µL) to RFT (0.1 mM) in the absence of **4** (top) and in the presence of **4** (0.1 mM, bottom) in MeCN.

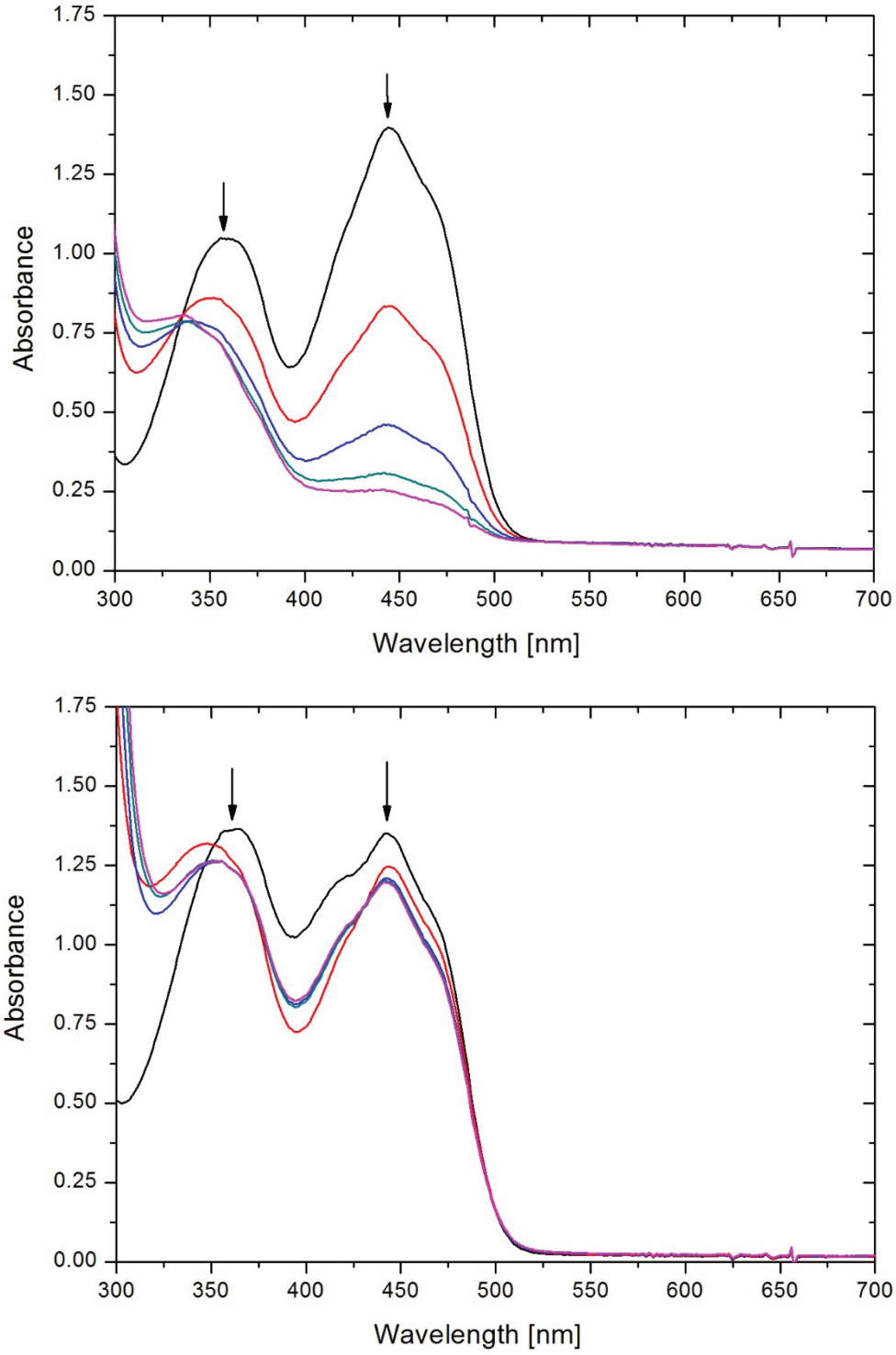

Figure S2. UV-vis absorption spectra of **4** (5.7 mM) and RFT (0.1 mM) in the absence of **1** (top) and in the presence of **1** (0.2 mM, bottom) during irradiation with blue light in 5 min steps in MeCN/water mixtures (1:1, v/v%) at 298 K under aerobic conditions**.**

3.5.4 Reaction time profiles of selected oxygenation reactions

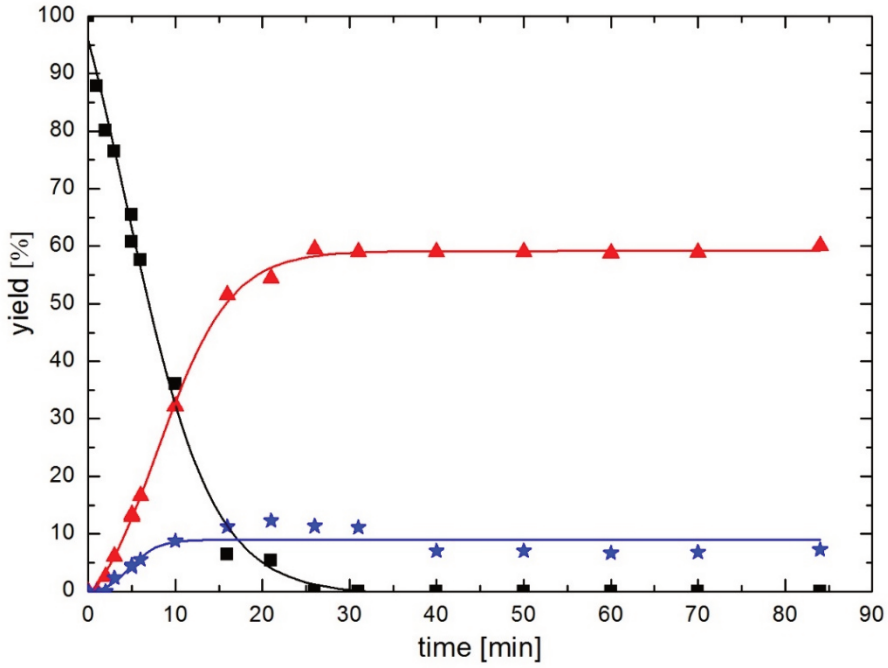

Figure S3. Reaction time profile of the photocatalytic oxygenation of **1** (■) to **2** (▲) and **3** (∗) in the presence of MnO_2 (3 mg, 60 mol%) and RFT (8 mol%) in MeCN/water (1/1 v/v). Lines are visual guides only.

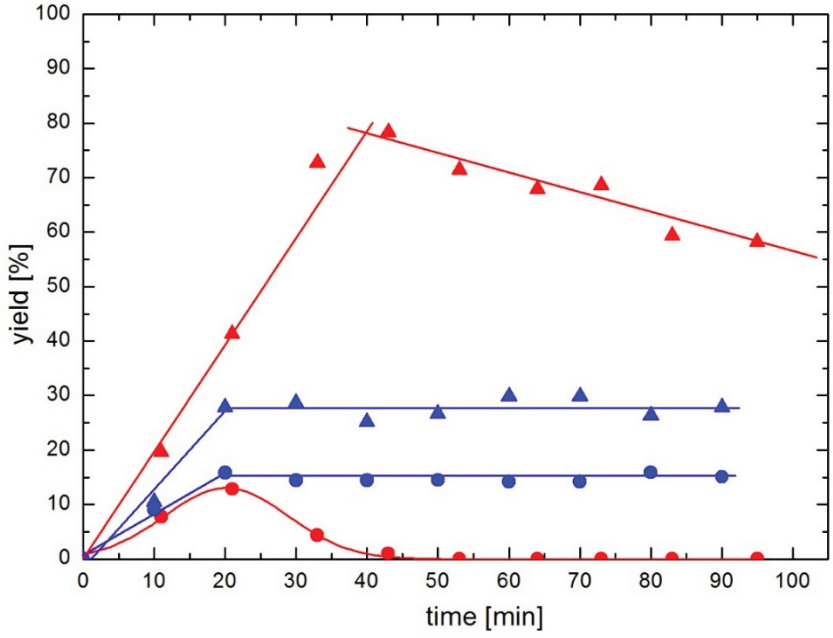

Figure S4. Reaction time profile of the photocatalytic oxygenation of **1** to **2** (▲) and **3** (●) in the presence of RFT (10 mol%) and a non-heme iron catalyst (8 mol%) in MeCN/water (1/1 v/v); **7** (▲, $[Fe(Ph\text{-}DPAH)_2](OTf)_2$), **8** (▲, $[Fe(Me_6TREN)(OTf)](OTf)$). Lines are visual guides only.

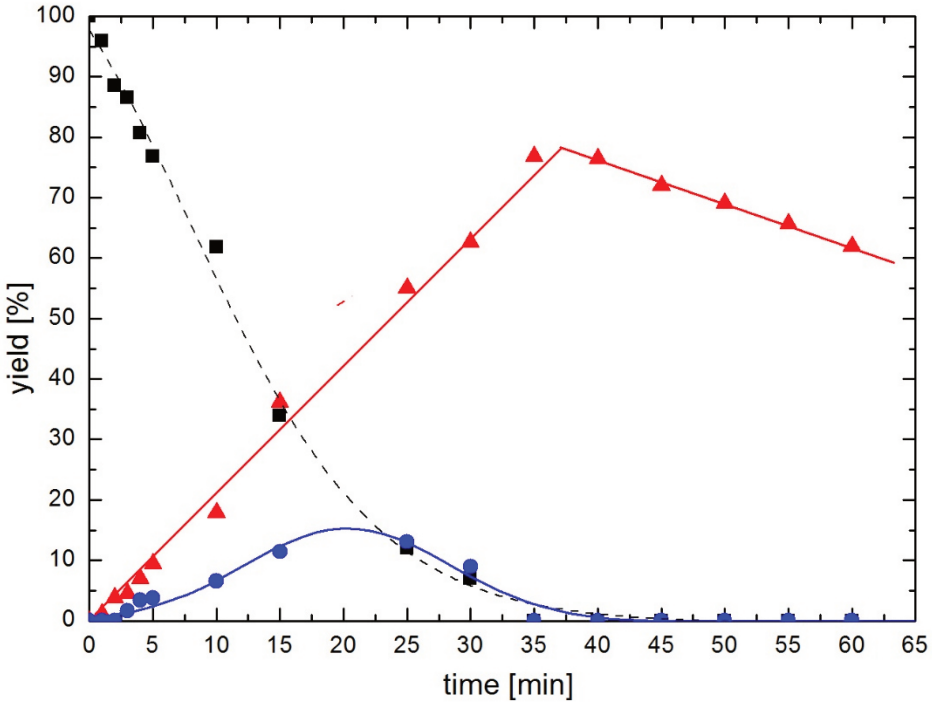

Figure S5. Reaction time profile of the photocatalytic oxygenation of **1** (■) to **2** (▲) and **3** (●) and in the presence of $Fe(ClO_4)_2$ (**9**, 8 mol%) and RFT (10 mol%) in MeCN/water (1/1 v/v). Lines are visual guides only.

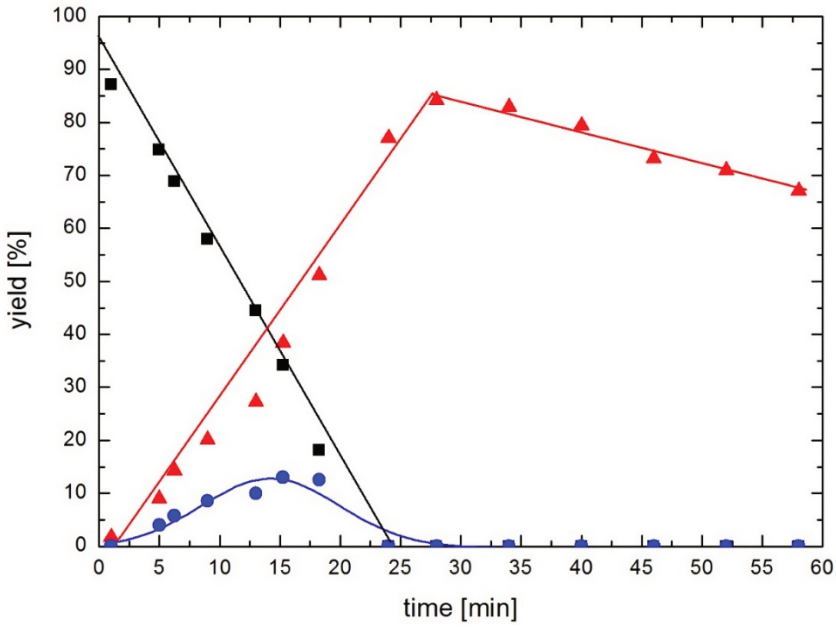

Figure S6. Reaction time profile of the photocatalytic oxygenation of **1** (■) to **2** (▲) and **3** (●) in the presence of $Fe(ClO_4)_3$ (**10**, 8 mol%) and RFT (10 mol%) in MeCN/water (1/1 v/v). Lines are visual guides only.

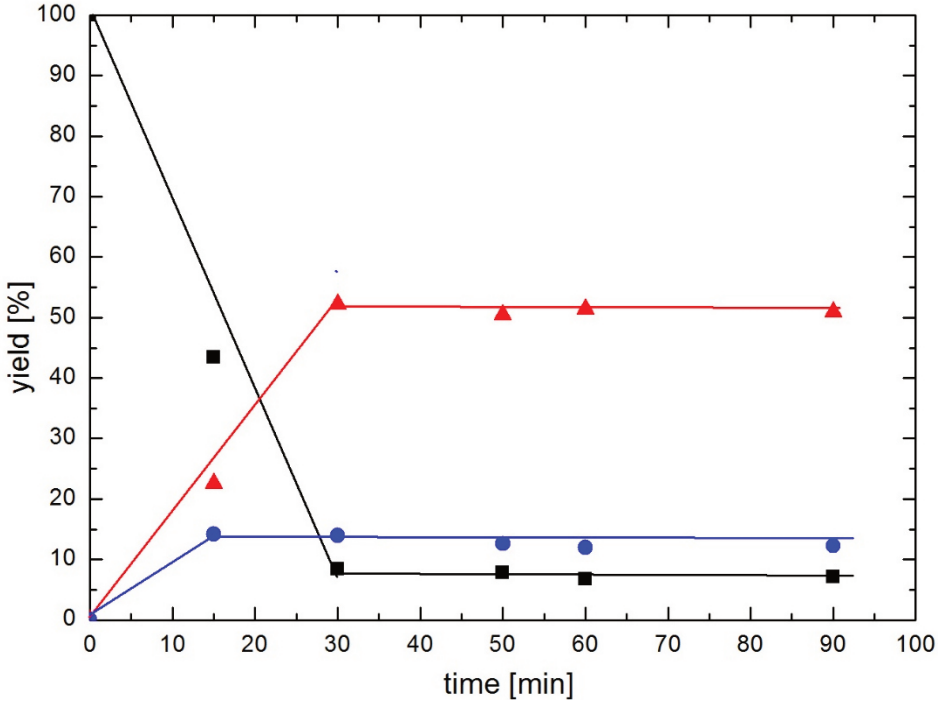

Figure S7. Photocatalytic oxygenation of **1** (■) to **2** (▲) and **3** (●) in the presence of $Fe(acac)_2$ (**11**, 8 mol%) and RFT (10 mol%) in MeCN/water (1/1 v/v). Lines are visual guides only.

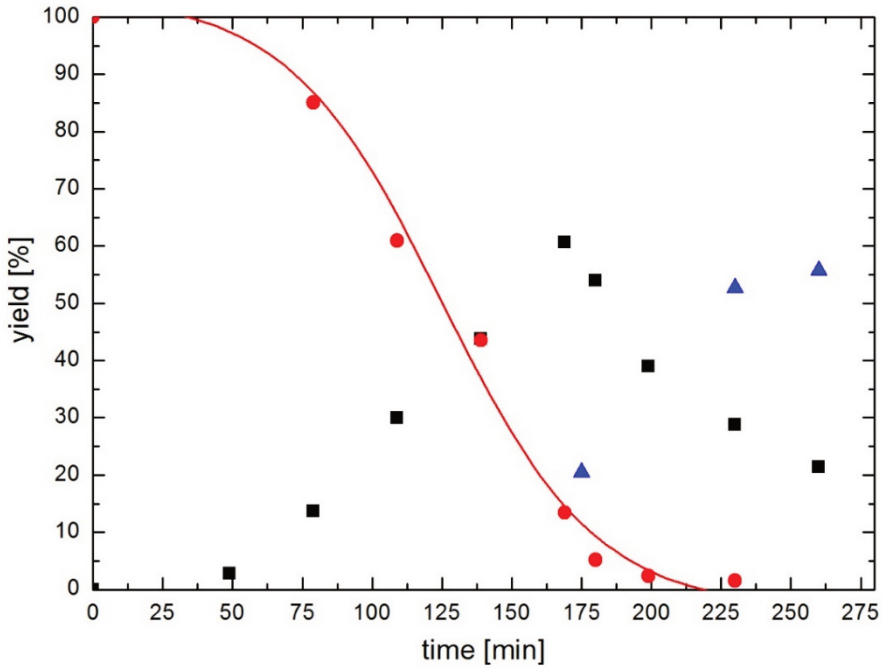

Figure S8. Reaction time profile of the photocatalytic oxygenation of 4-methoxytoluene (●) to 4-methoxybenzaldehyde (■) in the presence of RFT (8 mol%) and **4** (8 mol%) in MeCN. The formation of the corresponding 4-methoxybenzylester (▲) was confirmed by esterification with $TMSCH_2N_2$ (20 eq.). Lines are visual guides only.

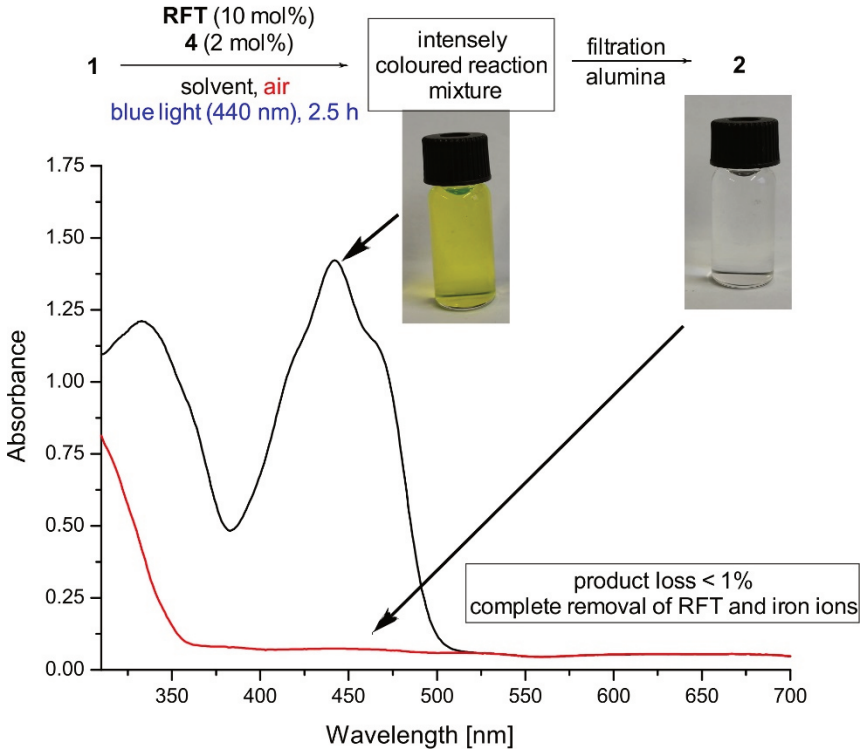

Figure S9. Removal of the catalysts by filtration through basic alumina; UV-vis spectra before (black) and after the filtration (red).

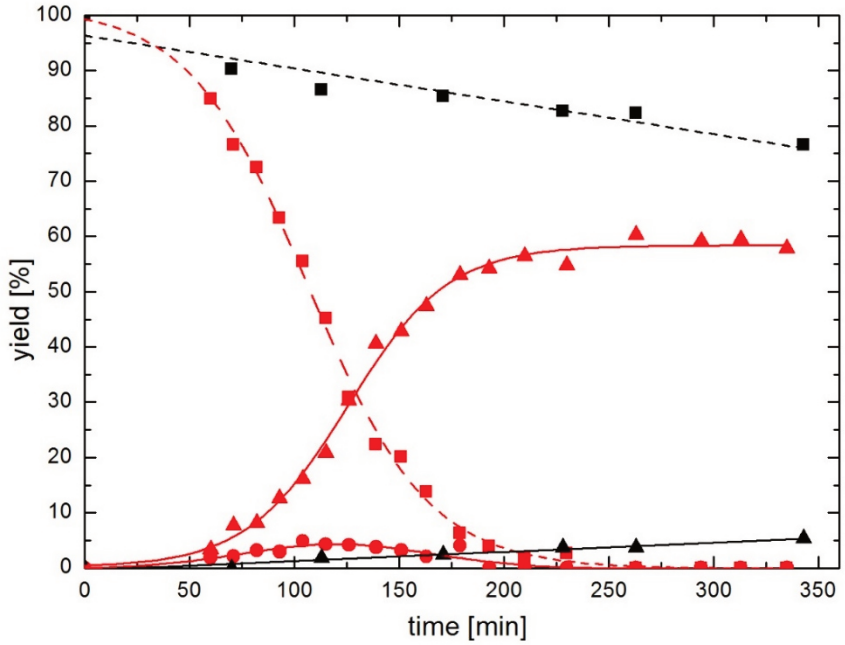

Figure S10. Reaction time profile of the photocatalytic oxygenation of **1** (■) to **2** (▲) and **3** (●) with RFT (10 mol%, black) and in the presence of **4** (8 mol%) in neat MeCN (red). Lines are visual guides only.

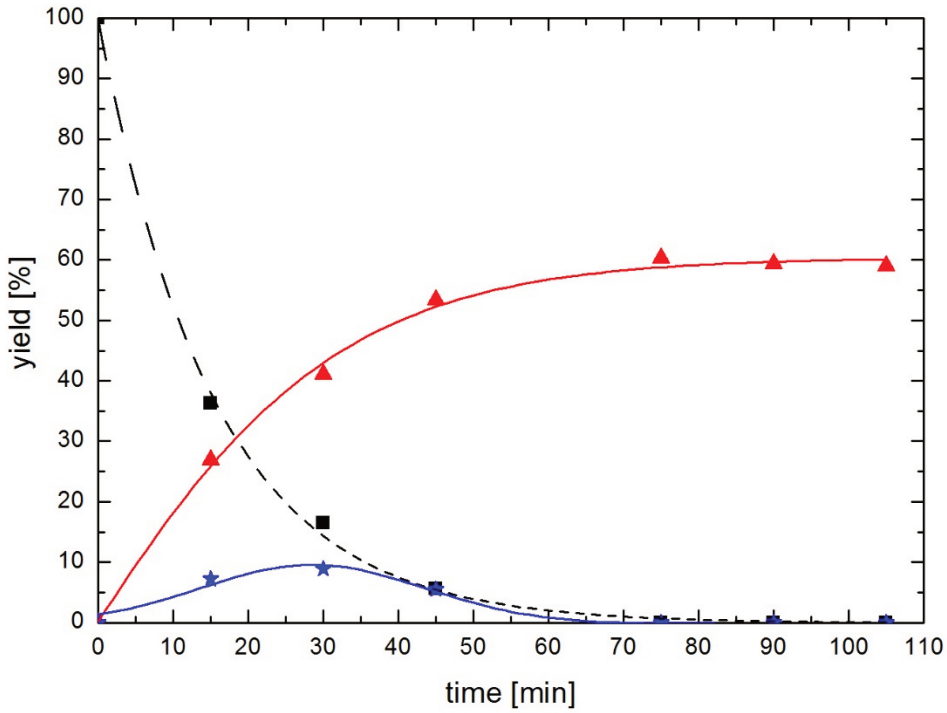

Figure S11. Reaction time profile of the photocatalytic oxygenation of **1** (■) to **2** (▲) and **3** (*) in the presence of **4** (8 mol%) and RFT (10 mol%) in CD_3CN/D_2O (1/1 v/v). Lines are visual guides only.

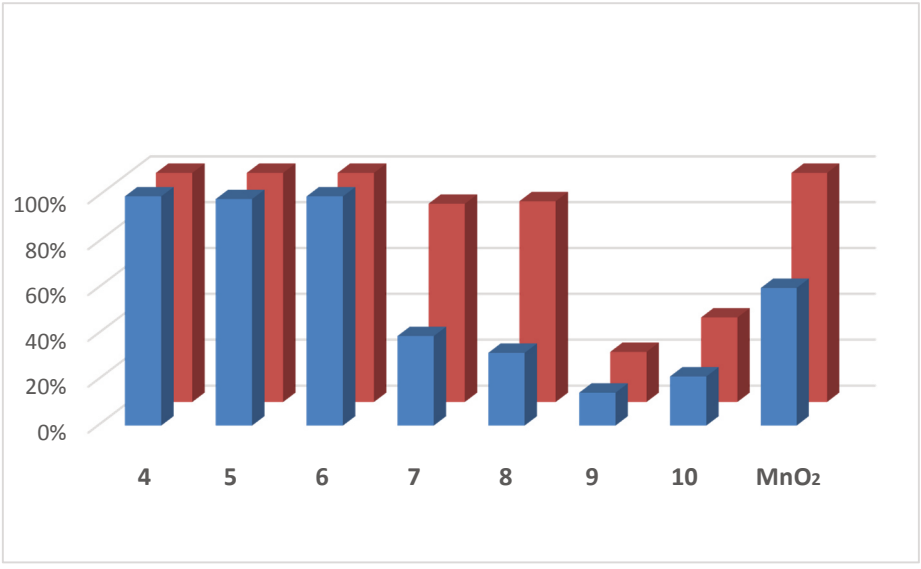

Figure S12. Decomposition of H_2O_2 (30%, 10 eq.) in the presence of an iron catalyst (**4** – **10**), and MnO_2 (10 mol%) after 1 min (blue) and after 10 min (orange). The percentage of H_2O_2 present in the reaction mixtures was determined by UV-vis spectroscopy.

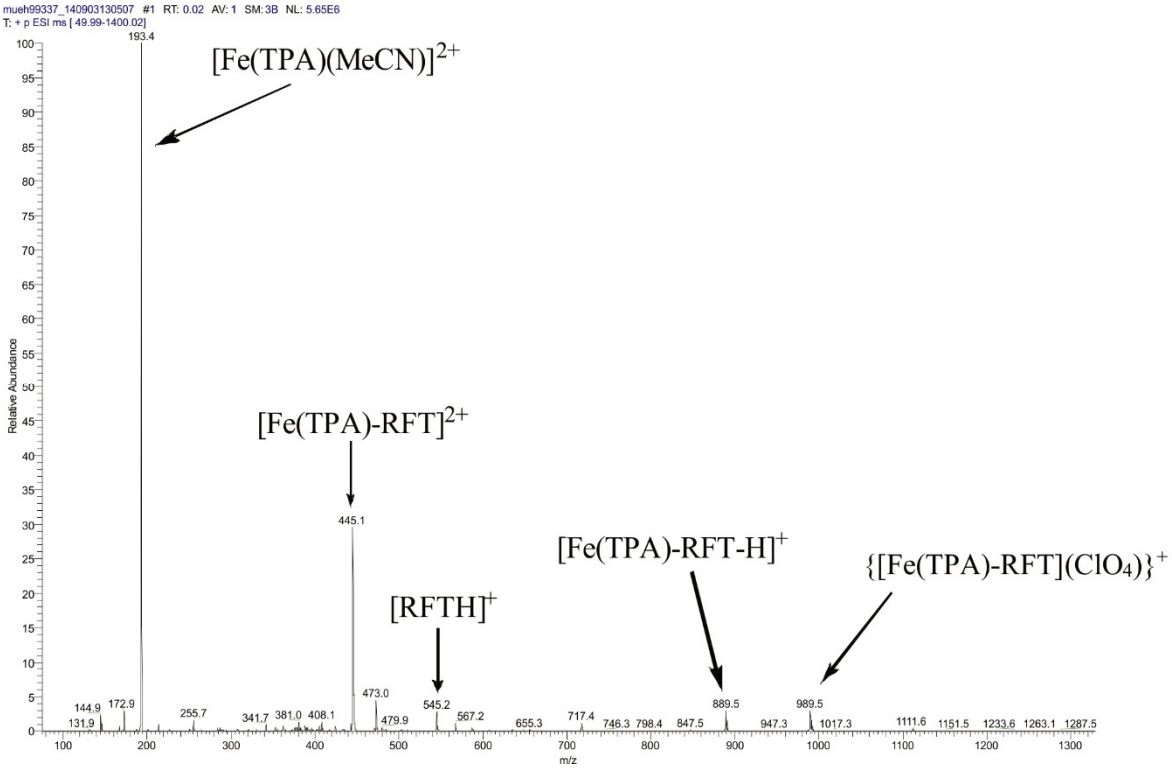

Figure S13. ESI-MS spectrum of a mixture containing RFT and **4**. Peaks at m/z of 193.4 and 545.2 correspond to $[Fe(TPA)(MeCN)]^{2+}$ and $RFTH^{+}$, respectively. Peaks at m/z of 445.1, 889.5 and 989.5 may indicate adduct formation between RFT and **4**.

3.5.5 References

[S1] A. Diebold, K. S. Hagen, *Inorg. Chem.* **1998**, *37*, 215–223.

[S2] I. Prat, A. Company, T. Corona, T. Parella, X. Ribas, M. Costas, *Inorg. Chem.* **2013**, *52*, 9229–9244.

[S3] G. J. P. Britovsek, J. England, A. J. P. White, *Inorg. Chem*. **2005**, *44*, 8125–8134.

[S4] P. D. Oldenburg, A. A. Shteinman, L. Que, *J. Am. Chem. Soc*. **2005**, *127*, 15672–15673.

[S5] S. Alagaratnam, N. J. Meeuwenoord, J. A. Navarro, M. Hervás, M. A. De la Rosa, M. Hoffmann, O. Einsle, M. Ubbink, G. W. Canters, *FEBS J*. **2011**, *278*, 1506–1521

4 Aerobic Photooxidation of Cycloalkenes Catalyzed by Riboflavin Tetraacetate and a Non-Heme Iron Complex[a]

Bernd Mühldorf and Robert Wolf

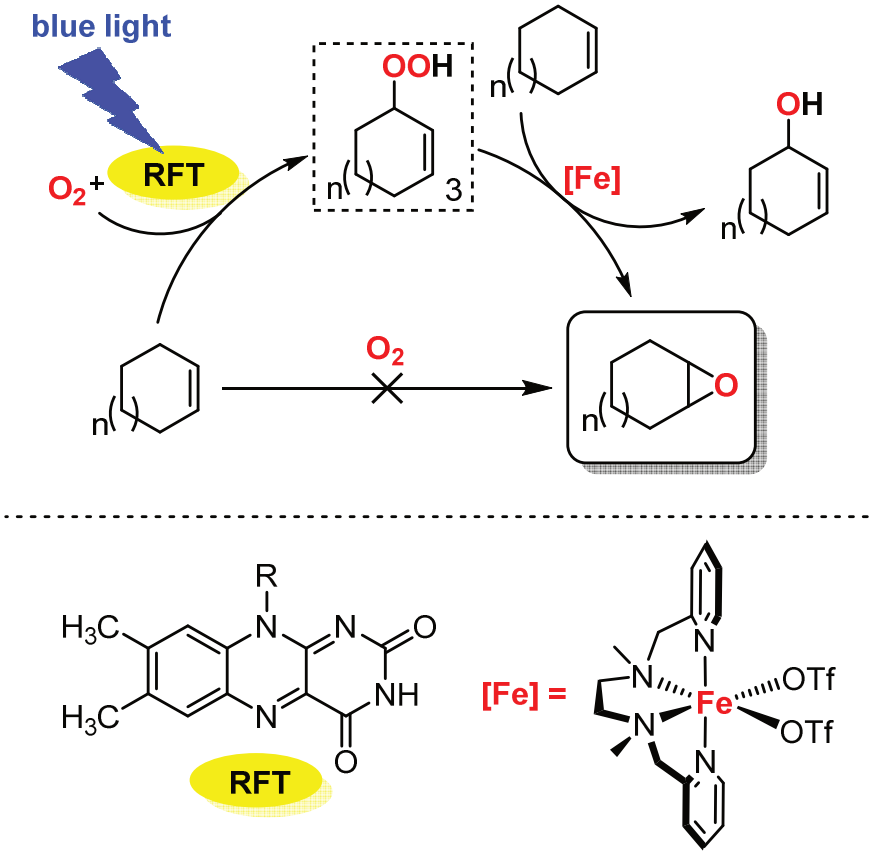

[a] Unpublished results

4.1 Introduction

Hydrocarbons are rather inert compounds requiring chemical functionalization such as oxygenation prior to use for further chemical transformations.[1] Oxygenated hydrocarbons – epoxides in particular – are useful synthetic intermediates for a variety of products. Traditionally, epoxides are prepared by reacting alkenes with stoichiometric amounts of high cost reagents such as peracids[2] or by alkaline dehydrochlorination of chlorohydrins,[3] which is a highly atom-uneconomic and waste generating process. Green chemistry requirements indicate that hydrogen peroxide or dioxygen are the most suitable reagents from an economic and environmental point of view.[4] Nature uses metalloenzymes (cytochrome P450 and non-heme based oxygenases) to perform selective oxyfunctionalizations with dioxygen under mild conditions.[5] Unfortunately, only a few examples, mainly manganese or ruthenium porphyrin complexes, are capable of performing the catalytic alkene epoxidations with aerobic dioxygen directly, nevertheless the yields are low and the selectivity is poor.[6,7]

Since the direct utilization of dioxygen as oxidant is challenging,[4] alternative procedures were developed. Ishii and co-workers reported a protocol for the epoxidation of cycloalkene derivatives of type **1** to epoxides **2a**, where stoichiometric quantities of ethylbenzene **A** were combined with the radical initiator **PINO** to generate an *in situ* formed alkyl hydroperoxide intermediate **B**, which acts as an oxidant for the epoxidation catalyst $Mo(CO)_6$ (Scheme 1).[8] **B** is reduced to the by-products alcohol **C** and ketone **D**, which is a common problem for this type of reaction. The reaction of alkyl hydroperoxides with metal complexes is well-known (Sharpless epoxidation, Halcon process, Shell process), but it is mainly restricted to high-valent d^0 transition-metal compounds of Ti^{IV}, V^{V}, Mo^{VI} and W^{VI}.[9] Importantly, catalysts common in autooxidation processes such as $Co^{II,III}$, $Mn^{II,III}$ or $Fe^{II,III}$ catalyze instead the homolytic decomposition of alkyl hydroperoxides[10] (Haber-Weiß mechanism) to alcohols and ketones (Russel-type termination steps) and thus are not suitable for selective oxygenations.

In recent years, bioinspired non-heme iron complexes with polydentate *N*-donor ligands were developed which gave access to distinct high-valent oxo-species when reacted with hydrogen peroxide[11] and alkyl hydroperoxides (such as *tert*-butyl hydroperoxide).[12] These non-heme iron catalysts perform regioselective C−H oxidations of alkanes and epoxidations or *cis*-dihydroxylations of alkenes.[12] Nevertheless, only a few of these catalysts give truly satisfactory results in terms of efficiency, chemo- and enantioselectivity. Additionally, the choice of the oxidant is crucial. For example $[Fe(bpmen)(OTf)_2]$ (bpmen = *N*,*N*′-dimethyl-*N*,*N*′-bis(2-pyridylmethyl)-1,2-diaminoethane, OTf = trifluoromethanesulfonate, Scheme 1), a typical and widely-used biomimetic epoxidation catalyst, shows striking differences in its reactivity towards

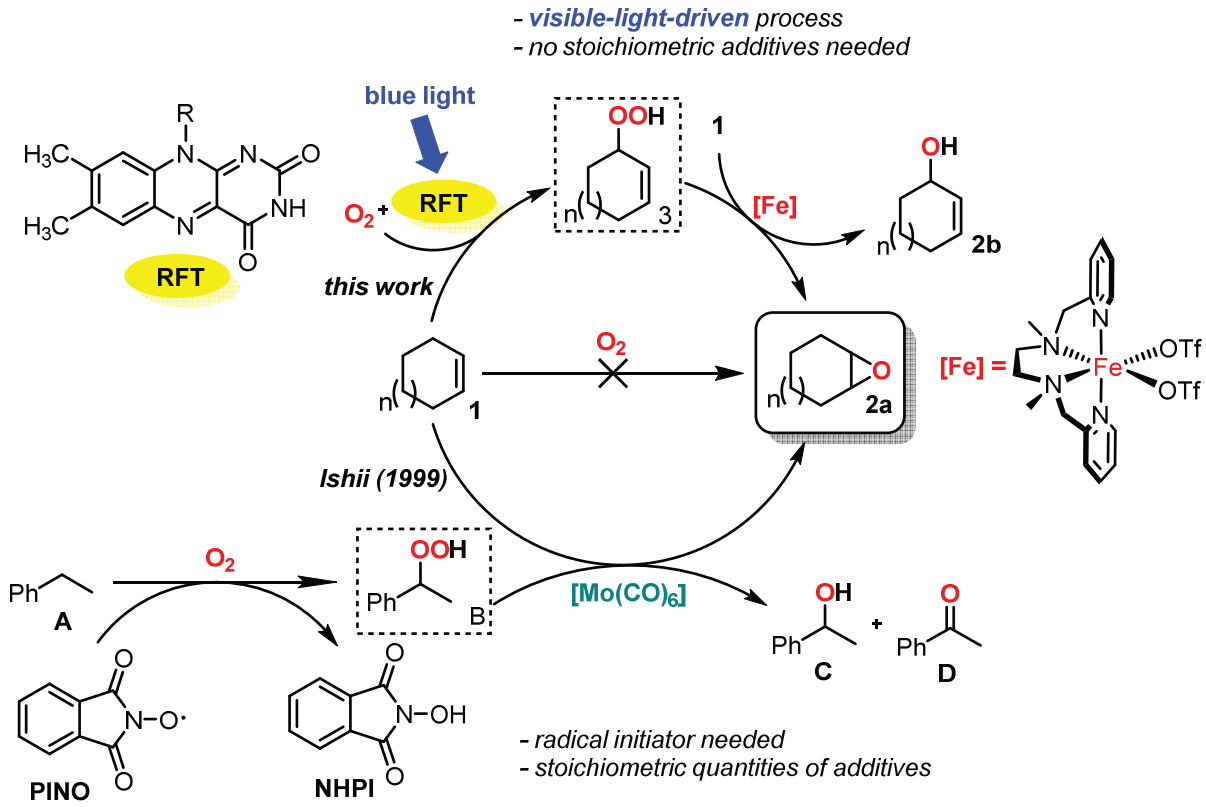

Scheme 1. Epoxidation of cycloalkanes (n = 1−3) via *in situ* generated alkyl- or allylic hydroperoxides; R=$CH_2(CHOAc)_3CH_2OAc$, **PINO** = hydroxyphthalimide-*N*-oxide radical, **NHPI** = *N*-hydroxyphthalimide.

different oxidants. For instance, when [Fe(bpmen)$(OTf)_2$] is reacted with hydrogen peroxide, an iron(V)-oxo species responsible for alkene epoxidation was observed by EPR spectroscopy. In contrast, no EPR evidence of an iron(V)-oxo species was found for the reaction of [Fe(bpmen)$(OTf)_2$] with the alkyl hydroperoxide ^{t}BuOOH.[13] This combination consistently failed to epoxidize olefins, indicating the importance of the reactive iron(V)-oxo species.[13]

Inspired by the work of Maldotti[14,15] and Tonellato[16] who photochemically generated an allylic hydroperoxide (AHP) from an alkene *via* singlet oxygen sensitization and utilized this AHP *in situ* as an oxidant for epoxidation reactions with iron(III) porphyrins or $Mo(CO)_6$, we conceived a photocatalytic protocol based on a flavin analogue as a singlet oxygen photosensitizer and a non-heme iron complex as epoxidation catalyst. According to Scheme 1, the excitation of the flavin analogue riboflavin tetraacetate (RFT) with blue light in the presence of air leads to singlet oxygen sensitization.[17][18] Singlet oxygen then reacts with the substrate **1**, producing the allylic hydroperoxide **3** *in situ* in a Schenck-ene type reaction. In the presence of a non-heme iron catalyst, **3** may act as an oxidant for the epoxidation of another equivalent of **1** to yield epoxide **2a**. The oxidant **3** is reduced to the allylic alcohol **2b**. This procedure should give access to the challenging epoxidation of

alkenes with air as the terminal oxidant *via* the photochemical generation of an allylic hydroperoxide as "true" oxidant, thus no stoichiometric quantities of additives or other oxidants such as described in traditional protocols are needed. Furthermore, we investigate if an allylic hydroperoxide is a suitable oxidant for non-heme iron catalysed epoxidation reactions.

4.2 Results and Discussion

Initial investigations focussed on the oxidation of *cis*-cyclooctene (**1**) in acetonitrile with various non-heme iron(II) complexes (**4** − **9**, 1−4 mol%) in the presence of RFT (1 mol %), blue light and dioxygen (Table 1). All reactions were performed in 10 mL Schlenk tubes purged with oxygen. The reaction mixtures were irradiated with a blue light-emitting diode (440 nm) overnight placed in a cooling block to exclude thermal activation pathways. The best results were obtained with catalyst **4** (Table 1), which gave 64% substrate conversion and a cyclooctene oxide (**2a**) yield of 31%. The formation of **2a** was also confirmed by GC-MS measurements (Figure S1). It is important to note that this procedure intrinsically limits the yield of **2a** to a maximum yield of 50%. The corresponding turnover number (TON) is 28, which is significantly higher than reported in the literature using catalyst **4** and H_2O_2 as the terminal oxidant.[19] For example, the epoxidation of **1** with **4** is performed with TON 7.5 using hydrogen peroxide as an oxidant. Only traces of 2-cyclooctene-1-one (**2c**) were detected. We assume that polymeric by-products, which cannot be detected in GC analysis (*vide infra*), are also formed. Catalysts **5**, **6** and **8** gave comparable results to catalyst **4**, but were less effective. As an example for a catalyst with two tridendate *N*,*N*,O-ligands, catalyst **7** favours the formation of allylic by-products (2-cyclooctene-1-ol (**2b**) and 2-cyclooctene-1-one (**2c**). Catalyst **9** does give any epoxide, but catalyzes the formation of allylic compounds **2b** and **2c**.

Next to cyclooctene (Scheme 2a), the mixture of RFT and **4** also catalyzes the oxygenation of cyclohexene (**10**, Scheme 2a) to cyclohexene oxide (**12a**) with a turnover number of 14 (6% yield) under concomitant formation of 2-cyclohexene-1-ol (**12b**, TON = 8, 3% yield), 2-cyclohexene-1-one (**12c**, TON = 27, 11% yield) and 2-cyclohexenone oxide (**12d**, TON = 10, 4% yield). An excess of cyclohexene was used due to its volatility. The formation of **12c** and **12d** proceeds mainly *via* oxidation of **12b** by singlet oxygen, which abstracts a hydrogen atom in C3 position of **12b** generating intermediate **13** (Scheme 2b).[20] This abstraction is very unlikely in the case of the more flexible backbone in 2-cyclooctene-1-ol (**2b**), thus, a higher selectivity is observed.[21]

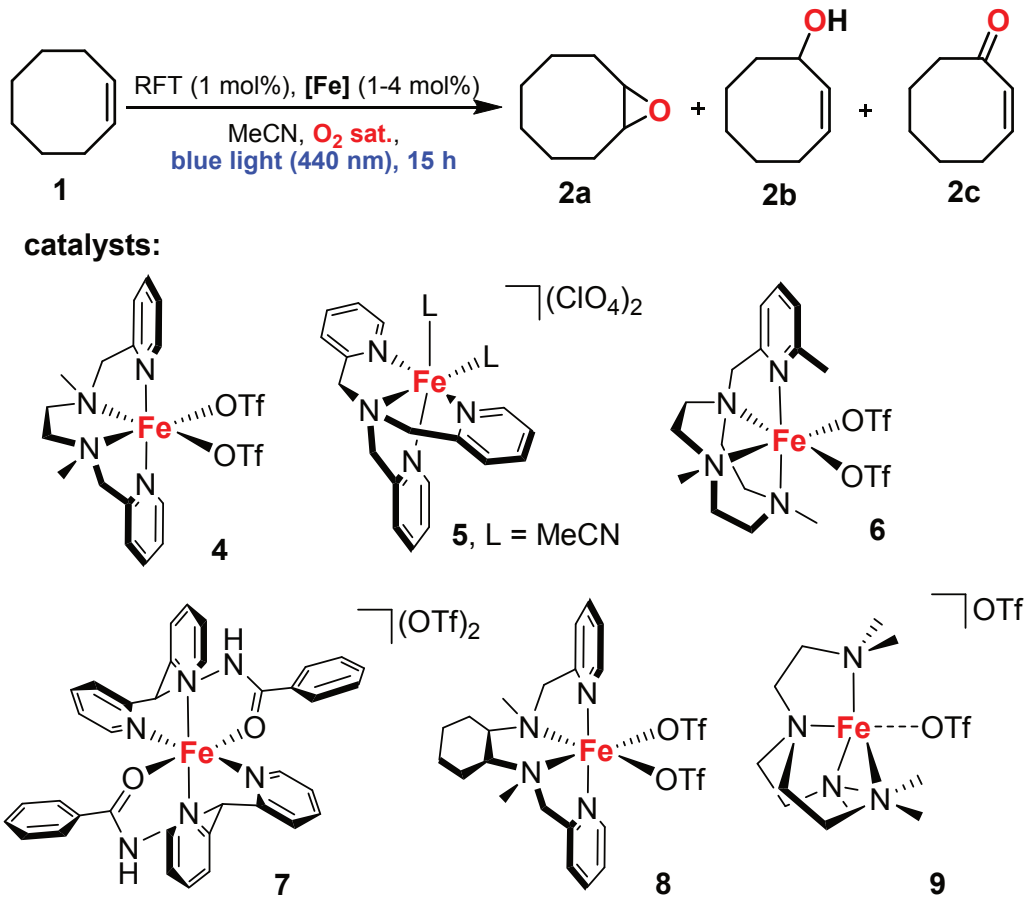

Table 1. Photocatalytic epoxidation of **1** – screening of non-heme iron catalysts

Entry	[Fe]	Conv. [%][b]	Yield 2a [%][b]	Yield 2b [%][b]	Yield 2c [%][b]	TON (2a)
1	**4**	64	31	0	4	28
2	**5**	61	24	0	10	15
3	**6**	44	16	0	5	9
4	**7**	79	14	11	21	12
5	**8**	34	14	0	2	9
6	**9**	47	Traces	14	14	n.d.

[a] All reactions were performed with *cis*-cyclooctene (0.2 mmol), RFT (1 mol%), iron catalyst (1-4 mol%) in 2 mL MeCN. The samples were purged with pure dioxygen, capped, and placed in a cooling block during irradiation (15 h) with blue light (440 nm). [b] Conversion and yield determined by GC-FID integration; TON (turn over number) was determined as the molar ratio of **2a** and the corresponding iron catalyst **4-9**; n.d. = not determined. Non-heme iron catalysts **[Fe]**: [Fe(bpmen)](OTf)$_2$ (**4**), [Fe(TPA)(MeCN)$_2$]$^{2+}$ (**5**), [Fe(Me$_2$PyTACN)OTf$_2$] (**6**), [Fe(DPAH)$_2$] (**7**), [Fe(bpmcn)(OTf)$_2$] (**8**), [Fe(Me$_6$TREN)OTf](OTf) (**9**).

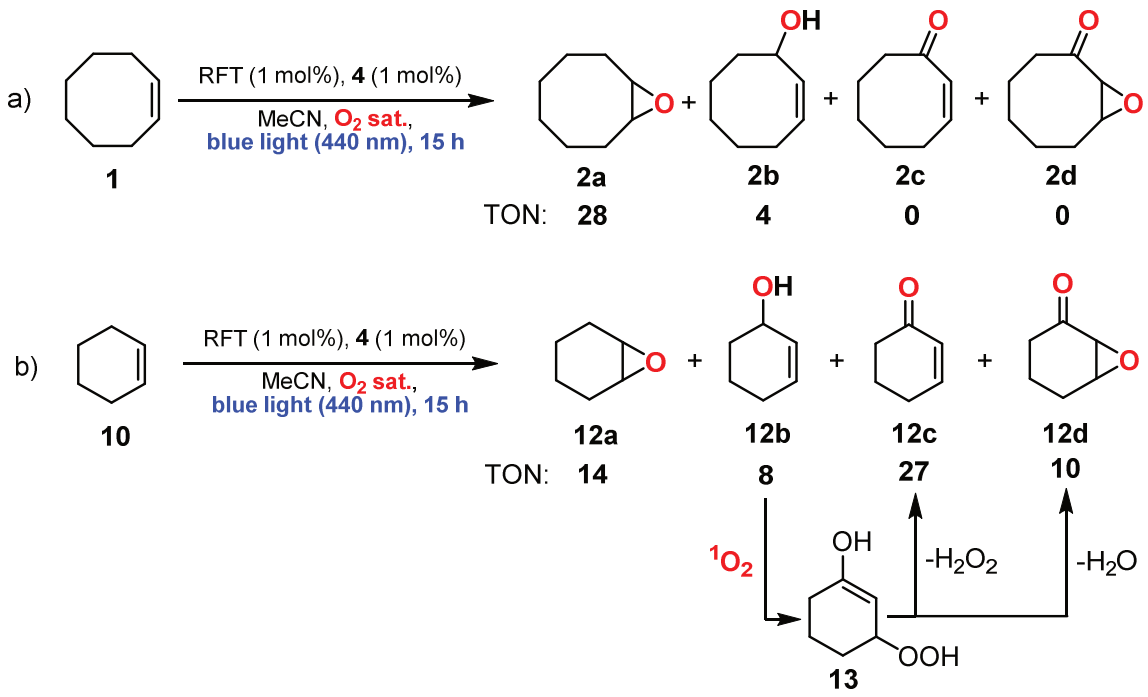

Scheme 2. Comparison of the reactivity of cyclooctene (**1**) with cyclohexene (**10**).

Control experiments showed that the epoxidation does not proceed in the absence of a non-heme iron catalyst, in the absence of RFT, in the dark or under an atmosphere of pure nitrogen (Table S1, entries 1−5). In addition, control experiments clearly show that the allylic product **2b** is not stable under the reaction conditions presumably due to polymerization (Table S1, entry 6), whereas **2c** is not prone to polymerization, decomposition or further transformations (Table S1, entry 7). Importantly, **1** is also consumed in the absence of an iron catalyst (44% conversion), but no epoxide is detected and only negligible amounts of **2b** and **2c** are observed (Table S1, entry 2). These oxidation products are formed by RFT *via* a singlet oxygen pathway. We tentatively attribute this mismatch in the mass balance, which is observed for all reactions under study, to the subsequent polymerization of **2b** to unidentifiable products. Indeed, **2b** was consumed (19% conversion) when **2b** was used as starting material in the presence of RFT in an additional control experiment (Table S1, entry 8). The conversion is even higher (79%) when **4** is added to RFT (Table S1, entry 6); the products were not identifiable.

Interestingly, inorganic salts, such as $Fe(ClO_4)_2$ and $Fe(ClO_4)_3$, are less effective epoxidation catalyst than complexes **4**–**9** (Table S1, entries 9−10), indicating that the tetradentate ligand is important. Traces of **2a** can be observed if the non-heme iron catalyst is substituted by ferrocene, excluding the role of the catalyst as an electron shuttle (Table S1, entry 11).

Reaction monitoring of the photocatalytic epoxidation of **1** in the presence of **4** and RFT (Figure 2) shows that the epoxide **2a** is continuously formed, while allylic alcohol **2b**

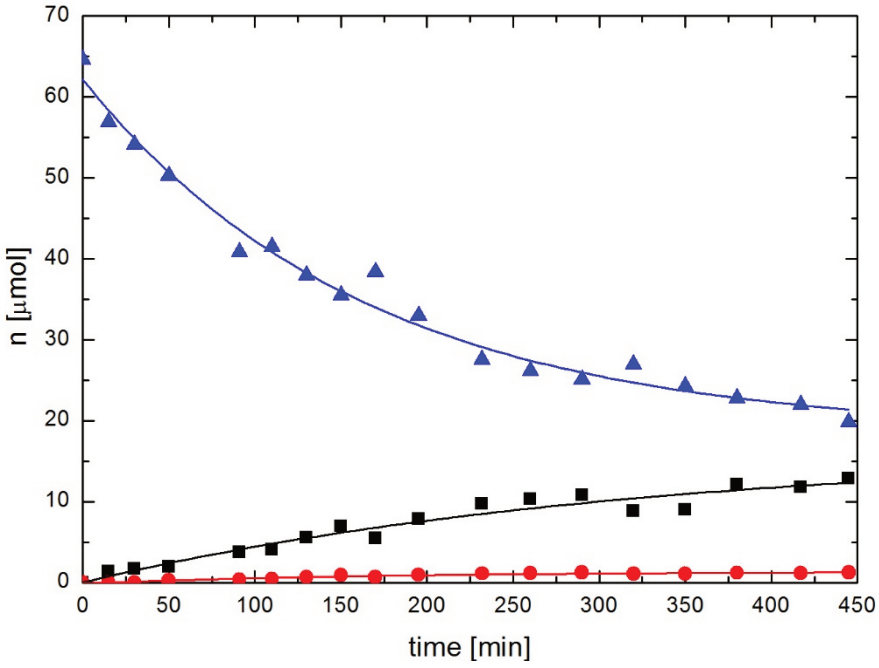

Figure 2. The epoxidation of *cis*-cyclooctene **1** (▲, 0.06 mmol) to epoxide **2a** (■) in the presence of **4** (3 mol%) and RFT (3 mol%) during irradiation with blue light (440 nm) in open vials, placed in a cooling block. The by-product **2c** (●) was detected in traces. Conversion and yield determined by GC-FID integration.

is not observed. Only negligible quantities of allylic ketone **2c** are detected. This indicates that the subsequent transformation of **2b** to presumably polymeric products by RFT is faster than the oxidation of **2b** to **2c** by the non-heme iron-catalyst **4**. The formation of epoxide **2a** is faster when the solvent mixture is purged with oxygen, emphasizing a possible singlet oxygen pathway.

4.3 Mechanistic Considerations

More insight into the reaction mechanism was gained by NMR spectroscopy. We illustrate our results with cyclohexene (**10**). The reaction was separated in two steps. In the first step allylic hydroperoxide **11** was generated by a Schenck-ene reaction (Scheme 2, step A). In the second step, the action of the non-heme iron complex as an epoxidation catalyst in the presence of **11** as oxidant is observed (step B).

First, we tested the ability of the chromophore RFT to sensitize singlet oxygen, which reacts with cyclohexene and forms allylic hydroperoxide **11**. We irradiated RFT in the presence of **10** and monitored the reaction by $^{13}C\{^{1}H\}$ NMR spectroscopy. The spectra unequivocally confirm the formation of 2-cyclohexen-1-yl-hydroperoxide (**11**) by the Schenck-ene reaction (Figure 3a). The spectrum obtained after irradiation with blue light for 12 h in acetonitrile is identical to that reported for **11** in literature.[22]

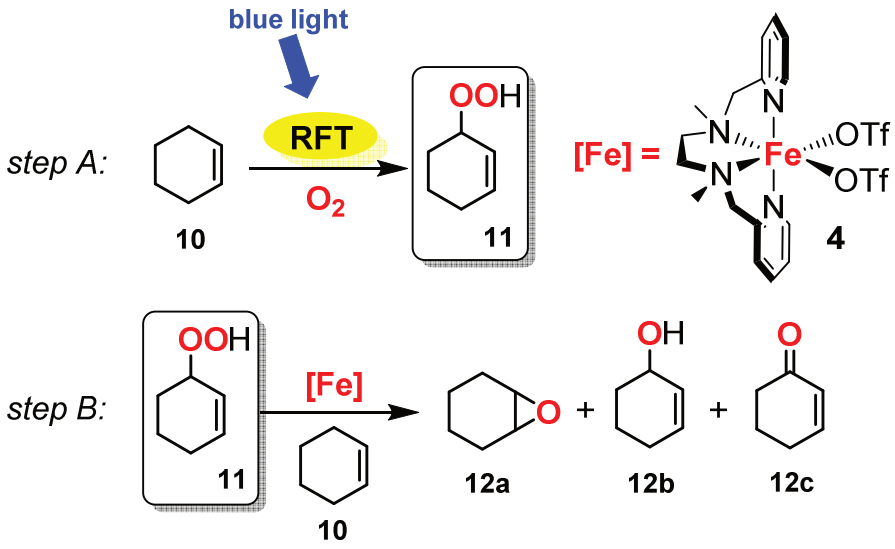

Scheme 2. Stepwise photocatalytic epoxidation of cyclohexene (**10**) as a model substrate; photocatalytic generation of key intermediate **11** by RFT in a Schenck-ene reaction (step A); epoxidation of **10** by non-heme iron catalyst **4** and **11** as the oxidant (step B).

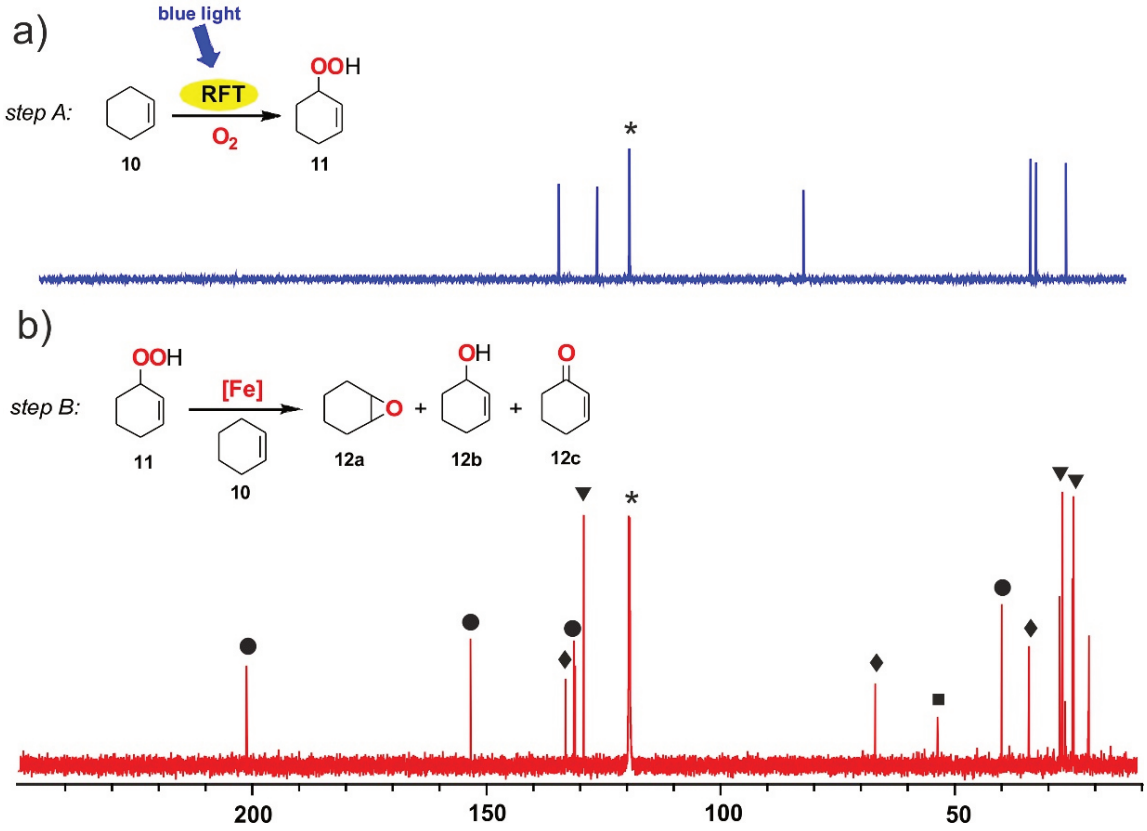

Figure 3. $^{13}C\{^{1}H\}$ NMR spectra (100.61 MHz, 300 K, CD_3CN): a) the formation of allylic hydrogen peroxide **11** by RFT and cyclohexene **10**, b) the reaction between **11** and non-heme iron catalyst **4** in the presence of an excess of **10**; signals are marked as follows: CD_3CN(*), **10** (▼), **12a** (■), **12b** (♦) and **12c** (●).

Second, allylic hydroperoxide **11** was slowly added to a mixture, containing **10** and non-heme iron catalyst **4** in the absence of RFT and in the dark. After stirring the solution for 10 minutes, **11** was fully consumed. The $^{13}C\{^{1}H\}$ NMR spectrum showed a mixture of **12a**, **12b** and **12c**. The assignment was confirmed by comparison with authentic samples.

If the described stepwise mechanism is valid, the yield of epoxide **2a** is intrinsically limited to 50% based on the starting material. One equivalent of **10** is utilized for the generation of allylic hydroperoxide **11** and another equivalent is needed to perform the epoxidation. To verify this assumption, we performed an additional control experiment. Allylic hydroperoxide **11** was generated in one separate step by RFT as described above (Scheme 3a). **11** was slowly added to cyclooctene **1** in the presence of non-heme iron catalyst **4** in *the absence of RFT and in the dark* (Scheme 3b). After 10 minutes, the reaction mixture was subjected to GC-FID analysis. If the assumption is valid, the amount of generated epoxide **2a** has to be equal to the amount of **12b** formed, or at least equal to the sum of **12b** and **12c**. The latter species is generated in an autoxidative iron-promoted reaction as confirmed by control experiments (*vide supra*). Indeed, the amount of generated epoxide **2a** was nearly identical to the sum of **12b** and **12b** (Scheme 3b).

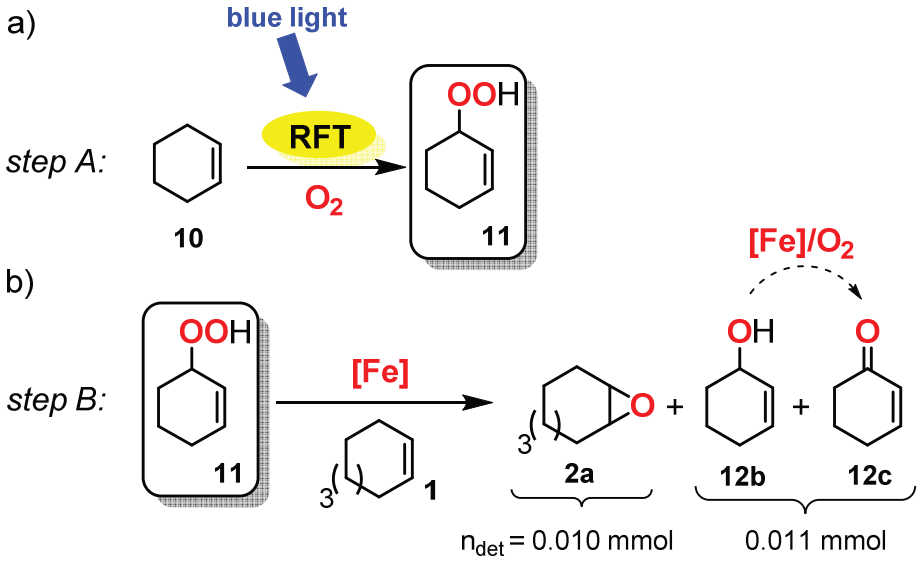

Scheme 3. a) Photocatalytic oxidation of cyclohexene to allylic hydroperoxide by RFT with singlet oxygen; b) epoxidation of cyclooctene **1** by the iron catalyst **4** and the oxidant **11**. The reduction of **11** yields **12b** which is subsequently oxidized to **12c**.

These results are summarized in our mechanistic proposal for the epoxidation of cyclooctene (Scheme 4). Based on our investigations, we propose the following reaction mechanism for the photocatalytic aerobic epoxidation of cyclooctene (Scheme 4). The excitation of the chromophore RFT leads to the rapid formation of ^{3}RFT *via* intersystem crossing (ISC) from the excited singlet state ^{1}RFT. The reaction of ^{3}RFT with $^{3}O_2$ affords

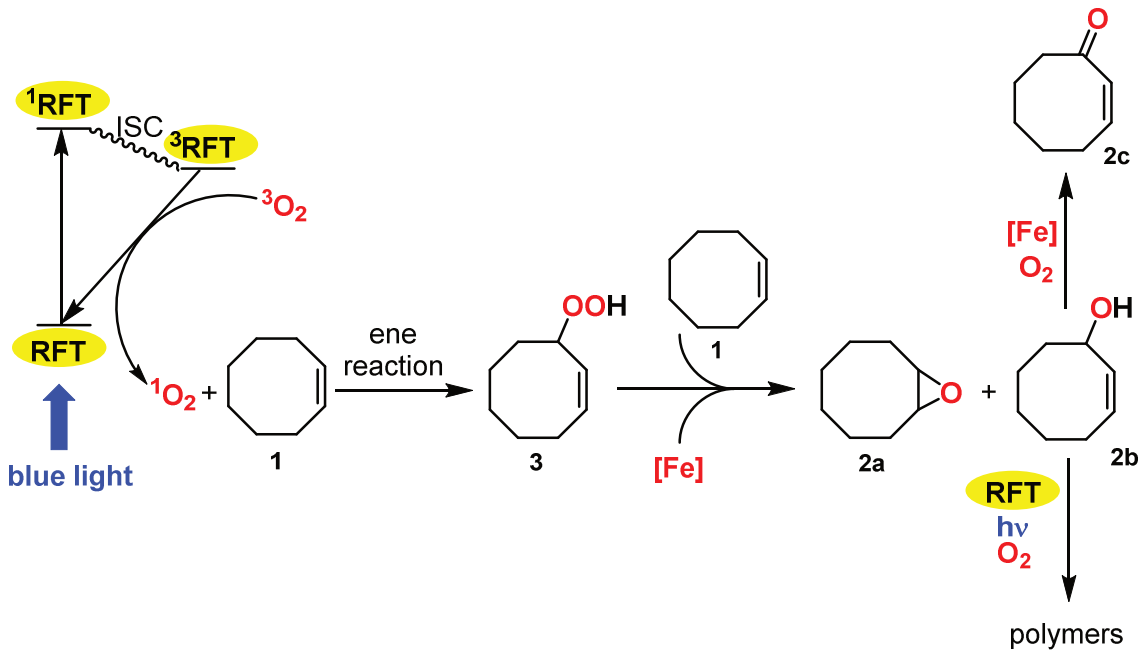

Scheme 4. Mechanistic proposal for the photocatalytic aerobic epoxidation of cyclooctene **1** in the presence of the photocatalyst RFT and the epoxidation catalyst **4**.

$^1O_2$, which subsequently reacts with cyclooctene **1** to the allylic hydroperoxide **3** in a Schenck-ene reaction. We propose that **3** is capable of oxidizing a non-heme iron catalyst to a high-valent iron-oxo species, yielding by-product **2b**. This iron-oxo species acts as an epoxidation catalyst for another equivalent of cyclooctene **1**, generating epoxide **2a**. Our control experiments confirmed that the by-product **2b** is not stable under our experimental conditions. **2b** is further oxidized to the corresponding allylic ketone **2c** in the presence of the iron-catalyst. Additionally, **2b** is prone to polymerization mainly initiated by RFT and $^1O_2$.

In the course of our investigations, we wondered if the combination of **4** and **11** yields epoxy alcohols of type **14** in the absence of **10**. This reaction is similar to the Sharpless epoxidation, where allylic alcohols are converted into epoxy alcohols in the presence of the catalyst Ti(O^iPr)$_4$ and the oxidant ^{t}BuOOH (Scheme 5). However, the addition of **11** to the iron catalyst did not give any indication of the formation of **14**. Instead, the formation of allylic alcohol **12b** and allyl ketone **12c** was observed (Figure S2). The formation of these species indicates that **4** is able to reduce **11** to **12b**, but the subsequent epoxidation of the double bond is in direct competition with the oxidation of the allylic alcohol to the corresponding ketone **12c**.

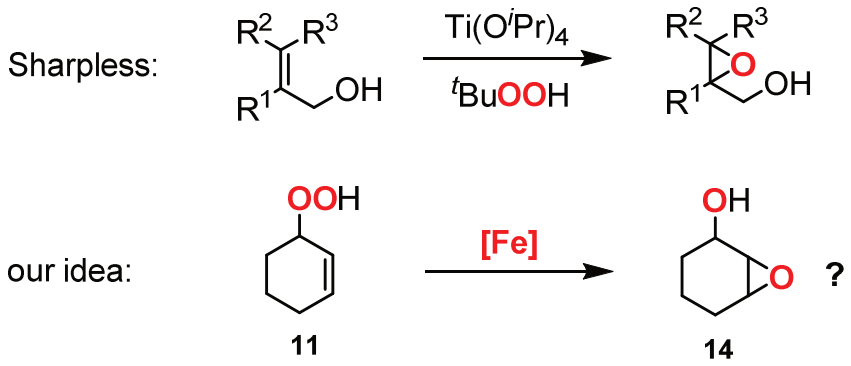

Scheme 5. Formation of epoxy alcohols from allylic alcohols in the Sharpless epoxidation (top) and intramolecular formation of epoxy alcohols of type **14** from allylic hydroperoxide **11** in the presence of a non-heme iron catalyst (bottom).

4.4 Conclusion and Outlook

We report the photocatalytic epoxidation of cyclooctene and cyclohexene to their corresponding epoxides by atmospheric oxygen as terminal oxidant and under visible light irradiation. The stepwise investigation of the reaction mechanism confirms that a) RFT is able to generate an allylic hydroperoxide by the Schenck-ene-reaction *via* singlet oxygen sensitization and b) the non-heme iron catalyst utilizes the *in situ* generated allylic hydroperoxide as an oxidant for the epoxidation of cycloalkenes. The reaction of allylic hydroperoxides and non-heme iron catalysts appears to be unknown in the literature, thus no detailed information of the reactive iron-oxo species is available so far.

4.5 Experimental Section

Materials

RFT was prepared according to a known literature procedure.[23] All other chemicals were obtained commercially (Sigma Aldrich, VWR). Cyclooctene and Cyclohexene were distilled prior to use and filtered over basic Al_2O_3. The iron catalysts were prepared as described in the literature: [Fe(bpmen)](OTf)$_2$ (**4**)[24], [Fe(TPA)(MeCN)$_2$](ClO$_4$)$_2$ (**5**)[25], [Fe(Me$_2$PyTACN)OTf$_2$] (**6**)[26], [Fe(DPAH)$_2$] (**7**)[27], [Fe(bpmcn)(OTf)$_2$] (**8**)[28], [Fe(Me$_6$TREN)OTf](OTf) (**9**)[24].

Representative procedure for the formation of epoxide 2a

Iron catalyst (1−4 mol%) was added to a mixture of *cis*-cyclooctene (0.2 mmol) and RFT (1 mol%) in 2 mL MeCN. The samples were purged with pure dioxygen, capped, and placed in a cooling block during irradiation (15 h) with blue light (440 nm). After 15 h of irradiation, *n*-pentadecane (internal standard), saturated Na_2CO_3 and brine were added. The organic phase was extracted with ethylacetate and subjected to GC-FID analysis. The retention time was verified with authentic samples. Conversion and yield were determined by GC-FID integration; TON (turnover number) was determined as the molar ratio of **2a** and the corresponding iron catalyst **4**−**9**.

4.6 Supporting Information

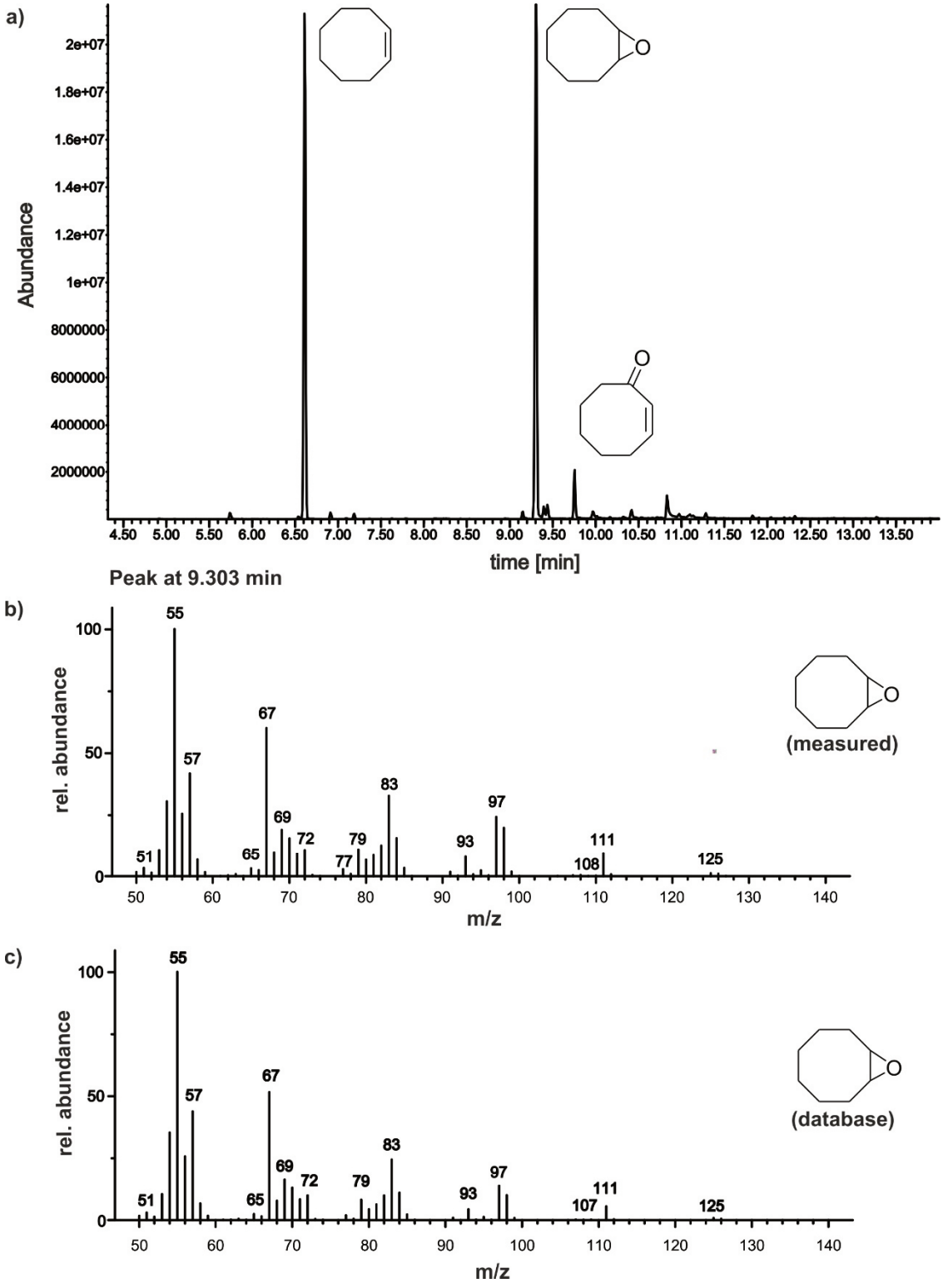

Figure S1. a) GC-MS spectrum of a mixture of *cis*-cyclooctene (**2a**, 0.2 mmol), RFT (1 mol%), $[Fe(bpmen)(OTf)_2](OTf)_2$ (1 mol%) in an oxygen purged solution of 2 mL MeCN which was irradiated over night with blue light (440 nm); the signals are assigned as follows: t_R=6.06 mins *cis*-cyclooctene (**1**), t_R=9.303 mins cyclooctene oxide (**2a**), t_R=9.756 mins 2-cyclooctene-1-one (**2c**); b) mass spectrum of the signal at the retention time t_R=9.303 mins which is assigned to **2a**; c) mass spectrum of an authentic sample of **2a**.

Table S1. Photocatalytic epoxidation of **1** – control experiments and further investigations

Entry	Cond.	Conv. [%][b]	Yield 2a [%][b]	Yield 2b [%][b]	Yield 2c [%][b]
1	**standard**	64	31	0	4
2	**no Fe**	44	traces	1	2
3	**no RFT**	28	0	0	0
4	**no light**	2	0	0	0
5	**N_2**	3	0	0	0
6[c]	**2b**	79	-	-	8
7[d]	**2c**	0	-	-	-
8[c]	**2b, no Fe**	19	-	-	0
9	**$Fe(ClO)_2$**	78	7	4	14
10	**$Fe(ClO)_3$**	70	7	3	10
11	**ferrocene**	62	traces	4	8

[a] All reactions were performed with *cis*-cyclooctene (**1**, 0.2 mmol), RFT (1 mol%), iron catalyst **4** (1 mol%) in 2 mL MeCN. Deviations from these standard conditions are assigned in column 2. The samples were purged with pure dioxygen, capped, and placed in a cooling block during irradiation (15 h) with blue light (440 nm). [b] Conversion and yield determined by GC-FID integration. [c] **2b** (0.1 mmol) was used instead of **1**. [d] **2c** (0.1 mmol) was used instead of **1**.

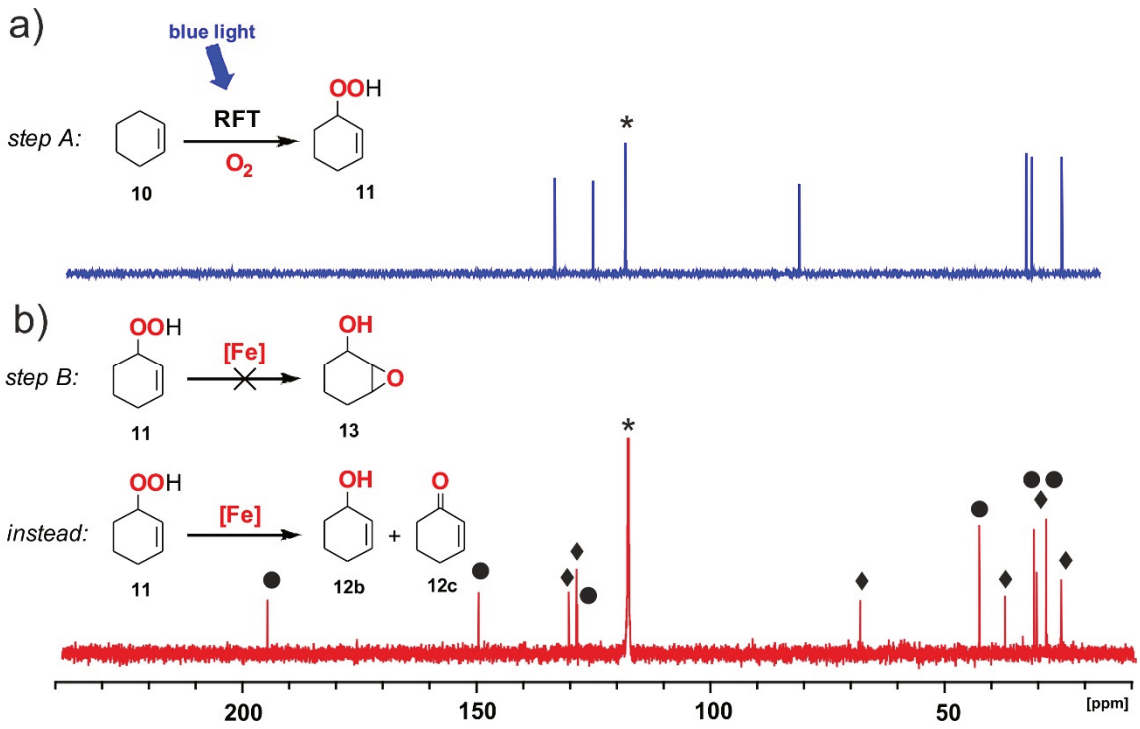

Figure S2. $^{13}C\{^{1}H\}$ NMR spectra (100.61 MHz, 300 K, CD_3CN): a) formation of allylic hydrogen peroxide **11** by RFT and cyclohexene **10**; b) the reaction between **11** and non-heme iron catalyst **4**. The desired product **13** was not obtained, instead products **12b** and **12c** were obtained; signals are marked as follows: CD_3CN(*), **12b** (♦) and **12c** (●).

4.7 References

[1] A. E. Shilov, G. B. Shul´pin, *Chem. Rev.* **1997**, *97*, 2879.

[2] Swern D., *Organic Peroxides*, Wiley-VCH, New York, **1972**.

[3] W. F. Richey, *Kirk-Othmer Encylcopedia of Chemical Technology*, Wiley, New York, **1993**.

[4] J. Piera, J.-E. Bäckvall, *Angew. Chem. Int. Ed.* **2008**, *47*, 3506–3523.

[5] L. Que, W. B. Tolman, *Nature* **2008**, *455*, 333–340.

[6] J. T. Groves, R. Quinn, *J. Am. Chem. Soc.* **1985**, *107*, 5790–5792.

[7] J. T. Groves, M. K. Stern, *J. Am. Chem. Soc.* **1988**, *110*, 8628–8638.

[8] T. Iwahama, G. Hatta, S. Sakaguchi, Y. Ishii, *Chem. Commun.* **2000**, 163–164.

[9] R. A. Sheldon, in *Chem. Funct. Groups Peroxides* (Ed.: S. Patai), J. Wiley, New York, **1983**.

[10] R. A. Sheldon, J. K. Kochi, *Metal-Catalyzed Oxidations of Organic Compounds*, Academic Press, New York, **1981**.

[11] E. P. Talsi, K. P. Bryliakov, *Coord. Chem. Rev.* **2012**, *256*, 1418–1434.

[12] W. Nam, *Acc. Chem. Res.* **2007**, *40*, 522–531.

[13] O. Y. Lyakin, K. P. Bryliakov, E. P. Talsi, *Inorg. Chem.* **2011**, *50*, 5526–5538.

[14] A. Maldotti, L. Andreotti, A. Molinari, S. Borisov, V. Vasil'ev, *Chem. – Eur. J.* **2001**, *7*, 3564–3571.

[15] A. Maldotti, A. Molinari, P. Bergamini, R. Amadelli, P. Battioni, D. Mansuy, *J. Mol. Catal. Chem.* **1996**, *113*, 147–157.

[16] S. Campestrini, U. Tonellato, *Eur. J. Org. Chem.* **2002**, *2002*, 3827–3832.

[17] S. Fukuzumi, K. Tanii, T. Tanaka, *J. Chem. Soc. Perkin Trans. 2* **1989**, 2103–2108.

[18] J. Dad'ová, E. Svobodová, M. Sikorski, B. König, R. Cibulka, *ChemCatChem* **2012**, *4*, 620–623.

[19] R. Mas-Ballesté, M. Costas, T. van den Berg, L. Que, *Chem. – Eur. J.* **2006**, *12*, 7489–7500.

[20] M. Prein, W. Adam, *Angew. Chem. Int. Ed. Engl.* **1996**, *35*, 477–494.

[21] U. Neuenschwander, I. Hermans, *J. Org. Chem.* **2011**, *76*, 10236–10240.

[22] V. J. Dungan, B. M.-L. Poon, E. S. Barrett, P. J. Rutledge, *Tetrahedron Lett.* **2013**, *54*, 1236–1238.

[23] S. Alagaratnam, N. J. Meeuwenoord, J. A. Navarro, M. Hervás, M. A. De la Rosa, M. Hoffmann, O. Einsle, M. Ubbink, G. W. Canters, *FEBS J.* **2011**, *278*, 1506–1521.

[24] G. J. P. Britovsek, J. England, A. J. P. White, *Inorg. Chem.* **2005**, *44*, 8125–8134.

[25] Y. Zang, J. Kim, Y. Dong, E. C. Wilkinson, E. H. Appelman, L. Que, *J. Am. Chem. Soc.* **1997**, *119*, 4197–4205.

[26] I. Prat, A. Company, T. Corona, T. Parella, X. Ribas, M. Costas, *Inorg. Chem.* **2013**, *52*, 9229–9244.

[27] P. D. Oldenburg, A. A. Shteinman, L. Que, *J. Am. Chem. Soc.* **2005**, *127*, 15672–15673.

[28] R. V. Ottenbacher, K. P. Bryliakov, E. P. Talsi, *Inorg. Chem.* **2010**, *49*, 8620–8628.

5 Aerobic Photooxidation of Aldehydes to Esters Catalyzed by Riboflavin Tetraacetate[a]

Bernd Mühldorf and Robert Wolf

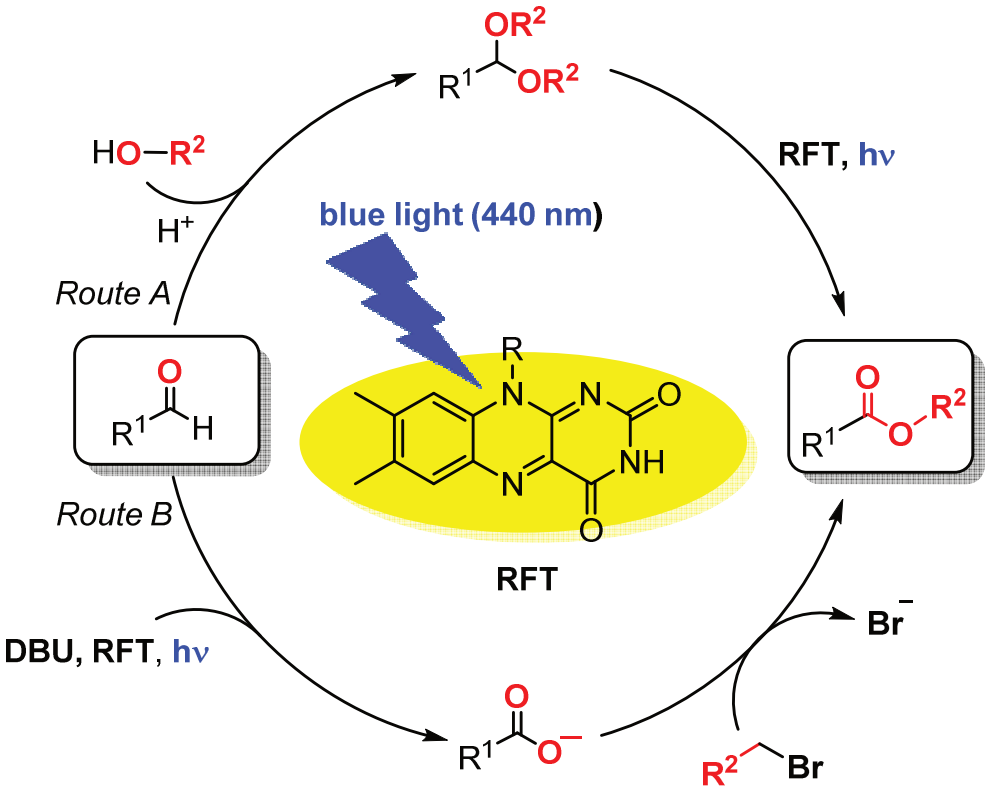

[a] Unpublished results

Ulrich Lennert performed the photocatalytic reactions and analysis shown in Table 5.

5.1 General Information and Introduction

Esters are an important class of compounds widely utilized as fine chemicals, pharmaceuticals, and food additives.[1] Classical methods for their preparation include the Brønsted or Lewis acid-catalyzed condensation of benzoic acids with alcohols at elevated temperatures,[2] and the reaction of activated carboxylic acids such as acyl chlorides or anhydrides with alcohols (Scheme 1, path A).[3] The latter approach requires a multistep process that often produces large amounts of by-products. The transition metal-catalyzed carbonylation of aryl halides with gaseous carbon monoxide (CO) in the presence of an alcohol represents an alternative approach (path B).[4,5] Unfortunately, this methodology suffers from the necessity of expensive precious metals such as Pd. Very recently, Jacobi von Wangelin and co-workers reported the metal-free visible-light-driven alkoxycarbonylation of arene diazonium salts using CO gas, an alcohol, and a redox active organophotocatalyst.[6,7] A further interesting approach to catalytic ester synthesis is the oxidative condensation of two alcohols (path C), which was achieved with air as oxidant in the presence of expensive palladium catalysts.[8],[9]

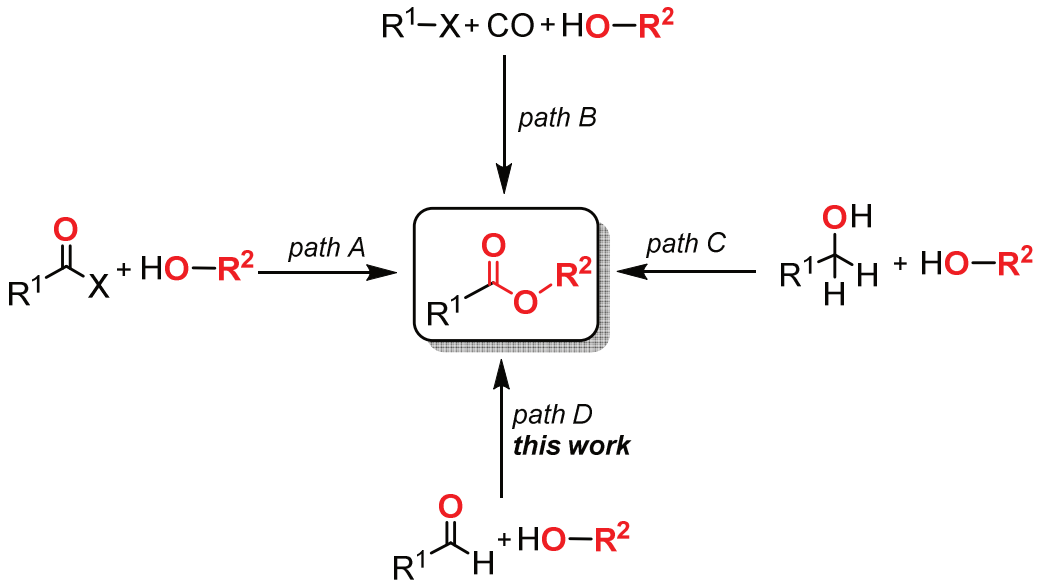

Scheme 1. Different approaches for the synthesis of ester groups.

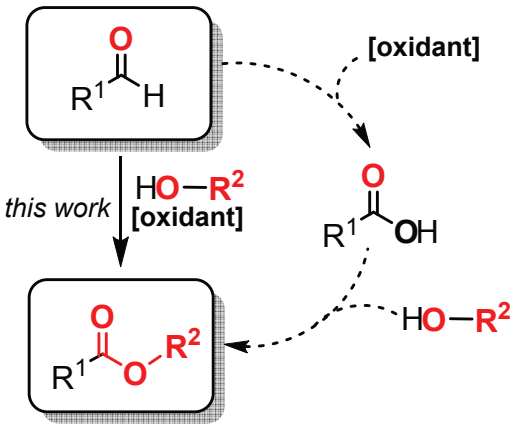

Scheme 2. Comparison of direct oxidative esterification of aldehydes with traditional two-step conversion of aldehydes to the corresponding esters.

The direct esterification of aldehydes has attracted much attention as alternative protocol in recent years (path D).[10] The direct formation of esters from aldehydes utilizes easily available starting materials, and an isolation of the corresponding carboxylic acid is not required (Scheme 2). This one-step transformation can be performed successfully using oxidants such as iodine (I_2)[11], pyridinum hydrobromide perbromide ($Py{\cdot}HBr_3$)[12], oxone ($KHSO_5$)[13], or peroxymonosulfuric acid (H_2SO_5).[14] Most of these oxidants are toxic and usually too strong to control selectivity. Additionally, the use of stoichiometric quantities or even excess of the oxidant leads to inefficient atom economy.

Inspired by the need for more efficient and environmentally benign procedures for aldehyde oxidation, catalytic methods using dioxygen as terminal oxidant have become an attractive field of research in recent years. Most of the established catalytic protocols rely on the use of N-Heterocyclic carbenes (NHCs) as organocatalysts.[15,16] A few of these utilize dioxygen as terminal oxidant (Scheme 3). A key step in these NHC-catalyzed transformations is the umpolung of the aldehyde **A** by the NHC.[17] This step provides the electron-rich enaminol of type **B**, which is known as the Breslow intermediate.[18] Liu and Xu showed that **B** can be used to access various esters **C** by reacting **B** with inactivated alky bromides in the presence of dioxygen.[19,20] Additionally, Gois and Anand reported the oxidative coupling of aromatic aldehydes with aryl boronic acids under an air atmosphere (**D**).[21,22] The development of a metal-NHC catalyst system made the direct use of phenols for the oxidative esterification of aldehydes under aerobic conditions possible.[23] A wide range of esters of type **E** were successfully obtained with $Fe(OTf)_2$ as metal catalyst. The combination of $Pd(OAc)_2$ with an NHC is also a potent catalyst for this kind of transformation,[25] while the use of $[RuCl_2(p\text{-cymene})]_2$ allows the use of benzylic alcohols as starting materials instead of aldehydes.[26] This tandem process starts with a ruthenium-catalyzed oxidation of the benzylic alcohol to the corresponding aldehyde **A** in

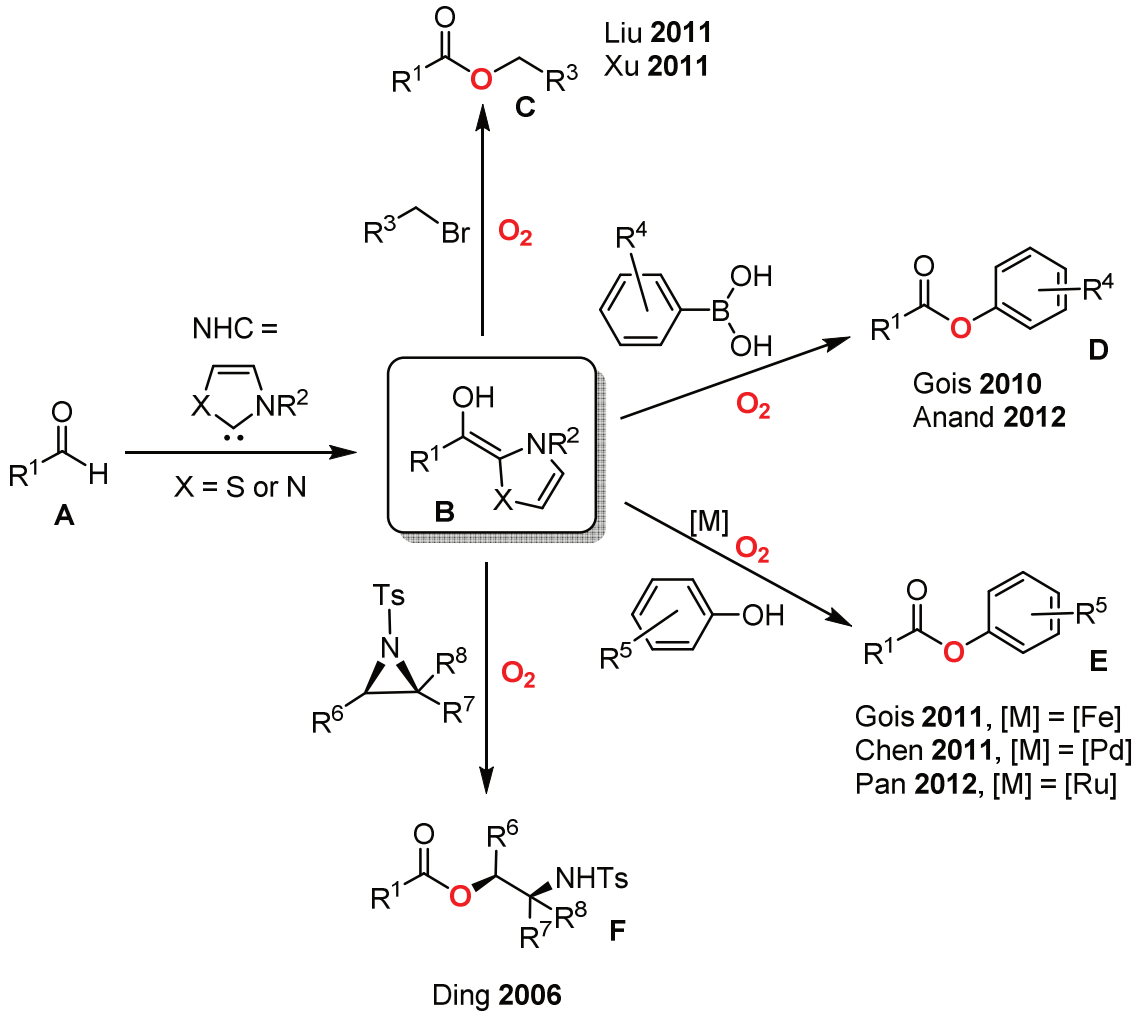

Scheme 3. NHC-catalyzed or NHC-mediated esterification of aldehydes using dioxygen as terminal oxidant; [Fe] = $Fe(OTf)_2$, [Pd] = $Pd(OAc)_2$, [Ru] = $[RuCl_2(p\text{-cymene})]_2$.

the first step, which is followed by the carbene-catalyzed oxidative esterification. Finally, it is worth mentioning that the formation of *O*-acylated *N*-tosylated 1,2-aminoalcohols **F** from the reaction of **B** with aziridines in the presence of air was reported by Ding *et al.*.[26] Despite its relevance in organocatalysis, NHCs are also known to be the catalytically active species in natural products such as the coenzyme thiamine (vitamin B1).[27,28] Based on mechanistic studies to the reactivity of thiamine, Yano[29] and Shinkai[30–33] independently developed a biomimetic two-component system for the oxidative esterification of aldehydes (Scheme 4a). The flavin analogue methyltetra-*O*-acetlyriboflain (MeFl) was combined with an *N*-hexadecythiazolium salt (HxdT) as carbene precursor in a cationic micelle generated by a surfactant. MeFl acts as oxidant for the *in situ* formed Breslow intermediate which is subsequently trapped by methanol to yield the corresponding ester. The reduced flavin analogue is easily regenerated by dioxygen forming hydrogen peroxide. The role of MeFl is crucial, since the well-known acyloin condensation of aldeydes occurs in the absence of MeFl. Diederich *et al.* used this MeFl/HxdT-system for

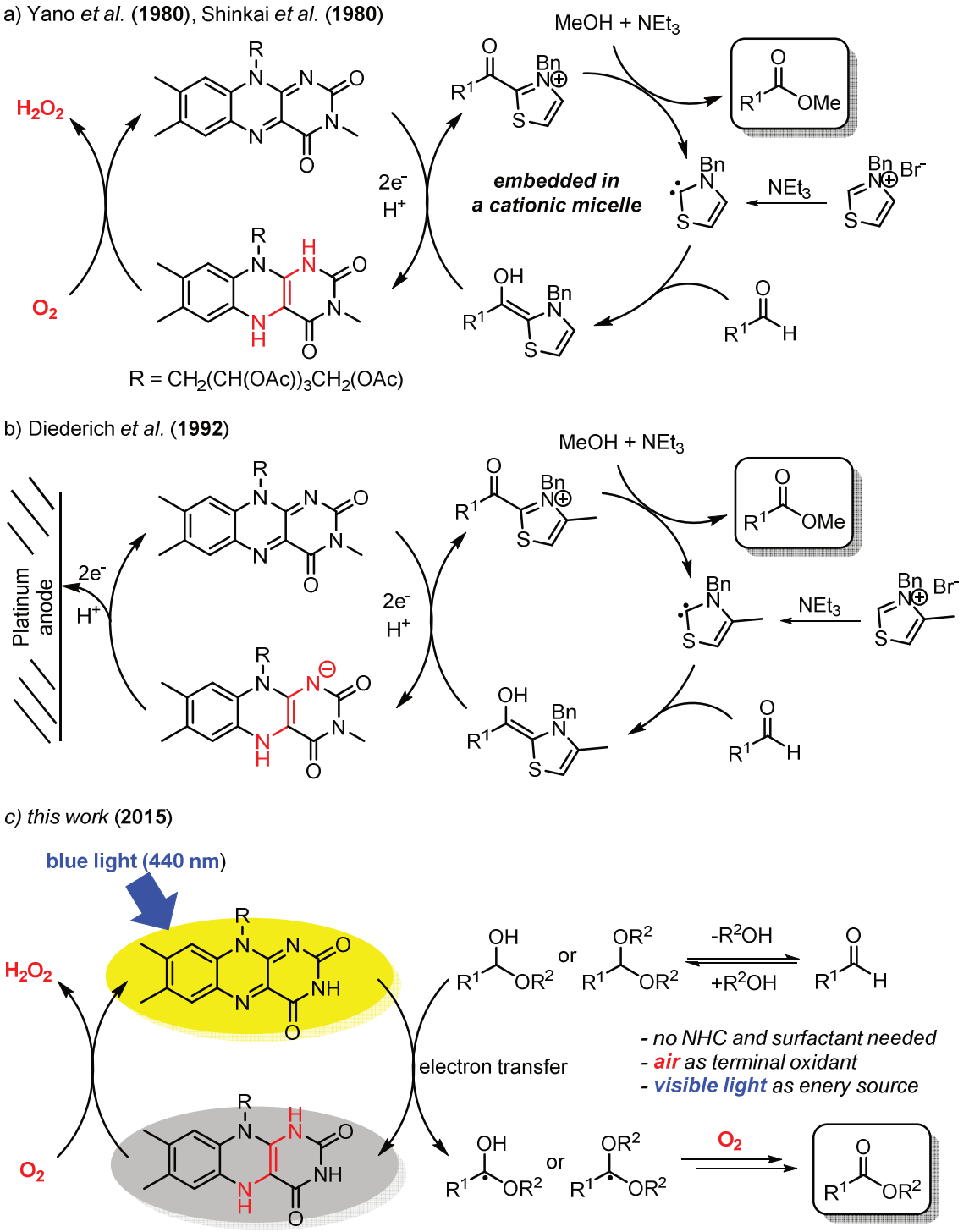

Scheme 4. a) Aerobic esterification of aldehydes catalyzed by a flavin analouge and a thiazolium carbene embedded in a cationic micelle generated by CTAB (cetyltrimethylammonium bromide) reported by Shinkai *et al.*; b) Electrochemical oxidation of aldehydes catalyzed by a flavin analogue and a thiazolium carbene reported by Diederich *et al.*; c) photocatalytic esterification of aldehydes by using riboflavin tetraacetate as photocatalyst and air as terminal oxidant as proposed in this work.

the electrochemical synthesis of methyl benzoates under anaerobic conditions (Scheme 4b).[34] Recently, Yashima reported the first enantioselective oxidative esterification by combining a flavin analogue with a chiral thiazolium-derived NHC.[35]

Building on recent developments in flavin-mediated photocatalysis,[36–41] we now report that riboflavin tetraacetate has been applied as a *photocatalyst* of the aerobic esterification of aldehydes for the first time. This protocol does not need an NHC precursor or a surfactant to achieve the desired esterification. Additionally, the use of atmospheric oxygen as terminal oxidant and visible light as abundant source of energy makes this protocol highly attractive.

5.2 Flavin-Catalyzed Aerobic Photooxidation of Aldehydes (Part 1): Synthesis of Methyl Esters

5.2.1 Introduction

Yano, Shinkai and Diederich described the flavin-mediated oxidation of the preliminary *in situ* formed Breslow intermediate in the presence of a suitable NHC precatalyst as the key step for the aerobic esterification of aldehydes (Scheme 4a and 4b). Herein, we report a photocatalytic protocol for the flavin-catalyzed oxidation of an aldehyde to the corresponding methyl ester with methanol as coupling reagent in the absence of any NHC precatalysts under acidic conditions (Scheme 4c). The *in situ* formation of the acetal is key for the formation of the desired ester.

5.2.2 Results and Discussion

We first investigated the photocatalytic oxidative esterification of 4-chlorobenzaldehyde (**1**, 0.02 mmol) to methyl 4-chlorobenzoate (**2**) in acetonitrile with riboflavin tetraacetate (RFT, 10 mol%) as a photocatalyst in the presence of HCl (100 eq.), aerobic conditions and an excess of methanol. Under these standard conditions, the desired ester is obtained in 65% yield (Table 1, entry 1). Control experiments confirmed that no formation of **2** occurs in the absence of RFT, HCl, in the dark or under a dinitrogen atmosphere (entries 2-5). The yield does not improve when the reaction is carried out in an atmosphere of pure dioxygen (entry 6) or in deuterated solvents (entry 7). This indicates that a singlet oxygen pathway seems very unlikely.[42,43]

For mechanistic investigations, we monitored the reaction course of **1** to **2** (Figure 1). In the initial stages of the reaction (<20 mins), the concentration of **1** decreases continuously, but the formation of the product **2** is negligibly low (<2% yield). 4-Chlorobenzaldehyde dimethyl acetal

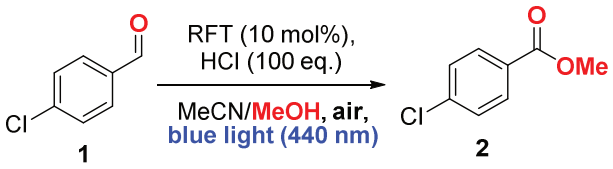

Table 1. Photocatalytic oxidation of 4-chlorobenzaldehyde – Control experiments.[a]

Entry	Conditions	Conv. [%][b]	Yield [%][b]
1	standard cond.	**100**	**65**
2	no RFT	41	0
3	no HCl	73	0
4	no irradiation	49	0
5	no (atmospheric) O_2	20	0
6[c]	O_2 (100%)	100	60
7	CD_3CN/CD_3OD	100	63
8	no MeOH	100	0[d]

[a] All reactions were performed with 4-chlorobenzaldehyde (0.02 mmol), RFT (10 mol%), HCl (37%, 167 µL) in 2 mL MeCN/MeOH (5/3, v/v). The samples were exposed to atmospheric oxygen and placed in a cooling block during irradiation (12 h) with blue light (440 nm). [b] Conversion and yield determined by GC-FID integration. [c] O_2: oxygen saturated solution. [d] The formation of 4-chlorobenzoic acid was confirmed by ^{1}H-NMR spectroscopy and GC-MS measurements.

(**1'**) is formed as an intermediate and identified by GC-MS measurements (Figure S1, SI) and authentic samples. The less stable hemiacetal was not observed. The concentration of **1'** subsequently decreases in the course of the reaction, and the formation of the desired ester **2** is observed (Figure 1). Based on this reaction time profile, we suggest that **1'** is a key reaction intermediate, which is further oxidized to the ester **2** in a photocatalytic process. Note that **1** is converted to 4-chlorobenzoic acid in the absence of methanol as ascertained by ^{1}H-NMR spectroscopy (Table 1, entry 8). Nonetheless, only traces of **2** are observed using 4-chlorobenzoic acid as a substrate. This observation indicates that the acid is not an intermediate in the oxidative esterification of **1** (Table S1, supporting information).

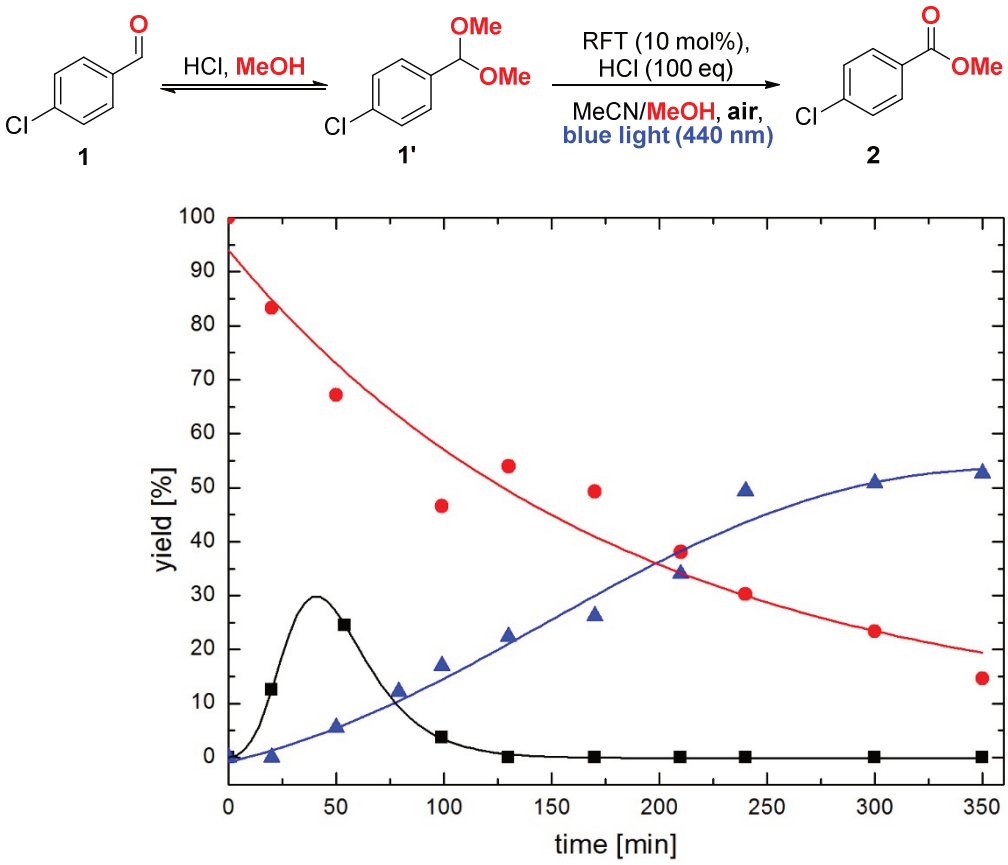

Figure 1. Reaction time profile of the photocatalytic esterification of **1** (●) to **1'** (■) and **2** (▲) in the presence of RFT (10 mol%), HCl (37%, 167 µL) in MeCN/MeOH (5/3 v/v). Lines are visual guides only.

To get further insight into this transformation, we applied UV-vis and fluorescence emission spectroscopy. First, we monitored the change of the absorption bands of RFT in the presence of HCl in MeCN/MeOH (5/3 v/v, Figure S2a, SI). The formation of an absorption band is observed at λ_{max} = 390 nm, which is assigned to the protonated species $RFTH^+$.[44] Excitation of $RFTH^+$ with blue light leads to the population of the first singlet excited state $^1RFTH^{+}$*. In order to investigate whether $^1RFTH^{+}$* is involved in the oxidative esterification of **1**, we investigated the influence of **1** and **1'** on the intensity of the emission of $^1RFTH^{+}$* by fluorescence emission spectroscopy. We added various equivalents of 4-chlorobenzaldeyde (**1**) or the observed intermediate 4-chlorobenzaldehyde dimethyl acetal (**1'**) to $^1RFTH^{+}$* and monitored the change of the intensity of the fluorescence emission of $^1RFTH^{+}$* (Figure S2b and S2c, SI). The intensity is unaffected by addition of **1** or **1'**, thus an energy or electron transfer between **1** or **1'** and $^1RFTH^{+}$* appears not to occur. These measurements indicate that $^1RFTH^{+}$* is not the excited state responsible for the performance of the photocatalyst. The triplet state, $^3RFTH^{+}$*, is accessible through an intersystem crossing (ISC) from $^1RFTH^{+}$*.[45] Based on investigations of

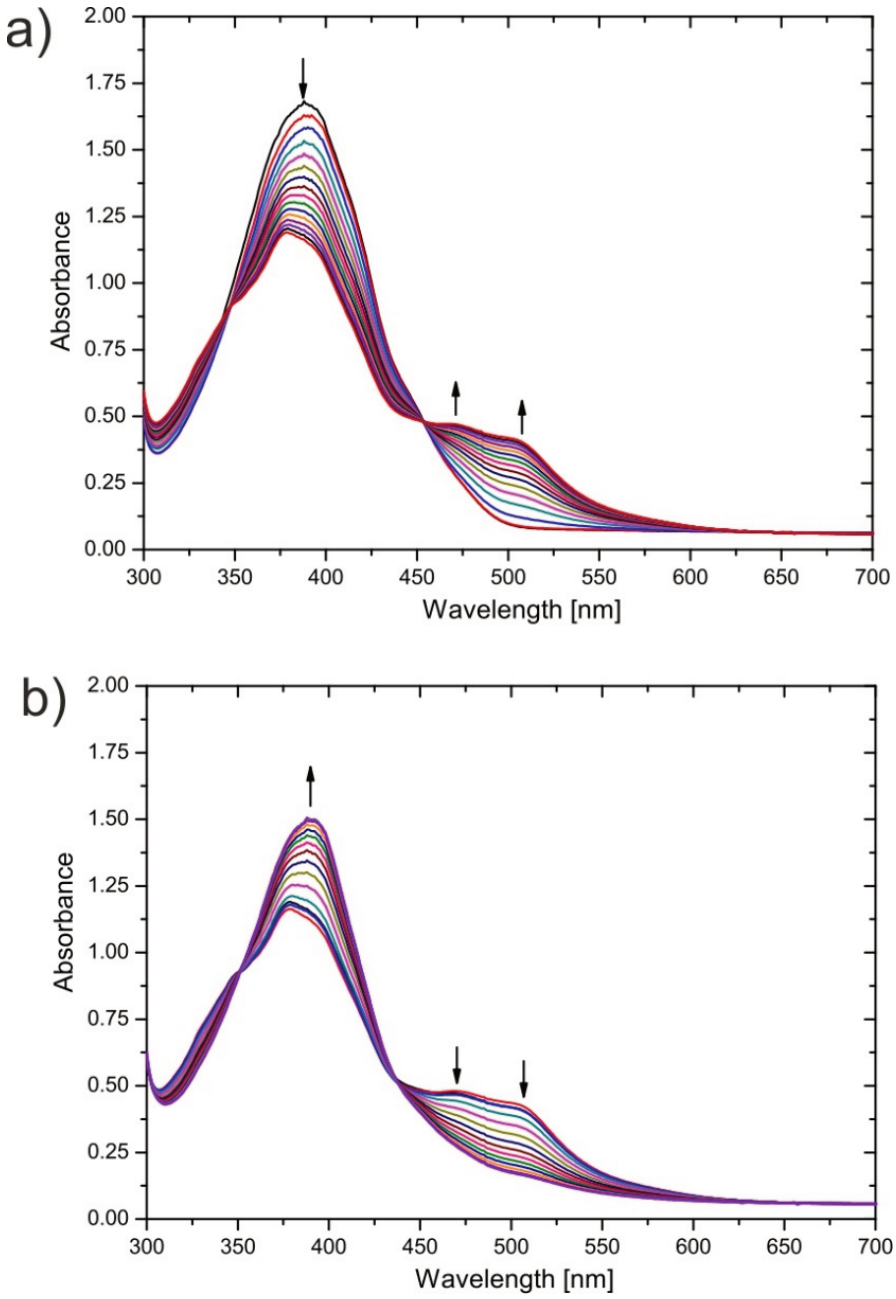

Figure 2. a) Electronic absorption spectra of 4-chlorobenzaldehyde (6.7 mM) and RFT (0.1 mM) in the presence of $HClO_4$ (67 mM) while irradiating with blue light in deaerated MeCN/MeOH (3/1 v/v) at 298 K. The spectra were measured over 1 h (120 s between each spectrum displayed; b) electronic absorption spectra of 4-chlorobenzaldehyde (6.7 mM) and RFT (0.1 mM) in the presence of $HClO_4$ (67 mM) at 298 K after 1 h of irradiation with blue light in deaterated MeCN/MeOH (3/1 v/v) (black) and exposing this solution to atmospheric oxygen. The spectra were measured over 20 minutes (120 s between each spectrum displayed).

Dick *et al.* and our experiments (fluorescence emission quenching), we assume that $^3RFTH^{+}$* is the reactive species.[45]

We further investigated which flavin species is generated by the electron transfer between **1** and $^3RFTH^{+}$*. Therefore, we irradiated a degassed mixture of RFT and **1** in MeCN/MeOH (5/3 v/v)

in the presence of $HClO_4$ (better dissociated than HCl, Figure 2a). The absorption band at λ_{max} = 390 nm subsequently decreases under irradiation, while the formation of a distinct broad band at λ_{max} = 460−530 nm is simultaneously observed. This broad band is characteristic for $^2RFTH_2^{\bullet+}$, which is generated by protonation of the reduced flavin species $^2RFTH^{\bullet}$ under acid conditions.[44] Additionally, it is known that $^2RFTH_2^{\bullet+}$ is easily reoxidized to $RFTH^+$ by atmospheric dioxygen and hydrogen peroxide is formed as a by-product.[45] Indeed, the regeneration of the absorption band at λ_{max} = 390 nm is observed when the solution is exposed to the atmosphere (Figure 2b). The formation of hydrogen peroxide is confirmed by UV-vis spectroscopy (see experimental section).

Based on these spectroscopic experiments, we propose the catalytic cycle displayed in Figure 3. The protonation of RFT by HCl yields $RFTH^+$ (**3**). Photoexcitation of **3** leads to the formation of $^1RFTH^{+}$* (step i), which is rapidly transformed to $^3RFTH^{+}$* *via* intersystem crossing (ISC, step ii). Aldehyde **1** is in equilibrium with acetal **1'**; the formation of the latter is catalyzed by HCl. An electron transfer from **1'** to $^3RFTH^{+}$* occurs, generating $^2RFTH^{\bullet}$ and the corresponding benzyl radical cation **4** (step iii). The latter species **4** is rapidly deprotonated† to yield the benzyl radical **5** (step vi). $^2RFTH^{\bullet}$ is protonated to yield $^2RFTH_2^{\bullet+}$ as confirmed by UV-vis spectroscopy under anaerobic conditions (Figure 3). The catalytic cycle is closed by atmospheric oxygen, which reoxidizes $^2RFTH_2^{\bullet+}$ to RFT or $RFTH^+$, respectively and generates H_2O_2 as by-product (step v). One conceivable way to connect the formed benzyl radical **5** with the desired product **2** is the direct trapping of **5** with dioxygen which forms a peroxo radical species **6**, which decomposes *via* a Russel mechanism to form the corresponding ester **2**.

We further investigated the substrate scope of the reaction of *para*-substituted benzaldehydes in the presence of an excess of methanol (Table 2). The esterification of 4-methoxybenzaldehyde proceeds in an excellent yield 93% in the presence of 10 eq. of HCl. Unfortunately, benzaldehyde derivatives with substituents such as Me, CO or CO_2Me only gave poor yields, whereas derivatives with electron-withdrawing substituents such Cl, Br or NO_2 gave good to excellent yields. In perspective of our recent work on the photooxidation of alkylbenzenes and benzyl alcohols by RFT in the presence of non-heme iron catalysts (see chapter 3)[38], we hypothesized that toluene derivatives or benzyl alcohols (instead of the corresponding aldehydes) could also be suitable starting materials for the direct formation of esters (Table 3). Therefore, we applied

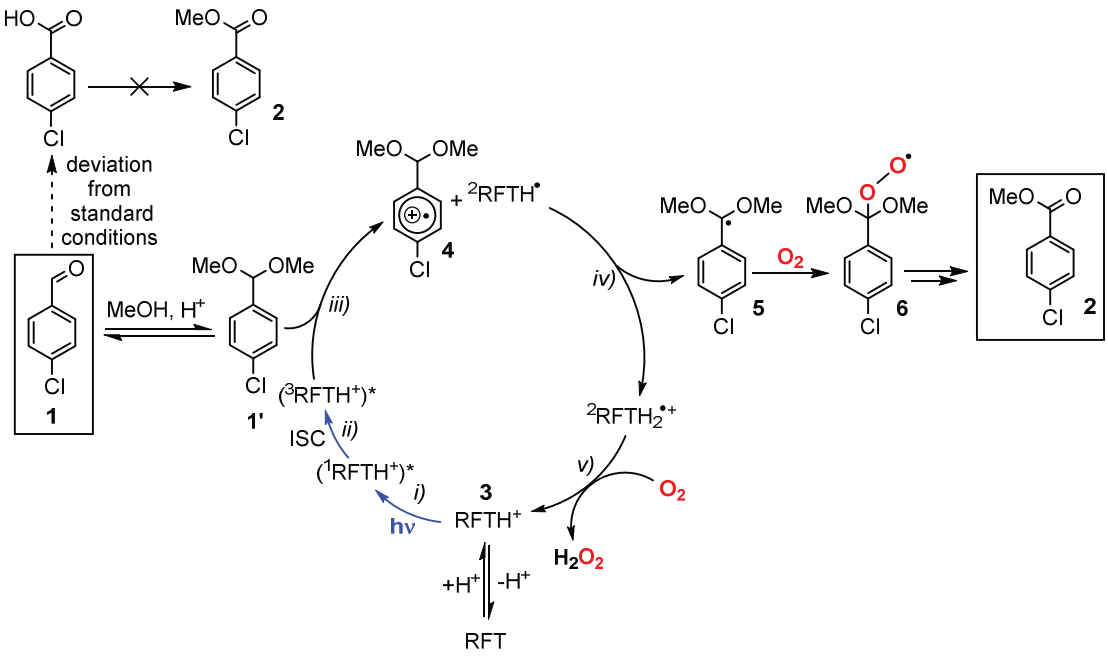

Figure 3. Proposed mechanism for the photocatalytic aerobic esterification of 4-chlorobenzaldehyde (**1**) to methyl 4-chlorobenzoate (**2**) with RFT in the presence of HCl and MeOH. Standard conditions are defined as follows: **1**, RFT (10 mol%) and HCl (37%, 167 µL) in 2 mL MeCN/MeOH (5/3, v/v) were irradiated for 12 h with blue light (440 nm) in the presence of atmospheric oxygen.

Table 2. Photocatalytic esterification of benzaldehyde derivatives with RFT[a]

Entry	Substrate	Product	R	Conv. [%][b]	Yield [%][b]
1	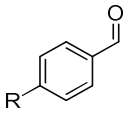	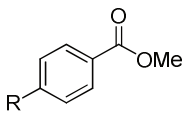	OMe[c]	100	**93**
			H	100	52
			Me	100	22
			CO	100	44
			CO_2Me	100	48
			^tBu	100	69
			Cl	100	65
			Br	100	**74**
			F	100	54
			CF_3	100	42
			NO_2	100	**83**

[a] All reactions were performed with substrate (0.02 mmol), RFT (10 mol%), HCl (37%, 167 µL) in 2 mL MeCN/MeOH (5/3, v/v). The samples were exposed to atmospheric oxygen and placed in a cooling block during irradiation (12 h) with blue light (440 nm). [b] Conversion and yield determined by GC-FID integration. [c] HCl (37%, 16.7 µL, 10 eq.)

RFT in the presence of the non-heme iron catalyst $[Fe(TPA)(MeCN)_2](ClO_4)_2$ (TPA = tris(2-pyridylmethyl)amine) for the photooxidation of various toluene derivatives (entry 1) or benzyl alcohols (entry 2) in a MeCN/MeOH-mixture. Our initial studies revealed that toluene

derivatives with electron–donating (OMe) or weakly electron–donating substituents (Me, ^{t}Bu) are converted smoothly to the desired methyl ester, whereas the reaction is unsuccessful with toluene and its derivatives with electron-withdrawing substituents (Br, Cl). We presume that the reduction potential of these derivatives is too positive to be oxidized by RFT or $RFTH^+$. The reduction potentials of the corresponding benzyl alcohols is significantly lower, allowing the reaction to proceed even though a mixture of aldehyde and ester is obtained in most cases (entry 2). In order to increase the reduction potential of RFT (see chapter 2)[37], we added $Sc(OTf)_3$ (20 mol%) to the reaction mixture under otherwise same conditions (Table S2). Unfortunately, no beneficial effect of $Sc(OTf)_3$ is observed. Control experiments revealed that both the solvent additive MeOH and the iron catalyst shut down the RFT/$Sc(OTf)_3$-mediated oxidation of the substrate, therefore this system is not suitable for toluene derivatives with an reduction peak potential $E^0_p(substrate^{\bullet+}/substrate) > 2.0$ V *vs.* SCE.

Table 3. Photocatalytic esterification of toluene derivatives and benzyl alcohol derivatives with RFT in the presence of a non-heme iron catalyst[a].

Entry	Substrate	Product	R	Conv. [%][b]	Yield [%][b]
1	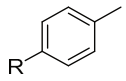	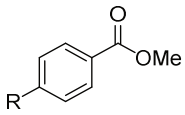	OMe	100	**94**
			Me[c]	100	**93**[d]
			^{t}Bu[c]	100	52
			H	57	0
			Br	38	0
			Cl	36	0
2	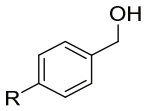	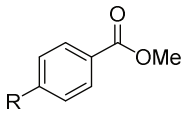	OMe	100	**>99**
			H	94	39[d]
			Cl	96	67[d]
			Br	94	49[d]

[a] All reactions were performed with substrate (0.02 mmol), RFT (10 mol%), $[Fe(TPA)(MeCN)_2](ClO_4)_2$ (10 mol%) and HCl (37%, 16.7 µL, 10 eq.) in 2 mL MeCN/MeOH (5/3, v/v); the samples were exposed to atmospheric oxygen and placed in a cooling block during irradiation (2 h) with blue light (440 nm). [b] Conversion and yield determined by GC-FID integration. [c] $HClO_4$ (70%, 17 µl), irradiation (5 h). [d] The corresponding aldehyde was detected: R = Me (6%), R = H (26%), R = Cl (14%), R = Br (16%).

We further investigated the range of alkyl benzoates accessible with RFT. Unfortunately, the reaction of various benzaldehyde derivatives in the presence of an excess of other alcohols such as ethanol, 2-propanol, *n*-butanol or *tert*-butanol gave unsatisfactory results compared to methanol (Table S3, SI). The reaction proceeds less efficiently in the presence of a sterically more demanding alcohol, which is line with the incomplete conversion of the starting material. The likely cause of the sluggish reactivity is the impaired formation of the corresponding acetal,

thus the subsequent electron transfer to $^{3}RFTH^{+}$* is less likely to occur. Additionally, the formation of the corresponding benzoic acid (see Figure 3) is favoured, thus diminishing the yield of **2**.

Assuming that an even larger excess of alcohol favours the formation of the key intermediate of type **1'**, the photocatalytic esterification of the test substrate 4-methoxybenzaldehyde was performed in various neat alcohol solutions (Table S4). Unfortunately, the yields are not significantly improved by using an alcohol as solvent.

5.2.3 Conclusion

In summary, we report a convenient photocatalytic protocol for the aerobic esterification of aldehydes to the corresponding methyl esters under visible-light irradiation, in the presence of methanol and under acidic conditions. Toluene and benzyl alcohol derivatives with a reduction potential lower than excited RFT are also suitable substrates. Mechanistic studies confirmed an electron transfer between the photoexcited chromophore RFT and the *in situ* formed acetal as the key step. Other alkyl benzoates only gave unsatisfactory yields, which is mainly caused by the impaired formation of the acetal in the case of sterically more demanding alcohols. Therefore, another photocatalytic approach to alkyl benzoates is needed, as described in the following chapter.

5.3 Flavin-Catalyzed Aerobic Photooxidation of Aldehydes (Part 2): Esterification of Aldehydes with Alkyl Bromides

5.3.1 Introduction

The autoxidation of aldehydes to carboxylic acids is a very-well known process, but this reaction is kinetically hindered and therefore occurs on a time scale which is too slow for useful synthetic applications. We observed that aldehyde **1** is fully consumed in in the presence of RFT, dioxygen, and blue light (Table 1, entry 8) and significant amounts of 4-chlorobenzoic acid (**7**) are formed (Scheme 5a). Therefore, we sought to exploit this photochemically enhanced autoxidative process of **1** to **7** (Scheme 5b). In the presence of a base, the effective deprotonation of **7** is achieved and the formed carboxylate **8** is a suitable nucleophile for various reagents. We sought to combine carboxylate **8** with ethyl bromide to yield ethyl 4-chlorobenzoate **9** in a S_N2-type reaction. The substrate scope of alkyl benzoates should easily be extended by applying other sterically more demanding alkyl bromides as electrophiles.

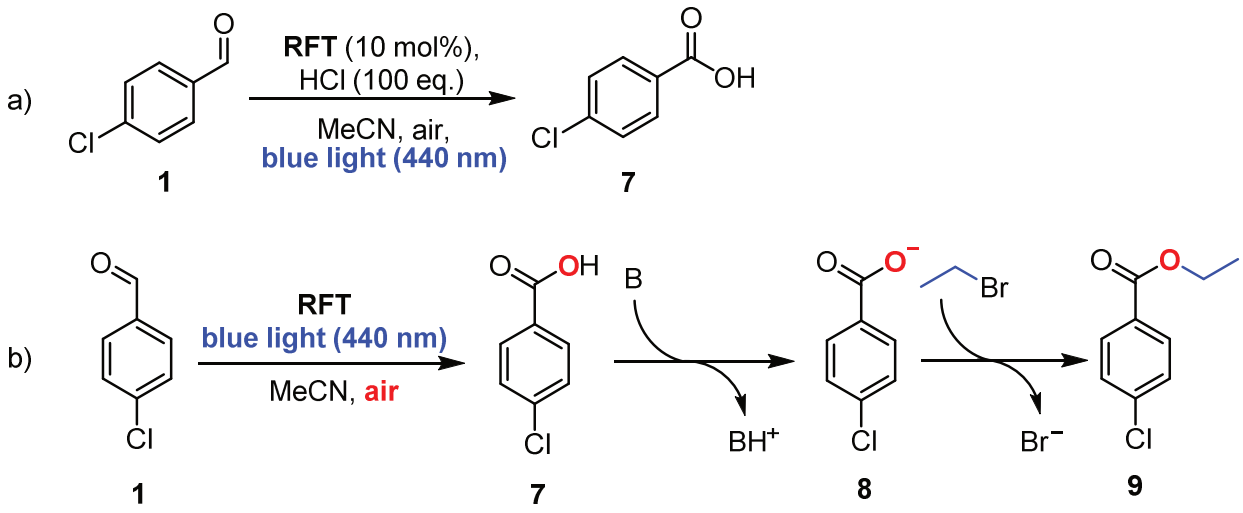

Scheme 5. a) Photochemically enhanced autoxidation of **1**; b) proposed mechanism for the formation of alkyl benzoates, B = base.

5.3.2 Results and discussion

We investigated the photocatalytic esterification of 4-chlorobenzaldeyde **1** to ethyl 4-chlorobenzoate **9** in the presence of a base, ethyl bromide, air and blue light in acetonitrile as solvent. Promising results were obtained with DBU (1,8-diazabicyclo[5.4.0]undec-7-ene) as a base in the presence of an excess of ethyl bromide (Table S5). A screening of the amount of base needed for full conversion of **1** revealed that nearly 30 equivalents of DBU are necessary to obtain satisfactory results (entry 1-4). Unfortunately, water (entry 5) and other bases such as $CsCO_3$, K_2CO_3 and Na_2CO_3 only gave yields below 25% (entry 6-8). Tertiary amines are not

suitable for this kind of transformation since they might interfere with the flavin-mediated process (entry 9-10). The formation of **9** was confirmed by GC-MS measurements (Figure S3) and with authentic samples.

Control experiments confirmed that no formation of **9** occurs in the absence of ethyl bromide RFT, DBU, in the dark or under a dinitrogen atmosphere (Table 4, entries 1-5). The yield does not improve when the reaction is carried out in an atmosphere of pure dioxygen (entry 6) or in deuterated solvents (entry 7). This indicates that a singlet oxygen pathway seems very unlikely.[42,43]

Table 4. Photocatalytic oxidation of 4-chlorobenzaldehyde – control experiments.[a]

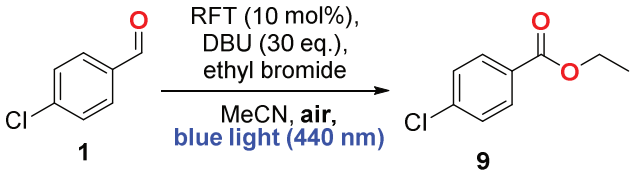

Entry	Conditions	Conv. [%][b]	Yield [%][b]
1	standard cond.	**100**	**84**
2‡	no DBU	100	0[c]
3	no RFT	10	10
4	no CH_3CH_2Br	100	0[d]
5	no irradiation	<2	0
6	no (atmospheric) O_2	34	0
7[c]	O_2 (100%)	80	80
8	CD_3CN	87	74

[a] All reactions were performed with 4-chlorobenzaldehyde (0.02 mmol), RFT (10 mol%), DBU (30 eq.), ethyl bromide (200 µL) in 2 mL MeCN. The samples were exposed to atmospheric oxygen and placed in a cooling block during irradiation (12 h) with blue light (440 nm). [b] Conversion and yield determined by GC-FID integration. [c] Methyl 4-chlorobenzoate (73%) detected after addition of $TMSCH_2N_2$. [d] Methyl 4-chlorobenzoate (19%) detected after addition of $TMSCH_2N_2$.

Special attention was drawn to control experiments, where the reaction was performed in the absence of DBU (entry 2) and in the absence of ethyl bromide (entry 4). Full conversion of the substrate **1** is observed in both cases, but no products were detected in GC-FID analysis. Thus, we added $TMSN_2CH_2$ (see experimental reaction) to the reaction mixtures. 4-chlorobenzoic acid

(**7**) or the corresponding carboxylate (**8**), which may be extracted into the aqueous phase during work-up will be detected as methyl 4-chlorobenzoate after addition of $TMSN_2CH_2$. Indeed, 73% and 19% of methyl 4-chlorobenzoate are formed in the absence of DBU and ethyl bromide, respectively. The low yield in the latter case might be due to inefficient esterification of the deprotonated 4-chlorobenzoic acid with $TMSN_2CH_2$ in the presence of a strong base such as DBU. Both experiments indicate that the carboxylate **8** is an intermediate in the photocatalytic esterification of **1**. When no strong base is present, the corresponding 4-chlorobenzoic acid **7** is formed and no S_N2-type reaction with the alkyl bromide occurs.

The esterification of benzoic acids in the presence of alkyl bromides and DBU is very well investigated.[46] Thus, we focussed on the photocatalytic transformation of **1** to **7** or the corresponding carboxylate **8**, which is significantly enhanced by RFT. It is noteworthy that autoxidation of the aldehyde **1** can be excluded in the given time frame, since only negligible quantities of **1** are converted in the absence of RFT (entry 3) or in the dark (entry 5).

To get further insight into the reaction mechanism, we divided the reaction into several steps. First, we monitored the influence of the strong base DBU on the chromophore RFT by UV-vis spectroscopy. The addition of DBU to RFT slightly changed the absorption spectrum of the chromophore (Figure S4). Comparable studies in aqueous NaOH solution,[47] suggest that strong bases are capable of deprotonating neutral RFT ($pK_a \sim 10$),[48] but the spectrum of deprotonated RFT only slightly differs from neutral RFT. Our studies indicate that an equilibrium between RFT and the deprotonated species (Scheme S1) is very likely in our system.

We further irradiated a mixture containing **1**, RFT and DBU under anaerobic conditions and monitored the change of the absorption of RFT (Figure 4). A rapid decrease of the absorption bands is observed, whereas no distinct absorption bands are formed (Figure 4a). After irradiation, we exposed this solution to atmospheric oxygen and the original absorption spectrum was obtained (Figure 4b). These observations suggest the formation of the reduced flavin species $RFTH_2$, which is easily recovered by dioxygen yielding RFT and hydrogen peroxide as a by-product. Unfortunately, we were not able to detect H_2O_2 in the reaction mixture by our standard techniques (see experimental section). Further tests revealed that this technique is not applicable in the presence of DBU. It is noteworthy that $RFTH_2$ is not formed in the absence of DBU, because no electron transfer occurs between **1** and $^1RFT^*$ or $^3RFT^*$ (Figure S5).‡

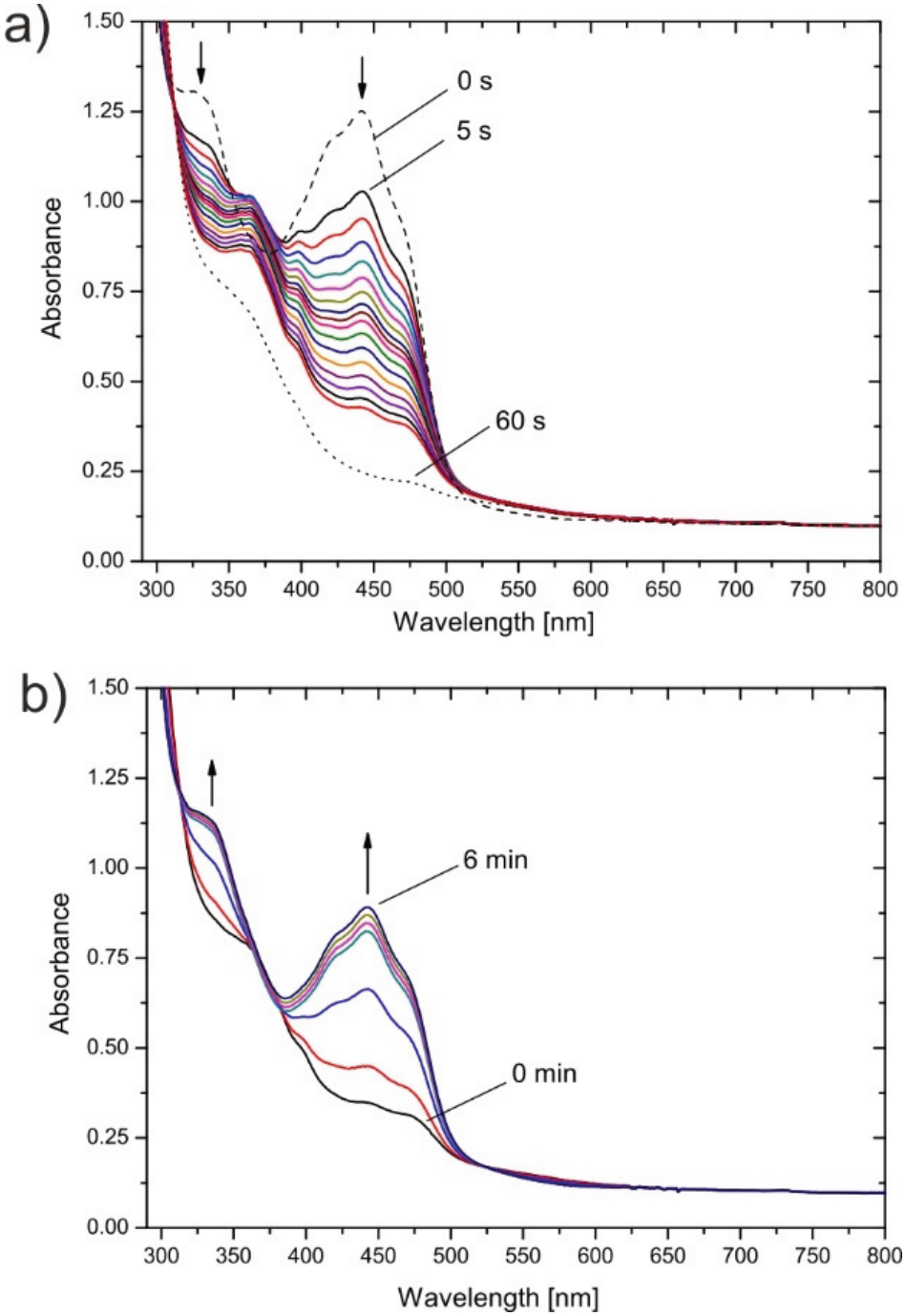

Figure 4. a) Electronic absorption spectra of **1** (6.7 mM) and RFT (0.1 mM) in the presence of DBU (30 µL) while irradiating with blue light in deaterated MeCN at 298 K. Dashed line (black): before starting to irradiate; the coloured spectra are obtained while irradiating for 15 seconds (1 s between each spectrum displayed); dotted line (black): after 60 seconds of irradiation; b) electronic absorption spectra of **1** (6.7 mM) and RFT (0.1 mM) in the presence of DBU (30 µL) while irradiating with blue light in deaterated MeCN at 298 K and exposing this solution to atmospheric oxygen. The spectra were measured over 6 minutes (one minute between each spectrum displayed).

These mechanistic investigations indicate that DBU does not only act as a strong base, but also serves as a sacrificial donor for excited RFT producing hydrogen peroxide (Scheme 6). The photooxidation of tertiary amines, in particular *N*-aryl-tetrahydroisoquinolines, is well

investigated.[49] No literature is known for the photooxidation of DBU, but we assume, that in the first step, the electron transfer from DBU to RFT yields the radical cation $DBU^{\bullet+}$, which is subsequently oxidized to yield 1,8-diazabicyclo[5.4.0]undec-7-en-11-one (DBU^{ox}). Indeed, the formation of DBU^{ox} was confirmed by GC-MS measurements (Figure S6).

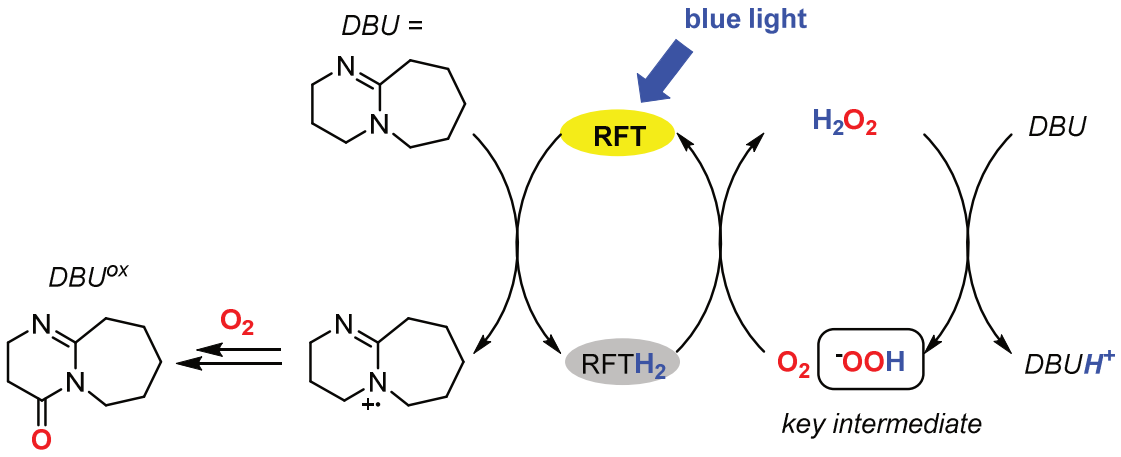

Scheme 6. Proposed mechanism for the formation of the hydroperoxide anion by flavin-mediated photooxidation of DBU.

In order to verify our mechanistic proposal, we wanted to prove that hydrogen peroxide is able to perform the oxidative esterification of **1** to **9** only in the presence of DBU and ethyl bromide. Therefore, we added various equivalents of H_2O_2 to a mixture containing **1**, DBU and ethyl bromide in the dark and in the absence of RFT (Table S6). Indeed, the yield of **9** increases with increasing quantities of hydrogen peroxide added to the reaction mixture. In the absence of DBU, no formation of **9** is observed (entry 6).‡ H_2O_2 is easily deprotonated by DBU yielding ^{-}OOH, which is a better nucleophile than hydrogen peroxide.

This reaction type strongly resembles the Dakin reaction (Scheme 7)[50], where aldehydes are converted to phenol derivatives or benzoic acids with hydrogen peroxide in the presence of NaOH. The *in situ* generated hydrogen peroxide anion ^{-}OOH reacts in a nucleophilic addition to the carbonyl atom yielding intermediate **G**. In the case of electron-donating substituents in *para*-position, a [1,2]-aryl migration is very likely and the phenyl ester **H** is formed, which is subsequently hydrolyzed by the nucleophilic hydroxide ion to phenol derivative **I** (Scheme 7a). On the contrary, electron-withdrawing substituents lead to the exclusive formation of the corresponding benzoic acids **J** (Scheme 7b). Electron-withdrawing substituents inhibit [1,2]-aryl migration in this case and favour hydrogen migration instead.

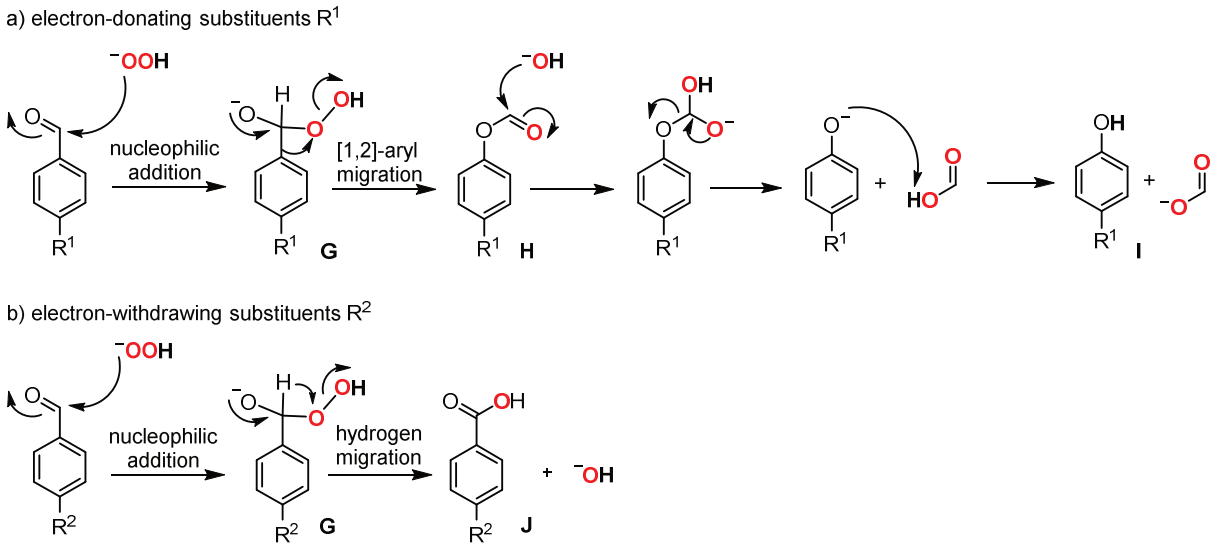

Scheme 7. Mechanism of the Dakin-reaction exemplified by (a) electron-rich aldehydes and (b) electron-poor aldehydes.[50]

These observations are in line with our initial studies of the substrate scope of the reaction (Table 5). The photoinduced oxidation of 4-methoxy- and 2-methoxybenzaldehyde does not give any alkyl ester, due to the electronic donating substituent in *para*- and *ortho*-position (see Scheme 7a). 3-Methoxybenzaldehyde is a suitable substrate, but only poor yields are obtained (Table 5, entry 1). As shown in Scheme 7b, electron-withdrawing substituents such as chlorine in the *para*- and *ortho*- position give good yields (entry 2), whereas no product is obtained in the case of 3-chlorobenzaldehyde. The yield significantly drops in the presence of sterically more demanding alkyl bromides. Benzaldehyde also gave poor yields (entry 4), presumably due to the competing formation of phenol derivatives (scheme 7a), which are further oxidized to unidentifiable polymeric products by RFT.[40] Therefore, we mainly focussed on substrates bearing electron-withdrawing substituents in *para*-position in combination with ethylbromide as coupling reagent (entry 5). As expected from our mechanistic studies, the combination of aldehydes bearing NO_2, Br, I and CN groups in the *para*-position with ethylbromide gave moderate to good yields.

Based on our mechanistic investigations, we propose the following reaction mechanism (Scheme 8). RFT oxidizes the sacrificial electron donor DBU to $DBU^{\bullet+}$, which is subsequently converted to DBU^{ox} (step *i*). The reduced flavin species is reoxidized by atmospheric oxygen and generates hydrogen peroxide as a by-product (step *ii*). Another equivalent of DBU deprotonates H_2O_2 to the nucleophilic hydroperoxo anion (step *iii*), which subsequently oxidizes the aldehyde **1** to the corresponding benzoic acid **7** analogous to a Dakin reaction (step *iv*). One equivalent DBU is needed to deprotonate the benzoic acid **7** to a carboxylate **8** (step *v*), which forms the desired ester **9** in the presence of an alkyl bromide (step *vi*).

Table 5. Photocatalytic esterification of benzaldehyde derivatives with RFT[a]

Entry	Substrate	Product	R	Conv. [%][b]	Yield [%][b]
1	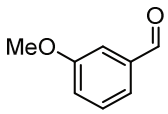	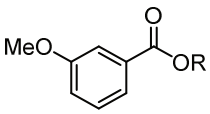	Et	94	**16**
			^{n}Bu	93	**20**
2	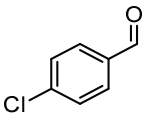	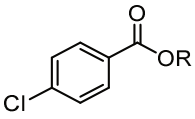	Et	100	**84/66**[c]
			^{i}Pr	84	**33**
			^{n}Bu	87	**8**
3	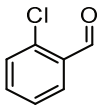	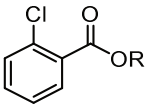	Et	92	**33**[d]
			^{i}Pr	86	**17**
			^{n}Bu	85	**3**
4	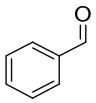	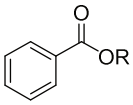	Et	87	**8**
			^{i}Pr	100	**30**
5	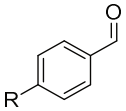	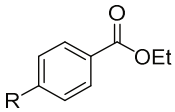	NO_2	100	**43**
			Br	96	**66**
			I	93	**37**
			CN	100	**80**

[a] All reactions were performed with substrate (0.02 mmol), RFT (10 mol%), DBU (30 eq.) and alkyl bromide (200 µL) in 2 mL MeCN. The samples were exposed to atmospheric oxygen and placed in a cooling block during irradiation (12 h) with blue light (440 nm). [b] Conversion and yield determined by GC-FID integration. [c] Isolated yield. [d] Yield determined by ^{1}H-NMR (internal standard: 1,2-dibromoethane).

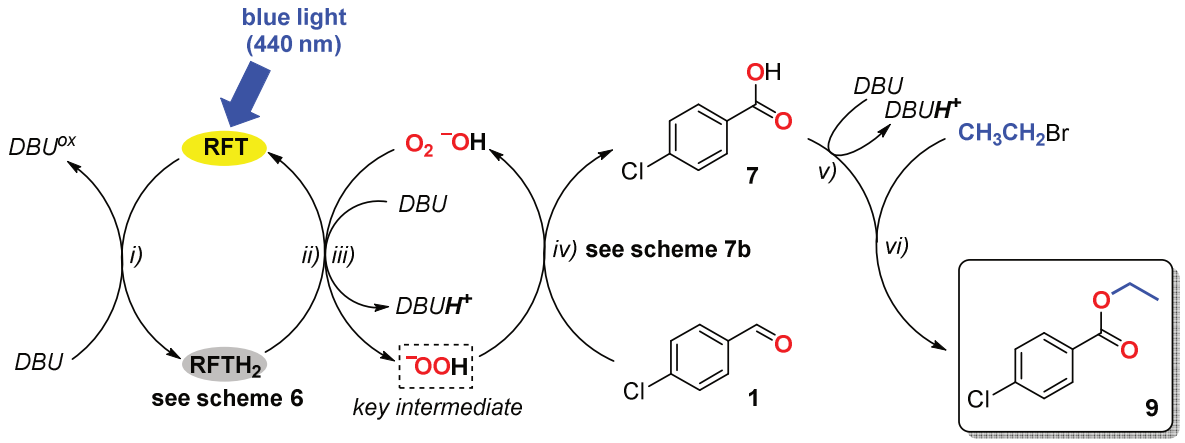

Scheme 8. Proposed mechanism for the photooxidation of 4-chlorobenzaldehyde **1** with ethyl bromide to ethyl 4-chlorobenzoate **9** in the presence of RFT as photocatalyst and DBU.

5.3.3 Conclusion and Outlook

We report the oxidative esterification of aldehydes by the chromophore RFT under visible-light irradiation in the presence of the strong base DBU and alkyl bromides as coupling reagents. The flavin-mediated oxidation of the sacrificial electron donor DBU leads to the *in situ* generation of the hydroperoxo anion, $^{-}$OOH, which subsequently oxidizes aldehydes to their corresponding benzoic acids. ´The deprotonation of the latter species by DBU gives carboxylates, which act as nucleophiles in the presence of alkybromides *via* an S_N2-type reaction to yield the corresponding esters. Unfortunately, this visible-light-driven esterification is limited to benzaldehydes bearing electron-withdrawing substituents due to the competing formation of phenol derivatives for electron-donating substituents. Nevertheless, this RFT/DBU system gives access to the highly nucleophilic species $^{-}$OOH directly from atmospheric dioxygen, which might be an easily accessible and useful oxidant for other oxygenation reactions

5.4 Experimental section

Materials

RFT was prepared according to a known literature procedure.[S1] All other chemicals were obtained commercially (Sigma Aldrich, VWR). Benzaldehyde derivatives with a melting point below r.t. were freshly distilled prior to use. The purity of benzaldehyde derivatives with melting point above r.t. was checked by NMR spectroscopy. All alkyl bromides were distilled prior to use. All other chemicals and solvents were used as received.

Representative procedure for the formation of methyl 4-chlorobenzoate (2)

4-Chlorobenzaldehyde (**1**, 0.02 mmol) was added to RFT (10 mol%) and HCl (37%, 167 µL or noted otherwise) in 2 mL solvent (acetonitrile/methanol 5/3 v/v). The reaction vial was placed in a cooling block to maintain ambient temperature, and the vials were irradiated with blue LEDs (440 nm, 3 W LED) while stirring with a magnetic stirring bar. After 12 h of irradiation, *n*-pentadecane (internal standard), saturated Na_2CO_3 and brine were added. The organic phase was extracted with ethylacetate and subjected to GC-FID analysis. The retention time was verified with authentic samples.

Representative procedure for the formation of ethyl 4-chlorobenzoate (9)

4-Chlorobenzaldehyde (**1**, 0.02 mmol) was added to RFT (10 mol%), ethyl bromide (200 µL) and DBU (30 eq.) in 2 mL acetonitrile. The reaction vial was placed in a cooling block to maintain ambient temperature, and the vials were irradiated with blue LEDs (440 nm, 3 W LED) while stirring with a magnetic stirring bar. After 12 h of irradiation, *n*-pentadecane (internal standard), saturated Na_2CO_3 and brine were added. The organic phase was extracted with

ethylacetate and subjected to GC-FID analysis. The retention time was verified with authentic samples.

Monitoring the formation of hydrogen peroxide

The formation of H_2O_2 was monitored by a standard method as follows: A diluted acetonitrile solution was treated with an excess of NaI(s). The concentration of I_3^- formed was determined by UV-vis spectroscopy (λ_{max} = 362 nm, ε = 13000 $M^{-1}cm^{-1}$).

Fluorescence emission quenching

A fluoresence cuvette containing RFT (c_{RFT} = $7.8 \cdot 10^{-6}$ $mol \cdot L^{-1}$) was placed in a fluoresence spectrometer (Casy Eclipse Varian). The solution was irradiated at 440 nm and the maximum emission intensity, $I_0^{max}(\lambda = 506$ nm), was determined. The addition of various volumina of a stock solution, containing RFT (c_{RFT} = $7.8 \cdot 10^{-6}$ $mol \cdot L^{-1}$) and the quencher, Q, yielded the concentration dependent emission intensity, $I^{max}(\lambda = 506$ nm). A Stern-Volmer plot of I_0^{max}/I_o *vs.* c(Q) provided the quenching constant, K_{SV}.

5.5 Supporting Information

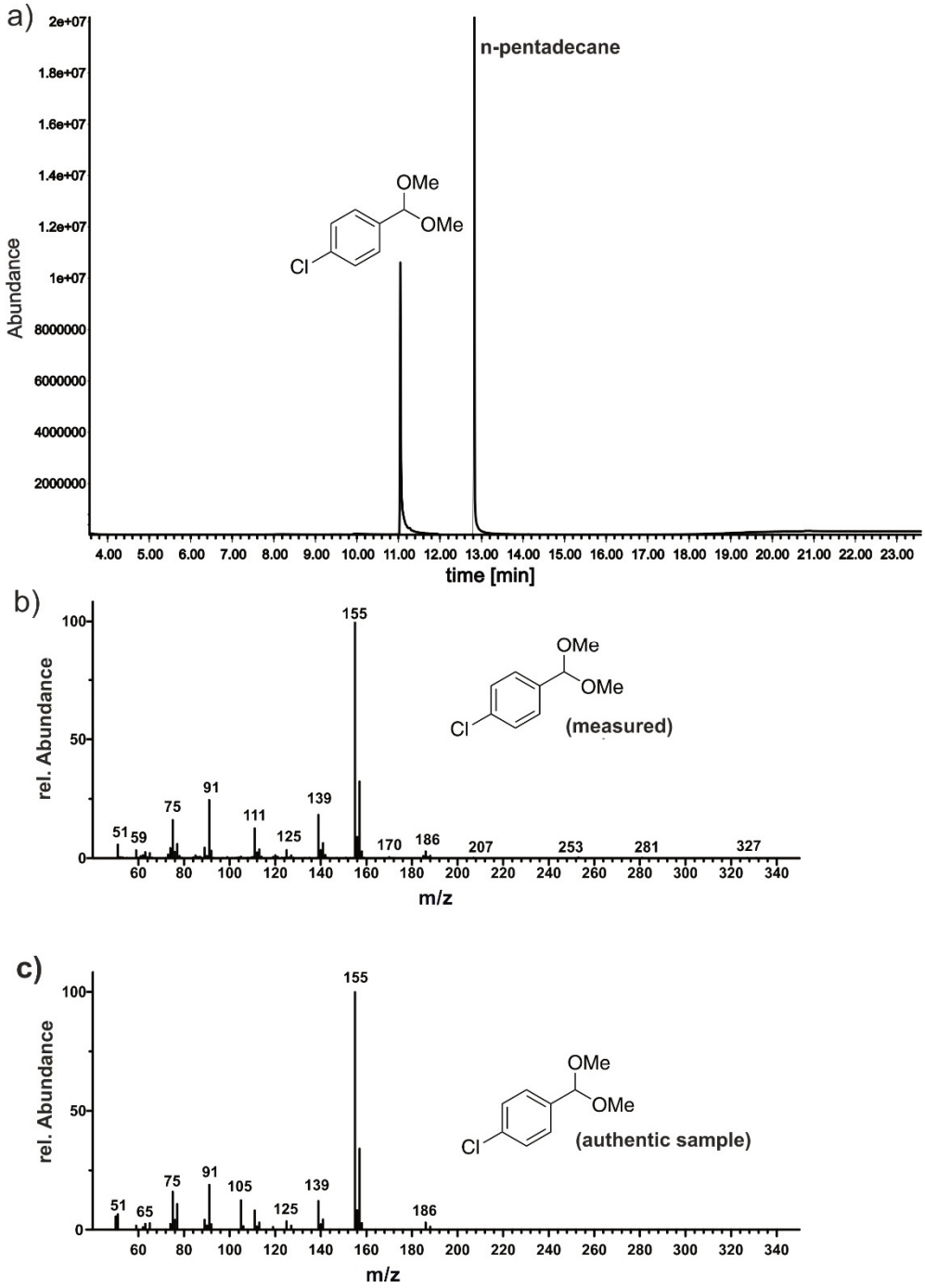

Figure S1. a) GC-MS spectrum of a mixture of 4-chlorobenzaldehyde (**1**, 0.02 mmol), RFT (10 mol%) and HCl (37%, 167 µL) in 2 mL MeCN/MeOH (5/3, v/v) which was irradiated for 40 min with blue light (440 nm); the signal at t_R = 12.8 minutes is assigned to the internal standard *n*-pentadecane; b) mass spectrum of the signal at the retention time t_R = 11 minutes which is assigned to **1'**; c) mass spectrum of an authentic sample of **1'**.

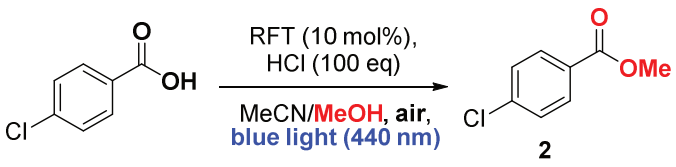

Table S1. Photocatalytic esterification of 4-chlorobenzoic acid – Control experiments.[a]

Entry	Conditions	Yield [%][b]
1	standard cond.	5
2	no RFT	2
3	no HCl	0
4	no irradiation	0

[a] All reactions were performed with 4-chlorobenzoic acid (0.02 mmol), RFT (10 mol%), HCl (37%, 167 µL) in 2 mL MeCN/MeOH (5/3, v/v). The samples were exposed to atmospheric oxygen and placed in a cooling block during irradiation (12 h) with blue light (440 nm). [b] The yield of **2** was determined by GC-FID integration.

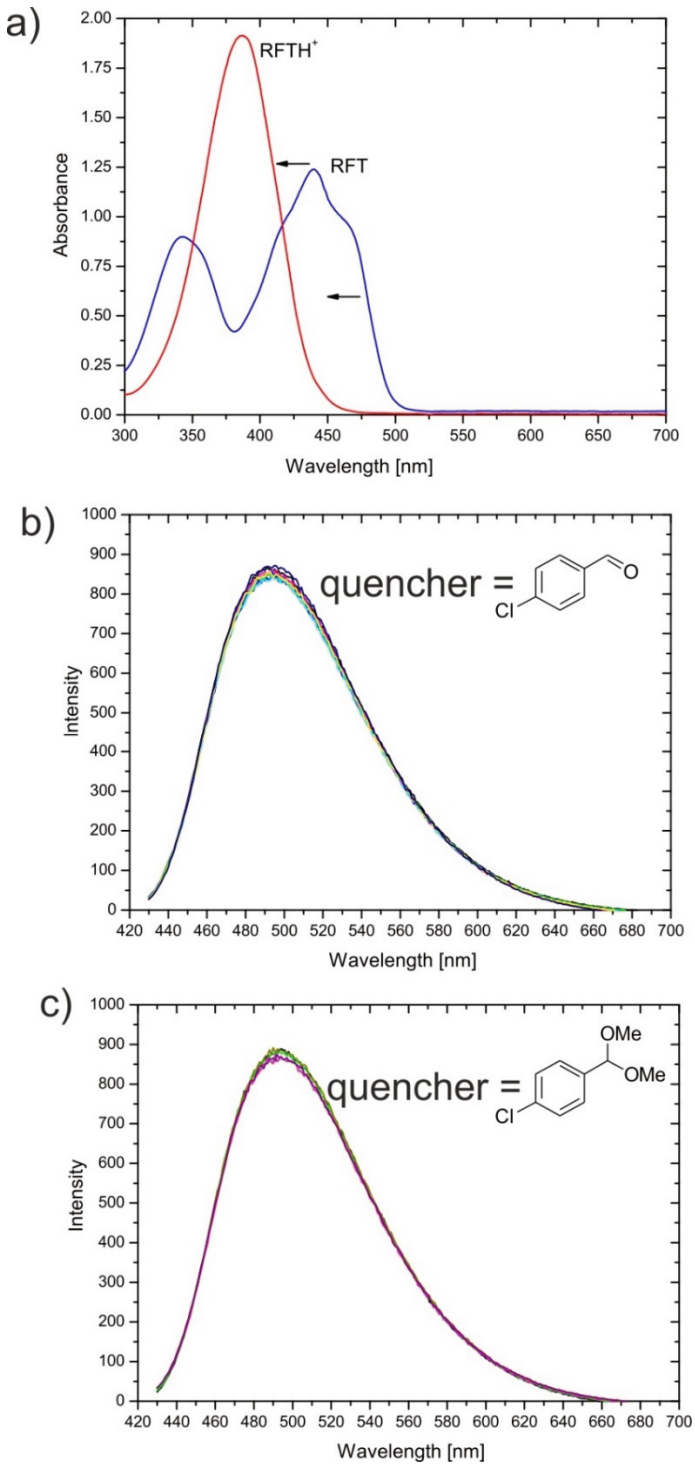

Figure S2. a) Electronic absorption spectra of RFT (0.1 mM, blue) and RFT (0.1 mM) in the presence of HCl (4 mM, red) in MeCN/MeOH at 298 K. b) Fluoresence emission spectra (excitation at 410 nm) of a mixture of RFT ($7.8 \cdot 10^{-6}$ M), HCl (4 mM) and various equivalents of quencher 4-chlorobenzaldehyde (**1**, 1 − 80 eq.) in MeCN at 298K. c) Fluoresence emission spectra (excitation at 410 nm) of a mixture of RFT ($7.8 \cdot 10^{-6}$ M), HCl (4 mM) and various equivalents of quencher 4-chlorobenzaldehyde dimethyl acetal (**1'**, 1 − 80 eq.) in MeCN at 298K.

Table S2. Photocatalytic esterification of toluene derivatives and benzyl alcohol derivatives with RFT[a] in the presence of a non-heme iron catalyst and $Sc(OTf)_3$.

Entry	Substrate	Product	R	Conv. [%][b]	Yield [%][b]
1	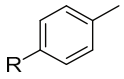	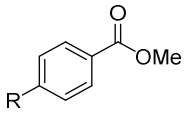	H	49	0
			Br	54	0
			Cl	35	0
2	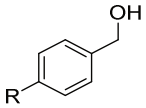	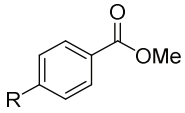	H	99	38[c]
			Cl	92	54[c]
			Br	82	44[c]
			F	89	44[c]
			CF_3	75	44
			NO_2	24	0[c]

[a] All reactions were performed with substrate (0.02 mmol), RFT (10 mol%), $Sc(OTf)_3$ (20 mol%), $[Fe(TPA)(MeCN)_2](ClO_4)_2$ (10 mol%) and HCl (37%, 16.7µL, 10 eq.) in 2 mL MeCN/MeOH (5/3, v/v). The samples were exposed to atmospheric oxygen and placed in a cooling block during irradiation (4 h) with blue light (440 nm); [b] Conversion and yield determined by GC-FID integration; [c] the corresponding aldehyde was detected: R = H (17%), R = Cl (11%), R = Br (10%), R = F (18%), R = NO_2 (4%).

Table S3. Photocatalytic esterification of 4-methoxybenzaldehyde with RFT in various alcohol/MeCN mixtures.[a]

Entry	Substrate	Product	R	Conv. [%][b]	Yield [%][b]
1[c]	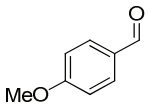	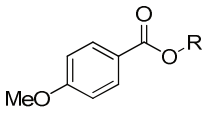	Me	100	93
			Et	87	58
			^{i}Pr	47	1
			^{n}Bu	62	27
2	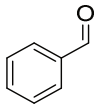	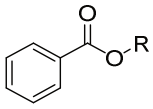	Me	100	52
			Et	53	22
			^{i}Pr	55	11
3	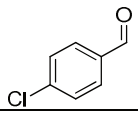	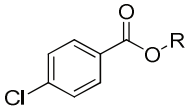	Me	100	65
			Et	73	47
4	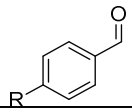	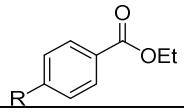	NO_2	95	45
			NMe_2	100	32

[a] All reactions were performed with substrate (0.02 mmol), RFT (10 mol%), HCl (37%, 167 µL) in 2 mL MeCN/ROH (R = Me, Et, ^{i}Pr, ^{n}Bu or ^{t}Bu, 5/3, v/v). The samples were exposed to atmospheric oxygen and placed in a cooling block during irradiation (12 h) with blue light (440 nm). [b] Conversion and yield were determined by GC-FID integration. [c] HCl (37%, 16.7 µL, 10 eq.)

Table S4. Photocatalytic esterification of 4-methoxybenzaldehyde with RFT using an alcohol as solvent[a]

Entry	Substrate	Product	R	Conv. [%][b]	Yield [%][b]
1	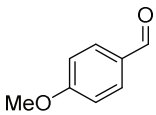	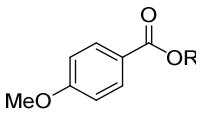	Me	100	91
			Et	100	57
			^{i}Pr	100	15
			^{n}Bu	100	25
			^{t}Bu	100	0

[a] All reactions were performed with substrate (0.02 mmol), RFT (10 mol%), HCl (37%, 16.7 µL, 10 eq.) in 2 mL alcohol ROH (R = Me, Et, ^{i}Pr, ^{n}Bu, ^{t}Bu). The samples were exposed to the atmosphere and placed in a cooling block during irradiation (12 h) with blue light (440 nm). [b] Conversion and yield determined by GC-FID integration.

Table S5. Photocatalytic oxidation of 4-chlorobenzaldehyde – screening of the base.[a]

Entry	Base	Conv. [%][b]	Yield [%][b]
1	DBU (20 mol%)	29	0
2	DBU (1 eq.)	33	0
3	DBU (10 eq.)	62	39
4	**DBU (30 eq.)**	**100**	**84**
5	H_2O (500 µL)	100	0
6	Cs_2CO_3 (10 eq.)	29	25
7	K_2CO_3 (30 eq.)	45	8
8	Na_2CO_3 (sat., 200 µL)	60	0
9	Et_3N (30 eq.)	51	8
10	DIPEA (30 eq.)	62	9

[a] All reactions were performed with 4-chlorobenzaldehyde (0.02 mmol), RFT (10 mol%), base, ethyl bromide (200 µL) in 2 mL MeCN. The samples were exposed to atmospheric oxygen and placed in a cooling block during irradiation (12 h) with blue light (440 nm). [b] Conversion and yield determined by GC-FID integration.

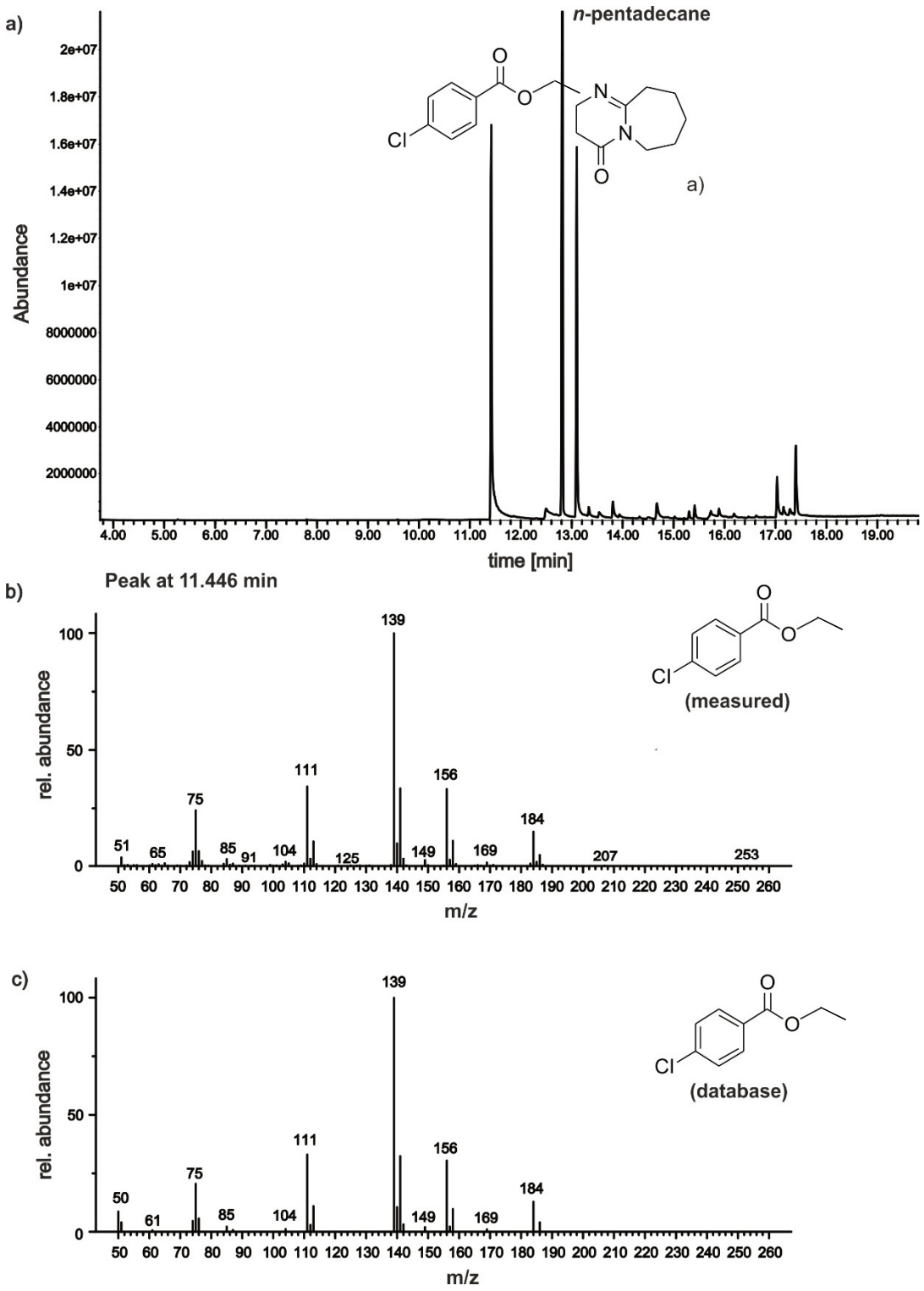

Figure S3. a) GC-MS spectrum of a mixture of 4-chlorobenzaldehyde (**1**, 0.02 mmol), RFT (10 mol%), DBU (93 µL) and ethyl bromide (200 µL) in 2 mL MeCN which was irradiated for 12 h with blue light (440 nm); the signal at t_R = 12.8 minutes is assigned to the internal standard *n*-pentadecane; b) mass spectrum of the signal at the retention time t_R = 11.446 minutes which is assigned ethyl 4-chlorobenzoate **3**; c) mass spectrum of an authentic sample ethyl 4-chlorobenzoate **9**.

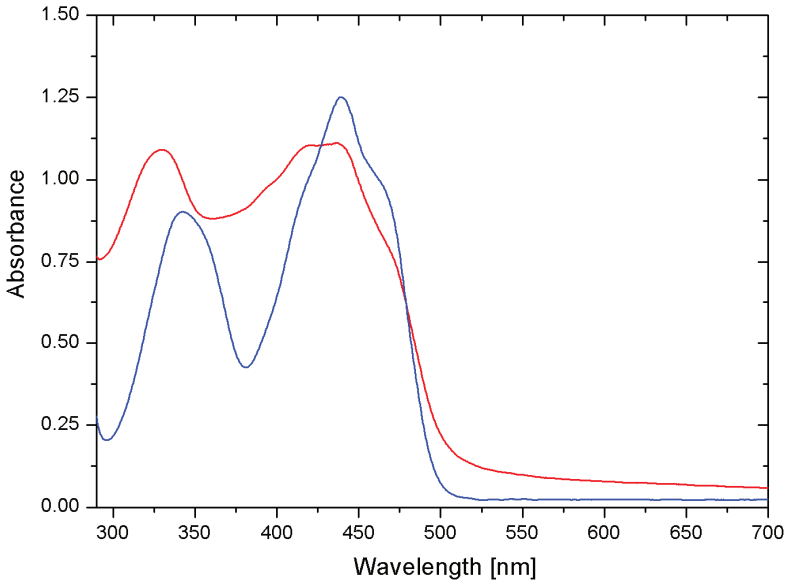

Figure S4. Absorption spectra of RFT (0.1 mM) in MeCN (blue) and of RFT (0.1 mM) in MeCN in the presence of DBU (30 µL, red).

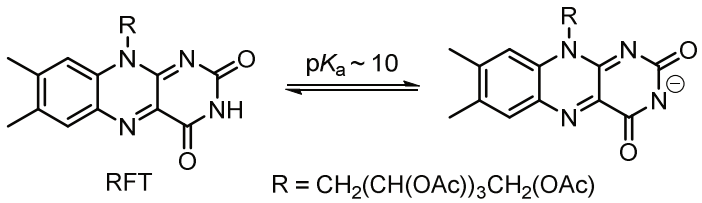

Scheme S1. Deprotonation of RFT by strong bases[48]

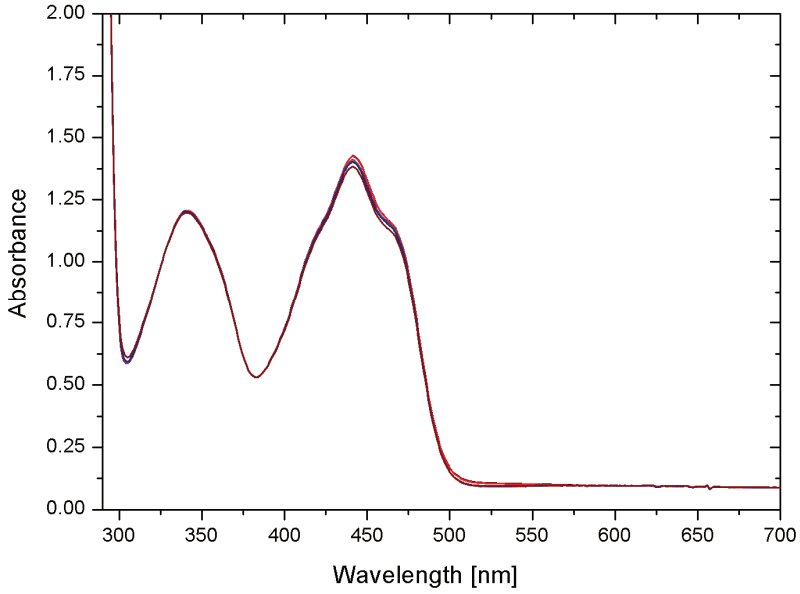

Figure S5. Electronic absorption spectra of 4-chlorobenzaldehyde (6.7 mM) and RFT (0.1 mM) while irradiating with blue light in deaterated MeCN at 298 K for one minute.

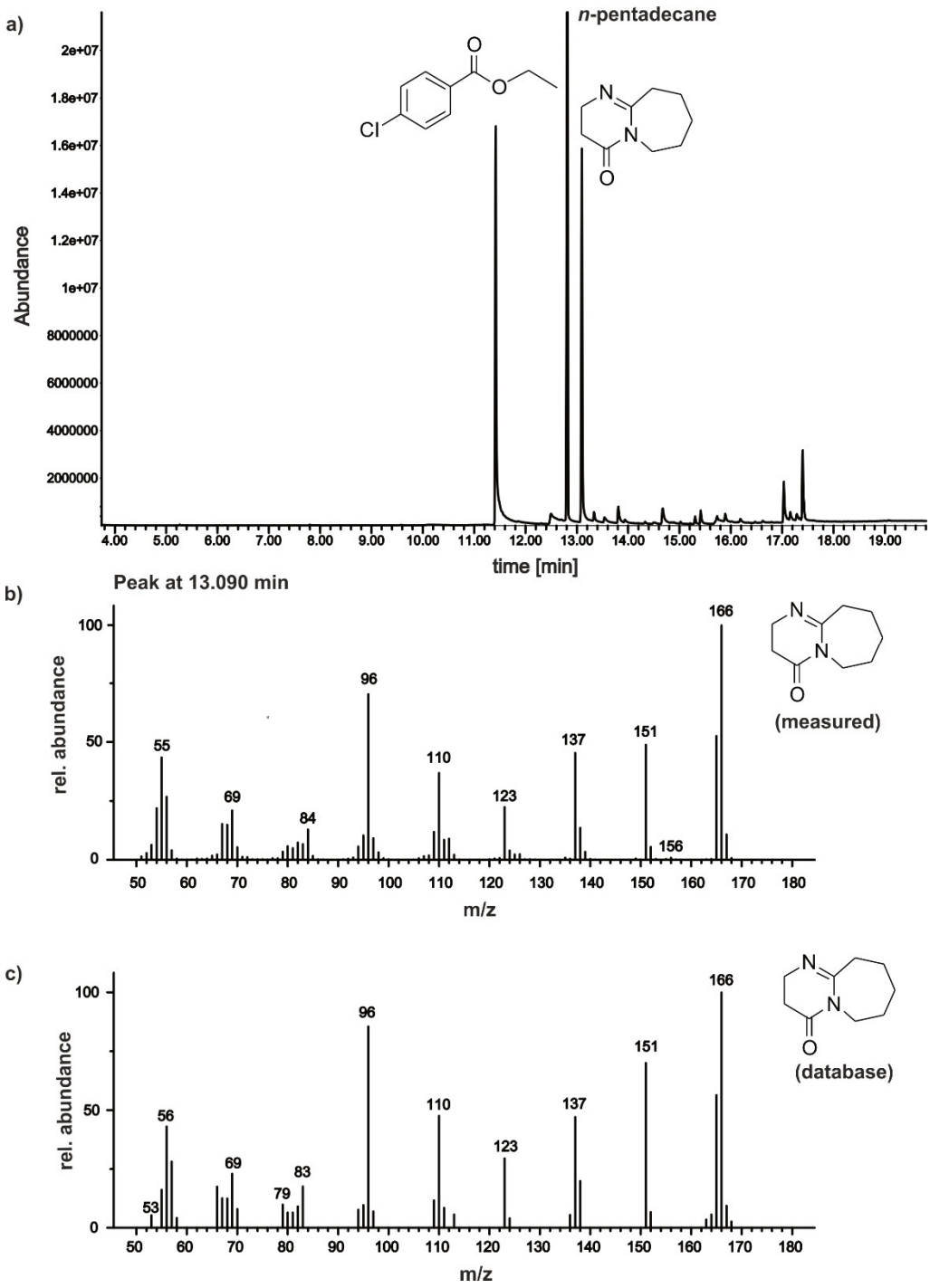

Figure S6. a) GC-MS spectrum of a mixture of 4-chlorobenzaldehyde (**1**, 0.02 mmol), RFT (10 mol%), DBU (93 µL) and ethyl bromide (200 µL) in 2 mL MeCN which was irradiated for 12 h with blue light (440 nm); the signal at t_R = 12.8 minutes is assigned to the internal standard *n*-pentadecane; b) mass spectrum of the signal at the retention time t_R = 13.090 minutes which is assigned to 1,8-diazabicyclo[5.4.0]undec-7-en-11-one (DBU^{ox}); c) mass spectrum of an authentic sample of 1,8-diazabicyclo[5.4.0]undec-7-en-11-one (DBU^{ox}).

Table S6. Esterification of 4-chlorobenzaldehyde with H_2O_2 in the presence of DBU and ethyl bromide[a]

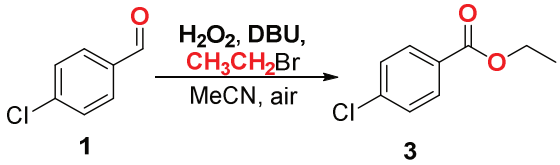

Entry	Eq. H_2O_2	Conv. [%][b]	Yield [%][b]
1	0.0	28	8
2	1.2	43	12
3	2.4	47	16
4	3.6	47	24
5	4.8	47	29
6[c]	1.2	98‡	0

[a] All reactions were performed with 4-chlorobenzaldehyde (0.02 mmol), DBU (30 eq.) and ethyl bromide (200 µL) in the presence of various equivalents of H_2O_2 (30%) in 2 mL MeCN. [b] Conversion and yield determined by GC-FID integration. [c] no DBU added.‡

5.6 Footnotes

†The pK_a of the $^2RFTH_2^{\bullet+}$ radical is approximately 2, while the pK_a of a toluene radical cation in MeCN is estimated to 12 to 13.[51,52]

‡The electron transfer only occurs between DBU and RFT. Nevertheless, control experiments revealed that **1** is fully consumed when irradiated in the presence of ethyl bromide in MeCN (see Table 4 (entry 2) and Table S6 (entry 6)). A closer examination of this reaction revealed that ethyl bromide initiates the consumption of **1** under irradiation. This reaction is supressed in the presence of DBU, hence we believe our mechanistic considerations are valid in the presence of DBU and alkyl bromide. We assume that a photoinitated formation of $Br^{\bullet}$ radicals occurs in the absence of any chromophore,[53] which abstract an aldehyde proton yielding an acyl radical. This acyl radical is easily trapped by dioxygen and fragments into the corresponding acid in the presence of traces of water. In the presence of DBU, $Br^{\bullet}$ radicals will abstract a proton from DBU instead, thus preventing the oxidation of **1**.

5.7 References

[1] W. Riemenschneider, H. M. Bolt, *Ullmann's Encyclopedia of Industrial Chemistry*, Wiley-VCH, Weinheim, **2005**.

[2] J. Otera, J. Nishikido, *Esterification: Methods, Reactions, and Applications*, Wiley-VCH, Weinheim, **2010**.

[3] R. C. Larock, *Comprehensive Organic Transformations: A Guide to Functional Group Preparations*, Wiley-VCH, New York, **1999**.

[4] A. Brennführer, H. Neumann, M. Beller, *Angew. Chem. Int. Ed.* **2009**, *48*, 4114–4133.

[5] A. Schoenberg, R. F. Heck, *J. Org. Chem.* **1974**, *39*, 3327–3331.

[6] W. Guo, L.-Q. Lu, Y. Wang, Y.-N. Wang, J.-R. Chen, W.-J. Xiao, *Angew. Chem. Int. Ed.* **2015**, *54*, 2265–2269.

[7] M. Majek, A. Jacobi von Wangelin, *Angew. Chem. Int. Ed.* **2015**, *54*, 2270–2274.

[8] Q. Xiao, Z. Liu, A. Bo, S. Zavahir, S. Sarina, S. Bottle, J. D. Riches, H. Zhu, *J. Am. Chem. Soc.* **2015**, *137*, 1956–1966.

[9] C. Liu, J. Wang, L. Meng, Y. Deng, Y. Li, A. Lei, *Angew. Chem. Int. Ed.* **2011**, *50*, 5144–5148.

[10] K. Ekoue-Kovi, C. Wolf, *Chem. – Eur. J.* **2008**, *14*, 6302–6315.

[11] N. Mori, H. Togo, *Tetrahedron* **2005**, *61*, 5915–5925.

[12] S. Sayama, T. Onami, *Synlett* **2004**, 2739–2745.

[13] B. R. Travis, M. Sivakumar, G. O. Hollist, B. Borhan, *Org. Lett.* **2003**, *5*, 1031–1034.

[14] A. Nishihara, I. Kubota, *J. Org. Chem.* **1968**, *33*, 2525–2526.

[15] S. De Sarkar, A. Biswas, R. C. Samanta, A. Studer, *Chem. – Eur. J.* **2013**, *19*, 4664–4678.

[16] K. Zeitler, *Angew. Chem. Int. Ed.* **2005**, *44*, 7506–7510.

[17] D. Seebach, *Angew. Chem. Int. Ed. Engl.* **1979**, *18*, 239–258.

[18] R. Breslow, *J. Am. Chem. Soc.* **1958**, *80*, 3719–3726.

[19] B. Maji, S. Vedachalan, X. Ge, S. Cai, X.-W. Liu, *J. Org. Chem.* **2011**, *76*, 3016–3023.

[20] Y.-C. Xin, S.-H. Shi, D.-D. Xie, X.-P. Hui, P.-F. Xu, *Eur. J. Org. Chem.* **2011**, *2011*, 6527–6531.

[21] J. N. Rosa, R. S. Reddy, N. R. Candeias, P. M. S. D. Cal, P. M. P. Gois, *Org. Lett.* **2010**, *12*, 2686–2689.

[22] P. Arde, B. T. Ramanjaneyulu, V. Reddy, A. Saxena, R. V. Anand, *Org. Biomol. Chem.* **2012**, *10*, 848–851.

[23] R. S. Reddy, J. N. Rosa, L. F. Veiros, S. Caddick, P. M. P. Gois, *Org. Biomol. Chem.* **2011**, *9*, 3126–3129.

[24] M. Zhang, S. Zhang, G. Zhang, F. Chen, J. Cheng, *Tetrahedron Lett.* **2011**, *52*, 2480–2483.

[25] D. Zhang, C. Pan, *Catal. Commun.* **2012**, *20*, 41–45.

[26] Y.-K. Liu, R. Li, L. Yue, B.-J. Li, Y.-C. Chen, Y. Wu, L.-S. Ding, *Org. Lett.* **2006**, *8*, 1521–1524.

[27] R. Kluger, *Chem. Rev.* **1987**, *87*, 863–876.

[28] M. Pohl, B. Lingen, M. Müller, *Chem. – Eur. J.* **2002**, *8*, 5288–5295.

[29] Y. Yano, Y. Hoshino, W. Tagaki, *Chem. Lett.* **1980**, *9*, 749–752.

[30] S. Shinkai, T. Yamashita, Y. Kusano, O. Manabe, *J. Am. Chem. Soc.* **1982**, *104*, 563–568.

[31] S. Shinkai, Y. Hara, O. Manabe, *Bull. Chem. Soc. Jpn.* **1983**, *56*, 770–774.

[32] S. Shinkai, T. Yamashita, Y. Kusano, O. Manabe, *Tetrahedron Lett.* **1980**, *21*, 2543–2546.

[33] S. Shinkai, T. Yamashita, Y. Kusano, O. Manabe, *J. Org. Chem.* **1980**, *45*, 4947–4952.

[34] S. W. Tam, L. Jimenez, F. Diederich, *J. Am. Chem. Soc.* **1992**, *114*, 1503–1505.

[35] S. Iwahana, H. Iida, E. Yashima, *Chem. – Eur. J.* **2011**, *17*, 8009–8013.

[36] V. Mojr, E. Svobodová, K. Straková, T. Neveselý, J. Chudoba, H. Dvořáková, R. Cibulka, *Chem Commun* **2015**, *51*, 12036–12039.

[37] B. Mühldorf, R. Wolf, *Chem. Commun.* **2015**, *51*, 8425–8428.

[38] B. Mühldorf, R. Wolf, *Angew. Chem. Int. Ed.* **2016**, 427–430.

[39] R. Lechner, B. König, *Synthesis* **2010**, *2010*, 1712–1718.

[40] R. Lechner, S. Kümmel, B. König, *Photochem. Photobiol. Sci.* **2010**, *9*, 1367.

[41] H. Schmaderer, P. Hilgers, R. Lechner, B. König, *Adv. Synth. Catal.* **2009**, *351*, 163–174.

[42] E. Sikorska, M. Sikorski, R. P. Steer, F. Wilkinson, D. R. Worrall, *J. Chem. Soc. Faraday Trans.* **1998**, *94*, 2347–2353.

[43] E. Sikorska, I. Khmelinskii, A. Komasa, J. Koput, L. F. V. Ferreira, J. R. Herance, J. L. Bourdelande, S. L. Williams, D. R. Worrall, M. Insińska-Rak, et al., *Chem. Phys.* **2005**, *314*, 239–247.

[44] S. Fukuzumi, S. Kuroda, *Res Chem Intermed* **1999**, *25*, 789.

[45] U. Megerle, M. Wenninger, R.-J. Kutta, R. Lechner, B. König, B. Dick, E. Riedle, *Phys. Chem. Chem. Phys.* **2011**, *13*, 8869.

[46] W.-C. Shieh, S. Dell, O. Repič, *J. Org. Chem.* **2002**, *67*, 2188–2191.

[47] K. H. Dudley, A. Ehrenberg, P. Hemmerich, F. Müller, *Helv. Chim. Acta* **1964**, *47*, 1354–1383.

[48] P. Hemmerich, C. Veeger, H. C. S. Wood, *Angew. Chem. Int. Ed. Engl.* **1965**, *4*, 671–687.

[49] M. Rueping, C. Vila, R. M. Koenigs, K. Poscharny, D. C. Fabry, *Chem. Commun.* **2011**, *47*, 2360–2362.

[50] Z. Wang, in *Compr. Org. Name React. Reag.*, John Wiley & Sons, Inc., **2010**.

[51] M. M. Green, S. L. Mielke, *J. Org. Chem.* **1984**, *49*, 1276–1278.

[52] A. M. de P. Nicholas, D. R. Arnold, *Can. J. Chem.* **1982**, *60*, 2165–2179.

[53] J. F. Franz, W. B. Kraus, K. Zeitler, *Chem. Commun.* **2015**, *51*, 8280–8283.

6 Halogenase-Inspired Oxidative Chlorination Using Flavin Photocatalysis[a]

Thea Hering, Bernd Mühldorf, Robert Wolf, and Burkhard König

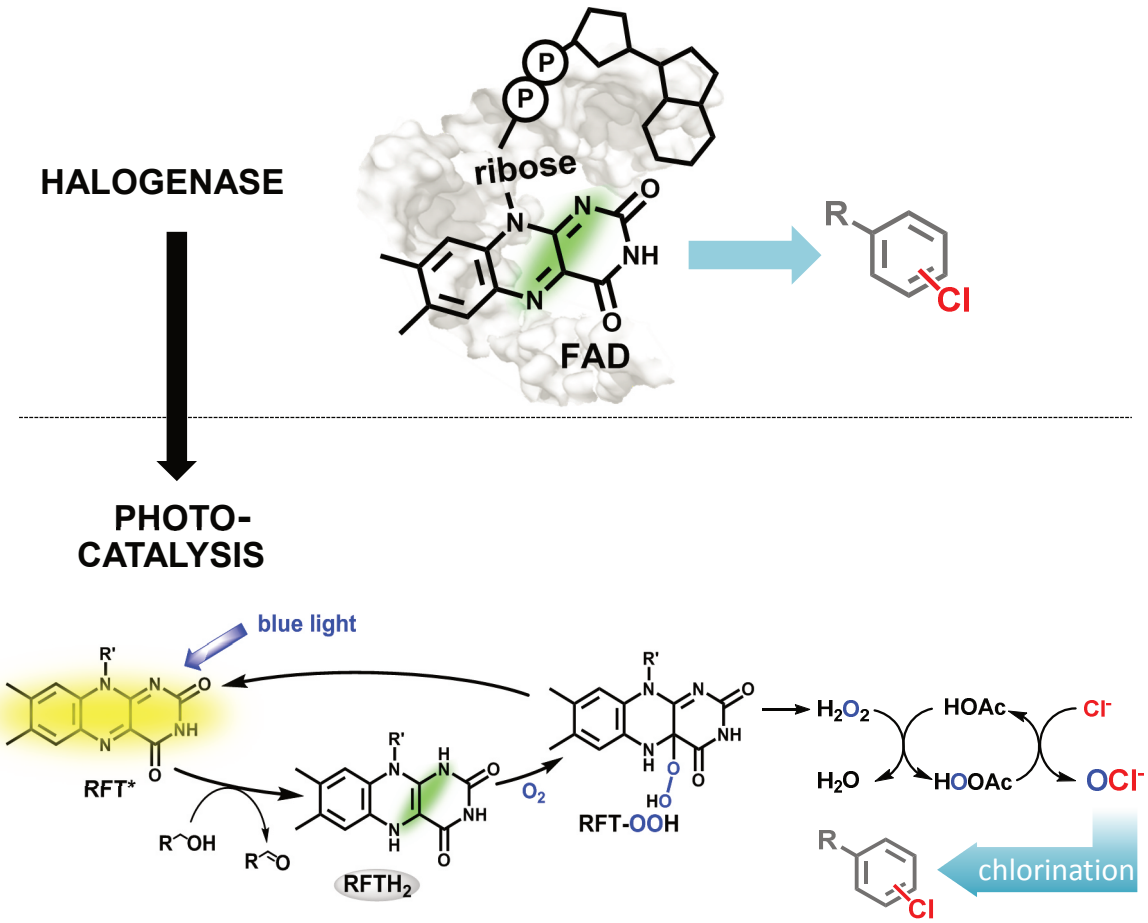

[a] Thea Hering, Bernd Mühldorf, Robert Wolf, and Burkhard König, Angew. Chem. DOI: 10.1002/anie.201600783R1, accepted on 02/15/2016.

TH wrote the manuscript in cooperation with BM, TH performed photocatalytic reactions, and the synthesis of the chlorinated products. BM performed photocatalytic reactions, work-up, and GC-FID calibration and analysis.

6.1 Introduction

Chlorinated aromatic compounds are ubiquitous in organic chemistry. They serve as key precursors for metal-catalyzed cross couplings and are widely employed in natural products, pharmaceuticals and material science to tune biological or electronic properties.[1] While traditional chemistry mostly relies on the use of hazardous and toxic chlorine gas or synthetic equivalents such as NCS and ^{t}BuOCl as the source of electrophilic chlorine, nature has developed a more elegant strategy based on the enzymatically catalyzed oxidation of abundant and non-toxic chloride ions in an oxidative chlorination.[2] Halogenases efficiently yield aryl halides from halide ions and aromatic compounds using either O_2 or hydrogen peroxide (haloperoxidases) as the oxidant.[3] With respect to environmental factors, these are the ideal oxidants as only water is produced as a by-product. For this reason a variety of chemical oxidative halogenations have been developed.[2] However, while great progress has been made in the area of oxidative bromination, oxidative chlorination remains challenging. The few examples known suffer from drastic conditions and low selectivity[2,4] or rely on stronger or metal based stoichiometric oxidants.[5] Over the last years, halogenases have been successfully isolated and used for the halogenation (mostly bromination) of aromatic compounds.[6] These reactions show high selectivity and have also been scaled up to gram amounts,[6b] but as the enzymes are naturally substrate specific the scope of accessible products is limited, and the isolation and handling of the enzymes is difficult.

We aimed to develop a biomimetic system inspired by flavin adenine dinucleotide (FAD)-dependent halogenases, which is one of the main families of this enzyme groups.[3a] The FAD dependent system combines several advantages: O_2 is used as oxidant avoiding the separate addition of H_2O_2 as required for heme and vanadate dependent haloperoxidases. The cofactor FAD is a purely organic, metal-free catalyst, and simple flavin derivatives are known to act as oxidative photocatalysts.[7] The enzymatic mechanism (Scheme 1) involves the reduction of FAD by $NADH_2$ to yield a reduced $FADH_2$, which reacts with oxygen to form a peroxo species FAD-OOH that is subsequently attacked by chloride ions to form the "Cl^+" equivalent HOCl.[8] Our system replaces FAD by the cheap dye riboflavin tetraacetate (RFT), which is known to form reduced $RFTH_2$ upon excitation with visible light in the presence of benzyl alcohols (Scheme 1).[7] This allows us to replace the biomolecules FAD and $NADH_2$ and to perform the reactions in organic solvents using a stable and inexpensive catalyst.

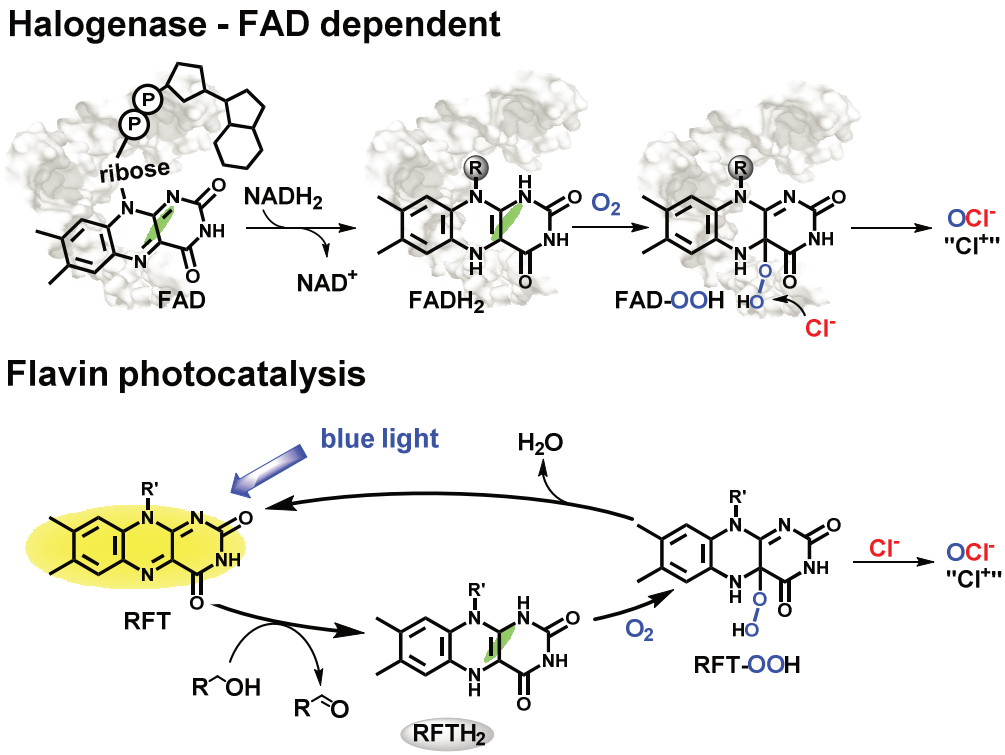

Scheme 1. Analogy of the mechanistic model of chloride oxidation by FAD-dependent halogenases (top) and the proposed photocatalytic halogenase mimetic system (bottom); R'=$CH_2(CHOAc)_3CH_2OAc$.

6.2 Results and Discussion

A key challenge in developing a photocatalytic halogenase mimetic system is the efficient generation of electrophilic hypochlorite. In analogy to the enzymatic system, $RFTH_2$ forms a short-lived flavin-peroxo species RFT-OOH, which should oxidize chloride ions to OCl^-. (Scheme 1) However, in the enzyme the reaction of the flavin peroxide to form hypochlorite and the subsequent chlorination of the substrate are catalyzed by the complex enzyme environment. For enzymes as RebH the mediation by a lysine residue in the active center is crucial for the reactivity and selectivity of the reaction. Moreover, X-ray studies of halogenases have shown that the substrate and the flavin peroxide (FAD-OOH) are brought in very close proximity (~10 Å) before a reaction takes place.[3a, 9] This is also the reason why the simple chemical system, using anisole (**1**) as the substrate, 10 mol% RFT as the photocatalyst under aerobic conditions and irradiation with blue light (λ_{max} = 455 nm) in the presence of HCl as the chloride source and *p*-methoxy benzyl alcohol (*p*MBA) as a replacement for $NADH_2$ in 2 mL acetonitrile, did not yield any chlorination product of anisole (Scheme 2).

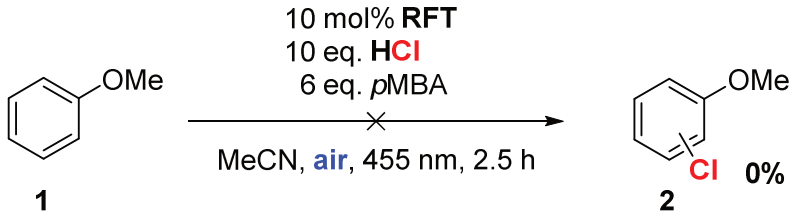

Scheme 2. Test reaction for the chlorination of anisole (**1**) with the photocatalytic system using 20 µmol of **1** in 2 mL acetonitrile.

In order to chemically mimic the enzymatic system, a mediator is needed, which is sufficiently long lived in order to enable the formation of perchloric acid. During the course of our investigations we discovered that peracetic acid can oxidize chloride ions and is able to perform oxidative chlorination of aromatic compounds (SI, Table S2).[10] Peracetic acid is highly explosive when isolated, but it can be formed in equilibrium with acetic acid and H_2O_2.[11] As it is known that RFT−OOH formed in the photocatalytic oxidation quickly releases one equivalent of H_2O_2,[7a] we added 10 eq. of acetic acid to the system described above and, to our delight, observed the chlorination of anisole (**1**).

Control reactions showed that all reaction components are essential to observe the chlorination reaction (SI, Table S1). Based on this we propose an *in situ* formation of peracetic acid as depicted in Figure 1, which acts as the described mediator and enables the chlorination via the following reaction cycle. In the first step, the photocatalyst RFT is excited by visible light irradiation (λ_{max} = 455 nm) to RFT* and reduced to $RFTH_2$ by oxidation of the benzylic alcohol (*p*MBA). $RFTH_2$ is re-oxidized by air forming H_2O_2, which does not directly oxidize chloride, but forms peracetic acid (HOOAc) in an equilibrium with acetic acid (HOAc). The hereby *in situ* generated HOOAc subsequently reacts with chloride to form the electrophilic chlorine species HOCl, which attacks anisole (**1**) in an electrophilic aromatic substitution reaction. However, we cannot exclude other electrophilic chlorine species in equilibrium with HOCl, e.g. Cl_2O, ClOAc, Cl_2 and H_2OCl^+, be involved.[4b, 12]

With this mechanistic model in hand we optimized the reaction conditions for the highest formation of peracetic acid (see SI). The equilibrium of H_2O_2 and acetic acid is known to be shifted towards the side of peracetic acid by strong acids.[11a] Therefore, hydrochloric acid proved to be the ideal chloride source as it dissolved well in acetonitrile and is a strong acid at the same time. The reaction with triethylammonium chloride (TEACl) and20 mol% H_2SO_4 also led to product formation, but with a slightly lower yield. No chlorination was observed with any of the tested chloride salts (TEACl, NaCl, KCl, and

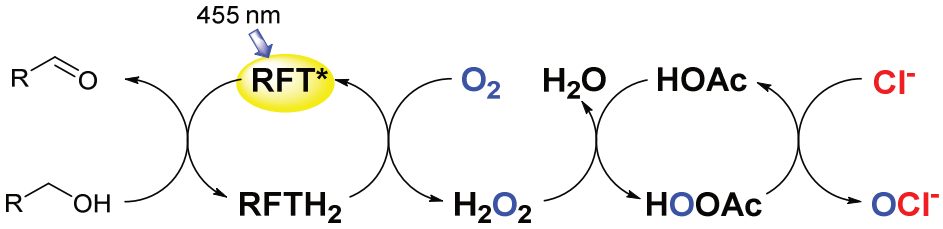

Figure 1. Proposed mechanistic scheme of the peracetic acid mediated oxidation of chloride by flavin photocatalysis.

NH_4Cl) in the absence of added acid. Furthermore, elevated temperatures are known to be beneficial for peracetic acid formation.[11b] An increase of the reaction temperature from 25 °C to 45 °C improved the yield of chloroanisole (**2**) from 28% to 66% (p:o 5:1); a further increase to 60 °C led to decomposition of the photocatalyst (SI, Table S4). We also varied the peracid and replaced acetic acid by the stronger acids formic acid and triflic acid (SI, Table S3). Formic acid showed significantly lower yields than acetic acid, while triflic acid with 5 eq. TEACl and 5 eq. HCl gave a comparable yield of the chlorinated anisole. Alternative reagents for the generation of peracetic acid such as acetic anhydride or acetyl chloride enabled product formation, but were less efficient than acetic acid.

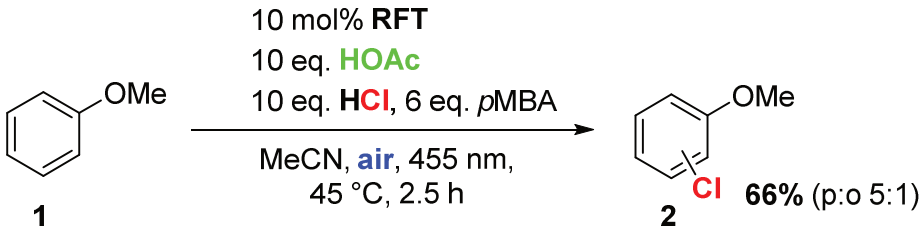

Scheme 3. Oxidative chlorination of anisole (**1**) with the photocatalytic halogenase mimetic system.

The optimized conditions depicted in Scheme 3 were used to investigate the substrate scope. While an enzyme usually has a highly specific binding pocket and thus a narrow substrate scope, but high selectivity, our system does not bind the substrate and should allow a broader substrate scope. The results are summarized in Table 1. The system works excellently for arenes with nitrogen +M substituents such as *N*,*N*-dimethylaniline (entry 1) or amides (entries 2,3). Substrates with an alkoxy group, such as anisole (entry 4) or diphenylether (entry 5), can also be successfully chlorinated in good to moderate yields. When the arene is too electron rich, as for example in dimethoxybenzene carrying two +M-substituents, the yield decreases due to the unselective direct oxidation of the substrate by the photocatalyst (entry 6). The acidic conditions lead to a protonation of RFT observable by UV/VIS measurements (SI, Table S4, S5). In its protonated form RFT is known to have a high oxidative power.[13] Substrates, which are too electron poor, e.g. trifluoromethoxybenzene (entry 7), are not attacked by hypochlorite and do not give

Table 1. Scope of the flavin-catalyzed oxidative chlorination and results obtained by direct addition of H_2O_2.[a]

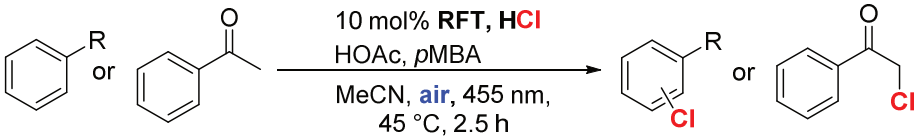

Entry	Substrate	Product	Conv [%][b]	Yield [%][b],[c]	H_2O_2[d]
1	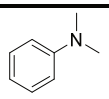 **3**	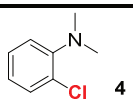 **4**	100	**96** (o:di 2:1)	14 (o:di 1:0)
2[e]	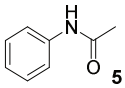 **5**	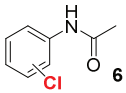 **6**	100	**97** (p:o 3:1)	37 (p:o 1:0)
3[e]	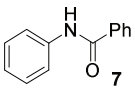 **7**	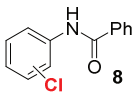 **8**	96	**98** (p:o 5: 1)	24 (p:o 1:1)
4	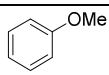 **9**	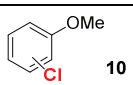 **10**	100	**66** (p:o 5:1)	17 (p:o 1:1)
5	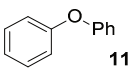 **11**	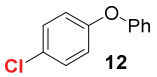 **12**	79	**80**	55
6	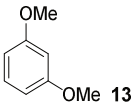 **13**	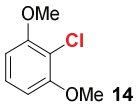 **14**	100	**40**	23
7	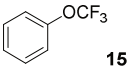 **15**	--	0	--	--
8	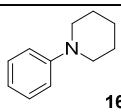 **16**	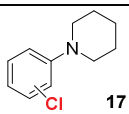 **17**	70	**64** (p:o 1:3)	68 (p:o 1:5)
9[f]	 **18**	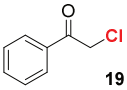 **19**	76	**63**	11
10[f]	 **20**	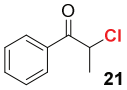 **21**	49	**64**	84

[a] Reactions were performed with 0.02 mmol of the substrate, 10 eq. HCl, 10 eq. HOAc, 6 eq. *p*MBA and 10 mol% RFT in 2.0 mL MeCN. The reaction mixtures were irradiated for 2.5 h at 45 °C. [b] determined by GC-FID using an internal standard [c] based on conversion [d] 6 eq. H_2O_2 10 eq. HOAc and 10 eq. HCl in 2 mL MeCN [e] with KCl additionl [f] with TFA.

chlorination products neither in the photocatalytic system nor when peracetic acid is added directly (SI, Table S2). Acetophenones (entries 9, 10) are mono-chlorinated in the α-position. The reaction proceeds via the enol form and therefore works better when the stronger triflic acid is used instead of acetic acid.[14] It is worth noting that aromatic amines (entries 1, 8) show *ortho* selectivity for the chlorination. This may be explained

by the intermediate formation of an *N*-chloramine. This selectivity is not observed with amides (entries 2, 3).

For comparison, Table 1 also shows the yields of chlorination obtained by adding 6 eq. of H_2O_2 directly to the reaction mixture instead of being generated by the photocatalytic process (reaction contained no RFT and *p*MBA). Even though the direct addition of H_2O_2 always gave full conversion of the substrate, the yields were considerably lower for most substrates than in the photocatalytic system. The slow generation of peroxide by the flavin-catalyzed process is beneficial for the reaction as it circumvents the problem of unselective side reactions and over-chlorination often observed for H_2O_2-based systems. The same observation was made for haloperoxidase-catalyzed reactions.[6e]

6.3 Conclusion

In conclusion, visible light flavin photocatalysis allows the oxidative chlorination of arenes inspired by FAD-dependent halogenases. The biomolecules FAD and $NADH_2$ were replaced by the cheap organic dye riboflavin tetraacetate and methoxybenzyl alcohol as the reducing agent. As a result, the reaction can be performed in organic media. Acetic acid was added to the system forming peracetic acid *in situ*, which acts as a mediator to activate the peroxide for chloride oxidation. Compared to the specific binding pocket of an enzyme, the activation by peracetic acid is a more general strategy and thus allows a broader substrate scope. The developed system allows the chlorination of electron rich arenes, e.g. anisole, methylanilines, diphenyl ether and amides, as well as the α-chlorination of acetophenones.

6.4 References

[1] a) J. Fauvarque, in *Pure Appl. Chem., Vol. 68*, **1996**, p. 1713-1720; b) A. F. Littke, G. C. Fu, *Angew. Chem., Int. Ed.* **2002**, *41*, 4176-4211; c) A. F. Littke, G. C. Fu, *Angew. Chem.* **2002**, *114*, 4350-4386; d) G. W. Gribble, *J. Chem. Educ.* **2004**, *81*, 1441-1449; e) H. Liu, X. Cao, Y. Wu, Q. Liao, A. J. Jimenez, F. Würthner, H. Fu, *Chem. Commun.* **2014**, *50*, 4620-4623.

[2] a) A. Podgoršek, M. Zupan, J. Iskra, *Angew. Chem., Int. Ed.* **2009**, *48*, 8424-8450; b) A. Podgoršek, M. Zupan, J. Iskra, *Angew. Chem.* **2009**, *121*, 8576-8603.

[3] a) F. H. Vaillancourt, E. Yeh, D. A. Vosburg, S. Garneau-Tsodikova, C. T. Walsh, *Chem. Rev.* **2006**, *106*, 3364-3378; b) A. Butler, M. Sandy, *Nature* **2009**, *460*, 848-854; c) J. M. Winter, B. S. Moore, *J. Biol. Chem.* **2009**, *284*, 18577-18581.

[4] a) A. O. Terent'ev, S. V. Khodykin, N. A. Troitskii, Y. N. Ogibin, G. I. Nikishin, *Synthesis* **2004**, *2004*, 2845-2848; b) R. Ben-Daniel, S. P. de Visser, S. Shaik, R. Neumann, *J. Am. Chem. Soc.* **2003**, *125*, 12116-12117.

[5] a) L. Gu, T. Lu, M. Zhang, L. Tou, Y. Zhang, *Adv. Synth. Catal.* **2013**, *355*, 1077-1082; b) K.-D. Umland, C. Mayer, S. F. Kirsch, *Synlett* **2014**, *25*, 813-816; c) J.-Y. Wang, Q. Jiang, C.-C. Guo, *Synth. Commun.* **2014**, *44*, 3130-3138; d) Z. Cong, T. Kurahashi, H. Fujii, *Angew. Chem., Int. Ed.* **2011**, *50*, 9935-9939; e) Z. Cong, T. Kurahashi, H. Fujii, *Angew. Chem.* **2011**, *123*, 10109-10113; f) A. K. Vardhaman, P. Barman, S. Kumar, C. V. Sastri, D. Kumar, S. P. de Visser, *Chem. Commun.* **2013**, *49*, 10926-10928; g) P. J. Hansen, J. H. Espenson, *Inorg. Chem.* **1995**, *34*, 5839-5844; h) R. Prebil, S. Stavber, *Adv. Synth. Catal.* **2014**, *356*, 1266-1274; i) P. Pandit, K. S. Gayen, S. Khamarui, N. Chatterjee, D. K. Maiti, *Chem. Commun.* **2011**, *47*, 6933-6935; j) P. B. Thorat, B. Y. Bhong, N. N. Karade, *Synlett* **2013**, *24*, 2061-2066.

[6] a) S. A. Shepherd, C. Karthikeyan, J. Latham, A.-W. Struck, M. L. Thompson, B. R. K. Menon, M. Q. Styles, C. Levy, D. Leys, J. Micklefield, *Chem. Sci.* **2015**, *6*, 3454-3460; b) M. Frese, N. Sewald, *Angew. Chem., Int. Ed.* **2015**, *54*, 298-301; c) M. Frese, N. Sewald, *Angew. Chem.* **2015**, *127*, 302-305; d) D. R. M. Smith, S. Grüschow, R. J. M. Goss, *Curr. Opin. Chem. Biol.* **2013**, *17*, 276-283; e) F. Sabuzi, E. Churakova, P. Galloni, R. Wever, F. Hollmann, B. Floris, V. Conte, *Eur. J. Inorg. Chem.* **2015**, *2015*, 3519-3525; f) E. Fernández-Fueyo, M. van Wingerden, R. Renirie, R. Wever, Y. Ni, D. Holtmann, F. Hollmann, *ChemCatChem* **2015**, *7*, 4035-4038; g) J. T. Payne, M. C. Andorfer, J. C. Lewis, *Angew. Chem., Int. Ed.* **2013**, *52*, 5271-5274; h) J. T. Payne, M. C. Andorfer, J. C. Lewis, *Angew. Chem.*

2013, *125*, 5379-5382; i) J. T. Payne, C. B. Poor, J. C. Lewis, *Angew. Chem., Int. Ed.* **2015**, *54*, 4226-4230; j) J. T. Payne, C. B. Poor, J. C. Lewis, *Angew. Chem.* **2015**, *127*, 4300-4304.

[7] a) U. Megerle, M. Wenninger, R.-J. Kutta, R. Lechner, B. König, B. Dick, E. Riedle, *Phys. Chem. Chem. Phys.* **2011**, *13*, 8869-8880; b) R. Lechner, S. Kümmel, B. König, *Photochem. Photobiol. Sci.* **2010**, *9*, 1367-1377.

[8] E. Yeh, L. J. Cole, E. W. Barr, J. M. Bollinger, D. P. Ballou, C. T. Walsh, *Biochemistry* **2006**, *45*, 7904-7912.

[9] E. Yeh, L. C. Blasiak, A. Koglin, C. L. Drennan, C. T. Walsh, *Biochemistry* **2007**, *46*, 1284-1292.

[10] a) Y. He, C. R. Goldsmith, *Synlett* **2010**, 1377-1380; b) Peracetic acid itself has not been extensively used for oxidative chlorination. However, we noticed that a number of oxidative chlorination reactions with hydrogen peroxide were performed in acetic acid as the solvent. We assume also that in these cases an *in situ* formation of peracetic acid might be responsible for the reactivity, see: a) references in A. Podgoršek, M. Zupan, J. Iskra, *Angew. Chem., Int. Ed.* **2009**, *48*, 8424-8450. b) N. I. Rudakova, Y. G. Erykalov, *Russ. J. Gen.Chem.* **2005**, *75*, 748-750. c) G. Jerzy, Ż. Slawomir, *Synth. Commun.* **1997**, *27*, 3291-3299.

[11] a) H. Klenk, P. H. Götz, R. Siegmeier, W. Mayr, in *Ullmann's Encyclopedia of Industrial Chemistry*, Wiley-VCH Verlag GmbH & Co. KGaA, **2000**; b) X. Zhao, T. Zhang, Y. Zhou, D. Liu, *J. Mol. Catal. A: Chem.* **2007**, *271*, 246-252.

[12] a) C. G. Swain, D. R. Crist, *J. Am. Chem. Soc.* **1972**, *94*, 3195-3200; b) P. B. D. de la Mare, I. C. Hilton, C. A. Vernon, *Journal of the Chemical Society (Resumed)* **1960**, 4039-4044.

[13] S. Fukuzumi, S. Kuroda, *Res. Chem. Intermed.* **1999**, *25*, 789-811.

[14] Incomplete conversion is observed as the required keto-enol equilibrium slows down the reaction. If the reaction of the substrate and the peracetic acid is not fast enough, a Bayer-Villiger type background reaction of the benzaldehyde consumes the peracid, see M. Matsumoto, K. Kobayashi, Y. Hotta, *J. Org. Chem.* **1984**, *49*, 4740-4741.

6.5 Supporting Information

6.5.1 General Information

Chemicals

RFT was prepared according to a known literature procedure.[1] All other chemicals were obtained commercially (Sigma Aldrich, VWR or TCI) or synthesized according to known literature procedures; **4**,[2] **8**,[3] and **17**[4]. Compounds **12** and **21** were synthesized using a scaled up reaction of peracetic acid described in the general procedure for reactions with peracetic acid.

Photochemical set-up, LEDs

Photocatalytic reactions were performed with 455 nm LEDs (OSRAM Oslon SSL 80 royal-blue LEDs, λ_{em} = 455 nm (± 15 nm), 3.5 V, 700 mA). Reaction vials (5 mL crimp cap vials, no cap) were illuminated from the bottom with LEDs and cooled or heated from the side using custom made aluminum cooling block connected to a thermostat. A magnetic stirrer is placed below the LED array.

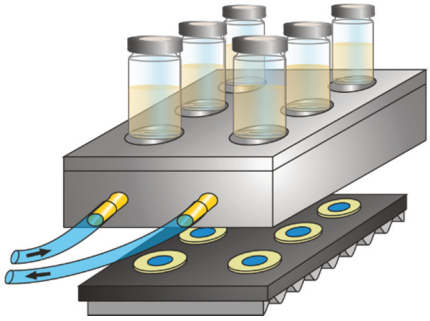

Figure S1. Photochemical set-up.

General Procedure for the photocatalytic chlorination

In a vial 0.02 mmol of the respective substrate, together with 10 mol% (0.002 mmol) RFT, 0.2 mmol (10 eq.) HCl, 0.2 mmol (10 eq.) HOAc (or TFA) and 0.12 mmol (6 eq.) *p*-methoxy benzylalcohol were dissolved in 2 mL of dry acetonitrile. The reaction mixture was irradiated under stirring for 2.5 h using the set-up depicted in Figure S1. After the irradiation the internal standard (0.01 mmol *n*-pentadecane) was added to the reaction and the reaction was immediately quenched with sat. Na_2CO_3-solution and brine. The mixture was extracted with ethyl acetate and subjected to GC-FID analysis.

GC-FID measurements

The GC oven temperature program was adjusted as follows: The initial temperature of 60 C was kept for 3 minutes, the temperature was increased at a rate of 20 °C/min until the final temperature (290 C) was reached and kept for 2 minutes; internal standard: *n*-pentadecane.

For substrates with lower boiling points a slightly different method was applied: The initial temperature of 60 °C was kept for 3 minutes, the temperature was increased at a rate of 25 °C/min until the final temperature (160 °C) was reached and kept for 5 minutes; internal standard: *n*-pentadecane.

GC was calibrated using a six-point calibration; the calibration curve for *o*-chloranisole is shown as an example. Authentic samples of each compound were used for calibration.

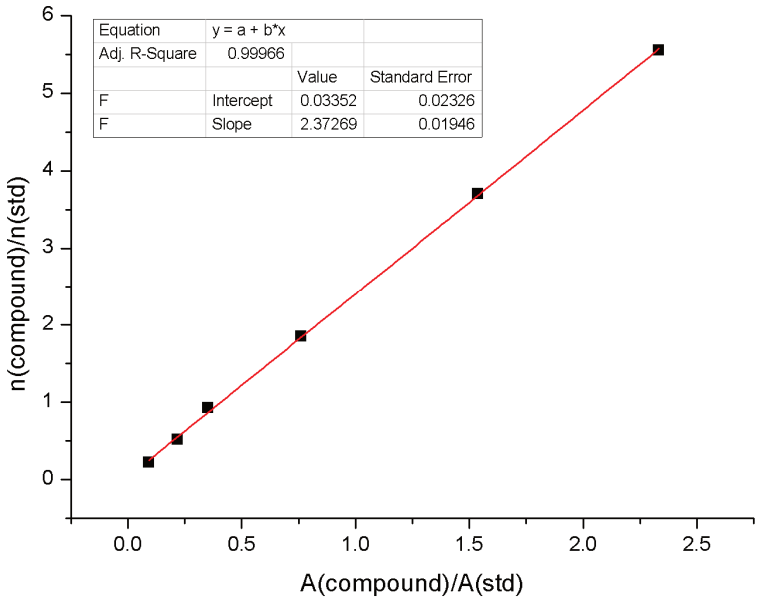

Figure S2. Exemplary calibration curve for *o*-chloranisole.

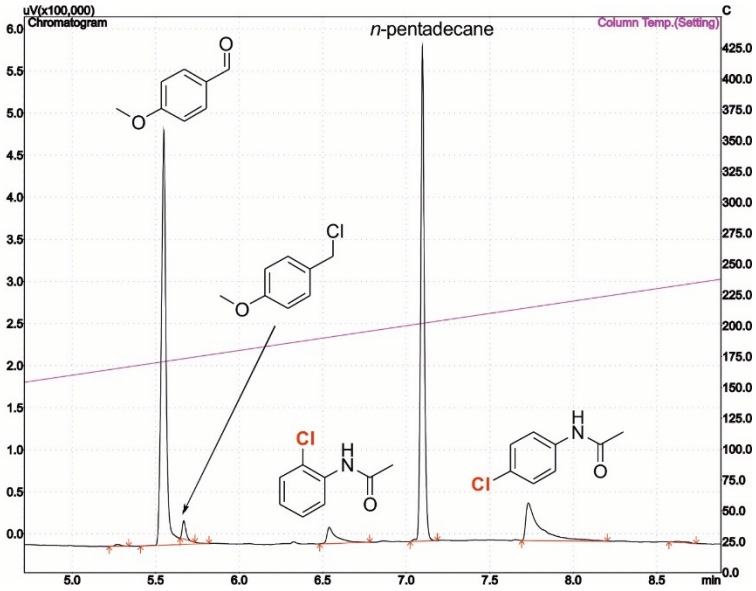

Figure S3. Example of the GC chromatogram obtained from the chlorination of acetanilide **5**.

6.5.2 Control Reactions

Control reactions were performed using equal amounts of the respective compounds as described in the general procedure. Work-up and analysis was done accordingly. No chlorination product was observed, when any of the components was omitted or the reaction was kept in the dark (entry 9). As described in the manuscript an unproductive background reaction occurred with protonated RFT.

Table S1 Control reactions.

entry	condition	Conv. /%	yield /%
1	RFT, anisole	17	0
2	RFT, anisole, HCl	100	0
3	RFT, anisole, HCl, HOAc	100	0
4	RFT, anisole, *p*MBA	24	0
5	RFT, anisole, *p*MBA, HOAc	100	0
6	RFT, anisole, *p*MBA, HCl	100	0
7	anisole, HCl	0	0
8	anisole, HOAc, HCl	0	0
9	no light	28	0

6.5.3 Reactions with Peracetic Acid

Peracetic acid can be used as a stoichiometric oxidant in oxidative chlorination. **Table 2** shows the yields of oxidative chlorination obtained for the substrates described in the manuscript. The results were obtained using the following procedure.

General procedure for the reaction with peracetic acid

In a vial 0.02 mmol of the respective substrate, 10 eq. HCl and 0.024 mmol (1.2 eq.) peracetic acid were dissolved in 2.5 mL MeCN. The reaction mixture was stirred for 2.5 h at r.t.. Afterwards the internal standard (0.01 mmol *n*-pentadecane) was added to the reaction and the reaction was immediately quenched with sat. Na_2CO_3-solution and brine. The mixture was extracted with ethyl acetate and subjected to GC-FID analysis.

For all substrates except for the electron poor compound **15** the corresponding chlorinated product was obtained. This observation proves that peracetic acid induces oxidative chlorination. However, for most substrates the use of peracetic acid employed directly will lead to an undesired double chlorination. The high reactivity of peracetic acid leads to overchlorination if used as a reagent directly, but is beneficial for the use as a mediator generated slowly in small amount as in the flavin photocatalysis.

Table S2. Oxidative chlorination using peracetic acid as the stoichiometric oxidant.

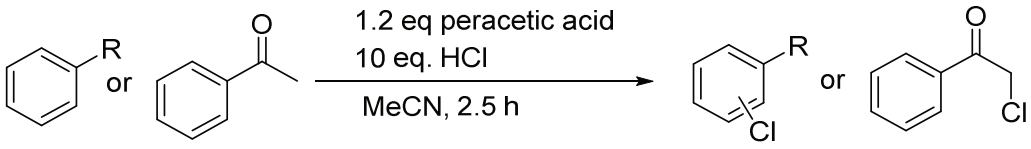

Entry	Substrate	Product	Yield/%[a]	Double chlorination/%[a]
1	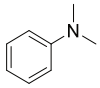 **3**	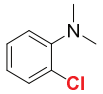 **4**	50 (p:o 0:100)	32
2	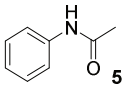 **5**	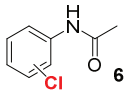 **6**	68 (p:o 5:1)	--
3	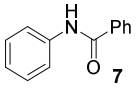 **7**	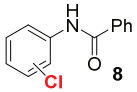 **8**	>99	0
4	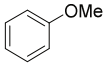 **9**	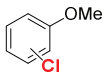 **10**	65 (p:o 15:1)	13
5[b]	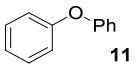 **11**	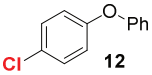 **12**	46	48[b]
6	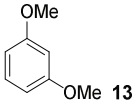 **13**	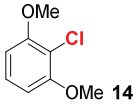 **14**	82	0
7	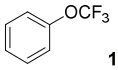 **15**	--	--	--
8[b]	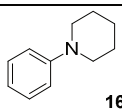 **16**	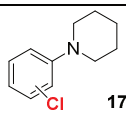 **17**	64 (p:o 1:11)	25
9	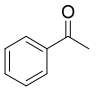 **18**	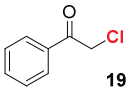 **19**	64	8
10[b]	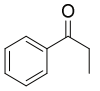 **20**	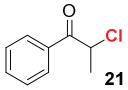 **21**	84	18[b]

[a] obtained by GC-FID analysis using n-petadecane as the internal standard. [b] Calibration factor for the monochlorinated product was used for estimation.

6.5.4 Optimization of the Reaction Conditions

As described in the manuscript, Table S3 summarized the results of the screening of different routes for the generation of peracetic acid (entries 1-6) and the variation of the peracid (entries 7-11). The most efficient generation of peracetic acid was achieved by a combination of acetic acid and hydrochloric acid (entry 1), even though acetic anhydride and acetyl chloride showed formation of chloroanisole, but in significantly lower yields. Triflic acid yielded the best results when a combination of hydrochloric acid and TEACl was used as the chloride source (entry 8).

Table S3. Variation of the peracid and chloride source.

entry	system	conv. /%	yield /%
1	HOAc (10 eq.), HCl (10 eq.)	100	66
2	HOAc (10 eq.), KCl	97	0
3	HOAc (10 eq.), TEACl (10 eq.), 20 mol% H_2SO_4	100	34
4	Ac_2O (10 eq.), HCl (10 eq.)	86	28
5	acetyl chloride (10 eq.)	100	17
6	acetyl chloride (10 eq.), HCl (5 eq.)	85	15
7	TFA (10 eq.), HCl (10 eq.)	65	27
8	TFA (10 eq.), HCl (5 eq.), TEACl (5 eq.)	100	57
9	TFA (10 eq.), KCl	100	30
10	HCOOH (10 eq.), HCl (10 eq.)	86	42
11	HCOOH (10 eq.), TEACl (10 eq.)	40	0

Table S4 shows the temperature dependence of the reaction.

Table S4. Temperature dependence of the reaction.

entry	temperature	yield / %[a]	conv. anisole / %
1	25 °C	28	98
2	35 °C	35	64
3	**45 °C**	**66**	**100**
4	45 °C (5 mol% RFT)	46	62
5	60 °C	0	16

Table S5 shows the screening of solvents known to lead to an efficient photooxidation of *p*MBA and hence formation of H_2O_2. Except for MeCN, none of the investigated solvents led to formation of the chlorinated product. Even though water is reported to be

beneficial for the oxidation of *p*MBA, it prevents productive formation of peracetic acid as it shifts the equilibrium (eq. 1) to the side of acetic acid.

$$HOAc + H_2O_2 \rightleftharpoons HOOAc + H_2O \qquad \text{(eq. 1)}$$

Table S5. Solvent screening at 45 °C.[a]

entry	solvent	yield 5 / %[b]	conv. anisole / %[b]
1	MeOH	0	9
2	MeOH/MeCN 1:1	0	64
3	DMSO	0	10
4	MeCN/H_2O 2:1	0	56
5	MeCN, dry	66	95

a) average of 2 reactions; b) yields determined by GC-FID analysis

6.5.5 UV-vis Spectroscopy

The UV-vis measurements with online irradiation were performed on a self-made apparatus using a fluorescence cuvette in a fluorescence cuvette holder, LED (Cree-XP, royal blue, 455 nm) placed perpendicular to the optical pathway of the Agilent 8453 UV-Vis Spectrometer. The measurement was performed in 10 mm Hellma fluorescence quartz cuvettes (117.100F-QS).

First, we monitored the change of the absorption bands of RFT in the presence of HCl in MeCN (Figure S4). The formation of an absorption band is observed at λ_{max} = 390 nm, which is assigned to the protonated species $RFTH^+$.[5] We irradiated a degassed mixture of RFT and *p*mBA in MeCN in the presence of HCl and HOAc (Figure S5). The absorption band at λ_{max} = 390 nm is decreases under irradiation, whereas the formation of a distinct broad band at λ_{max} = 460-530 nm is observed. This broad band is characteristic for $^2RFTH_2^{\bullet+}$, which is generated by protonation of the reduced flavin species $^2RFTH^{\bullet}$ under acid conditions.[5]

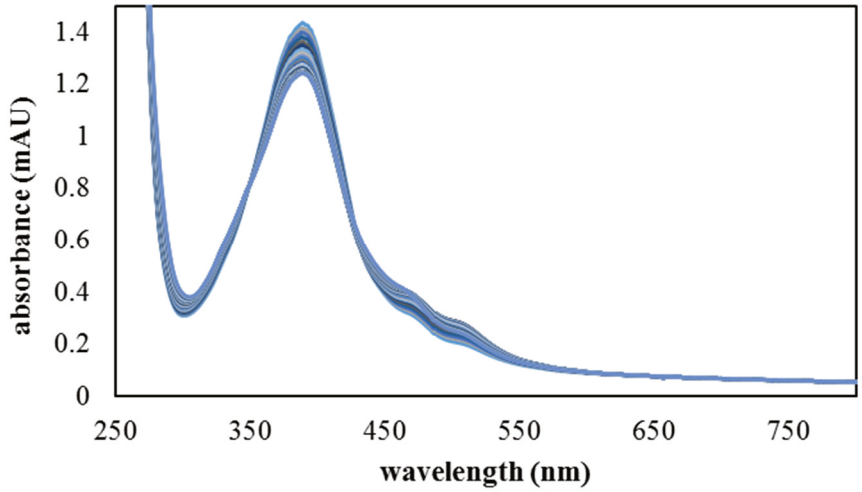

Figure S4. Electronic absorption spectra of RFT (0.1 mM, blue) in the presence of HCl in MeCN at 298 K.

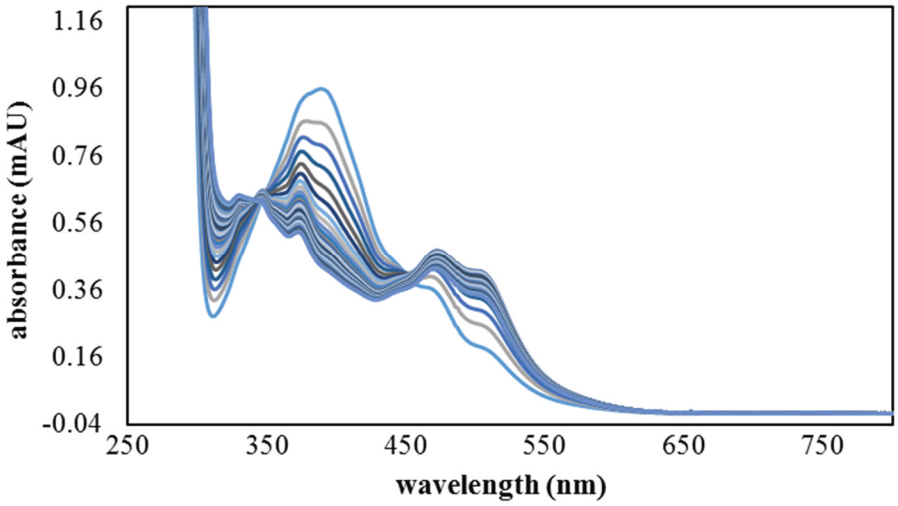

Figure S5. Electronic absorption spectra of *p*MBA (6.7 mM) and RFT (0.1 mM) in the presence of HCl while irradiating with blue light in MeCN at 298 K. The spectra were measured over 6 min recording one spectra every 10 s.

6.5.6 References

[1] S. Alagaratnam, N. J. Meeuwenoord, J. A. Navarro, M. Hervás, M. A. De la Rosa, M. Hoffmann, O. Einsle, M. Ubbink, G. W. Canters, *FEBS J.* **2011**, *278*, 1506-1521.

[2] Y. Lv, Y. Zheng, Y. Li, T. Xiong, J. Zhang, Q. Liu, Q. Zhang, *Chem. Commun.* **2013**, *49*, 8866-8868.

[3] A. M. C. H. van den Nieuwendijk, D. Pietra, L. Heitman, A. Göblyös, A. P. Ijzerman, *J. Med. Chem.* **2004**, *47*, 663-672.

[4] X.-Z. Shu, X.-F. Xia, Y.-F. Yang, K.-G. Ji, X.-Y. Liu, Y.-M. Liang, *J. Org. Chem.* **2009**, *74*, 7464-7469.

[5] S. Fukuzumi, S. Kuroda, *Res. Chem. Intermed.* **1999**, *25*, 789-811.

7 Summary

Chapter 1. Photocatalytic C−H Bond Oxygenation

In the first chapter of this thesis, recent developments in photocatalytic C−H bond oxygenation reactions are reviewed. Inspired by Nature, metal porphyrin and porphyrinoid catalysts have been designed to achieve the elusive goal of selective oxygenation reactions with dioxygen as oxidant. The visible-light-driven generation of distinct high-valent oxo-species is believed to be the key to trigger selective oxygenation reactions. Furthermore, $[Ru(bpy)_3]^{2+}$ and organic dyes such as methylene blue, eosin Y, and riboflavin tetraacetate were also applied in selected reactions. Over the last years, the development of acridinium-derived catalysts significantly improved the scope of oxygenation reactions. Interestingly, the combination of $[Ru(bpy)_3]^{2+}$ photocatalysis with transition metal porphyrins gave new insights into the oxygenation of substrates with water as oxygen source inspired by photosystem II. This oxidative activation of water led to the development of covalently linked dyads consisting of a light-harvesting chromophore and an oxygenation catalyst.

Chapter 2: Photocatalytic Benzylic C−H Bond Oxidation with a Flavin Scandium Complex[1]

One aim of this thesis was to expand the scope of visible-light-driven C−H bond oxygenation reactions with the purely organic, cheap and non-toxic chromophore riboflavin tetraacetate (RFT). This dye effectively catalyzes the aerobic photooxidation of benzyl alcohols, benzyl amines, and sulfoxides,[*i*] but has severe limits for the challenging oxygenation of alkylbenzenes to the corresponding aldehydes. The oxidation of only very few selected electron-rich substrates was achieved purely with RFT, because the reduction potential of photoexcited, ^{3}RFT*, is too low to trigger an electron transfer from substrates with higher oxidation potentials to ^{3}RFT*. An efficient electron transfer from the substrate to ^{3}RFT* is the key prerequisite for photocatalytic activity.

Building on pioneering work by Fukuzumi,[*ii*] who found that the reduction potential of RFT can be increased by metal ion coordination, we developed a photocatalytic $Sc(OTf)_3$/RFT system ($RFTH^+$-$2Sc^{3+}$, Scheme 1) which effectively catalyzes the aerobic oxidation of alkylbenzenes and electron-deficient benzyl alcohols under acidic conditions. The coordination of the Lewis-acidic scandium(III) ions enables an efficient electron transfer from the substrate to a photoexcited $RFTH^+$-$2Sc^{3+}$ complex (step *i*), which is not feasible in the absence of Sc^{3+} ions. The formed benzyl radical cation is trapped by dioxygen and subsequently yields the desired oxygenated product (step *ii*). The catalyst

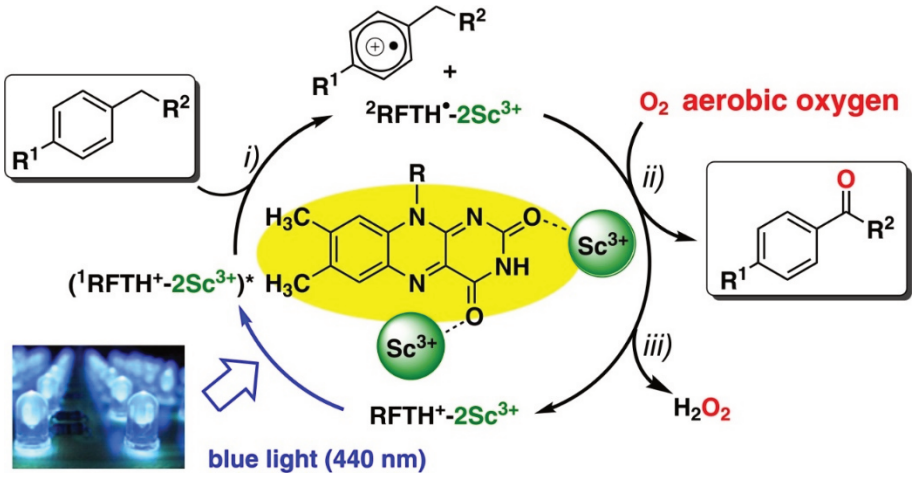

Scheme 1. Photocatalytic oxygenation of benzylic C−H bonds with an RFT-Scandium complex.

is regenerated in air under concomitant formation of H_2O_2 as the sole by-product (step *iii*). For example, toluene is converted to benzaldehyde in 71% yield. Benzyl ethers do not give the corresponding esters, but form benzaldehydes. Diarylmethylene derivatives and benzyl alcohols are oxidized with good to excellent yields as well. An exploration of the effect of redox-active metal ions on the catalytic performance of RFT is the subject of the next chapter.

Chapter 3: C–H Photooxygenation of Alkylbenzenes Catalyzed by Riboflavin Tetraacetate and a Non-Heme Iron Catalyst[2]

As shown in chapter 2, the additive $Sc(OTf)_3$ enables the oxygenation of alkylbenzenes with electron-withdrawing substituents, but this $Sc(OTf)_3$/RFT system still performs poorly for various other benzylic substrates. We became aware that the formation of hydrogen peroxide as a by-product is a major drawback of RFT-catalyzed oxygenations of benzylic substrates. This is exemplified by the oxygenation of 4-ethylanisole (**1**, Scheme 2, step *i*) established by König and co-workers which produces one equivalent of H_2O_2 per substrate molecule consumed. Unfortunately, H_2O_2 degrades RFT under irradiation quite rapidly. As a result, 4-acetylanisole (**2**) and 4-methoxy-α-methylbenzyl alcohol (**3**) are obtained as a product mixture in poor yields due to rapid photocatalyst bleaching. Feringa reported that bioinspired iron complexes with tetra- and pentadentate nitrogen ligands catalyze the oxidation of **1** using H_2O_2 as an oxidant (step *ii*), albeit with low yields and selectivities.[iii] Moreover, the ability of such iron complexes to catalyze H_2O_2 disproportionation (step *iii*) is well-known. Lower H_2O_2 concentrations could enable a higher photostability of RFT, allowing the flavin-mediated oxidation of the benzyl alcohol **3** to the ketone **2** (step *iv*) to proceed.

We discovered that the combination of the RFT with the bioinspired complex $[Fe(TPA)(MeCN)_2](ClO_4)_2$ (**4**, TPA = tris(2-pyridylmethyl)amine, Scheme 2) affords a

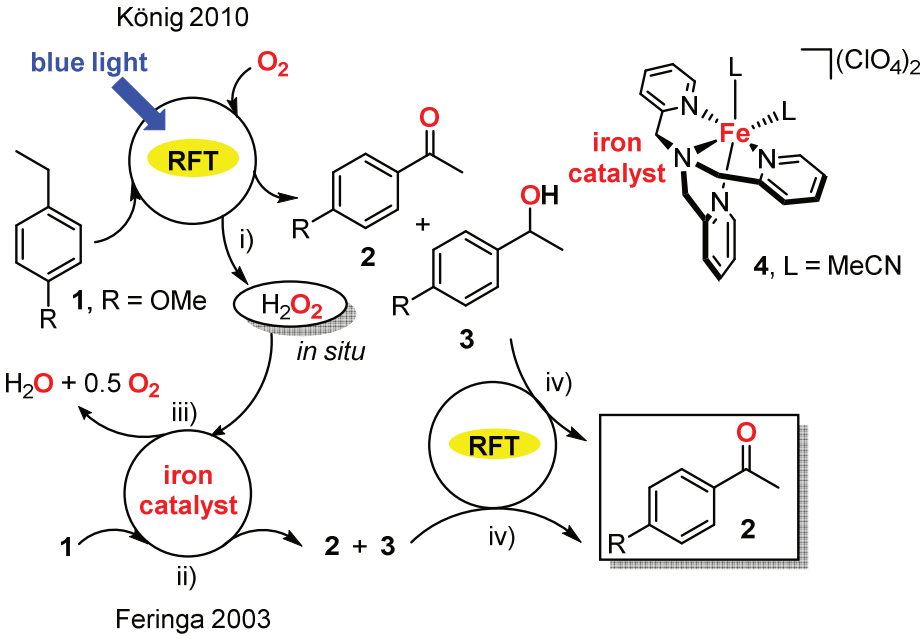

Scheme 2. Proposed dual catalysis for the oxidation of benzylic substrates exemplified for the oxidation of 4-ethylanisole (**1**) to 4-acetylanisole (**2**) and 4-methoxy-α-methylbenzyl alcohol (**3**).

readily accessible, cheap, and efficient catalyst for the visible-light-driven aerobic C–H bond oxidation of various alkylbenzenes. Contrary to the $Sc(OTf)_3$/RFT system, the reduction potential of RFT is not altered by the iron complex. Instead, the reactivity of the iron complex with photocatalytically generated H_2O_2 is key to ensure high conversions and selectivities. Co-catalyst **4** acts as a H_2O_2 disproportionation catalyst and an oxygenation catalyst at the same time. Different to the complementary enzyme-based photobiocatalytic tandem catalyst reported by Hollmann *et al.*,[iv] the present system uses a transition metal co-catalyst; a sacrificial electron donor is not required.

Chapter 4: Aerobic Photooxidation of Cycloalkenes Catalyzed by Riboflavin Tetraacetate and a Non-Heme Iron Complex[3]

In chapters 2 and 3, we reported the photooxygenation of a variety of benzylic substrates. In pursuit of our aim of expanding the scope of the flavin-mediated oxygenation reactions, we investigated the oxygenation of cycloalkenes. In this case, we exploited the ability of RFT to mediate energy transfer reactions and sensitize singlet oxygen. This in contrast to the $Sc(OTf)_3$/RFT- and non-heme iron/RFT-systems described in chapters 2 and 3, where the initial step is an electron transfer from the substrate to the catalyst and singlet oxygen is a negligible pathway.

The excitation of RFT leads to the formation of singlet oxygen ($^1O_2$), which readily reacts with cycloalkenes to allylic hydroperoxides in the well-known Schenck-ene reaction (Scheme 3, step *i*). A non-heme iron catalyst [Fe(bpmen)$(OTf)_2$] (**5**, bpmen = *N*,*N*′-dimethyl-*N*,*N*′-bis(2-pyridylmethyl)-1,2-diaminoethane, Scheme 3) utilizes the *in situ*

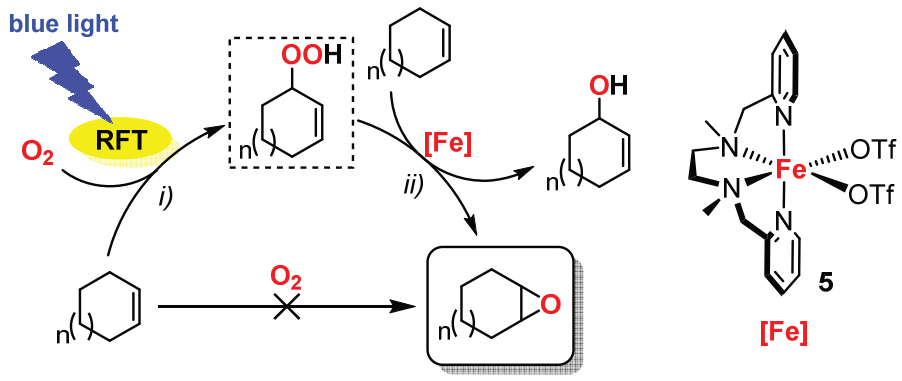

Scheme 3. Photocatalytic epoxidation of cycloalkenes *via* an *in situ* generated allylic hydroperoxides in the presence of the singlet oxygen sensitizer RFT and the oxygenation catalyst [Fe(bpmen)$(OTf)_2$] (**5**).

generated allylic hydroperoxide as an oxidant for the selective epoxidation of cycloalkenes with concomitant formation of the allylic alcohol (step *ii*). In the case of cyclooctene, the main product is cyclooctene oxide (31% yield) with a turnover number (TON) of 28, which is significantly higher than those reported reported in the literature for iron catalyst/H_2O_2 systems. Two equivalents of cycloalkene are needed to generate one equivalent of oxygenated substrate. Additionally, only traces of allylic alcohol are observed, which is presumably due to its polymerization. In the case of cyclohexene, the product distribution is significantly shifted from the epoxide (TON = 14) towards allylic oxygenation products.

Chapter 5: Aerobic Photooxidation of Aldehydes to Esters Catalyzed by Riboflavin Tetraacetate[4]

Esters are an important class of compounds widely utilized as fine chemicals, pharmaceuticals, and food additives. Classical methods for their preparation include the Brønsted or Lewis acid-catalyzed condensation of benzoic acids with alcohols at elevated temperatures. The direct formation of esters from aldehydes has attracted much attention as an alternative protocol to traditional methods, because it utilizes easily available starting materials, and an isolation of the corresponding carboxylic acid is not required.

We report a convenient photocatalytic protocol for the aerobic esterification of aldehydes to the corresponding methyl esters under visible light irradiation in the presence of methanol and acidic conditions (Scheme 4, Route A). Mechanistic studies revealed an electron transfer from the *in situ* formed acetal (Scheme 4, step *i*) to the photoexcited chromophore RFT as the key step (step *ii*). Other alkyl benzoates only gave unsatisfactory yields, which is mainly caused by the impaired formation of the acetal in the case of sterically more demanding alcohols. Therefore, another photocatalytic approach to alkyl benzoates was needed.

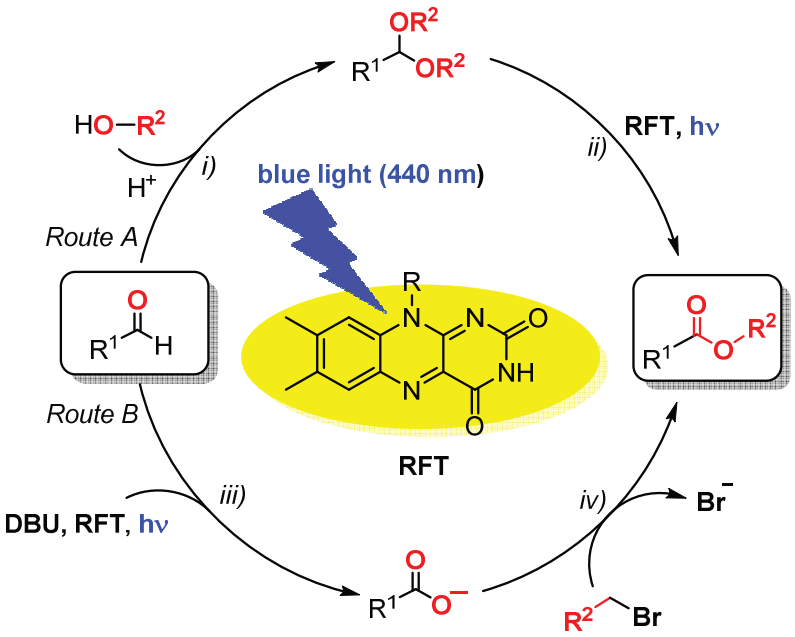

Scheme 4. Route A: Aerobic photooxidation of aldehydes to esters *via* the flavin catalyzed oxidation of an *in situ* formed acetal. This method is mainly limited to methyl esters; route B: Oxidation of aldehydes to carboxylates *via* the *in situ* photogeneration of $^{-}$OOH from RFT and the sacrificial substrate DBU; an S_N2 type reaction of the carboxylate with an alkylbromide yields the corresponding ester; this methodology was mainly applied for ethyl- and isopropylesters, but is limited to benzaldehydes bearing electron-withdrawing substituents.

Irradiation of a mixture of RFT and aldehydes in the presence of DBU (1,8-diazabicyclo[5.4.0]undec-7-ene) and alkyl bromides as coupling reagents turned out to be another suitable method for ester synthesis. The flavin-mediated oxidation of the sacrificial electron donor DBU leads to the *in situ* generation of the hydroperoxide anion, HOO^{-}, which subsequently oxidizes aldehydes to their corresponding benzoic acids or carboxylates (step *iii*). These nucleophilic species react to the corresponding esters in the presence of alkybromides *via* an S_N2-type reaction (step *iv*). This visible-light-driven esterification is limited to benzaldehydes bearing electron-withdrawing substituents due to the competing formation of phenol derivatives for electron-donating substituents. Nevertheless, this RFT/DBU system gives access to the highly nucleophilic species HOO^{-} directly from atmospheric dioxygen, which might be an easily accessible and useful oxidant for other oxygenation reactions.

Chapter 6: Halogenase-Inspired Oxidative Chlorination Using Flavin Photocatalysis[5]

Chlorinated aromatic compounds are ubiquitous in organic chemistry, which are classically synthesized by using hazardous and toxic chlorine gas or synthetic equivalents such as NCS and *t*BuOCl. Nature has developed a more elegant strategy based on flavin-dependent halogenase (FAD) enzymes, which elegantly oxidizes chloride to an

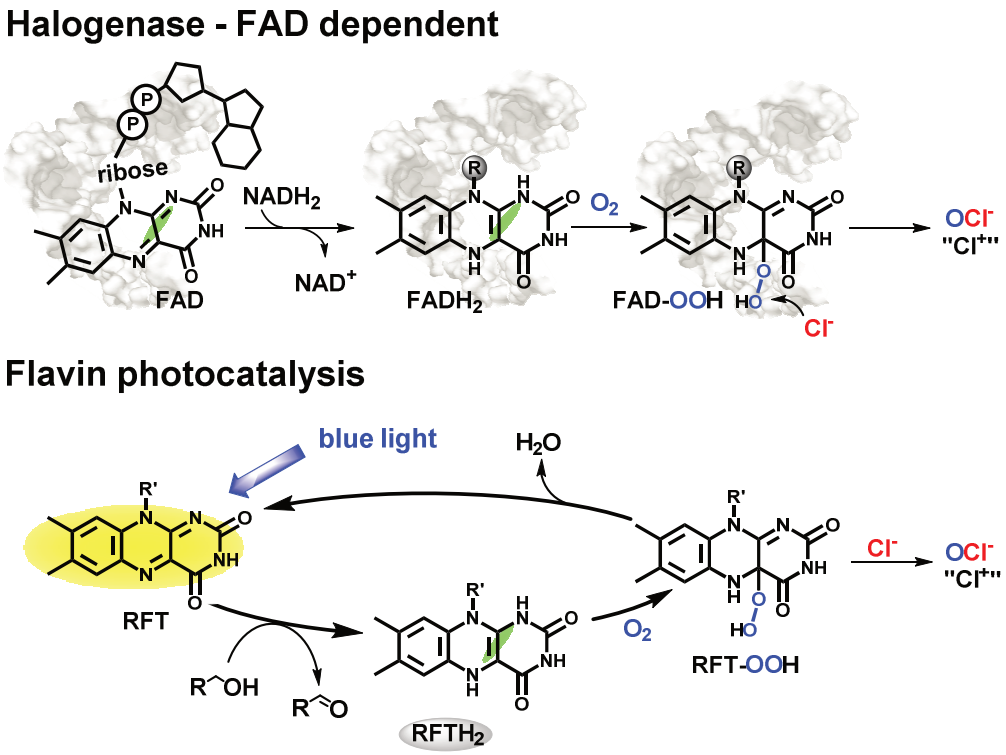

Scheme 5. Analogy of the mechanistic model of chloride oxidation by FAD-dependent halogenases (top) and the proposed photocatalytic halogenase mimetic system (bottom).

active species that functions as a "Cl^+" source in the presence of the co-factor $NADH_2$ and air (Scheme 5, top). Enzymes are substrate specific, thus, the scope of accessible products is limited. Moreover, the isolation and handling of the enzymes is difficult. Therefore, we sought to develop an artificial photocatalytic system based on our experience with RFT. We replaced the biomolecules FAD by RFT and $NADH_2$ by 4-methoxybenzyl alcohol, which serves as a cheap reducing agent (Scheme 5, bottom). It is noteworthy that no chlorination of the test substrate anisole was observed when the reaction was irradiated under these conditions. We assume that *in situ* photogenerated H_2O_2 and RFT do not form the same hydroperoxy species as in the FAD-dependent halogenase in the absence of the complex environment of the enzyme. Therefore, acetic acid was added, forming peracetic acid *in situ* which acts as a mediator for chloride oxidation (Scheme 6). Compared to the specific binding pocket of an enzyme, the activation by peracetic acid is a more general strategy and thus allows a broader substrate scope. The developed system allows the chlorination of electron rich arenes, e.g. anisole, methylanilines, diphenyl ether and amides, as well as the α-chlorination of acetophenones.

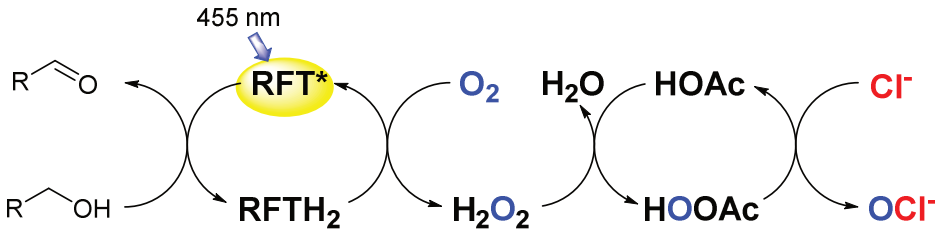

Scheme 6. Proposed mechanistic scheme of the peracetic acid mediated oxidation of chloride by flavin photocatalysis.

References:

[1] B. Mühldorf, R. Wolf, "Photocatalytic benzylic C−H bond Oxidation with a Flavin Scandium complex", *Chem. Commun.* **2015**, *51*, 8425−8428.

[2] B. Mühldorf, R. Wolf, "C−H Photooxygenation of Alkyl Benzenes Using Riboflavin Tetraacetate and a Non-Heme Iron Complex", *Angew. Chem.*, **2016**, *128*, 437−441; *Angew. Chem. Int. Ed.* **2016**, *55*, 427−430; Highlighted in *Nachrichten aus der Chemie*, February **2016**, Wiley-VCH.

[3] Unpublished results

[4] Unpublished results

[5] T. Hering, B. Mühldorf, R. Wolf, B, König, "Halogenase-Inspired Oxidative Chlorination Using Flavin Photocatalysis", *Angew. Chem. Int. Ed.*, **2016**, published in early view, DOI: 10.1002/anie.201600783R1.

[*i*] For selected examples of flavin-mediated photooxidations, see a) J. Dad'ová, E. Svobodová, M. Sikorski, B. König, R. Cibulka, *ChemCatChem* **2012**, *4*, 620−623; b) R. Cibulka, R. Vasold, B. König, *Chem. Eur. J.*, **2004**, *10*, 6223−6231; c) R. Lechner, B. König, *Synthesis* **2010**, 1712−1718; d) B. König, S. Kümmel, R. Cibulka in *Chemical Photocatalysis* (Ed.: B. König), De Gruyter, Berlin, **2013**, pp. 45–66.

[*ii*] For the modification of the reduction potential of RFT, see: a) S. Fukuzumi, K. Yasui, T. Suenobu, K. Ohkubo, M. Fujitsuka, O. Ito, *J. Phys. Chem. A*, **2001**, *105*, 10501–10510; b) S. Fukuzumi, S. Kuroda and T. Tanaka, *J. Am. Chem. Soc.*, **1985**, *107*, 3020–3027.

[*iii*] M. Klopstra, R. Hage, R. M. Kellogg, B. L. Feringa, Tetrahedron Lett. 2003, 44, 4581–4584.

[iv] For selected examples enzyme-based photobiocatalytic tandem systems a) E. Churakova, M. Kluge, R. Ullrich, I. Arends, M. Hofrichter, F. Hollmann, *Angew. Chem. Int. Ed.* **2011**, *50*, 10716–10719; b) D. I. Perez, M. M. Grau, I. W. C. E. Arends, F. Hollmann, *Chem. Commun.* **2009**, 6848–6850.

8 Acknowledgment

Mein besonderer Dank gilt Prof. Dr. Robert Wolf für die interessante Aufgabenstellung, die wertvollen Anregungen und die hervorragende Betreuung in der gesamten Zeit der Promotion. Der Versuchsballon „sich einen PCler in die AC zu holen um ihn dort OC und TC machen zu lassen“ ist nicht geplatzt.

Prof. Dr. Burkhard König danke ich zunächst dafür als Zweitgutachter zu fungieren. Desweitern möchte ich mich sehr herzlich für die vielen Diskussionsrunden im Rahmen des GRKs, wie auch für die außerplanmäßigen Besprechungen bedanken. Für die unkomplizierte Abwicklung organisatorischer Dinge in meiner Funktion als Graduiertensprecher bin ich ebenfalls sehr dankbar.

Prof. Dr. Arno Pfitzner (Drittprüfer) und Prof Dr. Richard Buchner danke ich ebenfalls dafür, dass sie sich bereiterklärt haben, das Prüfungskomitee zu komplettieren. Prof. Dr. Bernhard Dick, Prof. Dr. Axel Jacobi von Wangelin und Prof. Dr. Kirsten Zeitler bin ich für die Unterstützung in allen physikalischen sowie organischen Fragestellungen dankbar.

Dr. Michael Spörner (Univ. Regensburg) und Helmut Schüller (Zentrale Analytik) danke ich für die Hilfe bei den EPR Messungen, Dr. Gábor Balázs (Univ. Regensburg) für die Hilfe bei den Simulationen von EPR Spektren. Dank Dr. Rudolf Vasold (Univ. Regensburg) hatten wir zudem einen herausragend guten Zugang zu GC-MS Messungen. Regina Hoheisel danke ich für die Messung diverser CVs und die netten Gespräche.

Ich danke allen Mitglieder des GRKs für die interessanten Seminartage, besonders danke ich Tomáš Slanina, Hanna Bartling, Uwe Faltermeier und Fabian Brandl für die Unterstützung in allen spektroskopischen Fragen. Britta Badziura (Hüterin der Schatzkiste) danke ich für die schnelle und effiziente Abwicklung aller organisatorischer Dinge, Viola Rappenegger (Organisationsfee) danke ich für die enorme Unterstützung bei der teils sehr nervenaufreibenden Vorbereitung der Seminartage und für das sonstige Management.

Meiner Kooperationspartnerin Thea Hering danke ich für die sehr angenehme, lustige und effiziente Zusammenarbeit. Und natürlich das ganze drum herum!

Desweitern möchte ich bei Ester Heckel (F-Prak.), Thomas Föll (BA), Thomas Maier (BA), Rebecca Grünbauer (BA), Nadine Maue (ZuLA) und Ulrich Lennert (F-Prak.) für ihre Mitarbeit und Ideen bei den Projekten dieser Dissertation danken.

Ich danke allen Azubis, vor allem Vanessa Tomanek und Veronica Scheidler, dass sie mich so hervorragend in meiner Arbeit unterstützt haben und selbstständig alle die Dinge erledigt haben, die ich vergessen habe.

Allen jetzigen und früheren Mitgliedern des Arbeitskreises danke ich für die entspannte Laboratmosphäre und die kollegiale Zusammenarbeit. Mein besonderer Dank gilt Dr. Jennifer Bißmeyer (die mich zum Bouldern gebracht und mich viele neue, schöne Wörter und Sätze gelehrt hat), Dr. Babak Rezaei Rad (der mir den ersten positiven Eindruck in Form eines F-Praktikums vermittelt hat), Kapitän zur See Stefan Pelties (der mir mit seiner einmaligen nordischen Art zu jeder Zeit den Laboralltag versüßt hat), dem Obersten Kapellmeister und Fremdsprachenkorrespondenten Dirk Herrmann (der mir nicht nur das Gin trinken beigebracht hat, sondern auch ein einmaliger Laborkollege war), Philipp „the Phips“ Büschelberger (für die zahlreichen strammen Mäxe, hochphilosophischen Gespräche bis tief in die Nacht oder Morgen hinein, die Abifahrt Hirschegg 2015 und dafür, dass er mich als obersten Hofgrantler seiner Majestät abgelöst hat), dem Urlauber (für seine buddhistische Ruhe und Gelassenheit, wenn er denn mal da war), Christian „Petrosilius Zwackelmann“ Hoidn (für die fristgerechte und reibungslose Übernahme meines Schreibtisches und seine erhellende Art) und Uttam „the paper machine“ Chakraborty (for fruitful discussions and a lot of fun in the lab). Desweitern danke ich Julia „solvent girl“ Leitl, Thomas „nitrogen boy“ Maier und Ulrich „argon man“ Lennert für die kurze, aber sehr angenehme Zusammenarbeit.

Besonders danke ich Yvonne, Karl-Heinz und Franzi für die liebevolle Unterstützung über die ganze lange lange Zeit. Mein Dank dafür lässt sich wirklich nur schwer in Worte fassen.

Rosa bin ich für so vieles dankbar, Herbert und Angela danke ich besonders für ihre Unterstützung und ihre wohlschmeckenden Versuche, jemanden wie mir das Kochen beibringen zu wollen.

Viola danke ich für die hingebungsvolle Unterstützung in der finalen Phase dieser Arbeit, was wahrlich kein Zuckerschlecken gewesen sein muss. Vielen Dank!

Doris und Hubert danke ich ebenfalls für die langjährige Unterstützung und den Glauben, dass aus mir vielleicht doch noch mal irgendwann was werden könnte.

Meinem Vater Reinhold danke ich besonders für die finanzielle Unterstützung im Studium, die das hier erst möglich gemacht hat. Ich bin entgegen seiner Befürchtungen kein „langzottelter Bombenleger“ geworden. Petra danke ich im Speziellen für ihre Fürsorge um mein leibliches Wohl.

Zuletzt danke ich meiner Oma und meinem Opa! Für eure bedingungslose, fast schon aufopferungswillige Unterstützung über die ganze Zeit, vom Studium bis jetzt. Danke!

9 List of Publications

T. Hering, B. Mühldorf, R. Wolf, B. König, "Halogenase-Inspired Oxidative Chlorination Using Flavin Photocatalysis", *Angew. Chem. Int. Ed.*, **2016**, accepted, DOI: 10.1002/anie.201600783R1.

U. Chakraborty, M. Modl, B. Mühldorf, M. Bodensteiner, S. Demeshko, N. J. C. van Elzen, M. Scheer, S. Harder, R. Wolf, "Pentaarylcyclopentadienyl Iron, Cobalt and Nickel Halides" *Inorg. Chem.*, **2016**, published online at March 7, 2016; Article ASAP, DOI: 10.1021/acs.inorgchem.5b02896.

U. Chakraborty, B. Mühldorf, N. J. C. van Elzen, B. de Bruin, S. Harder, R. Wolf, "[CpArNi{Ga(nacnac)}]: An Open-Shell Nickel(I) Complex Supported by a Gallium(I) Carbenoid (CpAr = $C_5(C_6H_4$-4-$Et)_5$), nacnac = $HC[C(Me)N$-(C_6H_3)-2,6-$iPr_2]_2$)", *Inorg. Chem.*, **2016**, published online at March 7, 2016; Article ASAP, DOI: 10.1021/acs.inorgchem.5b02979.

B. Mühldorf, R. Wolf, "C─H Photooxygenation of Alkyl Benzenes Using Riboflavin Tetraacetate and a Non-Heme Iron Complex", Angew. Chem., 2016, 128, 437-441; *Angew. Chem. Int. Ed.* **2016**, *55*, 427-430; Highlighted in *Nachrichten aus der Chemie*, February **2016**, Wiley-VCH.

B. Mühldorf, R. Wolf, "Photocatalytic benzylic C-H bond oxidation with a flavin scandium complex", *Chem. Commun.* **2015**, *51*, 8425-8428.

B. Rezaei Rad, U. Chakraborty, B. Mühldorf, J. A. W. Sklorz, M. Bodensteiner, C. Müller, R. Wolf, "Synthesis, Structure, and Reactivity of Pentamethylcyclopentadienyl 2,4,6-Triphenylphosphinine Iron Complexes", *Organometallics* **2015**, *34*, 622-635.

10 Curriculum Vitae

Bernd Mühldorf

Lebenslauf

Daten zur Person

Familienstand:	ledig
Nationalität:	Deutsch
Geburtsdatum:	06.05.1987
Geburtsort:	Schwandorf

Ausbildung

Seit Nov. 2012	**DOKTORARBEIT** an der Universität Regensburg (Institut für Anorganische Chemie) im Arbeitskreis von Prof. Dr. R. Wolf: *"Visible-Light-Driven Aerobic Oxidation Reactions Catalyzed by Riboflavin Tetraacetate"*
Okt. 2010 – Sep. 2012	**MASTER OF SCIENCE** in **CHEMIE** an der Universität Regensburg mit Schwerpunkt physikalischer, theoretischer und anorganischer Chemie **MASTERARBEIT** im Arbeitskreis von Prof. Dr. R. Buchner (Institut für Physikalische Chemie): *"Dynamik, Hydratation und Ionenassoziation von Ionischen Flüssigkeiten auf Oligoethylenethercarboxylatbasis in wässriger Lösung"*
Okt. 2007 – Sep. 2010	**BACHELOR OF SCIENCE** in **CHEMIE** an der Universität Regensburg **BACHELORARBEIT** im Arbeitskreis von Prof. Dr. H. Yersin: *"Synthese und photophysikalische Untersuchungen von $[Pt(CN)_2(MeCN)_2]$ für OLED-Anwendungen"*
Sept. 1997 – Jun. 2006	**ABITUR** Johann-Michael Fischer Gymnasium, Burglengenfeld

Präsentationen

30.08 – 02.09.2015	Posterpräsentation – GDCh-Wissenschaftsforum Chemie 2015 in Dresden
23. – 28.08.2015	Vortrag – Wissenschaftliches Kolloquium von Arbeitsgruppen für Anorganische Chemie 2015 in Hirschegg, Österreich
22. – 24.07. 2015	Vortrag – 22. Seminartag des GRKs in München (LMU)
15. – 18.07. 2015	Posterpräsentation – 7th Pacific Symposium on Radical Chemistry in Singapur
13. – 18.07.2014	Posterpräsentation – XXVth IUPAC Symposium on Photochemistry in Bordeaux, Frankreich
26. – 28.03.2014	Vortrag – 17. Seminartag des GRKs in Kostenz

25. – 30.08.2013	Vortrag – Wissenschaftliches Kolloquium von Arbeitsgruppen für Anorganische Chemie 2013 in Hirschegg, Österreich
10. –.12.04.2013	Vortrag – 15. Seminartag des GRKs in Niederaltaich
05. – 09.09.2012	Posterpräsentation – European Molecular Liquids Group Annual Meeting, Eger, Ungarn; Posterpreis.

Mitgliedschaften

Gesellschaft Deutscher Chemiker e.V.

Graduiertenkolleg 1626 – Chemische Photokatalyse

TV Burglengenfeld, ATSV Kallmünz

Sonstige Erfahrung

Apr. 2015 – Apr. 2016	**GRADUIERTENSPRECHER** des GRK 1626 – Chemische Photokatalyse
Jan. 2012 – Sep. 2012	**WISSENSCHAFTLICHE HILFSKRAFT** am Institut für Physikalische Chemie an der Universität Regensburg im Arbeitskreis von Prof. Dr. R. Buchner
Okt. 2010 – Aug. 2011	**WERKSTUDENT** bei GENEART (Scientific Sale – Customer Contact Center)
Apr. 2007 – Okt. 2007	**KURZFRISTIGER BESCHÄFTIGTER** in der Fa. Läpple in Teublitz
Jul. 2006 – Mär. 2007	**GRUNDWEHRDIENST** im Gebirgsjägerbataillon 231 (Bad Reichenhall) und Wildflecken

11 Eidesstattliche Erklärung

Ich erkläre hier mit an Eides statt, dass ich die vorliegende Arbeit ohne unzulässige Hilfe Dritter und ohne Benutzung anderer als der angegebenen Hilfsmittel angefertigt habe; die aus anderen Quellen direkt oder indirekt übernommenen Daten und Konzepte sind unter Angabe des Literaturzitats gekennzeichnet.

Bernd Mühldorf